THE
PHYSICAL REVIEW
A Journal of Experimental and Theoretical Physics
VOL. 49, NO. 1 JANUARY 1, 1936 SECOND SERIES

The Probability of *KL* Ionization and X-Ray Satellites

ROBERT D. RICHTMYER, *Department of Physics, Massachusetts Institute of Technology*
(Received October 12, 1935)

A theory of the multiple ionizations produced by a fast cathode electron in the target of an x-ray tube is developed, based on the Born approximation of collision theory. The effective cross section for $1s2s$ ionization of potassium by an incident electron having five times the energy required for K-ionization or $1s$-ionization of potassium, and the distribution of energy and of angular momentum among the three electrons after collision is shown in detail. The probability of $1s2p$ ionization is also estimated roughly by the same method, and the two taken together are shown to be roughly in agreement with the experimental value of the integrated satellite intensity for $K\alpha$ of potassium. The predicted variation of the relative intensity with atomic number is also shown to be in rough agreement with experiment.

THE weak "satellite" lines of x-ray spectra require for their explanation transitions between doubly ionized states of the atom, and at the present time there are two theories concerning the nature of these transitions. The older theory[1] assumes that both the ionizations occur in interior shells of electrons, and that in the transition only one electron of the atom changes its quantum numbers, or "jumps." The absence of the second electron modifies the energies of, and increases the multiplicities of the initial and final states in such a way that several satellites should be found on the short wave-length side of the diagram line produced by the corresponding transition between singly ionized states. The other theory[2] assumes that the initial doubly ionized state is of the somewhat more probable type in which one of the ionizations occurs in an inner electron shell, and the other in a shell not far below the outermost filled shell of the atom; and that in the transition two electrons jump simultaneously into the two vacant places. Since in this case the coupling between the electrons is not enough greatly to alter the energy levels, the frequency of the satellite should be equal to the sum of the frequencies of the two transitions taken separately.

It seems evident that according to contemporary quantum theory both these proposed mechanisms must produce satellite lines, although some or all of the lines produced by either may be far too weak to observe. The wave-lengths as predicted by either theory[3] agree roughly with experiment, but it is not possible to predict wave-lengths with sufficient accuracy to decide between the two theories by this means alone. Ramberg[4] and Bloch[5] have estimated the intensities as predicted by the double jump theory, and it seems likely that some, at least,

[1] M. J. Druyvesteyn, Zeits. f. Physik **43**, 707 (1927).
[2] F. K. Richtmyer, J. Frank. Inst. **208**, 325 (1929).
[3] See Druyvesteyn, reference 1, H. C. Wolfe, Phys. Rev. **43**, 221 (1933), and Ramberg and Kennard, Phys. Rev. **46**, 1040 (1934) for the single jump theory, and Richtmyer reference 2 for the double-jump theory.
[4] E. Ramberg, Phys. Rev. **45**, 389 (1934).
[5] F. Bloch, Phys. Rev. **48**, 187 (1935).

of the lines are produced by double jumps. In this paper I consider intensities as predicted by the single jump theory. In 1927 Druyvesteyn[1] gave a rather crude semiclassical treatment of this problem, but since then nothing has been done with it.

The numbers of singly- and multiply-ionized atoms in the target are dependent upon the effective collision cross sections for single and multiple ionizations of an atom by a fast cathode electron, and for computing these cross sections we use the Born approximation of collision theory. Call the momentum vector (in atomic units) of the incident cathode electron $\mathbf{k}_0$. Then the cross section for collisions in which the atom is excited from the ground state to the nth state is

$$\Phi_n=\frac{k_n}{4\pi^2k_0}\int\left|\int V_{0n}(r_0)e^{i(\mathbf{k}_0-\mathbf{k}_n)\cdot\mathbf{r}_0}d\tau_0\right|^2d\omega(\mathbf{k}_n) \quad (1)$$

with

$$V_{0n}(r_0)=\int\Psi_n^*(r_j)\,U(r_0,r_j)\Psi_0(r_j)d\tau_j. \quad (2)$$

$\mathbf{k}_n$ is the momentum vector of the cathode electron after the atom has been excited; its magnitude is given by $k_n=(k_0^2-2E_n)^{\frac{1}{2}}$ where E_n is the energy of excitation of the atom, and its direction is the variable of integration $\omega(\mathbf{k}_n)$ in (1). r_0 refers to the three coordinates of the cathode electron; r_j (in which $j=1, 2, 3, \cdots, N$) refers to the coordinates of the N atomic electrons; $d\tau_0$ means integration over all space with respect to the coordinates of the cathode electron; and $d\tau_j$ means N-fold integration over all space with respect to the coordinates of the atomic electrons. The capital psi's are the complete atomic wave functions for the ground state and the nth excited state of the atom. $U(r_0, r_j)$ is the energy of interaction of the cathode electron with the atom. The outside integration in (1) is to be extended over the entire solid angle; that is, over all directions of scattering.

Let the excited state be a doubly ionized state in which a K electron and an L_{I} electron have been removed to "hyperbolic orbits" denoted by the quantum numbers k_1, l_1, m_1 and k_2, l_2, m_2, and represented by wave functions $\psi_{k_1l_1m_1}$ and $\psi_{k_2l_2m_2}$. We use N-rowed determinants of one-electron functions for Ψ_0 and Ψ_n, and if we retain only the first order of small quantities, we get

$$V_{0n}=\int\int\{\psi^*_{k_1l_1m_1}(r_1)\psi^*_{k_2l_2m_2}(r_2)-\psi^*_{k_1l_1m_1}(r_2)\psi^*_{k_2l_2m_2}(r_1)\}\cdot(1/r_{01}+1/r_{02})\varphi_1(r_1)\varphi_2(r_2)d\tau_1d\tau_2 \quad (3)$$

in which φ_1 and φ_2 are the K and L wave functions, respectively, in the normal atom, $r_{01}=|\mathbf{r}_0-\mathbf{r}_1|$, and $r_{02}=|\mathbf{r}_0-\mathbf{r}_2|$. It is to be noted that the φ's are not quite orthogonal to the ψ's, because the removal of each electron from the atom alters the field in which the other one moves. However, φ_1 will be much more nearly orthogonal to the ψ's than will φ_2, and so we shall drop terms in $1/r_{02}$.

This V_{0n} is to be substituted into expression (1). We introduce the quantity $q=|\mathbf{k}_0-\mathbf{k}_n|$, which is the magnitude of the change of momentum experienced by the cathode electron. We write the wave functions explicitly in terms of their angular and radial parts as

$$\psi_{klm}=Y_l^m(\theta,\varphi)S_{kl}(r);\qquad \varphi_1=S_1(r)/(4\pi)^{\frac{1}{2}};\quad \varphi_2=S_2(r)/(4\pi)^{\frac{1}{2}} \quad (4)$$

in which Y_l^m is a normalized spherical surface harmonic, the S's are solutions of Hartree's equations, and the continuous state functions $S_{kl}(r)$ are normalized so as to represent one particle per unit range of the momentum k. We then expand everything in sight in terms of spherical harmonics and Bessel functions, and boil down the result until we obtain

$$\Phi_n=\frac{16\pi^3}{k_0^2}\int_{k_0-k_n}^{k_0+k_n}\{O_{k_2}I_{k_10}(q)-O_{k_1}I_{k_20}(q)\}^2\frac{dq}{q^4} \quad \text{for } l_1=0,\ l_2=0 \quad (5a)$$

$$\Phi_n=\frac{32\pi^3}{k_0^2}(l_1+\tfrac{1}{2})O_{k_2}{}^2\int_{k_0-k_n}^{k_0+k_n}[I_{k_1l_1}(q)]^2\frac{dq}{q^4} \quad \text{for } l_1\neq 0,\ l_2=0 \quad (5b)$$

$$\Phi_n=0 \quad \text{for } l_2\neq 0. \quad (5c)$$

In these equations, O_k and $I_{kl}(q)$ have the following meanings:

$$O_k=\int\psi^*_{k_0}\varphi_2(2)d\tau_2=\int_0^\infty S_{k0}(r)S_2(r)r^2dr, \quad (6)$$

$$I_{kl}(q)=\frac{1}{(4\pi)^{\frac{1}{2}}}\int_0^\infty S_{kl}(r)S_1(r)J_{l+\frac{1}{2}}(qr)r^{\frac{1}{2}}dr. \quad (7)$$

Eq. (5c) shows that to our degree of approximation the L_I electron can be expelled only to states of zero angular momentum. The difference in appearance between (5a) and (5b) is due to an exchange effect between the two expelled electrons, which can take place only if the K electron is also expelled to a state of zero angular momentum. Exchange between the cathode electron and the atomic electrons is less important and has been neglected entirely.

In order, finally, to obtain the effective cross section for double ionization of the type in question (e.g., KL_1), the partial cross section as given by (5) must be integrated over all possible final states of the atom, that is over all possible hyperbolic orbits of the two expelled electrons. This requires a summation over l_1, and integrations in k_1 and k_2. The energetically possible final states will be given by the relations

$$\begin{gathered}k_1^2/2+k_2^2/2\leqslant k_0^2/2-W_K-W_L,\\ k_1\geqslant 0, \quad k_2\geqslant 0.\end{gathered} \quad (8)$$

These relations are approximate in that they assume that none of the three electrons involved stops in an optical orbit, but that all of them end up in states of positive energy. The relations require an integration of (5) over a 90° circle-sector in the k_1-k_2 plane. In the special case of $l_1=0$ only half of this sector is to be used, because of the symmetry properties of the wave functions. Otherwise the final states would be counted twice.

A completely numerical evaluation of the double-ionization cross section by this method would seem to be out of the question. One would have to obtain numerical solutions $S_{kl}(r)$ of Hartree's equation, then obtain the integrals O_k and $I_{kl}(q)$ by numerical integration, and then carry out the summation in l_1 and the integrations in q, k_1, and k_2 also numerically. One can approximate by taking the wave functions to be hydrogen-like functions, either corrected for external and internal screening, or uncorrected. Even then the amount of numerical work would be prohibitive, for one must still carry out the summation and the last three integrations numerically. We can further approximate, however, by replacing the product S_1S_{kl} by a function of simpler analytic form, but which is approximately equal to this product. Such a function must vary as r^l for small r, rise to a maximum for larger r, then become negative and have a much less pronounced minimum for still larger r, and after that be practically zero. Only the first maximum and first minimum of S_{kl} need be represented, because of the exponentially decreasing behavior of S_1. A function of the desired form, and which enables us to carry out the integration in q analytically is

$$S_1S_{kl}=(4\pi)^{\frac{1}{2}}(ar^l-br^{l+2})e^{-p^2r^2}. \quad (9)$$

The adjustable constants a, b, and p must be determined as functions of k_1 and l_1. For this purpose we suppose that the actual wave functions S_{kl} are solutions of the Schrödinger equation for a field of the form

$$V(r)=\begin{cases}V_0-Z/r & \text{for } r\leqslant r_0\ (=Z/V_0)\\ 0 & \text{for } r\geqslant r_0.\end{cases} \quad (10)$$

The solutions are hydrogen-like for small r, and essentially Bessel functions for larger r. The smooth joining at $r=r_0$ was carried out for energies greater than V_0 by means of the Wentzel-Kramers-Brillouin method. For small k the energies are less than V_0 and thus fall in a region which would be occupied by discrete levels if the Coulomb part of the field (10) were carried on out to infinity. For this case the smooth joining was carried out by means of some tables kindly supplied me by Professors Morse and Allis and which they had calculated in connection with their theory of the Ramsauer effect. V_0 and Z of the field (10) are chosen to make this field fit the actual atomic field in the neighborhood of the K shell,[6] and the K wave function S_1 is taken to be hydrogen-like with this same value of Z. Lastly a, b, and p are chosen so as to make the function (9) as nearly as possible equal to the product S_1S_{kl}. The method by which this was actually done is

[6] For potassium, $Z=18.5$, $V_0=37$, $r_0=0.50$; atomic units.

largely empirical, and since it is of no theoretical interest, it will not be described here.[7] The result is a set of graphs of a, b, and p as functions of k for various values of l. I believe that the fit is fully as good as the use of the Born approximation warrants. We now substitute (9) into (7), and put the resulting expression for $I_{kl}(q)$ into (5a) and (5b). In place of the integration variable q we introduce a new one given by $x=q^2/2p^2$, and we obtain

$$\Phi_n=\frac{\pi^3}{2k_0^2}\int_{u_1}^{u_2}e^{-x}\frac{[O_{k_2}(A_{k_10}+xB_{k_10})-O_{k_1}(A_{k_20}+xB_{k_20})]^2}{x^2}dx \quad \text{for } l_1=0, \tag{11a}$$

$$\Phi_n=\frac{\pi^3(l_1+\frac{1}{2})}{k_0^2 2^{l_1}}\int_{u_1}^{u_2}e^{-x}x^{l_1-2}[O_{k_2}(A_{k_1l_1}+xB_{k_1l_1})]^2dx \quad \text{for } l_1\neq 0, \tag{11b}$$

in which

$$A_{kl}=\frac{a}{p^{l+4}}+\frac{b(l+(3/2))}{p^{l+6}}; \quad B_{kl}=\frac{b}{2p^{l+6}}. \tag{12}$$

The integrals of (11) can be evaluated in terms of the exponential function and the exponential integral. The integration limits u_1 and u_2 depend on both k_1 and k_2 and are given by

$$u_1=\frac{(k_0-k_n)^2}{2p^2}, \quad u_2=\frac{(k_0+k_n)^2}{2p^2}. \tag{13}$$

k_n, the final momentum of the cathode electron, is given by conservation of energy as

$$k_n=(k_0^2-k_1^2-k_2^2-2W_K-2W_L)^{\frac{1}{2}} \tag{14}$$

in which W_K and W_L are the K and L ionization energies, respectively.

The calculation of the integrals O_k occurring in Eqs. (5) is by far the most important part of the work when the *relative* probability of double ionization is desired, since it is chiefly this factor which is responsible for the difference between the formulas for single ionization and for double ionization. In fact it can be shown that the relative probability can be roughly obtained from this quantity alone by integrating O_k^2 from $k=0$ to $k=$infinity. The other factors of (5) serve merely to give a variable weight to the various parts of this integration. O_k is to be contrasted with the integral $I_{kl}(q)$ in that it involves the L wave function of the atom while the latter involves the K wave function. For an actual atom the L wave function differs much more from a hydrogen-like wave function than does the K wave function. This means that although we may use hydrogen-like wave functions in connection with $I_{kl}(q)$, we cannot do so with O_k. The result of doing so depends in so sensitive a way on the effective nuclear charge and screening constant of the hydrogen-like functions that it seems best to use Hartree wave functions even in an approximate theory. The functions S_{k0} and S_2 of Eq. (6) were obtained by numerical solution of Hartree's equation, and then the integral O_k was obtained by numerical integration. This was carried out for the case of KL_{I} ionization of potassium. S_2 is just the $2s$ wave function as tabulated by Hartree, and the functions S_{k0} are positive-energy solutions of Hartree's equation for a potassium atom which has been ionized in the K and L_{I} shells. The results were checked by means of the identity

$$\int_0^\infty S_{k0}S_2dr=\frac{1}{W_{k0}-W_0}\int_0^\infty S_{k0}\delta V S_2dr \tag{15}$$

in which δV is the difference of the potential

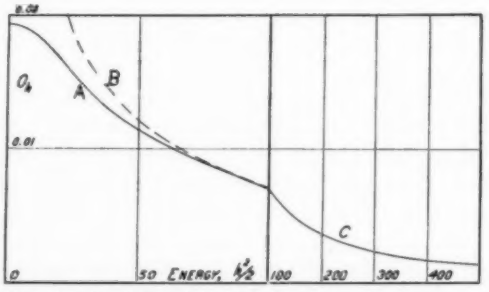

FIG. 1. The integral O_k for potassium. Curve A, computed by means of Hartree wave functions; curves B and C, computed by means of screened hydrogen-like wave functions. The energy is given in atomic units.

[7] It is described in complete detail in the writer's M.I.T. Doctor's thesis, 1935.

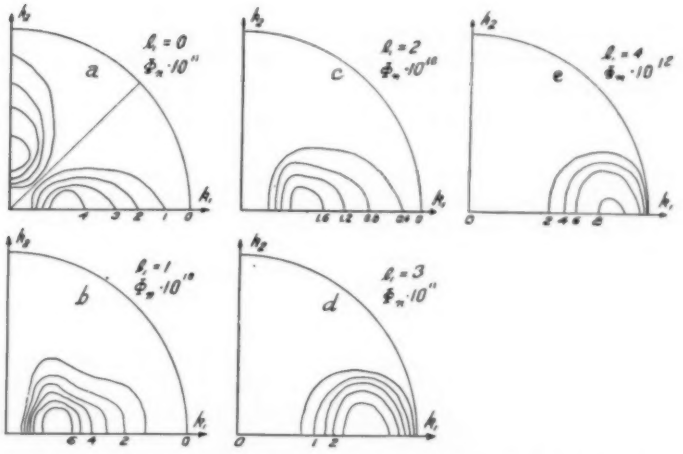

FIG. 2. Altitude charts of the partial cross section Φ_n, as a function of k_1 and k_2 for various values of l_1. Φ_n is zero along the k_2 axis and the circumference of the sector in charts b, c, d, and e, and along the 45° line and the circumference in chart a. Along the various curves it has the value indicated at the bottoms of the charts, multiplied by the proper power of 10.

functions for the normal and for the K-ionized atoms, W_0 is the energy parameter (a negative number) for the $2s$ wave function, and W_{k0} is the energy parameter (a positive number) for the function S_{k0}. For large values of k, or of energy, the numerical solution of Hartree's equation becomes increasingly difficult because of the rapid oscillations of the function S_{k0}, and a resort is had to hydrogen-like functions. For this purpose we use a screened Coulomb field of the type (10), choosing the constants V_0 and Z so as to fit the Hartree field near the L shell.[8] δV, which is the potential of a K electron in the atom, we take equal to $-\theta/r$, where θ is a constant, not far from unity, to be chosen by fitting the results onto the more accurate calculations of O_k with Hartree functions in the range of k for which both methods can be used. The results are shown in Fig. 1. In order to obtain a smooth joining of the two methods of calculation in the range $k^2/2$ equal to about 70 to 100 atomic units, it was necessary to take $\theta=0.65$.

The results of the calculation with Eqs. (5) are shown in Fig. 2, consisting of altitude charts of the partial cross section Φ_n as a function of k_1 and k_2, for various values of l_1. It is seen that the most important contribution to the total cross section will come from $l_1=1$, and for rather small values of the kinetic energy of the expelled electrons. The incident energy of the cathode electron was taken for the calculations to be five times the K ionization energy of potassium, or 665 atomic units. This value was chosen to make possible comparison with the experimental work of Mrs. Pearsall, who used a tube voltage of five times the K excitation voltage.

The functions of Fig. 2 were integrated in polar coordinates over the 90° circle sectors, by using Simpson's rule, integrating first with respect to the angular coordinate, and then with respect to the radial coordinate. The results are added together to give a total double ionization cross section of 1.12×10^{-7} atomic unit, or 0.29 percent of the K cross section as determined by the same method. The analogous calculation for the $KL_{II,\,III}$ cross section was not actually carried out, but the result can be easily estimated, and is slightly less, per electron, than the KL_I cross section. If we remember that there are two[9] L_I electrons and six $L_{II,\,III}$ electrons in

[8] This gives $Z=13.1$, $V_0=10.2$, $r_0=1.28$; atomic units.

[9] Strictly speaking the two L_I electrons must be treated differently. We have tacitly assumed that the L_I electron has the same direction of spin as the K electron. For the other L_I electron this is not true and the exchange effect which we found for $l_1=0$ will be missing. However, since the contribution of $l_1=0$ to the total cross section is small, the two L_I electrons have practically the same chance of being expelled.

the atom, we conclude that the number of KL ionized atoms of the target is about 2.0 percent of the number of K ionized atoms. This number can be directly compared with experiments on the relative intensity of satellites after discussing the transition probabilities.

The intensity of a given line is proportional to the number of atoms of the x-ray target in the initial state and to the transition probability for the given line. It is with the former quantity that this paper deals primarily, but the transition probabilities must of course also be considered. The way in which they enter in can best be understood by considering the following example:

Parent lines $(1s)\ {}^2S_{1/2}\rightarrow(2p)\ {}^2P_{3/2,\ 1/2}$
Satellites $(1s2s)\ {}^1S_0\ {}^3S_1\rightarrow(2p2s)\ {}^1P_1\ {}^3P_{012}$.

The electron configurations represent electrons missing from completed shells. There are two parent lines (the $K\alpha$ doublet) and six satellites (including intercombination lines) allowed by the selection rules. The transition probability for a line is given by a constant numerical factor times the cube of the frequency times the squared modulus of the matrix element of the electric moment. These matrix elements are rather complicated, since the wave functions for the initial and final states are linear combinations of determinants of one-electron functions. But the available experimental data deal with the integrated intensity of the whole satellite structure, and it is possible to show that the sum of the satellite intensities for transitions $(1s2s)$ to $(2p2s)$ is in the same ratio to the sum of the parent line intensities as the total number of atoms in the initial configuration $(1s2s)$ to the total number in $(1s)$. In other words the presence or absence of the $2s$ electron does not affect the total probability that a $2p$ electron will drop into a vacancy in the $1s$ shell. This neglects the variation of the frequency-cubed factor from line to line and assumes that the one-electron wave functions for the $1s$ and $2p$ electrons are the same in the configurations $(1s)$ and $(2p)$ as in the configurations $(1s2s)$ and $(2p2s)$.

The general case of this theorem or sum-rule will now be stated, and is true to the same degree of approximation as the special case discussed above. A and B are the initial and final configurations for the parent lines. The configuration AC differs from A only in the addition or omission of certain electrons and the configuration BC differs from B only in the addition or omission of the same electrons. We consider those satellite lines which are due to transitions from AC to BC.

Parent lines $A\rightarrow B$
Satellites $AC\rightarrow BC$.

If the total number of atoms of the target in states of configuration A is the same as the total number of atoms of the target in states of AC, then the sum of the intensities of the parents is equal to the sum of the intensities of the satellites.

The final theoretical prediction which we make is then that if all the satellites of $K\alpha$ are due to KL ionization, the integrated intensity of the satellites of $K\alpha$ should be 2.0 percent of the sum of the intensities of $K\alpha_1$ and $K\alpha_2$, when the tube voltage is five times the K excitation voltage. Strictly speaking this assumes a thin target, but we hope that the correction for the use of a thick target will not be very great; and we compare our result with the experimental result of Mrs. Pearsall,[10] who found a relative intensity of 3.0 percent, for all of the satellites of $K\alpha$ of potassium taken together and referred to the total intensity of the parent doublet $K\alpha$. The agreement is not as good as we might wish, but would seem to show conclusively that some, at least, of the satellites are produced by single transitions in KL ionized atoms. There is reason to believe that the Born approximation should give a slightly low result in this case, and some of the satellites may be due to other double and multiple ionizations such as KL^2, KM, etc., so that it seems not impossible that all the satellites are in this case to be explained by the single jump theory.

Having obtained the absolute value of the relative intensity, for one element, we can easily extend our results to neighboring elements by observing that according to our equations the result should vary roughly as the inverse cube of the effective nuclear charge near the L shell. This would be exactly the case if we used hydrogen-like wave functions throughout, and neglected external screening, thus setting $V_0=0$

[10] Anna W. Pearsall, Phys. Rev. **48**, 133 (1935).

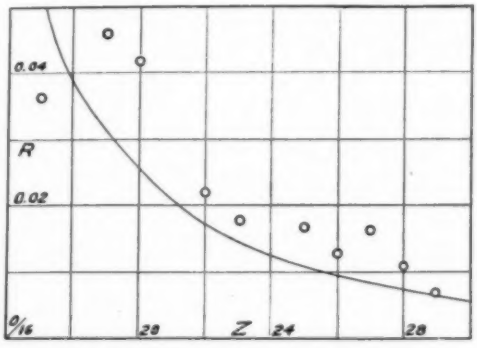

FIG. 3. The relative intensity of the $K\alpha$ satellites as a function of atomic number Z. R = integrated intensity of the satellites divided by the intensity of $K\alpha_1$. The circles are the experimental data of Mrs. Pearsall,[10] and the solid line gives the theoretical curve.

for both the K and L shells, and if we assumed a constant ratio between the effective nuclear charges near the K shell and near the L shell. In Fig. 3, therefore, we have compared the experimental values of relative intensity with the function $C/(Z-\sigma)^3$, in which σ is an internal screening constant which is practically independent of atomic number, and C is determined by our computation for potassium. The screening constant σ has the value 19−13 or 6 for potassium according to our method of determining it by fitting the Hartree potential to a screened Coulomb potential near the L shell. Other ways of estimating this screening constant give a somewhat lower value. Slater's value,[11] as determined by fitting actual wave functions, is 3. We have compromised, and taken $\sigma=4.5$. The agreement between the experimental points and the theoretical curve is seen to be quite satisfactory, although the theory gives consistently slightly low values.

We can derive from our equations a greatly simplified formula for the relative probability of double ionization in one limiting case, and by means of this simplification show the connection between our theory and a formula which has already been used by Bloch (p. 192) for rough calculation of double ionization probabilities. If we were to compute the cross section for removing electron number one alone by the method followed in this paper for the double ionization, we should arrive at equations very similar to (11a) and (11b), but differing from those in the following respects: the exchange effect for $l_1=0$ is of course missing; the integral O_k is missing throughout; and the integration limits u_1 and u_2 are slightly different, due to a difference in Eq. (14). The limiting case we consider is that in which one of the electrons to be removed lies much deeper in the atom than does the other. In this case we need consider only a limited range of values of k_2—a range limited by the condition that $k_2^2/2$ must be of the order of magnitude of the ionization energy of the outer electron, and therefore by hypothesis small compared to the ionization energy of the inner electron. This limitation of the range of k_2 comes from the nature of the function O_k of Fig. 1. This quantity involves the wave function S_2 of the outer electron in the normal atom, and has the property that it rapidly approaches zero as the energy $k_2^2/2$ is made large compared to the ionization energy of this outer electron. When the range of k_2 is limited in this way, the *only* difference between (11b) and the corresponding equation for single ionization is the presence of the factor $O_{k_2}^2$, so that after integrating over all possible final states in each case, we get

$$\frac{\text{double ionization cross section}}{\text{single ionization cross section}} = \int_0^\infty O_k^2 dk. \quad (16)$$

In order to get this result we have to consider Eq. (11a) a little further, because of the exchange effect which is present for the double ionization but not for the single ionization and which leads to cross product terms in the integrand of (11a) for double ionization but not for single ionization. However both $A_{k_1 0}$ and $B_{k_1 0}$ are practically zero for small values of k_1, and therefore the cross product terms are negligible in our limiting case, and Eq. (16) is established. In the case of KL ionization Eq. (16) gives a value which is about 25 percent too high as judged by our more exact calculation, but for KM and KN ionizations, etc., it should be much better.

The functions ψ_{k00} of (6) form a part of a complete orthogonal set. If we summed O_k^2 over all the members of this set, we should have, by a theorem in the theory of orthogonal functions,

[11] J. C. Slater, "Analytic Atomic Wave Functions," Phys. Rev. **42**, 33 (1932).

just $\int|\varphi_2|^2 d\tau$ or unity. The integral in k of (16) is a summation of O_k^2 over some of these functions, and therefore equal to unity minus the summation over the rest of the functions, which are just the ones occupied by electrons in the atom, so that

$$\frac{\text{double ionization cross section}}{\text{single ionization cross section}} = 1 - \left|\int \psi_2^* \varphi_2 d\tau\right|^2 - \sum_{n,\,l,\,m} \left|\int \psi_{nlm}^* \varphi_2 d\tau\right|^2 \quad (17)$$

in which the summation is to be extended over all the electrons of the atom except electrons numbers 1 and 2 themselves. This formula, with the summation missing, is the one which was used by Bloch in his "order of magnitude" calculations connected with the double-jump theory of satellites. The summation would probably be quite important in quantitative work.

The author wishes to express his gratitude to Professor Philip M. Morse of Massachusetts Institute of Technology for much helpful guidance and many valuable suggestions received from him during the course of this investigation.

Note added in proof: Dr. L. G. Parratt of Cornell University has kindly sent the writer some unpublished data of his on the relative intensities of the satellites of $K\alpha$. These were taken with a two-crystal spectrometer and an ionization chamber. They are more accurate than the data of Mrs. Pearsall, and cover a wider range of atomic numbers. When plotted on the graph of Fig. 3, the points so determined are somewhat closer to the theoretical curve, but still slightly above it. However, Parratt's experiments are so much better than my theory, that a more detailed comparison at this time is not worth while.

Since the manuscript was submitted for publication, the writer has had the privilege of discussing the subject on several occasions with Professor J. R. Oppenheimer. Professor Oppenheimer suggests that the interaction of the two *expelled* electrons may be of more importance than one might perhaps think at first. This interaction was of course entirely neglected in the theory, since Hartree wave functions were used for the doubly ionized state of the atom. This point cannot be quantitatively investigated until further calculations are made.

JANUARY 1, 1936 PHYSICAL REVIEW VOLUME 49

An Apparent Failure of the Photon Theory of Scattering

ROBERT S. SHANKLAND, *Ryerson Physical Laboratory, The University of Chicago*

(Received November 1, 1935)

A test has been made of the photon theory of the scattering of high frequency radiation. The pairs of scattered photons and recoil electrons predicted by this theory have been looked for by means of specially designed Geiger-Müller counters. Coincident discharges in the electron and photon counters were recorded by means of a vacuum tube amplifying and adding circuit. The scatterers used were air, aluminum, beryllium, filter paper and paraffin. The radiation was the gamma-rays from radium C. Experiments were performed with the counters set at various angles, some where the photon theory predicts coincidences, and others where coincidences should not be expected. The experiments uniformly gave fewer coincidences in the correct positions than were expected, and those observed could in every case be accounted for as chance coincidences due to the finite resolving time of the apparatus. It has not been found possible to bring the results of these experiments into accord with the photon theory of scattering. The wave-mechanical theory of the scattering process has not yet been extended to include the gamma-ray region so that it is impossible to compare this theory with the present experiments. Unless it is shown that the two theories disagree in the gamma-ray region it does not seem possible to reconcile the present experiment with the Bothe-Geiger and Compton-Simon experiments.

INTRODUCTION

THE discovery of the change in wave-length of x-rays when scattered by loosely bound electrons led A. H. Compton[1] to develop a photon theory based on the concept of light quanta to account for this phenomenon. This theory accounted for the interaction between radiation and matter by picturing the process as a mechanical collision between a light corpuscle and an electron which obeyed the laws of conservation of energy and momentum. At about the same time a virtual radiation theory was

[1] A. H. Compton, Phys. Rev. **21**, 483 (1923).

proposed by Bohr, Kramers and Slater.[2] This theory also accounted for the change in wavelength of the scattered radiation, and for the production of recoil electrons, which had been predicted by the photon theory and observed in the cloud expansion experiments of C. T. R. Wilson[3] and W. Bothe.[4]

It was evident, however, that the photon theory predicted four other phenomena, at that time unobserved, which the virtual radiation theory did not require. First, the recoil electron should appear at the same instant of time that the photon of radiation was scattered. Second, there should be a definite angular relationship between the direction in which the recoil electron is ejected and the direction in which the scattered photon travels away. Third, the momentum vectors of the incident photon, the scattered photon, and the recoil electron should be coplanar. Fourth, as a corollary of the second and third points, the momenta of the recoil electrons should be statistically distributed in magnitude and direction according to the angular distribution of the scattered photons.

More recently Wentzel[5] has discussed the problem by the methods of wave mechanics and obtained results for the ordinary x-ray region that agree in general with the older photon theory, but with a less definite physical picture of the scattering process. According to this theory there is a high probability that the scattered photon and the recoil electron will travel in the directions required by the photon theory so that both energy and momentum will be conserved. For an initially free electron this probability approaches unity in agreement with the older theory. The wave-mechanical theory does not require exact time coincidence between the appearance of the scattered photon and recoil electron since the motion of these corpuscles is determined by probability laws. However, the probable value of the time difference would be so small that it could hardly be experimentally detected.

The diverse predictions of these theories can only be cleared up by an appeal to experiment.

[2] N. Bohr, H. A. Kramers and J. C. Slater, Phil. Mag. **47**, 785 (1924).
[3] C. T. R. Wilson, Proc. Roy. Soc. **A104**, 1 (1923).
[4] W. Bothe, Zeits. f. Physik **16**, 319 (1923).
[5] G. Wentzel, Zeits. f. Physik **43**, 1 (1927).

Previous Experiments

Experiments designed to test the predictions of the theories were soon reported. The angular distribution of the recoil electrons was definitely established as being in statistical agreement with the photon theory by the cloud expansion experiments of Compton and Simon.[6] Further experiments by these investigators were carried out to determine whether the predictions of this theory were realized in the individual scattering events as well.[7] Within the rather large experimental uncertainties inherent in this type of experiment there was apparently an exact individual relationship between the angles as required by the photon theory.

At about the same time Bothe and Geiger[8] performed an experiment which was designed to determine if the recoil electron and scattered photon appear simultaneously. The primary radiation was supplied by an x-ray tube operated at 70 kv. Hydrogen was used to scatter the radiation, and point counters to record the coincidences. Under normal operating conditions with this apparatus the recoil electron counter discharged at the rate of about 400 times per minute, while the photon counter discharged about twice per minute. About one recoil electron counter discharge in 2000 was coincident with a photon counter discharge to an accuracy of about 1/1000 sec. These coincidences were not exact, for the discharge in one counter always seemed to lag behind that in the other to a measurable degree; but Bothe and Geiger concluded that this lag was not due to inductive effects between the counters, and calculated by probability theory that there was only one chance in 400,000 that the number of coincidences observed could be due to chance.

While this experiment was in progress, a similar experiment was undertaken at the University of Chicago by Bennett.[9] His apparatus consisted of a vacuum drum in which two Geiger point counters were mounted on spectrometer

[6] A. H. Compton and A. W. Simon, Phys. Rev. **25**, 309 (1925); also F. Kirchner, Ann. d. Physik **83**, 969 (1927).
[7] A. H. Compton and A. W. Simon, Phys. Rev. **26**, 289 (1925).
[8] W. Bothe and H. Geiger, Zeits. f. Physik **32**, 639 (1925).
[9] R. D. Bennett, Ph.D. Dissertation, University of Chicago (1925).

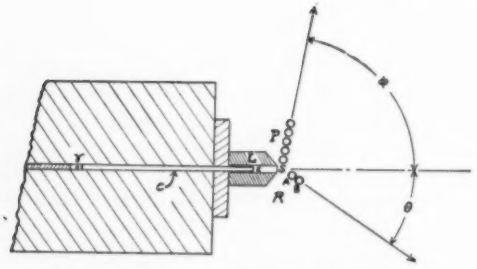

FIG. 1. Schematic arrangement of apparatus.

arms so that they could be set at the angles to the incident beam required by the photon theory. One counter was designed to record recoil electrons and the other to detect scattered photons. The primary radiation was supplied by an x-ray tube operated at 180 kv and was filtered through 7 mm of brass. In some of Bennett's experiments the scatterer was a thin piece of oiled paper or mica; in others it was air at atmospheric pressure. Because, as in the Bothe-Geiger experiment, there appeared to be a time lag in the action of the point counters so that the "coincidences" observed were not exact, the results of these experiments did not give a conclusive answer to the question.

A similar experiment was performed at the University of Chicago by J. A. Bearden. In this experiment the recoil electron counter was first placed in a position R_a where coincidences should have been observed according to the photon theory, and then in a second position R_b where coincidences should not have been observed. The position of the photon counter P was unchanged. The results were: "In position R_a there were 71 counts in P and 31,000 in R with only 8 coincidences. In position R_b there were 112 counts in P and 42,400 in R with 9 coincidences. Thus there were just as many coincidences in the wrong position according to the theory as in the correct position."[10]

The chief difficulties in these experiments are the time lag in the action of point counters and the fact that the recoil electrons produced by x-rays do not have as much energy as is desirable. The present experiment is an attempt to give a more definite answer to the question of the mechanism of scattering. To obtain recoil electrons of greater energy than in the experiments previously described, gamma-rays from radium C were used as the primary radiation. As an additional improvement specially designed Geiger-Müller counters were used to record the recoil electrons and scattered photons.

[10] Letter to A. H. Compton, July, 1935. In this letter Bearden reports also a repetition of these experiments with findings which confirm the earlier negative results and also those found in the present experiment.

DESCRIPTION OF THE EXPERIMENT

The general arrangement of the apparatus used in this experiment is shown in Fig. 1.

The source of gamma-rays (radon tube) was placed at γ and the beam of radiation which fell upon the scatterer at S was collimated by the system of lead shields shown. The Geiger-Müller counters at P and R were further protected from direct and scattered radiation by additional lead shields and lead shot which, for simplicity, have been omitted from the figure. To prevent the rays scattered from the end of the collimating tube at E from passing through the counters at P and R the lead cylinder L was used in the position shown. The arrangement was such that all parts of L were in the geometrical shadow of the bundle of rays collimated by the cylindrical hole C, thus to a large degree eliminating unwanted scattering.

The fraction F of the gamma-rays emitted by the radon tube which will strike the scatterer at S is determined by the solid angle subtended at γ by the scatterer. In the apparatus shown in Fig. 1 the distance γE is 28 cm and the diameter of the hole C is 0.80 cm. Therefore, $F = 5.13 \times 10^{-5}$. The fraction of the incident beam of gamma-rays scattered to the photon counters at P will be determined by several factors: the effective volume of the scatterer, the scattering coefficient for the radiation used, the distribution in angle of the scattered radiation, and the solid angle subtended by the counters. This fraction has been calculated for each of the experiments performed and used in computing the expected number of coincidences given in Tables I and II below. A photon scattered into the counter at R will record itself only when it ejects a secondary electron into the electric field of the counter. Since the absorption by the gas in the counter will be negligible, these secondary electrons must come from the walls of the counter cylinder. The

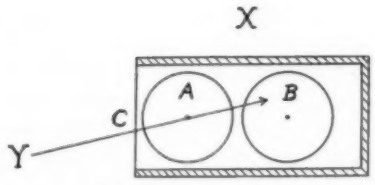

FIG. 2. β-ray counter.

cylinders used for the photon counters were gold tubes 3 cm long, 1 cm inside diameter, and of wall thickness $\frac{1}{2}$ mm. The reason for selecting gold as the material for constructing these counter cylinders was the following: The gamma-ray may be absorbed by the scattering process with the production of a recoil electron, or a photo-electron may be ejected when the whole quantum is absorbed. The number of recoil electrons that escape from the walls into the interior of the counter will increase only slowly with atomic number, because the increased scattering by elements of higher atomic number will be nearly canceled by their increased stopping power for beta-particles. On the other hand the absorption by the photoelectric process increases very markedly with atomic number. For elements of atomic number as high as that of lead or gold the photoelectric absorption for gamma-rays will be very important. Except for lead, which is slightly radioactive, the most convenient metal of high atomic number to use is gold. To further increase the chance of recording the photons, five of these gold counters were placed in a line and electrically connected so that if the photon were absorbed in any one of the five the discharge would be effective in contributing to a possible coincidence with a discharge in the recoil electron counter. The efficiency E of the photon counter can be determined by experiment by observing the discharge rate of the counter when a known number of gamma-ray quanta are passing through it in unit time. It was found that the chance of a photon's being absorbed was about one in 125, giving a value of $E=8\times10^{-3}$. The photon counters used in these experiments were filled with dry air at a pressure of 10.5 cm of mercury and were operated at about 1400 volts. Various experimenters have shown that the entire inside diameter of the counter is effective but that an end correction must be applied to allow for the decreased intensity of the electric field at the ends of the cylinder. Experiment proved that the effective volume of the cylinder was 0.92 of the geometrical volume.

According to the photon theory, with each photon scattered in the angular range $\phi\pm\Delta\phi$, a recoil electron should be ejected with the initial direction in the range $\theta\pm\Delta\theta$. The recoil electron counter was set at the mean value of θ in this range. In estimating the number of associated recoil electrons which will enter the recoil electron counter it is necessary to take account of the fact that the primary beam of gamma-rays is inhomogeneous and that the recoil electrons will be scattered by the matter between their point of origin and the recoil electron counter. These effects were taken into consideration in the computations which give the expected number of coincidences recorded in the tables below.

The problem of designing a counter to record the recoil electrons is very different from that discussed above for the photon counters. Here it is necessary to make the walls, etc., so thin that the beta-particles will be able to enter the counter easily. The final type of counter developed for this work is illustrated by Fig. 2.

The cylinders A and B are made of thin Al foil ($t=0.0007$ cm) supported upon a skeleton brass tube. The beta-rays entered the counter through a thin cellophane window C ($t=0.0017$ cm). The effective cross section of this counter was 3.2 $\times$0.9 sq. cm. This counter was used in two ways. First, counter A alone was used in such a way that coincidences were recorded when a recoil electron discharged counter A and at the same instant a scattered photon discharged any one of the gold counters P. This arrangement gave the data recorded below under the heading of Double Coincidence Experiments. In the second method, coincidences were recorded when a recoil electron passed through both A and B, discharging both, and at the same time a photon discharged one of the counters at P. The data from this type of experiment are listed below as Triple Coincidence Experiments. The principal advantage of the latter arrangement over the former is that it records a much smaller number of chance counts. These chance coincidences are due to the finite resolving time τ of the adding circuit of the vacuum tube amplifier. In addition to recoil

electrons entering the counters A and B, there will come from the scatterer gamma-radiation which will eject secondary electrons from the walls of the counter. These discharges will not contribute to true coincidences but will be effective in producing a certain number of false or chance coincidences. For the double and triple arrangements the number of these chance coincidences will be respectively:

$$D=2\tau N_A N_P, \quad (1)$$

$$T=2\tau(N_{AB}N_P+N_{AP}N_B+N_{BP}N_A) +3\tau^2 N_A N_B N_P. \quad (2)$$

Here N_A, N_B and N_P are the individual counting rates in counters A, B and P, respectively. N_{AB} is the number of true coincidences between counters A and B etc.; while τ is the resolving time, which was determined for the circuit used, to be $\tau=4.4\times10^{-6}$ min. The chance coincidences listed in column four of the tables were computed by these formulae.

Test experiments were performed to show that this double counter functioned properly by comparing the number of coincident discharges in A and B with the single counting rates of A or B. When this was done with a source of beta-rays at Y, the double discharges were found to be a large fraction of the single rates—showing that the beta-particles were actually passing through both counters. However, when a source of gamma-rays was placed at X, the coincidences were much fewer than the single discharge rates in either counter. The actual number of coincidences was found to agree with the prediction of Eq. (1) as would be anticipated because in this case only chance coincidences should be possible.

Tests were made to show that the counters and circuits as described were functioning properly and would record coincidences of the kind sought for in this experiment. These tests were performed by arranging the counters A, B and P in a vertical plane so that they could be used to record the passage of cosmic-ray particles. It was found that the number of triple coincidences observed agreed well with the number to be expected from the experiments of Hsiung[11] and others, showing that the counters and circuit were functioning properly. Another experiment similar to that described by Street and Woodward[12] was performed to determine the efficiency of the counters and circuits in recording coincidences when the single counting rates were approximately the same as in the main experiment. This test experiment showed the efficiency of both the photon counters and the electron counters for fast ionizing particles was about 85 percent and that the circuit was working properly to record coincidences.

[11] D. S. Hsiung, Phys. Rev. **46**, 653 (1934).

Experimental Results

The results of the present series of experiments are given in Tables I and II. The first column of these tables lists the scatterer and the second column the strength in millicuries of the radon tube used as a source of gamma-rays. In the third column are recorded the azimuths of the recoil electron counter measured from the direction of the incident beam of radiation. The

Table I. *Triple coincidence experiments.*

Scatterer	Source (mc)	θ	Chance Triples (hr.$^{-1}$)	Observed Triples (hr.$^{-1}$)	Expected Triples (hr.$^{-1}$)
Air	135	35°	0.4	0.0±0.5	13
Al t 0.0015 cm	140	35°	1.7	2.4±0.5	23
Al t 0.004	124	35°	4.9	4.7±1.5	48
Paraffin t 0.05	138	35°	9	14 ±3	69
Paraffin t 0.05	129	j35°	9	12 ±4	9
Be t 0.02	133	35°	8	9.5±2	48
Be t 0.02	131	j35°	8	9.5±2	8

Table II. *Double coincidence experiments.*

Scatterer	Source (mc)	θ	Chance Doubles (min.$^{-1}$)	Observed Doubles (min.$^{-1}$)	Expected Doubles (min.$^{-1}$)
Air	105	35°	0.67	0.92±0.07	0.89
Air	102	j35°	0.67	0.87±0.08	0.67
Filter paper t 0.015 cm	195	25°	2.5	1.9 ±0.18	5.7
"	191	−25°	2.5	2.2 ±0.28	2.5
Paraffin t 0.05	97	35°	1.5	1.8 ±0.09	2.8
"	94	j35°	1.5	1.8 ±0.17	1.5
"	95	35°	4.5	5.6 ±0.15	9.9
"	93	j35°	4.5	6.0 ±0.8	4.5
"	81	Hor	0.94	0.85±0.11	2.4

[12] J. C. Street and R. H. Woodward, Phys. Rev. **46**, 1029 (1934).

angles given without a symbol before them indicate that the counter was set at the angle required by the photon theory. A negative sign before the value of θ means that the counter was set on the same side of the incident beam as the photon counter; in which position, of course, no coincidences should be expected. When the symbol j is before the value of the angle, it signifies that the recoil electron counter was rotated about the primary beam as an axis into a position 90° from the plane containing the incident beam and the centers of the photon counters. The photon theory predicts no coincidences in this position because momentum could not be conserved. Column four gives the chance coincidences calculated from Eqs. (1) and (2) and the individual discharge rates of the several counters. Column five gives the observed coincidence rates together with the probable error. For each experiment a calculation was made of the number of coincidences to be expected from the photon theory, with the strength of the source, counter efficiency and geometrical arrangement known. This number added to the chance rate is given in the last column of each table and should be the number of coincidences per unit time which should be expected if the photon theory is correct. The experiment summarized in the last row of Table II was performed with all counters in the horizontal plane. This was to minimize the effect of the inhomogeneity of the incident rays by permitting a wide range of values of both ϕ and θ to be effective.

An examination of the tables will reveal the following facts: The number of coincidences observed are always fewer than predicted by the photon theory, and in fact agree rather well in each case with the number of chance coincidences to be expected. Further, when the recoil electron counter is set in the position $-\theta$ or $j\theta$ the number of coincidences observed is as great as in the correct position θ. This strengthens the view that all the observed coincidences are due only to chance and that the predictions of the photon theory are not verified by this experiment. Thus the present series of experiments, in common with the experiments of Bennett and of Bearden discussed above, yields results contrary to those obtained by Bothe and Geiger and by Compton and Simon. It seems difficult to understand how the present experiment could have failed to show the coincidences if they were real; but all the experiments performed by the writer have uniformly yielded a negative result.

The predictions of the photon theory should apparently apply to the scattering of gamma-rays studied in the present experiments. However, the wave-mechanical theory as developed by Wentzel contains approximations which limit its strict validity to the ordinary x-ray region, for which $h\nu \ll mc^2$. The further development of this theory to include gamma-ray scattering may give a less definite angular relationship than the photon theory predicts. Coincidences would be much more difficult to observe if the angular relationship is not valid because of the much smaller chance of capturing the scattered quantum. There is thus a possibility that the results of the present experiment will not be inconsistent with those of Bothe and Geiger and of Compton and Simon. In any event, the photon theory in its present form does not agree with the experiments reported here.

This experiment was suggested to the writer by Professor Arthur H. Compton and its completion has been possible because of his generosity and stimulating advice. It is also a pleasure to acknowledge the helpful criticism and discussion given by Professor Ralph D. Bennett of Massachusetts Institute of Technology; Professor J. A. Bearden of Johns Hopkins University; Professor W. Bothe of the Kaiser Wilhelm-Institut, Heidelberg; and Professor H. Geiger of the University of Tübingen.

Effects of Chemical Binding on the X-Ray $K\alpha_{1,2}$ Doublet Lines of Sulphur Studied with a Two-Crystal Spectrometer

LYMAN G. PARRATT,* *Cornell University*

(Received October 12, 1935)

Ionization curves of the $K\alpha_{1,2}$ doublet lines of sulphur have been recorded with the two-crystal spectrometer. Several sulphides and sulphates were used as targets. The effects of the chemical binding on the wave-length, on the $\alpha_1 \rightarrow \alpha_2$ separation and on the doublet contour were measured. With suitably chosen targets, the wave-length shift of the S $K\alpha_{1,2}$ lines from sulphates to sulphides was observed in the process of shifting.

SINCE first noticed in 1924 the effects of chemical binding on x-ray emission spectra have attracted the attention of numerous investigators.[1] Four of these effects have been studied: (1) The wave-length shift of the emission lines of light elements;[2, 3, 4, 5] (2) the different relative intensities;[6] (3) the possibly new lines with certain compounds;[6] and (4) the change in the line contours, particularly in the line widths at half-maximum intensity.[6, 7, 8] All of these effects have been investigated with the vacuum spectrograph by using the photographic method. The uncertainties in the photographic method of measuring intensities, especially of intensity distributions in wave-length (line contours), are well known and quantitative measurements require the ionization method and the high resolving power of the two-crystal spectrometer.[8] The present paper reports observations on the contour shape and the wave-length shift of the $K\alpha_{1,2}$ lines of sulphur with a two-crystal spectrometer.[9] With suitably chosen targets, the wave-length shift can be observed in the process of shifting.

Targets of several sulphur compounds were used. FeS, Cu_2S, $MgSO_4$ and $BaSO_4$, in powdered form, were pounded onto a roughened copper or aluminum water-cooled target. PbS was soft-soldered to copper. With the x-ray tube at low power, 10 kv and 10 to 15 ma, with the focal-spot about 2 mm in diameter, these targets operated satisfactorily, although, were the power increased, the powder substance would either change chemically or disappear from the target surface. FeS, by far the best target, would dissipate about 700 watts. The making of satisfactory targets for ionization recordings of intensities is a different problem than is the case for photographic measurements—the emitted intensity must remain constant (within 1 or 2 percent) throughout the time required to record a complete curve, about 30 minutes in the present work. Several sulphur compounds in addition to the ones mentioned above were tried but were found to be unsatisfactory.

In Fig. 1 are plotted the ionization curves of the S $K\alpha_{1,2}$ doublet lines with different targets—compounds and mixtures of compounds. These various targets are described in the caption to the figure. There can be no doubt that under the stress of the electron bombardment the sulphates decompose or react chemically, either by simple reduction or with the target material or both, and yield the spectra characteristic of the sulphides. In a sense these curves may be interpretated as x-ray pictures of the chemical reaction, each curve giving a quantitative measure, in fractions of the total number of molecules, of the extent of the reaction. The wave-length shift is clearly shown and differences in the widths of the lines and in the overlapping factor[10] are also evident. It so happens that the

* National Research Fellow.

[1] See Lindh, *Handbuch der Experimentalphysik* (1930), XXIV, part 2, pp. 314–325.

[2] Lundquist, Zeits. f. Physik **60**, 642 (1930); **77**, 778 (1932); **89**, 273 (1934).

[3] Faessler, Zeits. f. Physik **72**, 734 (1931).

[4] Svensson, Zeits. f. Physik **75**, 120 (1932).

[5] Valasek, Phys. Rev. **43**, 612 (1933); **47**, 896 (1935).

[6] Deodhar, Proc. Roy. Soc. **A131**, 647 (1931).

[7] Siegbahn and Magnusson, Zeits. f. Physik **96**, 1 (1935).

[8] Parratt, Phys. Rev. **45**, 364 (1934); Wilhelmy, Zeits. f. Physik **97**, 312 (1935).

[9] This instrument has been described in previous reports, Phys. Rev. **41**, 553 (1932); Rev. Sci. Inst. **5**, 395 (1934).

[10] This factor, a measure of the degree of overlapping of the two $K\alpha$ components, is defined as twice the ratio of the minimum ordinate between the lines to the maximum ordinate of the α_1 line. See Allison, Phys. Rev. **44**, 63 (1933); Parratt, Phys. Rev. **44**, 695 (1933).

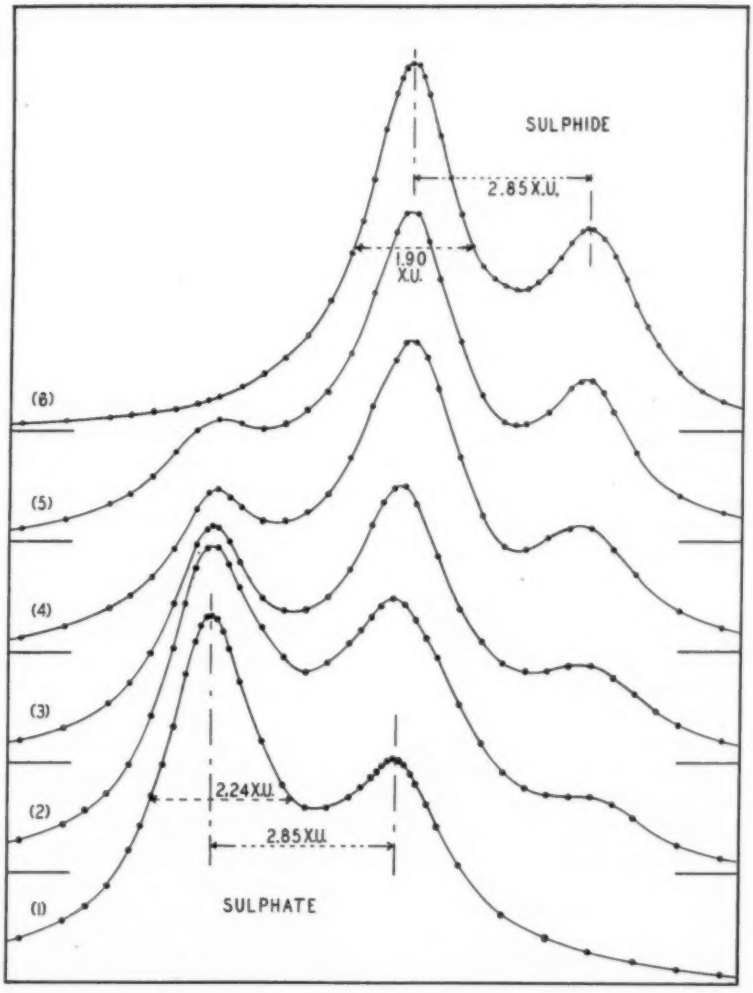

FIG. 1. Ionization curves of the S $K\alpha_{1,2}$ doublet lines. All six curves are plotted on the same abscissae scale. The targets used in recording these curves are:

Curve (1)—$BaSO_4$ on Al. The curve was recorded as soon as possible after applying the voltage to the tube, 8 kv and 8 ma.

Curve (2)—Same target as with curve (1) after the tube had been operating at 16 kv and 15 ma for two hours. After this "seasoning" the tube power was reduced to 10 kv and 15 ma and the curve recorded.

Curve (3)—$MgSO_4$ on Al. The curve was taken at 10 kv and 15 ma after the tube had been operating one hour at 15 kv and 15 ma.

Curve (4)—$MgSO_4$ on Cu. The curve was taken at 10 kv and 15 ma after the tube had been operating one hour at 15 kv and 15 ma.

Curve (5)—$MgSO_4$ on Cu. This target was the same as with curve (4) after three additional hours of operation at 15 kv and 25 ma. The curve was taken at 12 kv and 15 ma.

Curve (6)—Cu_2S on Cu. Taken at 10 kv and 10 ma. The target of curve (5) after 10 hours additional operation at 15 kv and 20 ma yielded a curve identical with curve (6) within the experimental error. Evidently after being subjected to the electron bombardment with the attending heat of the focal spot the $MgSO_4$ goes, with sufficient time, completely over to the sulphide, either Cu_2S or MgS or both.

Although an effort was made to record the intermediate curves in a minimum of time it is no doubt true that the chemical change was going on at the time of the recordings and the curves obtained do not represent truly static stages of the process.

wave-length of the α_2 line of the sulphates is in near coincidence, though not quite, with the wave-length of the α_1 line of the sulphides: There are actually four lines in the intermediate curves of the figure instead of the obvious three.

Measurements were made on the wave-length shifts, the wave-length interval $\alpha_1 \rightarrow \alpha_2$, the line widths at half-maximum intensity, and on the overlapping factors. Free sulphur was not used as a target so the wave-length shifts are referred to the position of the peak of the α_1 line of FeS. These data are given in Table I. The estimated maximum error in these measurements is indicated in the table.

A test with the FeS target showed no variations in the shape of the doublet contour as the tube voltage or current was altered. The voltage range in this test was 5 to 30 kv. This confirms and extends the results of similar tests by many investigators in the shorter wave-length regions.

TABLE I. *Measurements of the S $K\alpha_{1,2}$ doublet lines (5.36A) from various sulphur compounds as determined with the two-crystal spectrometer in the (1,+1) position.*
(The width data are not corrected for overlapping of the α_2 line.)

Target	Full Width of α_1			Separation $\alpha_1 \rightarrow \alpha_2$		Shift of α_1 Max. Ordinate (X.U.)	Overlapping Factor
	(sec.)	(X.U.)	"true"	(sec.)	(X.U.)		
FeS on Cu	275±5	1.88	1.63	416±3	2.85	0	0.77
Cu_2S on Cu	280±5	1.91	1.67	416±3	2.85	0.27±0.03	0.78
PbS	278±5	1.90	1.65	412±4	2.82	—	0.79
PbS*	144±3	2.30	(2.13)*	182±3	2.81	—	0.91
$MgSO_4$ on Cu after 12 hours of operation	282±7	1.93	1.68	415±3	2.84	0.27±0.03	0.78
$MgSO_4$ on Al taken as soon as possible with low power	326±10	2.24	1.99	415±4	2.84	3.28±0.04	0.93
$BaSO_4$ on Al taken as soon as possible with low power	327±6	2.24	1.99	416±4	2.85	3.28±0.04	0.91

* These data with PbS were recorded with quartz crystals, (10·0) planes, ground and etched. These quartz crystals, compared with calcites, have considerably less effective resolving power at this wave-length (5.36A) as determined from the (1,+1) width measurements; however, the (1,−1) width of the quartz specimens at this wave-length is less than the corresponding width with the calcites. The shape of the (1,−1) curve with quartz crystals is markedly different from the shape of the same curve with calcites. See Rev. Sci. Inst. 6, 113 (1935) and 5, 395 (1934). The relative effective resolving powers of these quartz and calcite crystals are in agreement with the discussion in Rev. Sci. Inst. 6, 387 (1935). It should also be pointed out that, in view of the great difference in the (1,−1) shapes with two types of crystals, the correction Eq. (1) will not apply to the width measurements with quartz—rather the correction should be greater than this equation gives. Furthermore, as pointed out in the last reference, the validity of the correction in the case of calcite is somewhat doubtful at this wave-length.

All the data in the present report, except those with the PbS target, were taken with calcite crystals A_4 B_4 which have been studied in other reports, Parratt, Rev. Sci. Inst. 6, 387 (1935) and Parratt and Miller, Phys. Rev. in press (1936).

The observed contours have not been resolved into the α_1 and α_2 components—the uncertainty of how this resolution should be made (due to our lack of knowledge of the true shapes of the individual lines) is too great to warrant the attempt at the present time. Hence, width measurements of the α_2 line and of the degrees of asymmetry of the lines are not given. The "true" widths of the α_1 line are obtained by applying to the observed widths the empirical correction for the finite resolving power of the crystals of the spectrometer as discussed in another article.[11] This correction is

$$W_T = W_0 - 2.9 W_C^{1.7}, \qquad (1)$$

where W_T is the true width, W_0 is the observed (1,+1) width and W_C is the observed width when the crystals are in the (1,−1) position. All the widths in Eq. (1) must be expressed in X.U. The (1,−1) width with calcites is 0.437 X.U. and with the quartz crystals is 0.353 X.U.

The measurements of the wave-length intervals are in good agreement with those obtained photographically. The photographic measurements, however, vary among themselves considerably. The $\alpha_1 \rightarrow \alpha_2$ separation of FeS, for example, is reported as 2.81 X.U. by Faessler[3] and 3.07 X.U. by Valasek[5]; and of $BaSO_4$ as about 2.84 X.U. by Faessler[3] and 3.00 X.U. by Lundquist.[2] The shift of the α_1 line, referred to FeS, of Cu_2S is given by Lundquist[2] as 0.05 X.U. and by Valasek[5] as 0.34 X.U.; of $BaSO_4$ by Lundquist[2] as 3.04 X.U. and by Faessler[3] as about 3.65 X.U. Such variations in the photographic measurements are not surprising when one considers the large widths of these doublet lines and the lack of resolution. Because of the higher resolving power of the two-crystal instrument and because of the greater accuracy of the ionization method in recording the intensity distributions in wave-length, the present measurements are more reliable.

The author is indebted to the University of Chicago for the loan of the double spectrometer with which these data were obtained.

[11] Parratt, Rev. Sci. Inst. 6, 387 (1935).

Theory of the Effect of Temperature on the Reflection of X-Rays by Crystals

I. Isotropic Crystals

CLARENCE ZENER AND G. E. M. JAUNCEY,* *Wayman Crow Hall of Physics, Washington University, St. Louis*

(Received October 16, 1935)

A short derivation of the Debye-Waller temperature factor in the reflection of x-rays from isotropic crystals is given. This short derivation clearly brings out the assumptions involved and paves the way for the extension of the theory to the more complex case of anisotropic crystals. One of the authors will give this extension in a subsequent paper.

1. INTRODUCTION

IN the reflection of x-rays from crystals and in the scattering of x-rays from gases, we meet two forms of the atomic structure factor. If we represent the structure factor relative to a lattice point in a crystal by F and that relative to the center of the atom by f, the relation between F and f is

$$F=fH, \tag{1}$$

where H is the temperature factor. This is given by

$$H=\int_{-\infty}^{\infty} p(z)\cos\left(\frac{4\pi z\sin\theta}{\lambda}\right)dz, \tag{2}$$

where $p(z)$ is the layer distribution function relative to a crystal plane of the atoms associated with that plane (the plane of x and y), the axis of z bisects the angle between the forward direction of the reflected rays and the backward direction of the primary rays, and θ is the glancing angle of incidence of the x-rays on the reflecting plane. The temperature factor is usually written in the form

$$H=e^{-M}. \tag{3}$$

The function M has been derived for isotropic solids by Debye.[1] Later, Waller[2] showed that Debye's formula for M should be multiplied by a factor of two. In this paper a new derivation is given. The authors believe that this third derivation is justified on two grounds. Firstly, the two previous derivations have been so lengthy, and the approximations so obscure, that it is difficult to see just what physical assumptions have been made. Secondly, one of the authors is communicating a paper in which the method of the present paper is extended to the derivation of M for anisotropic crystals. It is desirable to separate the case of isotropy from the more complex case of anisotropy.

2. THE LAYER DISTRIBUTION FUNCTION

We assume the displacements of the atoms from their equilibrium positions to be so small that the potential energy of the lattice is a quadratic function of the coordinates of the atoms. The actual displacement of a given atom from its lattice point is then given by the vector sum of the displacements arising from the various normal modes of vibration of the crystal. In particular, the component of the displacement of an atom along any axis, say along the z axis, is equal to the algebraic sum of the components of the displacements due to the vibrational modes. Since the probability of a displacement between z and $z+dz$ due to one vibrational mode is the same whether z is positive or negative, and since the displacements due to any two vibrational modes are independent, the calculation of the probability function $p(z)$ is identical with the calculation of the probability function for a net error which is due to a large number of independent errors,[3] or for the diffusion of Brownian particles from a plane.[4] The result is well known:

$$p(z)=\frac{1}{(2\pi\mu)^{\frac{1}{2}}}\cdot e^{-z^2/2\mu}, \tag{4}$$

* The authors were aided in part by a grant from the Rockefeller Foundation to Washington University for research in science.

[1] P. Debye, Ann. d. Physik **43**, 49 (1914).

[2] I. Waller, Zeits. f. Physik **51**, 213 (1923). A comprehensive list of references is given by Compton and Allison in *X-rays in Theory and in Experiment*, 435–436 (1935).

[3] See J. Rice, *Statistical Mechanics*, p. 10.

[4] A. Einstein, Ann. d. Physik **17**, 556 (1905).

where

$$\mu=\Sigma_s\mu_s. \tag{5}$$

Here μ_s is the mean square of the z component of the displacement due to the sth vibrational mode, and the summation is over all the vibrational modes of the crystal. Substitution of (4) into (2) gives

$$M=(8\pi^2\mu\sin^2\theta)/\lambda^2. \tag{6}$$

3. The Mean Square Displacement

In order to calculate μ, we must assume a definite model for the solid. We shall take that model introduced by Debye[5] in his theory of the specific heats of solids. The normal coordinates are taken to be the amplitudes of the vibrational modes which would be present if the solid were a continuous medium with the same gross elastic properties as the actual discontinuous solid. Since the number of normal coordinates must be $3n$, where n is the number of atoms in the solid under consideration, Debye found it necessary to exclude vibrational modes of a frequency greater than a certain maximum frequency, ν_m. It should be noted, however, that this method of obtaining the correct number of normal coordinates is not unique. In this paper we shall follow the procedure of Debye's theory of specific heats in excluding those vibrational modes with a frequency greater than ν_m.

The mean square μ is to be identified with the average square of the z component of the displacement vector $\mathbf{D}(\mathbf{r}, t)$ of the fictitious continuous medium. If we expand $\mathbf{D}$ into a Fourier series,

$$\mathbf{D}(\mathbf{r}, t)=2^{\frac{1}{2}}\sum\mathbf{a}_{j,\mathbf{k}}(t)\cos(\mathbf{k}\cdot\mathbf{r}+\delta_j),$$

and let $\gamma_{j,\mathbf{k}}$ be the cosine of the angle which $\mathbf{a}_{j,\mathbf{k}}$ makes with the z axis, then, in virtue of (5),

$$\mu=\sum\gamma^2_{j,\mathbf{k}}\cdot\overline{\mathbf{a}^2_{j,\mathbf{k}}}. \tag{7}$$

In the classical mechanics $\mathbf{a}_{j,\mathbf{k}}$ is a periodic function of time

$$\mathbf{a}_{j,\mathbf{k}}(t)=c_{j,\mathbf{k}}\cos(2\pi\nu t+\phi_{j,\mathbf{k}}),$$

the phases $\phi_{j,\mathbf{k}}$ being independent. In the quantum mechanics the $\mathbf{a}_{j,\mathbf{k}}$'s are independent dynamical variables. In both mechanics the average energy associated with $\mathbf{a}_{j,\mathbf{k}}$ is

$$\epsilon_{j,\mathbf{k}}=4\pi^2\nu^2M_0\overline{\mathbf{a}^2_{j,\mathbf{k}}}, \tag{8}$$

where ν is the classical frequency of $\mathbf{a}_{j,\mathbf{k}}$ and M_0 is the total mass of the solid. From the classical viewpoint this relation is obtained most readily by equating $\epsilon_{j,\mathbf{k}}$ to the kinetic energy $\frac{1}{2}M_0\dot{\mathbf{a}}^2_{j,\mathbf{k}}$ associated with $\mathbf{a}_{j,\mathbf{k}}$ at the instant when $\mathbf{a}_{j,\mathbf{k}}$ is zero. From the quantum viewpoint this relation is obtained via the virial theorem. By means of (8) and of the quantum formula

$$\epsilon_{j,\mathbf{k}}=\frac{h\nu}{\exp(h\nu/kT)-1}+h\nu/2 \tag{9}$$

($h\nu/2$ being the zero-point energy), we now transform (7) into

$$\mu=\frac{h}{4\pi^2M_0}\sum\gamma^2_{j,\mathbf{k}}\left\{\frac{1/\nu}{\exp(h\nu/kT)-1}+\frac{1}{2\nu}\right\}. \tag{10}$$

Eq. (10) is not restricted to isotropic crystals; it will in fact be used in a following paper on anisotropic crystals. Assuming isotropy, $\gamma^2_{j,\mathbf{k}}$ is replaced by its spatial average $\frac{1}{3}$, while, as in specific heat theory, the number of vibrational modes with frequencies between ν and $\nu+d\nu$ is $9n\nu_m^{-3}\nu^2d\nu$. Hence (10) may be replaced by an integral between the limits $\nu=0$ and $\nu=\nu_m$. Introducing the quantity $\xi=h\nu/kT$ and the characteristic temperature $\Theta=h\nu_m/k$, we obtain an expression for μ which when inserted in (6) gives the Waller formula

$$M=\frac{6h^2}{m_ak\Theta}\cdot\left\{\frac{\phi(\Theta/T)}{\Theta/T}+\frac{1}{4}\right\}\frac{\sin^2\theta}{\lambda^2}, \tag{11}$$

where $m_a=M_0/n$ is the mass of a crystal atom and

$$\phi(x)=\frac{1}{x}\int_0^x\frac{\xi}{e^\xi-1}d\xi, \tag{12}$$

the well-known Debye function.

[5] P. Debye, Ann. d. Physik **39**, 789 (1912).

Neutrons from the Disintegration of Deuterium by Deuterons

T. W. BONNER* AND W. M. BRUBAKER, *Kellogg Radiation Laboratory, California Institute of Technology*

(Received October 22, 1935)

The excitation functions for the emission of neutrons from the two reactions ${}_1H^2+{}_1H^2\rightarrow{}_2He^3+{}_0n^1$ and ${}_4Be^9+{}_1H^2\rightarrow{}_5B^{10}+{}_0n^1$ have been investigated in the energy range from 0.5 to 0.9 MEV. In this interval the yield of neutrons from a $H_3{}^2PO_4$ target increases nearly linearly with the bombarding energy while the yield from a Be target increases nearly exponentially. At 0.9 MEV three times as many neutrons were observed from the Be target as from the $H_3{}^2PO_4$ target. At the lower voltage of 0.5 MEV only 1/3 as many neutrons came from the Be as from the $H_3{}^2PO_4$. The neutrons from deuterium were found to be nearly homogeneous in energy with a maximum of 2.55 MEV when they are observed at right angles to the direction of the incident 0.5 MEV deuterons. The energy of the disintegration is 3.21 ± 0.13 MEV.

THE emission of neutrons in large numbers from the bombardment of deuterium by deuterons was first reported by Oliphant, Harteck and Rutherford.[1] They attributed the neutrons to the reaction:

$$ {}_1H^2+{}_1H^2\rightarrow{}_2He^3+{}_0n^1. \qquad (1)$$

They reported an equivalent yield of one neutron per 10^6 deuterons incident on a pure deuterium target at 0.1 MEV. This means an actual yield of about 1 in 10^7 from targets such as can be used conveniently ($H_3{}^2PO_4$, $(NH_4{}^2)_2SO_4$, $NH_4{}^2Cl$). This yield from deuterium at 0.1 MEV is comparable to the yield from a Be target at 0.8 MEV as reported by Crane, Lauritsen and Soltan.[2] However previous experiments in this laboratory as well as those at Berkeley[3] indicated that at high voltages the yield of neutrons from the beryllium reaction

$$ {}_4Be^9+{}_1H^2\rightarrow{}_5B^{10}+{}_0n^1 \qquad (2)$$

was considerably greater than that from deuterium. In the present experiment we have compared the yield of neutrons from targets of $H_3{}^2PO_4$ and Be when bombarded by deuterons of energies between 0.5 MEV and 0.9 MEV.

Oliphant, Harteck and Rutherford[1] have used a helium-filled ionization chamber connected to an amplifier and oscillograph to measure the maximum energy of the neutrons from deuterium. From the maximum oscillograph deflection they have estimated that the neutrons have a maximum energy of 2.2 MEV. From the ranges of 30 recoil-helium tracks in a cloud chamber Dee[4] has inferred that the neutrons are homogeneous and have an energy of 1.8 MEV. In the present experiment we have determined the energy distribution of the neutrons more accurately by observing a large number of recoil protons in a cloud chamber.

Excitation Curves

We have compared the excitation functions for the emission of neutrons from Be and $H_3{}^2PO_4$ targets by counting the number of recoil protons photographed in a cloud chamber. We placed the methane-filled cloud chamber close to the target so that a large number of recoil protons could be observed. All observed tracks were counted, regardless of their orientation. When the voltage was increased from 0.5 MEV to 0.9 MEV the average number of tracks per expansion increased from 2.7 to 42 with the Be target, and from 7.1 to 13.4 with the $H_3{}^2PO_4$ target. These data have been reduced to an absolute yield and plotted as shown in Fig. 1. From 1000 to 2000 tracks were counted to determine each point on the curve. The relative yields are much more accurate than the absolute ones; the latter may be in error by as much as a factor of 5 or possibly 10. The curve shows that the yield of neutrons is greater from an $H_3{}^2PO_4$ target for voltages less than 0.68 MEV, but that for higher voltages the yield from Be is greater. Since the hydrogen in the $H_3{}^2PO_4$ molecule is

* National Research Fellow.

[1] Oliphant, Harteck and Rutherford, Proc. Roy. Soc. **A144**, 692 (1934).

[2] Crane, Lauritsen and Soltan, Phys. Rev. **45**, 507 (1935).

[3] McMillan and Livingston, Phys. Rev. **47**, 452 (1935).

[4] P. I. Dee, Proc. Roy. Soc. **A148**, 623 (1935).

responsible for 1/8 of the molecular stopping power, one should multiply the experimental yield by 8 to get the yield from a pure deuterium target.

The Be excitation curve agrees quite well with the one obtained by Crane, Lauritsen and Soltan[2] who used a paraffin-lined ionization chamber to detect the neutrons. The curve is roughly exponential, doubling every 0.1 MEV. The deuterium excitation curve rises only 75 percent in the interval between 0.5 and 0.9 MEV. Since the height of the potential barrier for deuterons on deuterons is only about 0.1 MEV, this increase cannot be due to a greater probability of penetrating the potential barrier but to the increased range of the deuterons in the target. The range of a 0.9 MEV deuteron is approximately 90 percent greater than that of a 0.5 MEV deuteron, so the agreement is fairly good.

The yield from beryllium as compared to that from deuterium at 0.2 MEV can be found by extrapolating the curves down to this energy. This gives the ratio of the number of neutrons from Be to the number from H_3PO_4 as approximately 1/20. Thus it is apparent that, at potentials of the order of 0.2 MEV, deuterium contamination on targets may be responsible for an appreciable portion of the observed neutrons.

Energy Distribution of the Neutrons

In previous papers[5] we described our method of determining neutron energies by measuring the lengths of recoil proton tracks in a high pressure cloud chamber filled with methane. In the present experiment the procedure has been the same except that a pressure of only 2.70 atmospheres was used in the chamber. At this pressure the tracks of the highest energy recoil protons had a length of approximately 4.5 cm. From the stopping power of the gas[6] in the chamber and the range-velocity curve, we have computed the energy of the recoil protons.[7]

[5] Bonner and Brubaker, Phys. Rev. **47**, 910 (1935); Rev. Sci. Inst. **6**, 143 (1935); Phys. Rev. **48**, 742 (1935).

[6] The gas in the chamber was 85.1 percent CH_4, 13.5 percent C_2H_6, and 1.4 percent N_2. The corresponding stopping powers were 0.86 for methane, 1.52 for ethane, and 0.98 for nitrogen.

[7] G. Mano, J. de phys. et rad. **5**, 628 (1934).

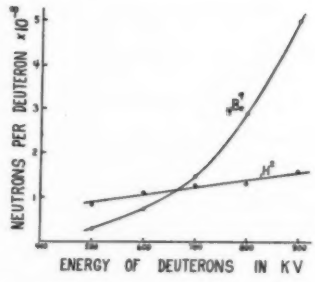

Fig. 1. The yield of neutrons from Be and $H_3{}^2PO_4$ targets when bombarded by deuterons.

Two series of runs were made. In the first we measured only those proton tracks which made angles of less than 8° with the forward direction (for neutrons which came directly from the source). The bombarding potential in this series of runs was 0.5 MEV. Under these conditions we photographed approximately 1200 recoil protons, 110 of which met our requirements for measurement. The energy distribution of these protons is given in the lower curve of Fig. 2. This curve indicates that the neutrons are nearly homogeneous in energy with a maximum of 2.55±0.10 MEV. We do not believe that the long tail on the low energy side of the maximum necessarily means that neutrons of this energy come from the source; it is at least partly due to scattered neutrons which made large angle collisions with protons and projected them in a direction such that they were measured.

The second set of data was obtained from photographs which had been taken in the excita-

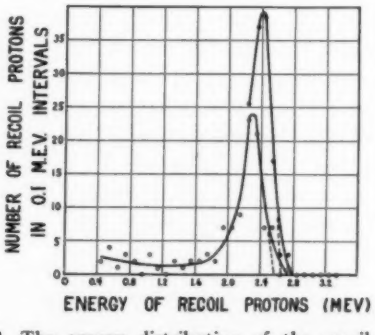

Fig. 2. The energy distribution of the recoil protons projected in the forward direction.

tion curve experiments. In this series of runs the chamber was so close to the target that the direction of the neutrons was not well defined. For this reason we could not investigate the entire energy distribution, but by measuring the long tracks we were able to get an independent value of the maximum energy of the neutrons. The distribution of the high energy protons so measured is given in the upper curve of Fig. 2.

Discussion of Results

When the neutrons are observed at right angles to the direction of the incident deuterons the energy of the neutrons is given by:

$$E_n = \tfrac{3}{4}Q + \tfrac{1}{4}E_d,$$

where E_n is the neutron energy, Q the energy released in the disintegration, and E_d is the energy of the deuteron.

When our bombarding potential was 0.5 MEV, a maximum of 0.125 MEV of this energy appeared in the kinetic energy of the neutrons emitted at right angles. Because we used a thick target and alternating current, disintegrations were effected by deuterons of all energies below the maximum. This gave the neutrons an energy spread of 0.125 MEV, with Q constant. A few neutrons which were emitted in a direction parallel to that of the incident deuteron beam made elastic collisions with little loss of energy in the 3 mm of brass which is directly below the target and so may have been scattered into the chamber. Such neutrons received a maximum of 0.9 MEV more energy than those emitted at right angles and so may have been responsible for a few tracks with energies greater than 2.55 MEV.

The maximum energy of the neutrons as obtained from the first series of runs is 2.55 $\pm$0.10 MEV, and from the second series is 2.62$\pm$0.10 MEV. The corresponding Q's are 3.23$\pm$0.13 and 3.19$\pm$0.13 MEV. Dee and Gilbert[8] have obtained the energy of the short range $_2He^3$ particles which are produced in the same disintegration and from this energy have calculated that Q is 2.8$\pm$0.2 MEV.

From the energy released in this disintegration, one can calculate the mass of $_2He^3$. Using the values Q=3.2 MEV, $_1H^2$=2.0142, and $_0n^1$ =1.0086, we obtain 3.0164 for the mass of $_2He^3$. This is smaller than the value 3.0172 calculated by Oliphant, Kempton and Rutherford[9] from the disintegration of lithium by protons:

$$_3Li^6 + {}_1H^1 \rightarrow {}_2He^4 + {}_2He^3.$$

It is not clear whether the disagreement is to be attributed to experimental errors or to the fact that the other masses involved in the calculation are not well enough known.

In conclusion, we wish to thank Professor C. C. Lauritsen for valuable suggestions and the Seeley W. Mudd Fund for financial support.

Note added in proof: In view of the discrepancy in the two calculated masses of He^3 and the disagreement in the He^4/H^2 ratio as determined by Bainbridge and by Aston by means of the mass spectrograph, it seems advisable to calculate the mass of the deuteron from disintegration data. The ratio He^4/H^2 can be found by solving the first four of the following equations for the mass of the deuteron

$$_1H^2 + {}_1H^2 = {}_2He^3 + {}_0n^1 + 3.21 \pm 0.13 \text{ MEV.}$$
$$_3Li^6 + {}_1H^1 = {}_2He^4 + {}_2He^3 + 3.6 \pm 0.1 \text{ MEV.}^9$$
$$_3Li^6 + {}_1H^2 = 2\,{}_2He^4 + 22.06 \pm 0.07 \text{ MEV.}^{10}$$
$$_1H^2 + h\nu = {}_1H^1 + {}_0n^1 - 2.26 \pm 0.08 \text{ MEV.}^{11}$$
$$_3Li^6 + {}_0n^1 = {}_2He^4 + {}_1H^3 + 4.6 \pm 0.2 \text{ MEV.}^{12}$$
$$_1H^2 + {}_1H^2 = {}_1H^3 + {}_1H^1 + 3.97 \pm 0.02 \text{ MEV.}^{10}$$

We get the relation $_1H^2 = \frac{1}{3}(He^4 + 23.93 \pm 0.20$ MEV). This relation toegther with a standard He^4 mass of 4.00336 gives a mass of the deuteron equal to 2.01458$\pm$0.00010; this value is considerably higher than Bainbridge's value 2.01423. A check on this mass of the deuteron is obtained by solving the last four of the equations for the mass of the deuteron. Here we get the relation $_1H^2 = \frac{1}{3}(He^4 + 23.69$ ± 0.23 MEV) or a mass of 2.01440$\pm$0.00012 which is also higher than 2.01423. From these two results we get a mean disintegration mass of 2.01449$\pm$0.00009 which is nearly the same as Aston's value 2.01443 when referred to the He=4.00336 scale; with such a deuteron mass the discrepancy in the two calculated masses of $_2He^3$ disappears.

If this mass of the deuteron proves to be more nearly correct than the old mass, then the masses of the other elements will be affected by such a change. If we use Bainbridge's mass spectrograph ratio of He^4/H^1 we can calculate the masses of the other elements appearing in the above set of reactions. The best values obtained are:

$_0n^1 = 1.00885 \pm 0.00010$	$_1H^3 = 3.01664 \pm 0.00010$
$_1H^1 = 1.00807 \pm 0.00002$ (mass spectrograph)	$_2He^3 = 3.01674 \pm 0.00014$
	$_2He^4 = 4.00336$ (standard)
$_1H^2 = 2.01449 \pm 0.00009$	$_3Li^6 = 6.01593 \pm 0.00011.$

[8] Dee and Gilbert, Proc. Roy. Soc. **A149**, 200 (1935).

[9] Oliphant, Kempton and Rutherford, Proc. Roy. Soc. **A150**, 241 (1935).

[10] Oliphant, Kempton and Rutherford, Proc. Roy. Soc. **A149**, 406 (1935).

[11] N. Feather, Nature **136**, 468 (1935).

[12] Chadwick and Goldhaber, Nature **135**, 65 (1935); Taylor and Goldhaber, Nature **135**, 341 (1935).

The Excitation Function of Lithium Under Proton Bombardment

M. OSTROFSKY, G. BREIT, *University of Wisconsin*
AND
D. P. JOHNSON, *Institute for Advanced Study, Princeton, New Jersey*

(Received October 18, 1935)

The yield of alpha-particles in the bombardment of lithium with protons is calculated for different depths and widths of the "potential well." It is found that agreement with experiment can be obtained either by using the part of the incident wave having an angular momentum $L=0$ or the part having $L=1$. For the first condition with a radius of 0.35×10^{-12} cm one needs a "potential well" about 35 MEV deep. For $L=1$ and the same radius a "well" about 21.5 MEV is needed. The latter depth fits in nicely with approximate estimates of this depth from nuclear binding energies. The calculations are made more carefully than is customary in the usual type of potential barrier penetration consideration. It is found that this is necessary and that even the order of magnitude of the collision cross section requires the more accurate type of calculation. The influence of the depth and width of the "potential well" is found to be pronounced and it is found possible to vary the shape of the excitation curve as well as the absolute value of the cross section by changing the depth and width of the "well." For energies sufficient to allow the proton to slip over the potential barrier classically, the collision cross section may increase or decrease with the energy depending on the "well." Thus the saturation of the yield with the voltage is not a good measure of the height of the barrier and of the nuclear radius. The position of stationary and resonance levels is found to be important for the shape of the excitation curve. The effect of the decay of the incident wave inside the nucleus is estimated and is found to be small in the present case. The asymptotic form of the dependence of the collision cross section on velocity at low velocities is const.$\times v^{-2}\exp\{-2\pi ZZ'e/\text{“}137\text{”}v\}$ within the limitations of the present theory. Estimates of the theoretically expected variation of the yield with velocity are made for Li^7+H^2 and compared with the experiments of Oliphant, Kinsey and Rutherford. A correspondence between different nuclear reactions is established by means of which one can use calculations for one reaction to obtain yields for another reaction with a corresponding "potential well." The "potential well" necessary for the quantitative representation of the alpha-particle reaction is compared with the mass of Be^8. It is found possible to fit both requirements by attributing the alpha-particle reaction to $L=0$ and the formation of Be^8 from Li^7 to the addition of a proton into a p level.

THE disintegration of lithium into two alpha-particles under proton bombardment was observed by Cockcroft and Walton[1] and the data were later extended to higher energies by Henderson.[2] Recently careful measurements of yields in thick as well as thin targets were made by Herb, Parkinson and Kerst.[3] According to these recent observations the yield of protons in thin targets increases steadily up to 400 kv. Measurements made up to 1000 kv by Hafstad and Tuve[4] show that here also the yield increases with the voltage. In this respect the data of Herb, Parkinson and Kerst as well as that of Hafstad and Tuve contradicts the observations of Henderson. In terms of the usual theoretical interpretation the results indicate that the potential barrier is not reached below 1000 kv.

It is tempting to connect these results with Goldhaber's discussion[5] of the relative improbability of this reaction because according to him the reaction can be reasonably attributed to incident protons having an orbital angular momentum $L=1$ (in units $\hbar$) and because the barrier for $L=1$ is appreciably higher than that for $L=0$. It is also of interest to know to what extent collision processes due to incident particles having $L=1$ are less probable than collision processes due to incident particles having $L=0$ and colliding "head on" with the bombarded nucleus. It is supposed by Goldhaber that the $L=0$ part of the incident wave is much more likely to produce a disintegration than the $L=1$ part and it would be very nice and simple if one could always use this point of view.

The probability of nuclear reactions is usually discussed[6] in terms of the following factors: (a) The probability that the bombarding particle

[1] J. D. Cockcroft and E. T. S. Walton, Proc. Roy. Soc. **A137**, 229 (1932).
[2] M. C. Henderson, Phys. Rev. **43**, 98 (1933).
[3] R. G. Herb, D. B. Parkinson and D. W. Kerst, Phys. Rev. **48**, 118 (1935).
[4] L. R. Hafstad and M. A. Tuve, Phys. Rev. **48**, 306 (1935). We are indebted to the authors for informing us of their results before publication.
[5] M. Goldhaber, Proc. Camb. Phil. Soc. **30**, 561 (1934).
[6] J. D. Cockcroft, International Conference on Physics, London (1934).

should perform a nuclear collision (this probability is usually computed by assigning to the process a collision cross section of the order of the square of the wave-length of the incident particles); (b) the probability that, once a collision within the area of the collision cross section takes place, the particle penetrates through the potential barrier; (c) the chance that once the particle penetrates through the barrier, a disintegration takes place. In terms of this description of the process one would expect the $L=0$ part of the incident wave to be more effective than the part represented by $L=1$ and one would further expect the process to reach saturation once the incident particles have an energy higher than the top of the barrier.

The incident particles must be supposed in many cases to be subjected to an attractive field of force when they are inside the bombarded nucleus because, for example, in the bombardment of Li by protons the final product of two alpha-particles is produced as a result of the binding of the incident proton into a H^3 combination in the Li^7 nucleus. The influence of the attractive forces can be treated schematically by means of a "well" in the potential. The influence of such a "well" is not taken care of by the usual description of the collision process. It is desirable to have a discussion in which this influence is taken into account. In order to do so we discuss below the same problem from a different point of view which is more closely related to a straightforward solution.

It is supposed in the calculations presented here that the incident particles can be treated as a wave incident on the bombarded nucleus. As usual the density of the particles can be represented by the square of the absolute value of the wave function ψ. The total chance of finding the particle inside the bombarded nucleus is $\int|\psi|^2 d\tau$ and can be calculated for any assumed form of the potential energy. The number of disintegrations per second is assumed to be $P\int|\psi|^2 d\tau$ where P is a constant characteristic of the colliding particles and of the end products of the reaction. The constant P may be described as the chance per second that a disintegration should take place when the incident particle is in the bombarded nucleus. Its order of magnitude may be roughly estimated as the relative velocity of the disintegration products divided by the nuclear radius and multiplied by the transparency of the potential barrier for the disintegration products. This point of view is closely related to the discussion in Chapter IV, §2 of Gamow's book.[7] One can justify it by a more general discussion in which the nucleus and the colliding particle are considered as a many-body problem.[8]

The essential limitations on the method from the point of view of the general wave equation for the composite parts of the nucleus are:

(a) It is sufficient to consider the wave function as represented by a sum of the functions representing the initial and final state.

(b) The wave functions representing the final state do not change appreciably with the velocity of the incident particles. This condition is satisfied if the energy liberated in the reaction is large compared to the incident energy and may be expected to be satisfied for $Li^7+H^1\rightarrow He^4+He^4$. This condition is not satisfied even approximately if the disintegration products separate with an energy which corresponds to a resonance level for their mutual potential energy.[9] In such a case we may speak of *resonance to the disintegration products* and it is possible that the resonance observed for the γ-rays from Li under proton bombardment is of this type.[9] It would then be attributable to the formation of one normal and one excited α-particle. The maximum energy of the rays is according to Crane, Delsasso, Fowler and Lauritsen[9a] nearly equal to the energy available in the formation of the 8 cm α-particles. We may provisionally suppose with these authors that in the emission of γ-rays one of the particles is excited to a level about 16 MEV high and the kinetic energy of the two particles is therefore small. The smallness of the kinetic energy is favorable for sharp resonance. Estimates show that a kinetic energy of about 500 kv would correspond approximately to a half-value breadth of 80 kv and this half-value breadth is sensitive to the kinetic energy. It is also possible that an excited Be^8 nucleus is formed. It is thus not necessary to consider the resonance to γ-rays in connection with the yield of 8 cm α-particles because the process involved may be essentially different.

(c) The weighting of the function which represents the incident particle is not important. The point is that this function enters the expression for the collision cross section through the matrix element of the interaction energy. It is thus weighted through the nucleus by quantities which involve the interaction energy and the wave function of the final state. It is laborious to make calculations with

[7] G. Gamow, *Nuclear Structure and Radicactivity.*

[8] Appendix I. (Justification of method used from point of view of many body problem.)

[9] L. R. Hafstad and M. A. Tuve, Phys. Rev. **47**, 507 (1935).

[9a] Crane, Delsasso, Fowler and Lauritsen, Phys. Rev. **46**, 531 (1934); **47**, 410 (1935).

the matrix element and attempts to do so show that the results are sensitive to assumptions about the interaction energy as well as assumptions about the state and constitution of the bombarded nucleus and the final products. In the present state of relative ignorance about the state of the particles inside nuclei it was felt desirable to have calculations in which the weighting of the incident wave is neglected. By doing so, one introduces in P an arbitrary adjustable constant and loses definiteness of theoretical prediction, but one gains freedom from special assumptions about nuclear binding forces.

(d) It is assumed that one may neglect the absorption of incident particles due to the fact that they cause disintegrations.[10] This restriction would make the theory inapplicable if the nuclear diameter and P were large. The incident wave would then decay approximately exponentially inside the nucleus and calculations neglecting the effect of such a decay would be invalid. It is complicated to try to fit experimental material by taking this effect into account in all of the calculations. It is simpler to first neglect the effect of absorption on the incident wave and to derive from comparison of theory and experiment a value of P. The calculations can then be repeated with this value of P and the experimental data fitted by successive approximations. This is the plan followed below and the corrections due to absorption are found to be negligible in the case considered.

In standard notation an incident plane wave

$$e^{ikz}=(\pi/2\rho)^{\frac{1}{2}}\sum_0^\infty(2L+1)i^L P_L(\cos\theta)J_{L+\frac{1}{2}}(\rho) \quad (1)$$

is modified by the Coulombian field of the nucleus into

$$\sum_0^\infty(2L+1)i^L P_L(F_L/\rho)e^{i\sigma_L}. \quad (2)$$

Here $k=\mu v/\hbar$ where μ = reduced mass, v = relative velocity; $\rho=kr$ with r = distance between colliding particles; P_L = Legendre polynomial of order L; $J_{L+\frac{1}{2}}$ = Bessel function of order $L+\frac{1}{2}$. The function F_L is the regular solution of

$$[d^2/d\rho^2+1-2\eta/\rho-L(L+1)/\rho^2]F_L=0, \quad (3)$$

where $\eta=1/ka$, $a=\hbar^2/\mu ZZ'e^2$, Ze, $Z'e$ are the charges on the particles and e is the electronic charge. The function F_L is normalized so as to be asymptotic for large ρ to a sine wave with unit amplitude. We also use G_L which is asymptotic to a cosine wave with unit amplitude. The constant σ_L depends on k but not on ρ and drops out in the present application. The nuclear well inside the nuclear radius r_0 modifies the function F_L into $\bar{F}_L$ which also satisfies (3) for $r>r_0$ and satisfies

$$[d^2/d\rho^2+1+2U/\mu v^2-L(L+1)/\rho^2]\bar{F}_L=0, \quad (3')$$

where U is the depth of the "well" for $r<r_0$.

$$\bar{F}_L=[F_L/(1-F_LG_L\delta_L-iF_L^2\delta_L)]_{r=r_0}u,$$
$$\delta_L=(F_L'/F_L-\bar{F}_L'/\bar{F}_L)_{r=r_0}, \quad (4)$$

where u is the regular solution of (3′) normalized so that $u(r_0)=1$. Replacing F_L by $\bar{F}_L$ in the expression (2), one can calculate the probability of disintegration on the assumptions already discussed. The effective collision cross section is then found to be

$$\sigma=(\Lambda^2/\pi v)P\sum_0^\infty(2L+1)\int_0^{r_0}\bar{F}_L^2dr \quad (5)$$

or

$$\sigma=\frac{4\pi Pr_0^2}{v}\sum_0^\infty\frac{(2L+1)(F_L^2/\rho^2)\overline{u_L^2}}{(1-F_LG_L\delta_L)^2+F_L^4\delta_L^2};$$
$$\overline{u_L^2}=\frac{1}{r_0}\int_0^{r_0}u_L^2dr. \quad (6)$$

In the last formula F_L, G_L are supposed to be taken at $r=r_0$. Formula (5) is reminiscent of the procedure used by Cockcroft. In it $\Lambda=\hbar/\mu v$ occurs in the combination Λ^2/π and one may treat this factor separately. The quantity $\bar{F}_L^2$ under the integral sign depends on the transparency of the barrier to the incident waves. It will be noted, however, that the integral in Eq. (5) brings in the nuclear radius r_0 so that in addition to the usual factors there is present a factor Pr_0/v which has the significance of the chance of a disintegration due to a sojourn of the proton during a time r_0/v in the nucleus. It is not present in the usual discussions and brings in an additional factor $1/v$ into the velocity dependence of σ. It should be also remembered

[10] The possible importance of this factor was emphasized by Fermi in a colloquium of the Ann Arbor 1935 summer school where some of the present results were discussed. We are very grateful to Professor Fermi for this and several other valuable discussions.

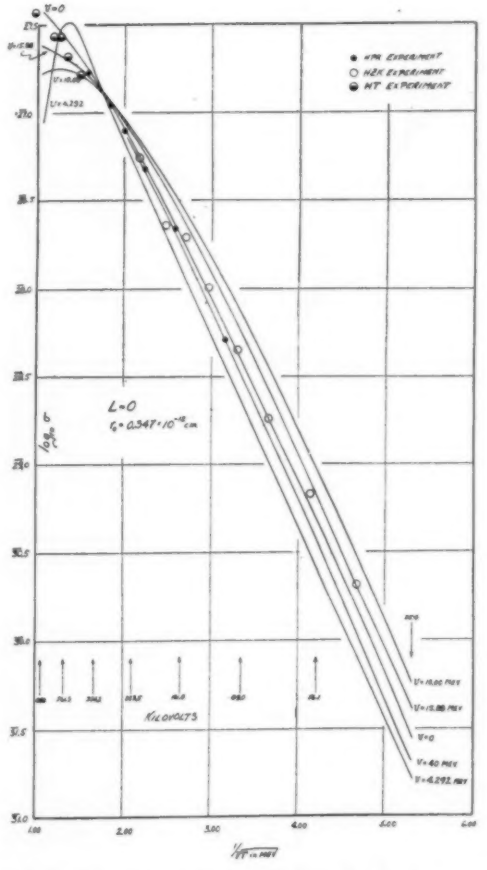

FIG. 1. $L=0$, $r_0=0.347\times10^{-12}$ cm, $U=0$, 4.292, 10.00, 15.88 MEV, $\rho/ak=0.316$.

that the integral in Eq. (5) is a function of the velocity quite apart from the penetrability of the barrier. Thus for $L=0$ and in the absence of a "nuclear well" one can approximate F_0 by $C_0\rho$, $C_0=[2\pi\eta/(-1+\exp 2\pi\eta)]^{\frac{1}{2}}$. The factor C_0 for large η [small energies] represents something like the penetrability of a one-dimensional barrier on account of the presence of $\exp(2\pi\eta)$. In addition C_0 contains $(2\pi\eta)^{\frac{1}{2}}$ which varies as v^{-1}. Finally ρ varies as v. The integral in Eq. (5) thus varies roughly as $v\exp(-2\pi\eta)$ and the cross section as $v^{-2}\exp(-2\pi\eta)$. This rough estimate thus leads to the type of velocity dependence used by Cockcroft. The reasons for the dependence are seen, however, to be different inasmuch as both the factors $(2\pi\eta)^{\frac{1}{2}}$ and $\rho/r=v$ are not usually considered. In this limiting case of small r_0 and "no well" one has approximately due to $L=0$

$$\sigma\leqq(4Pr_0/3v)\pi r_0^2(2\pi\eta)/[-1+\exp 2\pi\eta]. \quad (7)$$

This formula shows that there is not very much point in speaking of Λ^2 rather than r_0^2 determining the order of magnitude of the cross section.[11] The factor πr_0^2 present in (7) shows, as one would expect, that σ vanishes with r_0 which is not the case in the method used by Cockcroft. On the other hand, the velocity dependence is the same in the two methods to within the limitations of Eq. (7).

The nuclear radius and the wave-length of the protons inside a reasonable "potential well" are of the same order of magnitude and the approximation of Eq. (7) is very poor. In applications to experimental material it is found necessary to use Eq. (6). According to Goldhaber it is probable that nuclear reactions are due to at most a few values of L. The contributions due to different L are, therefore, treated separately and the discussion in Appendix I shows that the values of P which can be expected to correspond to different L from the point of view of the many-body problem are different. The contribution to σ due to an individual L is denoted below by σ_L.

The denominator of an individual term of the summation in Eq. (6) determines the proximity of resonance.[12] Thus for small energies $F^2\delta$ is small and there is a maximum in σ_L whenever $1-FG\delta=0$. The function $\bar{F}$ is in this case identical with G. For large energies $F^2\delta$ is of the same order of magnitude as $1-FG\delta$ and one has no sharp resonance under these conditions. Nevertheless the variation of σ_L with velocity may be strongly affected by having a blunt resonance at high energies. By arranging the "potential well" in this manner one can decrease the ratio of σ_L at low velocities to σ_L at high velocities without introducing a pronounced resonance peak. Again by properly arranging the depth and width of the potential well it is

[11] Cf. G. Breit, Phys. Rev. **34**, 817–818 (1929) for a very similar formula $\sigma=\pi r_0^2(2\pi\eta)/[-1+\exp(2\pi\eta)]$ which applies for small r_0 on supposition that the flux of particles through the nucleus determines the probability of disintegration. The difference of a factor v is due to the fact that at present the density is used instead of the flux.

[12] G. Breit and F. L. Yost, Phys. Rev. **48**, 203 (1935).

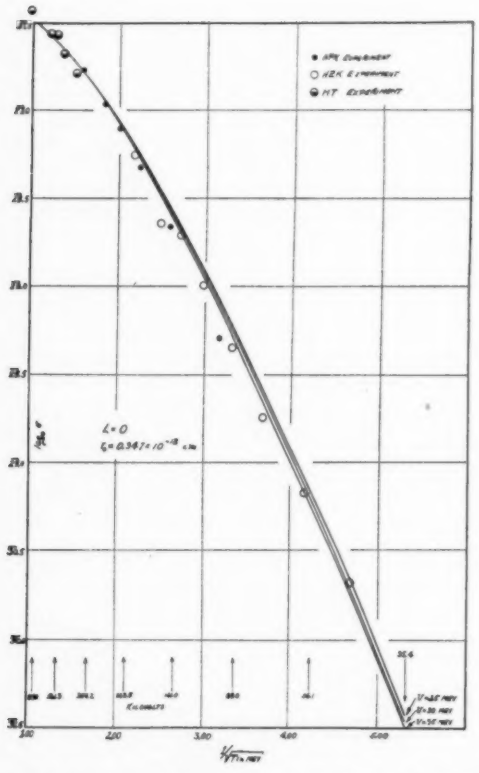

FIG. 2. $L=0$, $r_0=0.347\times10^{-12}$ cm, $U=25$, 30, 35 MEV, $\rho/ak=0.316$. Single line to the left of 354 kv is for $U=35$ MEV.

possible to produce the opposite effect of increasing the ratios of the low velocity values of σ_L to the values at high energies. This can be accomplished by arranging for a stationary level to lie slightly below the level of zero energy. The effect is then very similar to what one would have if there were resonance at very low energies. Both of these effects are obvious in the curves showing the theoretical dependence of σ_L on the energy reproduced above in Figs. 2 and 3. The theoretical value of σ_L for fixed P can be varied by *orders of magnitude* by changing the depth and width of the "well" without introducing pronounced resonance in the experimental region. It is thus at times rather unsatisfactory to speak of reactions as "probable" or "improbable" in the manner of Goldhaber unless one specifies a given width, depth and shape of the "potential well."

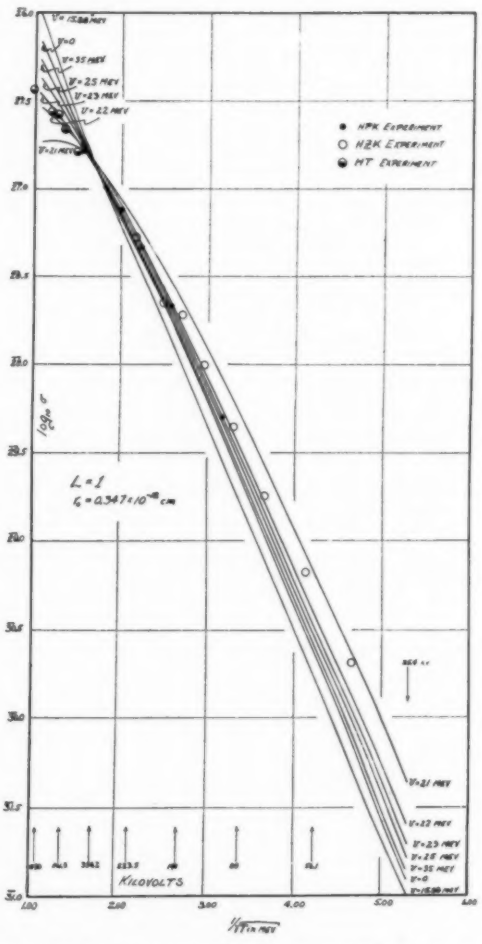

FIG. 3. $L=1$, $r_0=0.347\times10^{-12}$ cm, $U=0$, 15.88, 21, 22, 23, 25, 35 MEV.; $\rho/ak=0.316$.

Calculations with Eq. (6) are somewhat laborious and it is often desirable to have a more convenient formula. For $L=0$ one can obtain such a formula by neglecting the "well" altogether, i.e., by supposing that the inverse square field applies everywhere. The nuclear radius has then only the significance of defining a sphere of action within which the incident particle is effective in producing disintegrations. In the notation previously used[12]

$$F_0=C_0\rho\Phi_0;\quad C_0^2=2\pi\eta/[e^{2\pi\eta}-1]. \qquad (8)$$

Introducing this into Eq. (5) one has to perform

an integration involving Φ_0^2. For low energies Φ_0 can be approximated[13] by

$$\Phi_0 \leqq J_1(ix)/(ix/2) = \hat{\Phi}_0; \quad x = (8\rho\eta)^{\frac{1}{2}} = (8r/a)^{\frac{1}{2}}, \quad (9)$$

where J_1 is the usual Bessel function. This approximation is fair even if one approaches energies in the neighborhood of the barrier energy for given r. Integrating one finds

$$\sigma = (4\pi P r_0^3/3v) C_0^2 f, \quad (10)$$

where

$$f = |2I_1(x)/x|^2 - |2I_2(x)/x|^2, \quad (11)$$

where the I are the usual Bessel functions of an imaginary argument. For work with tables given in Watson's *Bessel Functions* it is convenient to use

$$f = (2I_1/x)^2 - (2/x)^2(I_0 - 2I_1/x)^2. \quad (11')$$

A few values are given in Table I.

TABLE I.

x	1.0	1.2	1.4	1.6	1.8	2.0
f	1.20	1.30	1.43	1.59	1.80	2.04

For use of the tables of Φ being prepared for publication[13] it is convenient to express f in terms of $\hat{\Phi}_0$, $\hat{\Phi}_1$. One has

$$f = \hat{\Phi}_0^2 - (r/2a)(\hat{\Phi}_0 - (r/3a)\hat{\Phi}_1)^2. \quad (11'')$$

Substitution of numbers gives Table II.

TABLE II.

$f/\hat{\Phi}_0^2$ =	0.892	0.869	0.844	0.814	0.778	0.742
$\log_{10}(r/a)$ =	1.4	1.5	1.6	1.7	1.8	1.9

(The third figure is not quite certain in these ratios.) Similar formulas can be worked out for $L=1$. In the approximation of Eq. (10) one obtains the same velocity dependence as by means of Eq. (7). The absolute value can be estimated more accurately by means of Eq. (10). Numerical trial shows that Eq. (10) gives a velocity dependence of σ and absolute values similar to those obtained from Eq. (6) for $U=0$. It is good only as a starting point.

For very low energies ($\eta \gg L$) the velocity dependence for all L becomes the same in the general case. The asymptotic form of σ_L is then

$$\sigma_L \sim \frac{\pi^2 P r_0^3 2^{2L+3}(r/a)^{2L}(F_L'/F_L - G_L'/G_L)^2 \overline{u_L^2}}{(2L)!(2L+1)!(\bar{F}_L'/\bar{F}_L - G_L'/G_L)^2} \frac{\eta}{v} e^{-2\pi\eta}. \quad (12)$$

The first fraction approaches a constant value because $\rho F'/F$, $\rho G'/G$, $\rho \bar{F}'/\bar{F}$ as well as $\overline{u_L^2}$ approach constant values.

The effect of absorption of incident protons within the nucleus can be estimated by using a wave equation with a complex potential energy

$$\Delta\psi + (2\mu/\hbar^2)(E - V + i\hbar P/2)\psi = 0. \quad (13)$$

Here E is the energy, V is the real part of the potential energy, and the extra term in P was added so as to represent absorption. It follows from this equation that

$$(\hbar/2\mu i)\ \mathrm{div}\,[\psi^*\nabla\psi - \psi\nabla\psi^*] = -P\psi^*\psi. \quad (14)$$

Particles may be said to disappear at the rate $P\psi^*\psi$ per unit volume and per unit time. For $L=0$ and a constant V Eq. (13) gives

$$\sigma = \frac{2\pi(P/v)[Sh/k_1' - s/k_0]}{|k'|^2(Ch+c)(G^2+F^2) + k^2(Ch-c)(G'^2+F'^2) - 2ks[k_0'(GG'+FF') + k_1'] - 2kSh[k_1'(GG'+FF') - k_0']}, \quad (15)$$

where

$$k' = k_0' + ik_1' = (2\mu/\hbar^2)^{\frac{1}{2}}[E - V + i\hbar P/2]^{\frac{1}{2}}, \quad (15')$$

$$Ch = \cosh 2k_1' r_0, \quad Sh = \sinh 2k_1' r_0, \quad c = \cos 2k_0' r_0, \quad s = \sin 2k_0' r_0. \quad (15'')$$

[13] F. L. Yost, John A. Wheeler and G. Breit in preparation for publication.

For very low energies the terms in G^2 and GG' predominate strongly and one has the asymptotic form

$$\sigma \sim \frac{2\pi[Sh/\zeta_1 - s/\zeta_0](Pr_0^3/v)(F^2/\rho^2)(FG/\rho)^{-2}}{\zeta^2(Ch+c)+(Ch-c)(\rho G'/G)^2-2\zeta_0 s(\rho G'/G)-2\zeta_1 Sh(\rho G'/G)}, \tag{16}$$

$$\zeta_0 = k_0' r_0, \quad \zeta_1 = k_1' r_0, \quad \zeta = |\zeta_0 + i\zeta_1|. \tag{16'}$$

Comparing this with Eq. (12) the asymptotic dependence on the velocity for very low energies is seen to be the same because FG/ρ, ζ_0, ζ_1, $\rho G'/G$ approach finite limits. The factor in Eq. (16) which contains the main velocity dependence is $F^2/v\rho^2$ which for $L=0$ behaves as the $(\eta/v)\exp(-2\pi\eta)$ of Eq. (12). The argument applies also for $V=0$. Eq. (12) behaves as usual while in Eq. (16) the ζ approach finite limits $\zeta_0=\zeta_1=r_0(\mu P/2\hbar)^{\frac{1}{2}}$ so that $Sh/\zeta_1 - S/\zeta_0$ does not vanish as long as $P\neq 0$. Thus in the limit of $v\to 0$ the dependence $v^{-2}\exp(-2\pi\eta)$ may be expected to apply with and without absorption. The quantity Pr_0/v is therefore not the primary determining parameter for the applicability of Eq. (6) to the velocity dependence as one is tempted to suppose.

It is instructive to consider the special case of $ZZ'=0$ which corresponds to neutron capture. Instead of Eq. (15) we now have

$$\sigma = 2\pi[Sh/k_1' - s/k_0'](P/v)[|k'|^2(Ch+c)+k^2(Ch-c)-2kk_1's+2kk_0'Sh]^{-1}. \tag{17}$$

For very low velocities and vanishing V, $k_0'^2=k_1'^2=\mu P/2\hbar$ and

$$\sigma \sim (2\pi\hbar/\mu v k_1')(Sh-s)/(Ch+c). \tag{17'}$$

If on the other hand, $P\to 0$, V is finite, and $v\to 0$

$$\sigma = 2\pi k_0^{-2}(1-s/2k_0r_0)(Pr_0/v)/\cos^2 k_0 r_0. \tag{17''}$$

Here also the velocity dependence is the same for very low velocities and the cross section varies as $1/v$ with or without absorption. According to Eq. (17') high values of P give small σ for small v which is just the opposite of the behavior without absorption given by Eq. (17''). This is due to the fact that a large absorption shifts the phase of the sine curve for $\bar{F}$ towards zero at the nuclear boundary and thus decreases the absolute value of $\bar{F}$ at r_0. These special cases indicate that the influence of absorption of the incident wave is more likely to show itself in the dependence of σ on P than on v. In connection with the discussion of experimental material numerical calculations made by means of Eq. (15) will be presented and it will be seen that in the special case considered the effect of absorption is not important.

Discussion of Experimental Material

The data considered here are those of Herb, Parkinson and Kerst[3] from 100 to 400 kv, of Hafstad and Tuve[4] in the region from 400 to 1000 kv and of Heydenburg, Zahn and King[14] from 200 kv to 46 kv. The data of Herb, Parkinson and Kerst give yields of α-particles in thick as well as thin targets and can be used to obtain absolute values of cross sections. The uncertain element enters in the range of protons in a solid Li target and in the dependence of the range on velocity. In deriving the absolute values of σ the 3/2 power dependence of range on energy was used. The data of Hafstad and Tuve and of Heydenburg, Zahn and King are used below to give values of σ by comparison with the absolute values of Herb, Parkinson and Kerst. Thus only ratios of σ's at different voltages are supposed to be given correctly by these data.[4, 14]

Assuming the 3/2 power dependence of range

[14] N. P. Heydenburg, C. T. Zahn and L. D. P. King, unpublished.

on kinetic energy, the number of disintegrations per proton is

$$Y=Nx_0\bar{\sigma}, \quad \bar{\sigma}=(3/2)T_0^{-\frac{3}{2}}\int_0^T \sigma(T)T^{\frac{1}{2}}dT, \quad (18)$$

where $\sigma(T)$ = collision cross section for kinetic energy T; x_0 = range of protons at kinetic energy T; N = number of Li^7 nuclei per unit volume of target. Nx_0 can be obtained by comparison of a standard material (oxygen) with the stopping power of Li. Using the stopping powers of N_2, O_2, H_2O, CO_2, H_2 relative to oxygen, as given by Rutherford, Chadwick and Ellis, one obtains 0.948 for the stopping power of air relative to oxygen. From the Cavendish laboratory graphs the range of protons in air at 2 MEV = 7.2 cm. Using these numbers and 0.519 for the stopping power of Li relative to oxygen, one finds $Nx_0 = 6.03\times10^{19}$ at 400 kv. At this voltage the number of disintegrations caused by a single proton on a thick target[3] is $Y=46.4\times10^{-9}$. Hence $\bar{\sigma}=7.69\times10^{-28}$ cm² at 400 kv. From the thin target data of Herb, Parkinson and Kerst, the value of $\bar{\sigma}/\sigma$ was computed for 400 kv and was found to be 0.461 with a probable accuracy of 1 percent. Hence at 400 kv, $\sigma=1.668\times10^{-27}$ cm². No correction was made here for the 1 : 12 ratio of Li^6 to Li^7. From this σ the thin target results of Herb, Parkinson and Kerst give values of σ also for voltages down to 100 kv. The data of Heydenburg, Zahn and King were obtained for thick targets and were reduced by them to thin target data by differentiation. The use of these data thus presupposes the approximate validity of the 3/2 power range energy relation not only in obtaining the absolute value of σ at one voltage but also in obtaining the relative values at different voltages. One should not attach therefore as much weight to this set of data as to the thin target experiments.

The experiments of Hafstad and Tuve give preliminary values for the yield in a very thin film of lithium salts which probably had a negligible stopping power. We have summarized the data in Table III.

The number of significant figures is, of course, exaggerated in Table III both with respect to the absolute value of 400 kv and the relative values at different energies. Extra decimals were kept in the calculations only in order to avoid accumulation of errors. In the comparison of theory and experiment given in Figs. 1, 2, 3, 4, 5 the data of HPK are represented by closed circles, those of HZK by open circles and those of Hafstad and Tuve by circles, whose lower halves are black. The calculation of the theoretical values of σ was made with values of $\log_{10}ka=\bar{1}.6$, $\bar{1}.7$, $\cdots$ 0.3 and in some cases 0.4, 0.5. Computation for these values does not require interpolation of tables of Coulomb wave functions.[13] Throughout the kinetic energy of the bombarding particle was computed with

$$T=24.83mZ^2Z'^2(ka)^2 \text{ kv}. \quad (19)$$

Here m is the mass of the bombarding particle in terms of the mass of the hydrogen atom and the kinetic energy is expressed in kilovolts and Z, Z' are the atomic numbers of the colliding particles. The nuclear radius is given by

$$r_0=2.88\times10^{-12}(\rho/ka)/(ZZ'/\mu) \text{ cm}, \quad (20)$$

where μ is the reduced mass for the collision, also expressed in terms of the mass of the hydrogen atom. When the kinetic energy of relative motion is

$$ZZ'e^2/r_0=49.66Z^2Z'^2(\mu/m_H)(ka/\rho) \text{ kv}, \quad (21)$$

the incident particle has enough energy to slip over the barrier. The kinetic energy which the incident particle must have in order to clear the

TABLE III. *Kinetic energy (T) of protons and collision cross section of (σ).*

T in MEV	(T in MEV)$^{-\frac{1}{2}}$	$10^{27}\sigma$	OBSERVER
0.100	3.162	0.0503	HPK
.150	2.582	.2061	
.200	2.236	.4692	
.250	2.000	.7693	
.300	1.826	1.070	
.350	1.690	1.367	
.400	1.581	1.668	
.450	1.488	1.64	HT
.550	1.347	2.21	
.625	1.264	2.70	
.700	1.194	2.78	
1.050	.976	3.72	
.2125	2.170	.546	HZK
.1875	2.309	.4395	
.1625(?)	2.481	.2258	
.1375	2.697	.1908	
.1125	2.981	.1008	
.0915	3.306	.04438	
.0748	3.656	.01787	
.0584	4.138	.006682	
.0460	4.662	.001908	

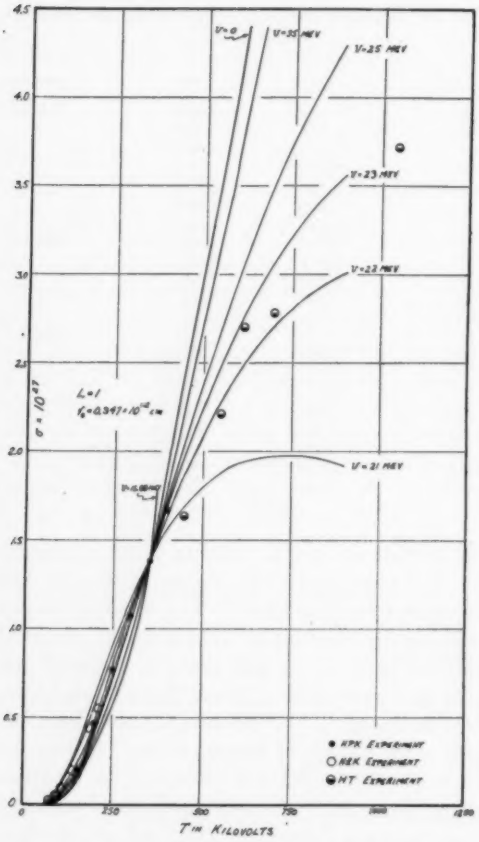

FIG. 4. $L=1$, $r_0=0.347\times10^{-13}$ cm; $\rho/ak=0.316$.

barrier is $(m/\mu)ZZ'e^2/r_0$, i.e.,

$$T_{\text{barrier}}=49.66Z^2Z'^2(m/m_H)(ka/\rho)\text{ kv}. \quad (21')$$

Calculations for constant U (see Eq. (3')) involve the use of the phase of the wave function for $r\leqq r_0$ at $r=r_0$. This is

$$z=r_0[(2\mu/\hbar^2)(U+\mu T'/m)]^{\frac{1}{2}}. \quad (22)$$

Thus, e.g., for $L=0$, $\bar{F}=$const. sin z for $r<r_0$. The formula

$$z=(2\rho/ka)^{\frac{1}{2}}[U/(ZZ'e^2/r_0)+\tfrac{1}{2}ka\rho]^{\frac{1}{2}} \quad (23)$$

combined with Eq. (22) is convenient for the calculation of z.

A set of numerical calculations for protons colliding with Li or any other nucleus can be interpreted by means of Eqs. (19) . . . (23) together with Eq. (6) so as to give values of σ for protons and deuterons colliding with any other nucleus provided the value of U is properly chosen. Thus keeping ρ and ka fixed the terms in the summation in (6) are left unchanged provided z is also kept fixed. In order that this be the case we must have the same values of $U/(ZZ'e^2/r)$ in the two reactions according to Eq. (23). By Eq. (21) this is accomplished by keeping

$$U_1\mu_1^{-1}Z_1^{-2}Z_1'^{-2}=U_2\mu_2^{-1}Z_2^{-2}Z_2'^{-2}, \quad (24)$$

where the indices 1,2 refer to the two reactions. Collision processes in which this correspondence is maintained may be called *corresponding* processes. The only part of the formula for σ which is different for *corresponding* processes is the factor Pr_0^3/v. Values of σ in corresponding processes which belong to the same ka may be called *corresponding* values. The ratios of *corresponding* collision cross sections at different voltages are thus the same for *corresponding* processes. The values of U which must be used for deuterons colliding with the same nucleus as protons in order to give corresponding processes are nearly twice those for protons. This is convenient because the binding of a deuteron to a nucleus may be expected to be roughly twice the binding of a proton.

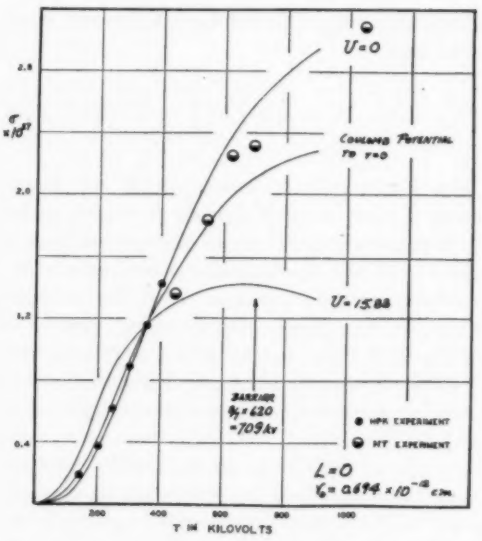

FIG. 5. $L=0$, $r_0=0.694\times10^{-13}$ cm, $U=0$, 15.88 MEV and Coulomb potential to $r=0$; $\rho/ak=0.631$.

In Fig. 1 the values of $\log_{10}\sigma$ are plotted as ordinates and those of $(T \text{ in MEV})^{-\frac{1}{2}}$ as abscissae for $L=0$, $\rho/ka=0.3162$, $r_0=0.347\times10^{-12}$ cm and $U=0$, 4.292, 10.00, 15.88 and 40.00 MEV. In this as well as the succeeding figures P was adjusted so as to make the theoretical and experimental curves intersect at 354 kv. It will be noted that $U=0$ agrees fairly well with the experimental data. The agreement is not perfect and $U=0$ is presumably an unreasonable value because it allows for no binding of the proton to the Li^7 nucleus. When U is increased the first effect is to spoil agreement with experiment. The values of U at low voltages become anomalously small as is seen from the curve for $U=4.292$ MEV. The maximum in σ shows that this effect of increasing U can be attributed to resonance above the barrier. As U increases further the resonance level moves through the experimental region towards lower voltages and finally becomes a stationary level. This condition is shown by $U=10.00$ MEV. Here the expected yield is too high for low voltages on account of the fact that $1-FG\delta$ decreases with the voltage. In order to obtain agreement with experiment the stationary level must be moved down into the "well." The effect of doing so is shown by $U=15.88$ and $U=40$ MEV. Relatively large changes in U are seen to be necessary to produce an appreciable effect. Fig. 2 gives similar curves for $U=25$, 30, 35 MEV. Above 400 kv the theoretical values appear to be definitely too high. However, it should be remembered that the experimental values are not very certain in this region. We may thus consider the agreement as being moderately satisfactory. $U=35$ MEV appears to be the best fit.

Fig. 3 shows similarly the condition for $L=1$. $U=0$, gives a too steep increase of σ with velocity. The immediate effect of increasing U is to increase the disagreement between theory and experiment as is shown by $U=15.88$ MEV. This is due to the fact that a resonance level is moving down into the experimental region as U increases. The level is at $T=0$ when $U=20.5$ MEV. By adjusting U in the neighborhood of this value one can obtain a large range of variation in the dependence of σ on T. Thus for $U=21$ MEV the deviation from experiment is in an opposite direction from that at $U=0$. The experimental points are seen to be bracketed by $U=21$ and $U=22$ MEV. Fig. 4 shows a direct plot of σ against T for the same conditions as Fig. 3.

Calculations for radii $r_0=0.694\times10^{-12}$ cm and 0.501×10^{-12} cm were made for σ for several values of U. The results are very similar to those given by the curves and can be foreseen by remembering that the important thing is the position of stationary and resonance levels.

It will be noted from the above graphs that it is not proper to describe the problem only as one of penetration through the barrier. The depth and width of the "well" are seen to have a very pronounced effect and one may have a decrease of σ with T at the barrier as well as an increase. The description of the disintegration phenomenon by means of penetration through a barrier is particularly poor for high energies and it begins to be poor before the energy exceeds the barrier height. For a fixed P the order of magnitude of the expected collision cross section varies with the "well." Thus the values of $(4Pr_0/3v)$ at 354 kv are as in Table IV for $L=0$, $r_0=0.347\times10^{-12}$ cm and in Table V similarly for $L=1$. Comparing these values with the general slope of the curves for $\log_{10}\sigma$ against $T^{-\frac{1}{2}}$ it is seen that there is considerable parallelism between them. Thus for example for $L=1$ the $4Pr_0/3v$ is nearly the same for $U=35$ and for $U=0$ and the slopes of the curves are also nearly the same. Both effects are due to the distance of the experimental region from the stationary level. It is also obvious that one cannot, in general, consider a reaction due to $L=1$ as much less prob-

TABLE IV. $L=0$.

U	$4Pr_0/3v$	U	$4Pr_0/3v$
0	0.034	20	0.135
4.29	.0028	23	.160
10	.0153	25	.164
15.88	.0820	27	.158
18	.111	30	.134

TABLE V. $L=1$.

U	$4Pr_0/3v$	U	$4Pr_0/3v$
0	1.415	22	0.0225
4.29	.887	23	.0453
10	.359	25	.114
15.88	.0560	35	.818
21	.00755		

able than for $L=0$. The variation of P for fixed L due to changing U can be just as important as the variation of P with fixed U due to changing L.

For the radius $r_0=0.347\times10^{-12}$ cm ($\rho/ka=0.3162$) the potential barrier is reached when $T=1413$ kv. It has already been pointed out that the shape and slope of the yield curves at the barrier varies with U. In order to show that this condition is not a characteristic of the radius used we give in Fig. 5 the theoretical yield curves for $\rho/ka=0.631$, $r_0=0.694\times10^{-12}$ cm, $L=0$. The barrier is reached in this case when $T=709$ kv which falls within the range of experiments of Tuve and Hafstad. For $U=0$ the yield goes on increasing at the barrier. For $U=15.88$ MEV it decreases after the barrier voltage is exceeded.

The effect of absorption of the incident waves discussed in connection with Eqs. (13), (14), (15) was estimated for $L=0$, $U=15.88$ MEV, $r_0=0.347\times10^{-12}$ cm. According to Table IV the experimental value of the cross section of 354 kv demands $4Pr_0/3v=0.0820$. The complex potential energy used in Eq. (15) is connected more directly with Pr_0/v_i where v_i is the velocity which the proton would have classically inside the "well." For the $Li^7+H^1\rightarrow He^4+He^4$ reaction we have thus $4Pr_0/3v_i=0.01134$. This reaction, in the classification of Goldhaber, is an "improbable" one. Compared with $Li^6+H^1\rightarrow He^3+He^4$ it is perhaps thirty times less probable. In order to have a more typical case we multiply the above value of $4Pr_0/3v_i$ by 40 which corresponds to using $Pr_0/v_i=0.3435$. We use this value for very small v and calculate the corresponding values for larger v. The formulas which determine the necessary quantities in Eq. (15) are:

$$\zeta_0=k_0'r_0;\quad \zeta_1=k_1'r_0;$$

$$\zeta=|k'|r_0=(\zeta_0^2+\zeta_1^2)^{\frac{1}{2}};\quad v_i=\hbar\kappa/\mu \qquad (25)$$

$$\kappa^2=2\mu(E-V)/\hbar^2;\quad z=\kappa r_0 \qquad (25')$$

$$\zeta_0^2=(z^2/2)\{1+[1+(Pr_0/zv_i)^2]^{\frac{1}{2}}\};$$

$$\zeta_1^2=(z^2/2)\{-1+[1+(Pr_0/zv_i)^2]^{\frac{1}{2}}\}. \qquad (26)$$

In Eq. (15) the difference of ζ_0 from z and the difference of ζ_1 from 0 determine the effect of absorption. A numerical calculation gives the following values:

TABLE VI.

T	z	ζ_0	ζ_1	σ/σ_{ab}
35.4 kv	2.852	2.857	0.1713	1.01
89.0	2.857	2.862	.1710	1.04
223.5	2.867	2.872	.1704	1.04
354.2	2.877	2.882	.1698	1.04
890	2.919	2.924	.1674	1.07
2235	3.020	3.024	.1618	1.09

The last column of the above table gives the ratio of σ, the theoretical cross section neglecting the decay of the incident wave, to σ_{ab} the theoretical cross section taking this decay into account. The first values may be somewhat inaccurate on account of inaccuracies in the Coulomb functions. As the kinetic energy increases σ_{ab} increases slightly in comparison with σ. However, the effect is not serious and is usually too small to be of interest. It is thus likely that calculations neglecting the decay of the incident wave inside the nucleus are usually sufficiently good. It is not intended to say, however, that this will be always so. Small z and large Pr_0/v_i will doubtless make the effect of absorption important and an estimate of its importance seems to be advisable.

It is of interest to compare the deuteron reactions on Li with the corresponding proton reactions. According to Oliphant, Kinsey and Rutherford[15] the increase with energy in the efficiency of the deuterons is more marked than that for protons. Thus according to their graph the deuteron yield is lower than the proton yield below about 120 kv and is considerably greater than the proton yield at 170 kv. This crossing over of the yield curves can be understood as the effect of the difference in velocity of protons and deuterons at the same voltage. The deuterons having the lower velocity, the exponent $-\pi ZZ'e/$"137"v in the C_L is larger in absolute value for deuterons than for protons and varies therefore more rapidly. For the lower range of voltages used by Oliphant, Kinsey and Rutherford the exponential factor in C_L is the most important factor of σ and a crossing over of the yield curves is thus to be expected.

[15] Oliphant, Kinsey and Rutherford, Proc. Roy. Soc. **A141**, 722 (1933).

According to the consideration of corresponding collision processes discussed in connection with Eq. (24) we would expect the graphs of Fig. 1 to apply to the deuteron reactions provided the abscissa $(T_{\text{proton}})^{-\frac{1}{2}}$ is multiplied for each point by $2^{-\frac{1}{2}}=0.707$. The deuteron graphs are thus steeper than those for protons. The graphs of Fig. 1 ($\rho/ka=0.3162$) when applied to Li^7+H^2 correspond to a nuclear radius of 0.195×10^{-12} cm. This is appreciably smaller than the 0.347×10^{-12} cm used for Li^7+H^1. It is fairer to use a larger radius for the H^2 collision such as $r_0=0.39\times10^{-12}$ cm which corresponds to $\rho/ka=0.631$. The yield curves corresponding to this radius for Li^7+H^1 are shown in Fig. 5. According to Eq. (24) $U_{\text{proton}}=15.88$ is equivalent to $U_{\text{deuteron}}=28.2$ MEV. For such a well the factor by which the yield under deuteron bombardment should increase from 150 to 175 kv should be about 1.82 while actually it is about 2.5 for the 10.3 cm absorber and 1.8 for the 2.7 cm absorber. It is presumably the latter value that corresponds to the Li^7+H^1 reaction and there is at least a rough agreement between experiment and theory. However, it is felt that a more careful study of the deuteron reactions would be proper.

The value $U\leqq20$ MEV for Li^7+H^1, $L=1$ fits in reasonably with estimates from the nuclear binding energies. Using Wigner forces and statistical considerations one would estimate 18 MEV to be the value of U and roughly the same for Majorana-Heisenberg forces. This agreement may be partly accidental on account of the crudeness of the present theory as well as the theory of nuclear binding energies.

The two possibilities $L=0$, $U\leqq35$ MEV and $L=1$, $U\leqq22$ MEV can be compared with the probable mass of Be^8 which is approximately[16] 8.0071. With this mass, and Bethe's masses for Li^7 and H^1, the energy liberated in the formation of Be^8 when a proton is captured by Li^7 is 16.7 MEV. If $U=22$ MEV this capture cannot occur into the stationary level with $L=1$ because this level is too high by $16.7-1.5=15.2$ MEV. For this U the level with $L=0$ would be approximately in the right position to give the 16.7 MEV binding energy. However, this level of Li^7 is filled by two protons and the exclusion principle makes the addition of a third proton impossible. One can increase U so as to bring the second level for $L=1$ into about the same position as the first one is for $U=22$. This would give approximately the right dependence of the α-particle yield on velocity considering $L=1$ as responsible for the disintegration. However, the required depth would be about 80 MEV which is unreasonably large. For $U=35$ MEV the α-particle yield dependence on velocity can be fitted by using $L=0$ for the proton and simultaneously the mass of Be^8 can be accounted for by supposing that Be^8 is formed through the capture of a proton into the first level with $L=1$. In Li^7 there is only one proton in this level and the addition of a second proton to form Be^8 is possible and probable. The mass of Be^8 thus indicates that $U=35$ MEV and $L=0$ for the proton should be used for the α-particle yield. According to Tables IV, V for this U the $L=0$ process is more probable than the process for $L=1$ if P is the same. The angular momentum of the alpha-particles with respect to each other after disintegration must be $l=2$ if $L=0$ while it may be 0 or 2 if $L=1$. One generally supposes that $l=0$ is more probable than $l=2$. However, the wave-length of the relative motion of the alpha-particles is in this case of the same order as the nuclear radius and their kinetic energy is large. The two values $l=0$ and $l=2$ may be equally probable and there appears to be no general objection to regarding $L=0$, $l=2$ as the main process. It should be, nevertheless, remembered that in this process the total orbital angular momentum of the particles is changed from 1 to 2. This change occurs simultaneously with a change of total particle spin from 1 to 0. The interaction between orbital and spin angular momenta must therefore be supposed sufficiently strong to make this interchange possible. Such an interaction is not necessary for $L=1$, $l=0$, 2.

Briefly the above discussion indicates that one may suppose that there is only a weak interaction between orbital and spin angular momenta at the sacrifice of even an approximate agreement with the mass of Be^8 or else one may account for that mass but then one must suppose a strong spin orbit interaction.

[16] Oliphant, Kempton and Rutherford, Proc. Roy. Soc. **A150**, 241 (1935).

Appendix I

The collision of a proton with a Li^7 nucleus and the subsequent formation of two alpha-particles can be treated schematically by thinking of three particles A, B, C. Particles A and B are thought of as being bound to each other initially, particle C collides with the combination, knocks out B and attaches itself to A. The combination $A+B$ represents the Li^7 nucleus and C represents the proton. A may be thought of as an H^3 combination within Li^7 and B as an alpha-particle inside the same nucleus. The combination $A+C$ is then a newly formed alpha-particle recoiling from B. We introduce coordinates $x_A{}^i$, $x_B{}^i$, $x_C{}^i$, $i=1, 2, 3$ for the three particles. We introduce also

$$x_B-x_A=\xi,\ x_C-x_A=\eta,\ x=x_B-(M_Ax_A+M_Cx_C)/(M_A+M_C),$$
$$y=x_C-(M_Ax_A+M_Bx_B)/(M_A+M_B). \quad (I\ 1)$$

The energy of the system will be supposed to be the sum of the kinetic energy and of the potential energies $V_{AC}(\eta)$, $V_{AB}(\xi)$, $V_{BC}(\eta-\xi)$. Corresponding to the initial state of the system one can separate the wave equation in the variables ξ, η and the coordinates of the center of mass provided one neglects V_{AC}, V_{BC}. Similarly if one neglects V_{AB}, V_{BC} the wave equation can be separated in the variables η, x and the coordinates of the center of mass. Approximately the wave function can be represented for the initial state as $\Phi_0(\xi)g_0(y)$. Here Φ_0 represents the initial state of relative motion of A and B while $g_0(y)$ describes the state of relative motion of B with respect to the center of gravity of A and B. Similarly the final state can be represented by $\Psi_m(\eta)f_m(y)$. Here the index m refers to different possible final states. The wave function can be expanded into a linear combination of $\Phi_n(\xi)g_n(y)$ and $\Psi_m(\eta)f_m(y)$. It will be supposed that the coefficient of $\Phi_0(\xi)g_0(y)$ is much larger than the coefficients of the other functions and also that in determining the coefficients of the other functions one may neglect all coefficients except that of $\Phi_0(\xi)g_0(y)$. On these assumptions one finds

$$[T_y+E_0{}^\xi-E+\int\Phi_0{}^*(\xi)[V_{AC}(y+q\xi)+V_{BC}(y+(q-1)\xi)]\Phi_0(\xi)d\xi]g_0(y)=0, \quad (I\ 2)$$

$$[T_x+E_m{}^\eta-E+\int\Psi_m{}^*(\eta)[V_{AB}(x+(1-p)\eta)+V_{BC}(-x+p\eta)]\Psi_m(\eta)d\eta]f_m(x)$$
$$+\int\Psi_m{}^*(\eta)[V_{AC}(\eta)+V_{BC}(p\eta-x)-\{\int\Phi_0{}^*(\xi)[V_{AC}(y+q\xi)+V_{BC}(y+(q-1)\xi)]\Phi_0(\xi)d\xi\}_{y=-qx+s\eta}]$$
$$\Phi_0(x+(1-p)\eta)g_0(-qx+s\eta)d\eta=0, \quad (I\ 3)$$

$$p=M_A/(M_A+M_C),\quad q=M_B/(M_A+M_B),\quad s=1-q+pq \quad (I\ 4)$$

and where T_y, T_x are the kinetic energy operators for the relative motions represented by y, x; E=total energy; $E_0{}^\xi$, $E_m{}^\eta$ are the energies of internal motion represented by ξ, η. Eq. (I 2) determines the function $g_0(y)$. The potential energy is a properly taken average of $V_{AC}+V_{BC}$ over the initial state of the combination $A+B$. Eq. (I 4) is an inhomogeneous equation which allows one to determine f_m. By the method of Chapter VI of Mott and Massey's book on *The Theory of Atomic Collisions* one can obtain f_m by analyzing it and the integral involving g_0 in (I 4) into a series of spherical harmonics and then determining the coefficient of each spherical harmonic (a radial function) in the expansion of f_m by an integration over the radius $(x_1{}^2+x_2{}^2+x_3{}^2)^{\frac{1}{2}}$. The asymptotic form of this coefficient for large radii is proportional to the result of multiplying the $\int d\eta$ in (I 4) by the regular normalized solution of the radial homogeneous equation for f_m [obtained by omitting $\int d\eta$ in (I 4)] and then integrating over x. Thus g_0 enters into the expression for the asymptotic form of f_m under $\int d\eta$ and is weighted in accordance with operations just described. The expected dependence of σ on g_0 is therefore more complicated than a simple proportionality to the integral of $|g_0|^2$ through the interior of the nucleus. Qualitatively the difference of the approximation used from the more exact result given by (I 4) cannot be significant as long as the shape of $|g_0|^2$ through the nucleus does not vary much with bombarding voltage. If g_0 becomes large on account of resonance as determined by Eq. (I 2) f_m will also be large. Similarly, if the regular normalized solution of the homogeneous equation for a radial part of f_m shows resonance at the energy $E-E_m{}^\eta$, the solution of (I 4) for f_m will be large and we have then *resonance to the disintegration products* which may be the explanation of the resonance for γ-rays from Li^7+H^1.

Numerical estimates show that one may treat Eq. (I 4) approximately by passing to the limit $M_A\to\infty$, $p=1$, $q=0$, $s=1$. In this case V_{AC} does not enter into the $\int d\eta$ in (I 4). For a spherically symmetric Φ_0 and $V_{BC}=e^2/r_{BC}$ one has

$$\sigma_L=\frac{4\pi}{2L+1}\frac{v_B}{v_Ck_B{}^3(E-E_m{}^C)^2}\left|\int\bar{F}_L{}^B(\rho_B)R_L(\rho_B)\rho_Bd\rho_B\right|^2,$$
$$R_L(\rho_B)=e^2\Phi_0(B)\int\Psi_m{}^*(C)S_L(r_B,r_C)(\bar{F}_L{}^C(\rho_C)/\rho_C)d\tau_C, \quad (I\ 5)$$
$$S_0(r_B,r_C)=\frac{1}{r_B}-\frac{1}{r_C}\int_{B'<C}|\Phi_0(B')|^2d\tau_{B'}-\int_{B'>C}\{|\Phi_0(B')|^2/r_{B'}\}d\tau_{B'};\ S_L=r_1{}^L/r_2{}^{L+1},\ r_2>r_1;\ (r_1,r_2)=(r_B,r_C)\text{ or }(r_C,r_B).$$

The indices B, C here indicate that one uses the coordinates of particles B, C and $\rho_B=k_Br_B$, $\rho_C=k_Cr_C$ where k_B, k_C are the values of k for B and C; the functions $\bar{F}_L{}^B$, $\bar{F}_L{}^C$ are analogous to $\bar{F}$ of Eq. (3′). The example of Eq. (I 5) shows that $\bar{F}_L{}^C$ enters into σ_L in essentially different ways for different L because S_L, $\bar{F}_L{}^B$ vary with L. We thus expect P to vary with L.

From the above formula (I 5) one finds that if Φ and Ψ are each of the form $e^{-r/R}$ and if $\bar{F}^C$ is small in the nucleus then σ is proportional to R^4 for $L=0$ and to R^6 for $L=1$. Besides, the value of the matrix element depends on the overlapping of wave functions. Thus the cross section is quite sensitive to the nuclear radius and relatively small changes in assumptions about the state of the nucleus may account for large changes in the values of P.

Angular Distribution of the Products of Artificial Nuclear Disintegration

JOSEPH GIARRATANA AND CORNELIUS G. BRENNECKE, *Department of Physics, New York University, University Heights*

(Received October 3, 1935)

Measurements were made of the angular distribution of the alpha-particles emitted during the disintegration of lithium (7) by fast protons. The protons were generated in a low voltage arc and accelerated down a three-section vertical tube by potentials obtained from a rectifying and doubling system. The bombarding beam was analyzed by an electromagnet, defined by a series of circular slits, and allowed to impinge on the target in a special chamber designed to permit observation of the particles at positions spaced by 15° in the plane of the beam. The alpha-particles were recorded by an ionization chamber which actuated a linear amplifier and oscillograph. Readings taken at three voltages between 200 and 240 kilovolts indicate that within the limits of experimental error, estimated as approximately eight percent, emission of alpha-particles is random in direction.

INTRODUCTION

IN the observation of disintegration phenomena it is usually possible to observe only the particles coming from the target within a relatively small solid angle. The total number of particles emitted is then obtained by multiplying the number actually observed by the ratio of 4π to the solid angle through which measurements are made. This is not without justification, for Kirchner,[1] observing the yield at various angles by means of cloud-chamber photographs, reported the probability of emission to be the same for all directions between 80° and 160° with the incident beam. Kirchner, however, gives no information as to the constancy of voltage and ion currents in his experiments, nor does he give any estimate of the absolute accuracy of his result other than to say that the fluctuations observed lie within the statistical limits of error. In view of the fact that this result must enter into all determinations of absolute yield, it was felt desirable to investigate further the angular distribution by a different and independent method. In the present paper this has been done by using as a recording device an ionization chamber together with a linear amplifier and oscillograph. The particles studied were the alpha-particles originating in the transformation

$$_3Li^7+{}_1H^1\rightarrow 2{}_2He^4.$$

APPARATUS

Protons were obtained from a low voltage arc of a conventional type, the construction of which is shown in Fig. 1. The total ion currents obtained depended upon the arc current, the relation being roughly a linear one. At 150 ma of arc current approximately 10 microamperes of ion current were obtained, while at 400 ma of arc the ion current rose to 30 microamperes. The percentage of protons present in the ion beam varied from 10 to 20 percent, being higher for higher pressures, in agreement with the results of Fowler and Gibson[2] and of Lamar and Luhr.[3] In the experiments which follow about 150 ma arc current were used. Variation of the voltage on the electrode F permitted nice adjustment of the size of the ion spot striking the target. The sylphon bellows S permitted the position of the source within the first electrode of the accelerating tube to be varied for preliminary rough focusing. The flow of hydrogen gas to the arc chamber was regulated by means of a simple capillary leak of the type described by R. D. Fowler.[4] Commercial tank hydrogen was found quite satisfactory, without preliminary drying. Care was taken, however, to prevent as far as possible the mixture of air and other gases with the hydrogen in the storage tank and connecting tubes.

The current supply for the source was contained in a shielded box mounted on insulating supports of textalite tubing. It consisted of a 300-watt 110-volt direct-current generator, a 150-watt 110-volt direct-current to 110-volt alternating-current converter, and the necessary transformers, rectifiers, rheostats, etc. The fila-

[1] Kirchner, Physik. Zeits. **34**, 777 (1933).

[2] Fowler and Gibson, Phys. Rev. **46**, 1075 (1934).

[3] Lamar and Luhr, Phys. Rev. **46**, 87 (1934).

[4] R. D. Fowler, Rev. Sci. Inst. **6**, 26 (1935).

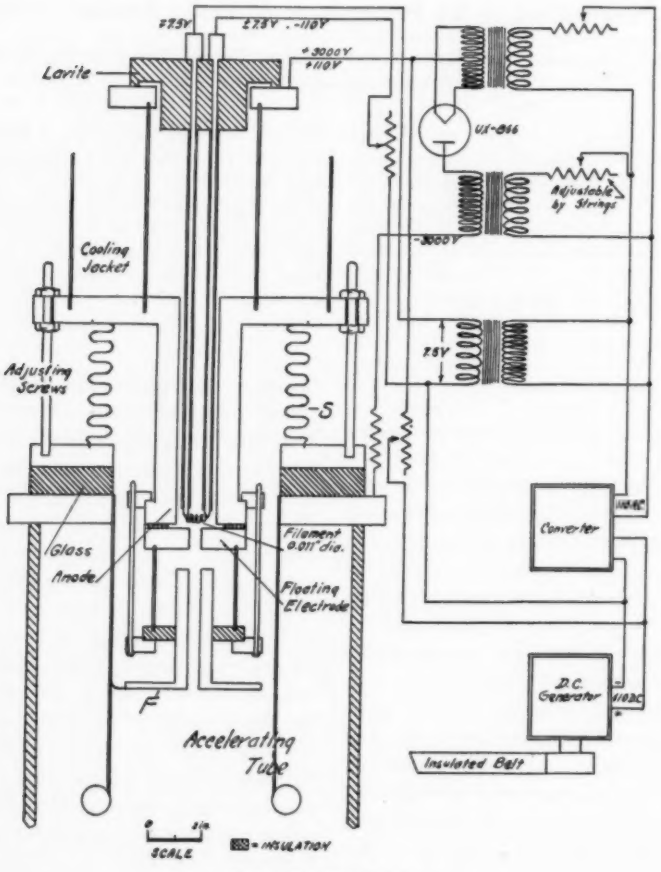

FIG. 1. Proton source.

ment transformer supplied 7.5 volts a.c. to the filament. A rectifier of the UX-866 type, operating from a 5000-volt neon sign transformer supplied direct current voltage for the focusing electrode F of the source.

During the early stages of this work the accelerating tube was a single section one made from a glass cylinder 12 inches in diameter and 26 inches in length. This tube proved very unstable, however, and it was found necessary to convert it into a two section tube, isolating the two parts electrically by a flat metal shield clamped in place by an adjustable expansion ring. This tube proved very stable in operation. Because of its short length, however, it would stand only about 170 kilovolts before flashing down the outside surface. This was corrected by the addition of a third section constructed from an 11-inch length of 6-inch diameter Pyrex tubing. In this form (Fig. 2) the tube has stood the maximum available voltage; i.e., 250 kilovolts, with no sign of breakdown.

The various ions, emerging from the accelerating tube, were sorted by means of an electromagnet, giving a field variable from 1000 to 1500 gauss, and a system of diaphragms. The first two diaphragms were grounded, while the third and the target chamber (Fig. 3) to which it was attached, were insulated from ground. The hole in the third diaphragm was $\frac{1}{2}$ inch, that in the second $\frac{3}{8}$ inch, and that in the first $\frac{1}{4}$ inch. Placing the third one immediately be-

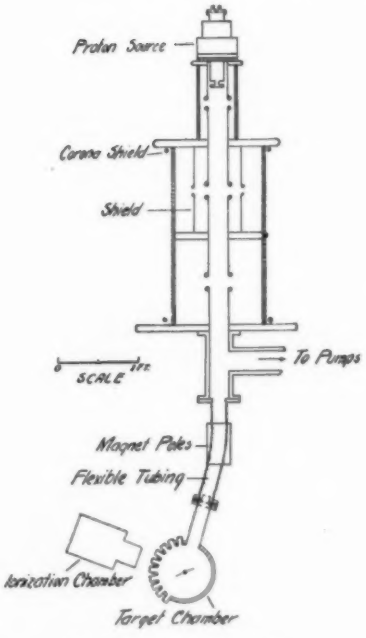

FIG. 2. Accelerating tube.

hind the second prevented the ions striking any surface of the target chamber until they struck the target itself. Because of the geometry of the chamber, the number of secondary electrons escaping through the diaphragms was very small. A microammeter connected between the chamber and ground read, therefore, the true ion current striking the target.

The target backing was of sheet aluminum, supported by a mica sheet which was in turn attached to a metal rod waxed into the large stopcock shown in the figure. The mica sheet served as a thermal insulator between the target, which sometimes became quite hot, and the wax.

The target was prepared by wetting the surface of the backing plate with a concentrated solution of pure lithium fluoride, and then evaporating the water by applying heat. It was found advisable to heat the target rather gently during evaporation, to avoid subsequent cracking of the surface of lithium salt.

The windows through which alpha-particles emerged from the target were of mica sheet, $\frac{3}{8}$ inch in diameter.

The accelerating potential was furnished by a 150-kilovolt transformer working into a rectifying and doubling circuit of the type described by Cockcroft and Walton.[5] The voltage was measured by means of a sphere gap, and it should be noted in this connection that recent checks of the A. I. E. E. standard sparkover potentials for sphere gaps[6, 7] have indicated these standards to be high by 16 to 20 kilovolts in the range of our measurements.

The linear amplifier used to record the disintegration products was constructed after a design kindly furnished this laboratory by Dr. M. A. Tuve, and is an adaptation of the amplifier developed by Wynn-Williams and Ward[8] to American tubes.

For oscillographs we used Peerless dynamic loudspeakers, from which the paper cones were removed. The voice coil was connected to a pivoted mirror by means of a strip of spring brass. These oscillographs were simple of construction and proved rugged in use, but the moving parts had too long a period to make them completely satisfactory for the purpose.

PROCEDURE AND RESULTS

The ionization chamber was very carefully aligned with the particular window of the target chamber through which observations were to be made, and the voltage and magnet current varied until protons of the desired energy entered the target chamber. The disintegration alpha-particles were then counted by the linear amplifier, and oscillograph records were made for periods of from three to ten minutes, the time depending upon the rate at which the products of disintegration were being recorded and upon the constancy of conditions.

The results are tabulated (Tables I, II, and III), and a graph summarizing them is shown in Fig. 4. As will be shown presently, the conditions during these experiments were such that an accuracy of better than 8 percent is not to be expected. The results indicate that within these limits the yield is independent of direction. In

[5] J. D. Cockcroft and E. T. S. Walton, Proc. Roy. Soc. **A149**, 406 (1935); **137**, 229 (1932).
[6] Henderson, Goss and Rose, Rev. Sci. Inst. **6**, 63 (1935).
[7] J. R. Meador, Elec. Eng. **53**, 942 (1934).
[8] Wynn-Williams and Ward, Proc. Roy. Soc. **A136**, 391 (1931).

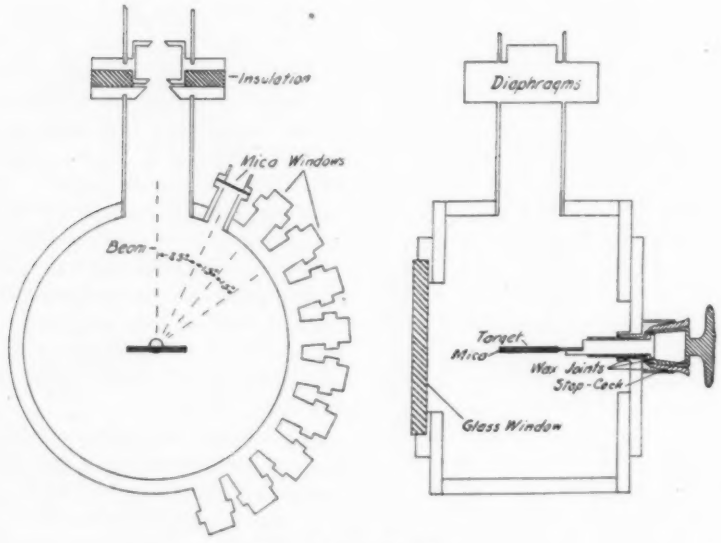

FIG. 3. Target chamber.

Tables I and II, in fact, the variations from mean yield are well within the limits of error, and are comparable in magnitude to the statistical fluctuations to be expected.

It is well to note that in determining the mean corresponding to a given voltage all the points are not of equal weight. This is true since, as was previously pointed out, the time of observation, and hence the number of disintegration products counted, varied from window to window. The statistical fluctuation, taken to be $\sqrt{N}$, where N is the total number of recorded alpha-particles, thus varies from one angle to the next. The magnitude of this fluctuation, expressed in percent, is shown for each point in the tables.

TABLE I.

Angle with Forward Direction of Beam	Proton Energy (kv)	Total Protons (microcoulombs)	Total Counts	Counts per Microcoulomb	% Statist. Fluct.	% Dev. from Mean
65 deg	220	174	370	2.13	5.21	4.46
80	220	184	415	2.25	4.90	0.45
95	220	162	382	2.36	5.13	5.36
110	220	384	856	2.23	3.41	0.45
140	220	399	894	2.24	3.34	0.00
Total all windows		1303	2917			
Mean for all windows				2.24		

TABLE II.

Angle with Forward Direction of Beam	Proton Energy (kv)	Total Protons (microcoulombs)	Total Counts	Counts per Microcoulomb	% Statist. Fluct.	% Dev. from Mean
35 deg	240	751	3006	4.00	1.83	4.99
50	240	329	1355	4.12	2.72	8.14
65	240	344	1262	3.66	2.82	3.94
80	240	720	2700	3.76	1.92	1.31
95	240	537	1955	3.64	2.26	4.46
110	240	352	1255	3.56	2.83	6.53
140	240	822	3171	3.86	1.78	1.31
Total all windows		3855	14704			
Mean for all windows				3.81		

TABLE III.

Angle with Forward Direction of Beam	Proton Energy (kv)	Total Protons (microcoulombs)	Total Counts	Counts per Microcoulomb	% Statist. Fluct.	% Dev. from Mean
35 deg	200	434	657	1.51	3.91	10.13
50	200	430	733	1.70	3.69	1.19
65	200	434	757	1.75	3.64	4.17
80	200	393	658	1.67	3.91	0.60
95	200	402	603	1.50	4.07	10.72
110	200	507	866	1.70	3.40	1.19
125	200	486	867	1.78	3.40	5.96
140	200	548	974	1.77	3.20	5.36
Total all windows		3634	6115			
Mean for all windows				1.68		

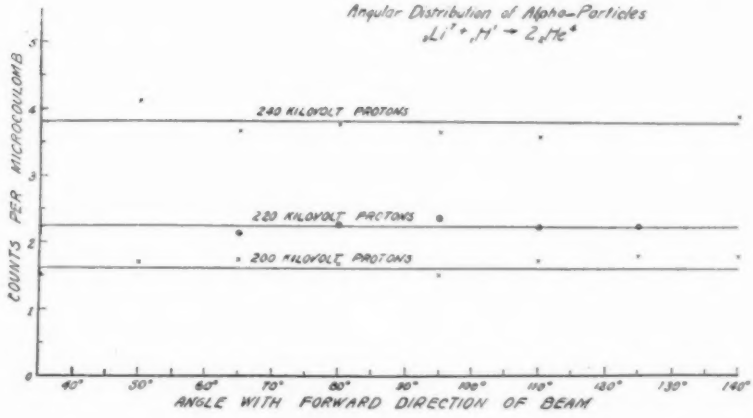

FIG. 4. Results.

The mean at a given voltage is obtained by adding all the counts taken at that voltage at all the windows and dividing the sum by the total number of microcoulombs. This automatically gives each point its proper weight.

DISCUSSION OF ERRORS

One of the main sources of error was the fluctuation of ion current. It was found quite difficult to keep the proton current, measured at the target, constant to better than 5 percent. The fluctuation may be traced to several causes, chief among which were the variations of accelerating voltage due to changing vacuum conditions in the accelerating tube and in the rectifier, and to variations of input to the source.

To keep the current as constant as possible one observer kept watch on the microammeter connected between the target and ground, reading the ion current and counteracting the changes by varying the voltage on the focusing electrode of the source. This was done by means of strings attached to a rheostat placed in the primary of the transformer supplying the focusing electrode voltage. This method of current control has the advantage that it tends to balance out in part the decrease or increase of voltage across the accelerating tube. However, on account of lag in the reaction of the observer to changes in the meter reading, errors in reading the meter, etc., the constancy of the current was at best no better than within 4 percent of the mean value. There were, in fact, brief periods during which the current would suddenly change by as much as 10 percent before the change could be detected and balanced out. Fortunately, the duration of such periods was short, and insofar as it was possible to recognize them the portions of the record corresponding to them were not counted.

The most important source of error, however, was variation of accelerating voltage, both in time and in angle. The latter variations occurred as a result of the shutting down of the analyzer magnet while the ionization chamber was being adjusted to a new position. The same value of magnetizing current was then reset for the new angle, and the assumption made that the voltage was correct when the ion beam attained its former position.[9] This assumption neglects the presence of hysteresis in the magnet iron, of course, but the lack of a convenient direct check on field strength at all times and the high quality of the magnet used made it desirable to run the risk of introducing error in this way. The maximum width of the hysteresis loop for the

[9] It may easily be shown that if the voltage is varied in such a way that the curvature of the ion path through the field remains the same, change in the voltage will be proportional to the change in field strength. Each particle will have a kinetic energy E, where

$$E = \tfrac{1}{2}mv^2 = m^2v^2/2m = \tfrac{1}{2}H^2\rho^2e^2, \qquad \text{since } H\rho = mv/e.$$

Thus for a constant value of curvature ρ and a particle of mass m and charge e

$$E = \text{const.} \times H^2; \qquad dE/E = 2dH/H$$

where H is the magnetic field.

magnet was found to be no more than 3 percent of the total field.

Voltage variations in time were due chiefly to changing vacuum conditions in the accelerating tube and in the rectifiers. Although frequent shut-downs were necessary to adjust the hydrogen leak and refill the cooling jacket of the source, care was taken to "break in" the tubes with voltage until vacuum conditions were fairly steady before resuming readings, since according to the results of Henderson[10] a change of voltage of 2½ percent at 250 kv results in a change of 6 percent in the number of disintegrations.

The stopping power of the windows in the target chamber was approximately 3 cm, while the distance from the windows to the ionization chamber was 1½ cm. The total stopping power of mica and air in the path of the alpha-particles was, accordingly, only 4½ cm. Since the range of the particles was 8.4 cm, slight variations in the thickness of the windows introduced no error in determining the number of particles reaching the ionization chamber.

In order to avoid variations due to the thickness of the target traversed by alpha-particles on their way to the window at which observations were being made, the target was always adjusted so that it occupied a symmetrical position with respect to the incident beam and the direction of observation. (See Fig. 5.) There is, therefore, no correction necessary for target penetration, since conditions are similar for all windows.

In our discussion thus far we have spoken of the target as though it had a perfectly smooth surface. Although this is, of course, not true, we have estimated that the error introduced by neglecting to consider the alpha-particles which may be absorbed by crystals of the salt is negligible.

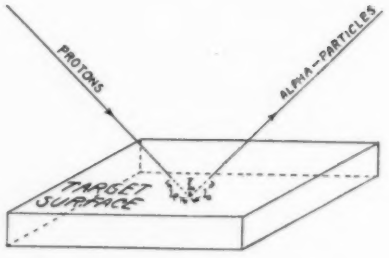

FIG. 5. Target penetration.

There still remains to be considered the effect of the change in size and shape of the ion spot on the target as the target is changed in position for the various windows. As the spot changes shape and becomes longer or shorter the solid angle of each of its elements as seen from the window of observation changes from one window to the next. This effect was calculated for the window at 35° and for the window at 140° from the incident beam. The result of the calculations showed the necessary correction to be negligible and of no importance for this range of angles and for a proton beam of ¼-inch diameter.

After considering the various sources of error and their relative importance we have concluded that the accuracy to be expected from these experiments is approximately eight percent. The results indicate that within these limits the emission of alpha-particles is random in direction.

The authors wish to express their appreciation to Professor G. Breit, who suggested the investigation and directed its earlier portions, and to Dr. W. H. Crew, and Messrs. R. Cortell, A. Roberts, and T. Zandstra for assistance in constructing the apparatus and taking the readings.

[10] M. C. Henderson, Phys. Rev. **43**, 98 (1933).

Erratum: Fine Structure of $D\alpha$ with Increased Resolution

ROBLEY C. WILLIAMS AND R. C. GIBBS, *Department of Physics, Cornell University* (Phys. Rev. **48**, 971 (1935))

IN the sixth line from the end the word *increased* should be changed to *decreased*. The conclusion that follows is correctly stated.

Band Spectra of BiBr, BiCl, BiF, and BiI in Absorption

FRANK MORGAN, *Mendenhall Laboratory of Physics, Ohio State University*

(Received August 3, 1935)

The band spectra of BiBr, BiCl, BiF, and BiI have been examined in absorption and a vibrational analysis made for each of the observed systems. For BiBr there are two systems for each of the isotopes Br^{79} and Br^{81} with origins at 4045.7A and 4869.1A. The lower frequency system degrades to the red, but the direction in which the other degrades is in doubt. In BiCl a band system lying between λλ3600 and 4000A has been found for each of the isotopes Cl^{35} and Cl^{37} in addition to the system at λλ4300–5500A reported by Saper. The vibrational analyses are confirmed by the respective isotope shifts. One band system between λλ4150 and 4900A for BiF and one between λλ4150 and 4300A for BiI have been observed and analyzed.

INTRODUCTION

EDER and Valenta[1] photographed the flame spectrum of various compounds of bismuth and found band systems lying in the region of λλ4300–6700A, which they ascribed to BiO. Their photographs also show a group of lines in the neighborhood of 3900A. Mecke and Guillery,[2] using previous data, arranged some of these bands in a Deslandres' scheme in which the constants correspond to those expected for BiO. Ghosh[3] rephotographed the bands lying between 4300 and 6700A in a flaming arc fed with metallic bismuth or bismuth trichloride and made a vibrational analysis of the observed heads. He attributed them to BiO. Saper[4] had previously studied the band system lying between 4300 and 5500A, having excited it by introducing bismuth trichloride vapor into active nitrogen His vibrational analysis of this band system is nearly identical with that given by Ghosh for the systems he assigned to BiO. The assignment of Saper is, however, reinforced by the fact that he observed an isotope shift in agreement with the expected shift for Cl=35 and Cl=37. Howell and Rochester[5] using a high frequency electrical discharge have produced emission band spectra in BiBr and BiF, but no analysis of the observed systems seems to have been made.

In view of the apparent disagreement between Saper and Ghosh and the meagerness of data and analysis of the band systems of the bismuth halides, the present investigation was undertaken.

[1] Eder and Valenta, *Atlas Typischer Spektren*.
[2] Mecke and Guillery, Physik. Zeits. **28**, 514 (1927).
[3] C. Ghosh, Zeits. f. Physik **86**, 241 (1933).
[4] Saper, Phys. Rev. **37**, 1710A (1931).
[5] Howell and Rochester, Univ. Durham Phil. Soc. Proc. **9**, 196 (1934).

EXPERIMENTAL

To obtain these absorption spectra, light from a 500-watt incandescent lamp was passed through the vapor under investigation in an electric furnace heated to a temperature ranging from 700°C to 1400°C and then focused on the slit of the spectrograph. The spectrograms were taken with four different types of spectrographs according to experimental needs. An E-1 Hilger quartz spectrograph was used essentially to explore the region under consideration and to determine suitable experimental conditions. Some of the measurements on the bands of bismuth chloride were made on photographic plates taken on a Hilger-185 quartz spectrograph. This instrument has a dispersion of about 9.5A/mm at 4500A and 7A/mm at 3900A. The lower frequency system of bismuth chloride was photographed in the first order of a 21-ft. concave grating with 30,000 lines to the inch, giving a dispersion of 1.25A/mm at 4500A. The other system in bismuth chloride was photographed both in the first and second order of this grating. The dispersion in the second order is 0.48A/mm at 3900A. The remainder of the spectrograms from which measurements were made were taken on a 10-ft. concave grating on a Littrow mounting. This instrument has a dispersion of about 5.7A/mm in the first order. Both the first and second orders were used.

A standard iron arc was used as a comparison spectrum and measurements of wave-lengths were made on a Geneva Society comparator.

Two types of electric furnaces were used, one a Hoskins carbon resistor furnace giving temperatures up to 1600°C, the other a Hoskins

resistance furnace with which temperatures up to 1000°C can be attained.

To get the band systems of BiBr, bromine was passed over molten bismuth in an iron tube in the resistance furnace heated to about 900°C. The tube was open to the air at atmospheric pressure.

The BiCl bands were obtained by heating solid $BiCl_3$ in an open iron or quartz tube in the resistance furnace until the temperature was sufficiently high to vaporize the bismuth trichloride and dissociate it to form BiCl. They were also obtained by heating metallic bismuth in one of these tubes to the desired temperature and passing pure chlorine gas over the molten metal. Similarly the bands of BiI were produced by heating bismuth and iodine together at a temperature of 600 to 700°C and the same band system was obtained when BiI_3 was heated to the necessary temperature.

To develop the band systems of BiF a higher temperature is required. Hence bismuth trifluoride was heated in the Hoskins carbon resistor furnace to a temperature of about 1200°C. At this temperature a well-defined band system is developed in absorption.

BiBr Bands

In BiBr two band systems have been observed for each of the two isotopes of bromine, Br = 79 and Br = 81. The intensities of the corresponding bands are nearly equal as might be expected from the fact that the abundance of the isotopes is essentially the same. The lower frequency band system for each of the isotopes degrades

TABLE I. *BiBr band systems.*

LESS REFRANGIBLE SYSTEM

v′	v″	I	νobs.	νobs. −νcalc.
1	11	0	18385.6*	−1.1
		0	404.6	−0.9
0	10	1	450.8*	−0.6
		1	469.2	−0.6
1	10	2	585.0*	−0.9
		2	603.4	0.3
0	9	4	652.2*	0.7
		4	668.1	−0.2
1	9	0	786.8*	0.8
		0	802.2	0.6
0	8	6	852.6*	−0.1
		6	867.5	−0.1
2	9	0	917.4*	−1.1
0	7	10	19054.6*	−0.1
		10	067.9	0.0
0	6	9	257.6*	−0.2
		9	268.6	−0.5
2	7	1	320.9*	−0.8
		1	330.5	−0.1
0	5	8	461.4*	−0.3
		8	470.5	−0.7
1	5	7	596.3*	0.1
		7	604.6	0.1
0	4	4	666.8*	0.1
		4	674.5	0.3
1	4	5	801.3*	0.3
		5	807.8	0.3
2	4	0	932.7*	−0.8
		0	937.6	−0.2
1	3	4	20007.6*	0.8
		4	012.6	1.1
0	2	0	079.1*	0.1
2	3	5	140.0*	1.1
		5	143.4	1.6
1	2	2	215.5	2.0
3	3	1	268.8*	1.6
2	2	8	347.8*	1.8
3	2	6	476.7*	2.8
2	1	5	555.3*	1.6
4	2	3	600.9*	−1.7
3	1	6	683.3*	−0.2
4	1	5	809.9*	0.0
5	1	4	930.8	1.1
4	0	2	21018.3*	−0.5
6	1	2	015.9	0.3
5	0	2	047.6	0.2
7	1	4	140.7*	−0.8
6	0	4	135.6	−1.8
7	1	1	163.1	−1.6
6	0	5	258.0*	−2.0
7	0	3	254.1	−0.9
8	0	5	372.5*	−0.8
9	0	5	365.7	−1.8
10	0	5	480.1*	−0.6
11	0	5	473.1	1.6
		4	582.4*	0.5
		4	574.2	−1.2
		3	678.1*	1.9
		3	670.4	0.8
		1	763.1*	0.2
		1	756.0	−0.3

MORE REFRANGIBLE SYSTEM

v′	v″	I	νobs.	νobs. −νcalc.
6	10	00	24209.3*	0.9
		00	213.8	0.6
7	11	00	246.9*	−0.6
		00	251.6	−0.2
2	4	2	431.8*	1.6
		2	434.2	1.4
3	5	2	480.0*	0.5
		2	482.1	1.2
4	6	1	525.3*	−0.2
		1	527.0	−0.2
0	1	0	530.0*	−0.3
5	7	1	568.3*	−0.4
		1	569.6	−0.4
1	2	2	585.0*	0.5
		2	585.9	0.2
6	8	0	608.5*	−0.4
		0	609.6	−0.4
2	3	2	636.2	−0.2
3	4	2	683.9*	0.0
4	5	1	728.5	−0.6
0	0	10	738.6*	0.0
5	6	2	770.8*	−0.5
1	1	10	792.1*	0.3
6	7	3	810.5*	−0.4
2	2	9	842.0*	−0.1
7	8	2	846.2*	−0.7
8	9	1	877.8*	−2.3
3	3	8	889.1*	0.2
4	4	7	933.0*	−0.5
		7	931.3	−0.3
5	5	5	974.3*	−0.6
		5	972.4	−0.2
1	0	5	999.8*	−0.2
		5	997.0	−0.5
6	6	3	25012.7*	−0.4
		3	010.6	−0.2
7	7	overlapped by (2,1)		
2	1	7	049.2*	−0.2
		7	046.0	−0.2
8	8	1	078.7*	−1.9
		1	076.2	−2.1
3	2	6	095.3*	−0.4
		6	091.9	−0.3
4	3	5	138.6*	−0.6
		5	135.1	−0.1
5	4	4	179.3*	−0.1
		4	175.4	0.1
6	5	3	216.8*	0.1
		3	212.7	0.2
7	6	2	251.0*	−0.1
		2	246.8	0.0
2	0	3	257.3*	−0.3
		3	252.5	−0.3
8	7	0	280.1*	−0.3
		0	276.9	−1.3
3	1	5	303.0*	0.0
		5	297.8	0.2
4	2	6	345.3*	0.0
		6	339.9	0.1
5	3	6	385.0*	0.3
		6	379.2	0.3
6	4	6	421.5*	0.4
		6	415.6	0.4
7	5	5	455.0*	0.3
		5	449.1	0.6
8	6	4	484.2*	−0.8
		4	478.1	−1.0
3	0	1	511.1*	−0.1
		1	504.5	0.3
4	1	2	552.9*	0.3
		2	545.6	0.4
5	2	3	591.6*	0.5
		3	584.1	0.6
6	3	4	627.3*	0.8
		4	619.5	0.7
7	4	4	659.7*	0.6
		4	652.1	0.9
8	5	3	688.1*	−0.5
		3	680.5	−0.3
5	1	0	798.9*	0.5
		0	789.9	1.0
6	2	1	834.2*	1.3
		1	825.0	1.4
7	3	2	865.7*	1.2
		2	856.1	1.3
8	4	2	892.9*	−0.1
		2	883.4	−0.1

* The bands marked with an (*) are bands due to $BiBr^{79}$.

toward the red. It was not possible to determine unambiguously in which direction the bands of the other system degrade. In some cases they appear to degrade to the red, but ordinarily they have the appearance of lines. This uncertainty may arise because of branches that rise almost vertically on a Fortrat diagram. According to the rule of Birge and Mecke they should degrade toward the violet since $\omega_e' > \omega_e''$.

The observed wave numbers, the difference between the observed and calculated wave numbers, the estimated intensities, and the vibrational quantum numbers are recorded in Table I for the bands corresponding to each of the isotopes of bromine.

These band heads are represented within the experimental error by the following formulas:

For the lower frequency system:

$$\text{BiBr}^{79}: \nu = 20{,}532.0 + [135.91u' - 0.534u'^2 - 0.1030u'^3] - [209.50u'' - 0.466u''^2];$$
$$\text{BiBr}^{81}: \nu = 20{,}532.0 + [134.69u' - 0.524u'^2 - 0.1002u'^3] - [207.61u'' - 0.458u''^2],$$

where $u' = v' + \frac{1}{2}$ and $u'' = v'' + \frac{1}{2}$.

For the higher-frequency system:

$$\text{BiBr}^{79}: \nu = 24{,}710.9 + [265.34u' - 1.956u'^2] - [209.17u'' - 0.469u''^2];$$
$$\text{BiBr}^{81}: \nu = 24{,}710.9 + [262.95u' - 1.921u'^2] - [207.29u'' - 0.461u''^2],$$

where $u' = v' + \frac{1}{2}$ and $u'' = v'' + \frac{1}{2}$.

The constants for $BiBr^{81}$ were derived from the constants for $BiBr^{79}$ from the well-known formula,

$$G(v) = \rho\omega_e(v+\tfrac{1}{2}) - \rho^2 x_e\omega_e(v+\tfrac{1}{2})^2 + \rho^3 y_e\omega_e(v+\tfrac{1}{2})^3 \cdots,$$

for the vibrational terms of different isotopes, where ρ^2 is the ratio of the reduced masses of $BiBr^{79}$ and $BiBr^{81}$. It will be observed from the vibrational formula for the system toward the red that the coefficient of the third-degree term of the excited level is large. It has been necessary to introduce this third-degree term with a large coefficient to take account of the rapid convergence of the band heads (Fig. 1b). That this convergence is very rapid is immediately evident from the second-order grating plates. The convergence point, as calculated from the band-head formula, is at about 4520A.

TABLE II. *Intensities of BiBr bands.*

Less Refrangible													More Refrangible											
v' \ v''	0	1	2	3	4	5	6	7	8	9	10	11	v' \ v''	0	1	2	3	4	5	6	7	8	9	10	11
0			0		4	8	9	10	6	4	1		0	10	0										
1			2	4	5	7				0	2	0	1	5	10	2									
2		5	8	5	0			1		0			2	3	7	9	2	2							
3		6	6	1									3	1	5	6	8	2	2						
4	2	5	3										4		2	6	5	7	1	1					
5	4	4											5		0	3	6	4	5	2	1				
6	5	2											6			1	4	6	3	3	3	0		00	
7	5	1											7				2	4	5	2	*	2			03
8	5												8					2	3	4	0	1	1		
9	4																								
10	3																								
11	1																								

* Overlapped by (2,1).

The intensities of the band heads lie on well-defined Franck-Condon parabolas (Table II). For the system lying toward the red the parabola is much more open than for the other system as might be expected from the magnitude of the constants. The matrix scheme for the more refrangible system closely resembles that given by M. Wehrli and E. Miescher[6] for the indium halides.

BiCl BANDS

For bismuth chloride two band systems were also observed for each of the isotopes of chlorine, Cl = 35 and Cl = 37. One of these systems, the one lying toward the red, has already been reported and analyzed by Saper.[4] The other seems not to have been previously observed. The intensity of the bands for $BiCl^{35}$ is about three times the intensity of the corresponding bands for $BiCl^{37}$ as might be expected from the abundance of the isotopes. As in the band systems due to bismuth bromide the longer wave-length system degrades toward the red and the behavior of the other band system in this respect is uncertain.

Table III gives the observed wave numbers, the differences between observed and calculated wave numbers, the estimated intensities and the vibrational quantum numbers for the band systems due to $BiCl^{35}$ and $BiCl^{37}$.

Within experimental error the vibrational analyses of these heads are given by the following formulas:

For the longer wave-length system:

[6] M. Wehrli and E. Miescher, Helv. Phys. Acta. **7**, 298 (1934).

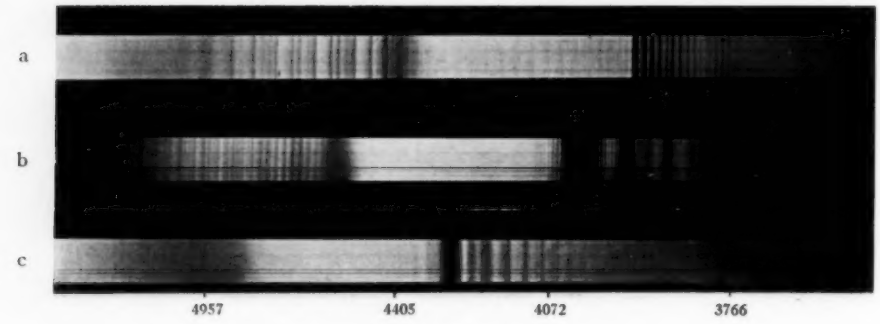

FIG. 1. Comparison of spectra: (a) BiCl; (b) BiBr; (c) BiI. Between λλ4500 and 4570 in (b), the absorption appears to be continuous. The band heads of the longer wave-length system converge to a point in this region. In (c), the bands to the extreme left are due to diatomic bismuth. The same bands appear in the case of BiBr, BiCl, or BiF, but at progressively higher temperatures. It is possible, of course, that there may be BiI bands mixed in with the Bi_2 bands.

TABLE III. *BiCl band systems.*

Less Refrangible System										More Refrangible System									
v'	v''	I	$\nu_{obs.}$	$\nu_{obs.}-\nu_{calc.}$	v'	v''	I	$\nu_{obs.}$	$\nu_{obs.}-\nu_{calc.}$	v'	v''	I	$\nu_{obs.}$	$\nu_{obs.}-\nu_{calc.}$	v'	v''	I	$\nu_{obs.}$	$\nu_{obs.}-\nu_{calc.}$
3	13	0	18552*	−2	0	2	8	146.7*	0.2	1	3	0	25024.9*	0.7	3	1	3	399.7*	1.2
4	13	0	754*	0			3	162.2	−0.5	2	4	0	113.5*	1.4			2	379.0	0.4
3	12	1	837*	−1	1	2	7	361.5*	−0.3	3	5	0	197.5*	3.0	9	8	00	441.5*	−0.6
2	11	1	917*	0			3	372.1	0.0	4	6	0	273.8*	2.3	4	2	4	467.9*	0.0
5	13	1	947*	−3	0	1	5	450.8*	−0.2	1	2	0	328.6*	2.5			1	446.2	−0.8
1	10	1	994*	0			2	459.5	0.3	5	7	0	344.4*	1.1	5	3	4	530.9*	−1.1
4	12	1	19037*	1	3	3	4	475.4*	0.9	2	3	1	415.7*	3.6			2	508.3	−2.2
3	11	0	124*	1	2	2	0	572.1*	0.2			0	417.2	2.8	6	4	3	588.7*	−2.0
2	10	2	204*	0			0	576.2	−1.4	3	4	0	494.9*	2.3			1	565.6	−3.2
		1	262	−1	1	1	10	666.0*	−0.3	0	0	10	539.9*	−0.6	7	5	3	642.1*	−2.1
1	9	2	284*	0			3	670.4	0.9			5	537.9	−1.4			1	618.4	−3.9
4	11	0	322*	0	0	0	1	756.2*	−1.2	4	5	1	568.5*	0.7	8	6	3	690.7*	−1.1
0	8	1	360*	1	2	1	10	876.4*	0.0	1	1	2	632.0*	2.0			1	666.8	−0.3
3	10	2	410*	0	1	0	5	972.3*	−0.4			4	628.1	1.1	3	0	2	705.9*	1.7
2	9	2	494*	0	3	1	1	22081.7*	0.0	5	6	0	636.6*	−0.9			0	678.0	0.4
		1	548	2			0	071.4	−4.5	6	7	1	702.7*	−0.7	9	7	2	733.8*	−0.7
1	8	2	575*	0	2	0	7	182.8*	0.0			1	700.2	−0.3			1	710.4	−2.6
0	7	2	653.5*	0.8			2	176.7	2.3	2	2	8	716.4*	2.4	10	8	1	770.5*	−1.1
		1	702.2	0.5	3	0	10	388.1*	0.0			4	710.9	1.5			0	747.5	−3.3
2	8	3	785.0*	0.1			4	374.5	−0.7	7	8	0	759.1*	−1.9	4	1	2	772.1*	0.3
5	10	1	805*	−1	5	1	2	476.0*	−1.5			0	755.4	−3.7			1	743.3	−0.6
1	7	3	868.3*	−0.4	4	0	8	588.4*	0.4	3	3	7	794.0*	1.3	5	2	2	833.1*	−0.8
		1	911.2	−0.8			3	571.5	0.2			4	787.2	0.4			1	803.6	−1.9
4	9	0	898*	−1	6	1	2	665.2*	0.8	8	9	0	812.9*	−1.8	6	3	2	889.2*	−1.5
0	6	4	948.2*	0.6			1	647.1	−2.7			0	808.4	−4.3			1	859.2	−3.0
		1	991.1	1.1	8	2	1	727.0*	0.7	4	4	6	865.8*	−0.2	7	4	2	940.6*	−1.7
5	9	1	20095*	0			0	706.6	−4.5			3	858.0	−0.9			1	910.3	−2.3
1	6	2	163.5*	0.6	5	0	4	783.4*	−0.5	5	5	2	932.4	−1.4	8	5	2	987.2*	−0.9
4	8	1	191*	0			1	760.1	−2.6	1	0	6	937.0*	1.3			1	956.7	−2.8
0	5	6	244.5*	0.1	7	1	3	849.6*	−2.5			3	926.2	0.6	9	6	2	27028.7*	0.0
		3	280.6	0.3			1	828.1	−3.5	6	6	1	993.8*	−2.4			1	26998.5	−2.1
6	9	0	284.3*	0.3	9	2	1	906.0*	5.0			0	984.1	−4.0	10	7	1	27063.2*	−0.8
0	4	7	543.1*	0.0			0	882.1	−1.3	2	1	5	26020.0*	2.1	4	0	00	477.7*	0.2
		3	572.2	−0.1	6	0	3	971.1*	−1.7	7	7	2	007.6	1.4	5	1	1	137.3*	−0.5
3	6	0	578.3*	0.0			1	946.0	−3.1			3	051.5*	−1.9			00	100.7	−1.6
2	5	1	669.6*	−0.2	8	1	2	23031.0*	0.2	3	2	1	041.1	−3.8	6	2	1	191.6*	−1.0
0	3	9	843.9*	0.1			0	005.7	−2.9			5	096.0*	0.4			0	154.4	−2.6
		3	866.0	−0.1	10	2	1	071.3*	0.6	8	8	2	082.2	0.4	7	3	1	240.8*	−1.6
2	4	1	969.8*	1.3	7	0	1	158.3*	−0.2			1	103.8*	−1.4			0	203.8	−2.1
1	3	2	21058.3*	−0.8			0	125.1	−5.8	4	3	4	166.0*	0.0	8	4	1	27285.7*	−0.6
		1	074.6	−1.8	9	0	1	512.6*	0.7			2	151.2	−0.9			0	248.3	−2.5
										5	4	3	26230.7*	−2.1	9	5	2	325.4*	0.4
												2	215.0	−2.5			0	288.3	−1.7
										6	5	3	290.5*	−2.0	10	6	1	358.0*	−0.2
												1	274.2	−3.3	8	3	1	586.0*	−0.3
										2	0	4	325.7*	2.1			00	543.3	−0.7
												2	306.3	1.7	9	4	0	623.7*	0.5
										7	6	2	345.7*	−1.9			00	579.8	−1.5
												1	328.9	−3.6	10	4	00	654.7*	0.2
										8	7	0	396.6*	−1.0					

* The bands marked with an asterisk are $BiCl^{35}$.

$$BiCl^{35}: \nu = 21{,}801.8 + [220.3u' - 2.50u'^2] - [308.4u'' - 0.96u''^2];$$

$$BiCl^{37}: \nu = 21{,}801.8 + [215.1u' - 2.38u'^2] - [301.2u'' - 0.92u''^2].$$

For the shorter wave-length system:

$$BiCl^{35}: \nu = 25{,}493.7 + [402.55u' - 3.650u'^2] - [307.66u'' - 0.954u''^2]:$$

$$BiCl^{37}: \nu = 25{,}493.7 + [393.12u' - 3.481u'^2] - [300.45u'' - 0.910u''^2],$$

where $u' = v' + \frac{1}{2}$ and $u'' = v'' + \frac{1}{2}$.

As in the case of the BiBr bands, the coefficients for the equation for $BiCl^{37}$ were calculated from theory involving the isotope shift.

The constants for the longer wave-length system differ only slightly from those reported by Saper.[4] They also differ only slightly from those given by Ghosh[3] for BiO if the origin used by Ghosh is properly displaced. In view of the agreement between these results and those of Saper, the similarity of this band system to the corresponding band systems of BiBr and BiF, and the satisfactory confirmation of isotope theory, it seems that Ghosh has incorrectly assigned this band system to BiO. In this connection it may be of interest to recall that Barratt[7] has shown that much confusion may arise in the identification of band systems because of the presence of chlorine as an impurity.

It is evident that the deviation of the calculated from the observed wave numbers for the higher frequency system is much greater for BiCl than for BiBr. This deviation apparently originates in perturbation of the upper levels because in the Deslandres' arrangement the values of $\Delta G''$ are quite consistent with what might be expected while $\Delta(\Delta G')$ first decreases and then increases as one goes to higher values of v'. The constants for the upper level are only average ones and only approximately fit the data. The error in observed frequencies should be less in this system than in any of the others because the heads were relatively sharp and the dispersion in the second order was only a little more than 3 cm^{-1}/mm. There is also a rather consistent, but unexplained, deviation between the observed and calculated isotope displacement of the bands of this system.

Even in the second order of the 21-ft. grating, no rotational structure was resolved. The bands appeared essentially as lines somewhat diffuse on the red side.

The intensities of band heads of both systems lie on Franck-Condon parabolas quite similar to those shown in Table II for BiBr.

[7] Barratt, Trans. Faraday Soc. **25**, 758 (1929).

BiF Bands

With bismuth fluoride (BiF), one strong and one weak band system were found. The weaker system lying toward the violet was not developed sufficiently well for measurement and analysis. The other system lying toward the red was similar to the corresponding system found for BiBr and BiCl except for the absence of the bands due to isotopes. Like the bands due to BiBr and BiCl, these bands degrade to the red.

The data for this system together with the vibrational analysis are recorded in Table IV. The band heads are represented by the equation:

$$\nu = 22{,}958.5 + [383.6u' - 3.28u'^2] - [512.0u'' - 2.25u''^2],$$

where $u' = v' + \frac{1}{2}$ and $u'' = v'' + \frac{1}{2}$.

TABLE IV. *BiF bands.*

v'	v''	I	$\nu_{obs.}$	$\nu_{obs.} - \nu_{calc.}$	v'	v''	I	$\nu_{obs.}$	$\nu_{obs.} - \nu_{calc.}$
3	7	00	20548.0	0.5	4	4	00	360.2	0.3
2	6	00	664.6	0.5	0	1	7	386.5	−0.1
1	5	00	780.3	1.6	3	3	4	494.4	−2.1
4	7	0	906.3	1.4	2	2	3	630.6	−0.5
3	6	1	21027.0	−1.0	0	0	10	894.2	0.1
2	5	2	148.5	−0.5	3	2	0	992.6	−2.5
1	4	3	268.2	0.1	2	1	5	23132.9	−1.2
0	3	3	385.1	0.0	1	0	9	271.2	0.1
3	5	0	512.3	−0.7	4	2	4	351.2	−1.2
2	4	4	637.4	−1.2	3	1	8	497.2	−0.8
1	3	5	761.8	−0.3	2	0	9	641.2	−0.3
0	2	6	883.4	−0.2	5	2	1	706.9	3.7
2	3	000	22134.6	2.0	4	1	1	854.7	−0.7
1	2	4	260.3	−0.3	3	0	4	24003.8	−1.6

BiI Bands

With bismuth iodide only one band system was observed. It corresponds to the system lying farther toward the violet in the other bismuth halides. As in the corresponding system in BiBr and BiCl the direction in which the bands degrade is uncertain.

It might be expected that there should be another system corresponding to the longer

TABLE V. *BiI bands.*

v'	v''	I	$\nu_{obs.}$	$\nu_{obs.}-\nu_{calc.}$	v'	v''	I	$\nu_{obs.}$	$\nu_{obs.}-\nu_{calc.}$
4	6	0	23202.0	0.9	4	4	4	522.3	0.2
5	7	0	220.5	−5.2	1	0	4	601.3	−0.4
0	1	1	242.5	0.0	2	1	4	631.1	−0.1
1	2	2	275.5	−0.2	3	2	3	658.8	0.3
2	3	4	308.5	2.0	4	3	2	683.9	0.4
3	4	4	335.2	0.1	5	4	0	706.9	0.6
4	5	4	361.5	0.2	2	0	2	794.5	−0.1
0	0	10	406.1	0.1	3	1	2	821.6	−0.6
1	1	9	438.3	−0.1	4	2	1	845.8	0.3
2	2	6	468.5	0.0	5	3	0	864.0	−3.7
3	3	4	496.6	0.1	4	1	0	24008.2	0.0

wave-length bands of BiBr and BiCl, but such a system was not observed. Judging from the way this system shifts in going from BiF to BiCl to BiBr, it would be expected in BiI at wave-lengths greater than 4500A, but if it appeared in that region it would be completely masked by the strongly developed diatomic bismuth bands. It may be that BiI is too unstable at the temperature used in these experiments to obtain this system in absorption.

Table V, together with the following equation, gives the data and vibrational analysis of this system:

$$\nu = 23{,}388.9 + [198.6u' - 1.44u'^2] - [163.9u'' - 0.31u''^2],$$

where $u' = v' + \frac{1}{2}$ and $u'' = v'' + \frac{1}{2}$.

The distribution of intensities is represented by a Franck-Condon parabola closely resembling the parabola for the corresponding system in BiBr and BiCl.

DISCUSSION OF RESULTS

Vibrational constants

According to the rule of Rosen[8] $\omega_e''^2 Z_1 Z_2$ should be constant for these halides where Z_1 and Z_2 are the atomic numbers of the atoms in the molecule, and according to Mecke[9] $\omega_e''^2 \mu (Z_1 + Z_2)$ is constant for molecules of this type, where μ is the reduced mass of the molecule.

TABLE VI.

MOLECULE	$\mu 10^{24}$	ω_e''	$\omega_e''^2 Z_1 Z_2 10^{-7}$	$\omega_e''^2 \mu (Z_1+Z_2)\,10^{24}$
BiF	28.7	512.0	19.6	6.9
BiCl	50.0	308.0	13.5	4.8
BiBr	95.3	209.4	12.8	4.9
BiI	130.2	163.9	11.8	4.8

[8] B. Rosen, Naturwiss. **14**, 978 (1926).
[9] R. Mecke, Zeits. f. Physik **42**, 390 (1927).

From Table VI it is evident that $\omega_e''^2 Z_1 Z_2$ decreases with increasing molecular weight and that $\omega_e''^2 \mu (Z_1 + Z_2)$ is nearly constant if BiF is excluded.

Dissociation energies

It is not in general possible to calculate the dissociation energies of these halides from the vibrational constants, because the band systems do not converge rapidly enough. In the case of the longer wave-length band system in BiBr the convergence of the excited levels is sufficiently rapid to permit the necessary extrapolations to be made with some accuracy. Both band systems in BiCl converge very slowly so that long extrapolations are necessary and the accuracy of the calculated dissociation energies is small. Table VII shows the dissociation energies for BiBr and

TABLE VII.

BiBr			BiCl		
LEVEL	DISSOCIATION* ENERGY D (volts)	$D-Dz$	LEVEL	DISSOCIATION* ENERGY D (volts)	$D-Dz$
C	4.1	1.2	C	4.5	1.5
B	2.7	−0.2	B	3.3	0.3
X	2.9	0	X	3.0	0
ATOMIC EXCITATION			ATOMIC EXCITATION		
PROBABLE PRODUCTS	ENERGY** (volts)		PROBABLE PRODUCTS	ENERGY** (volts)	
$Br(^2P^\circ_{3/2})+Bi(^2D^\circ_{5/2})$	1.9		$Cl(^2P^\circ_{3/2})+Bi(^2D^\circ_{5/2})$	1.9	
$Br(^2P^\circ_{3/2})+Bi(^2D^\circ_{3/2})$	1.4		$Cl(^2P^\circ_{3/2})+Bi(^2D^\circ_{3/2})$	1.4	
$Br(^2P^\circ_{1/2})+Bi(^4S^\circ_{3/2})$	0.45		$Cl(^2P^\circ_{1/2})+Bi(^4S^\circ_{3/2})$	0.1	
$Br(^2P^\circ_{3/2})+Bi(^4S^\circ_{3/2})$	0		$Cl(^2P^\circ_{3/2})+Bi(^4S^\circ_{3/2})$	0	

* For states C and B, $D = D' + E_{mole.}$
** Calculated from values given in *Atomic Energy States* by Bacher and Goudsmit.

BiCl calculated in the usual way[10] from the vibrational constants. Two of these atomic energy differences, *viz.*, 1.2 volts for BiBr and 1.5 volts for BiCl, suggest that in these cases the dissociation products are $Br(^2P^\circ_{3/2})+Bi(^2D^\circ_{3/2})$ and $Cl(^2P^\circ_{3/2})+Bi(^2D^\circ_{3/2})$, respectively, although the more probable[11] energy difference would be 1.9 volts if the $^2D^\circ_{5/2}$ state of bismuth is more probable than the $^2D^\circ_{3/2}$ state.

The author wishes to express his appreciation to Professor Alpheus W. Smith and Dr. R. V. Zumstein for the valuable advice given in the course of this investigation.

[10] Jevons, *Band Spectra of Diatomic Molecules.*
[11] G. M. Almy and F. M. Sparks, Phys. Rev. **44**, 365 (1933).

Absorption Spectra of PbF, PbCl and PbBr

FRANK MORGAN, *Mendenhall Laboratory of Physics, Ohio State University*

(Received October 30, 1935)

A vibrational analysis has been made of absorption band systems due to PbF, PbCl, and PbBr. A single system of double-headed bands lying between λλ4100 and 5300A has been observed for PbF. The separation of the heads is nearly constant. In PbCl a band system with the origin at 4571.8A has been found for each of the isotopes Cl^{35} and Cl^{37}. Similarly a system of bands between λλ4400 and 5400A has been observed for each of the isotopes Br^{79} and Br^{81}. The vibrational analyses are confirmed by the respective isotope shifts. All the bands degrade to the red.

BARRATT[1] has reported, without analysis, absorption spectra which he attributed to lead chloride. Howell and Rochester[2] have produced emission band spectra in PbF and PbBr by the use of a high frequency electrical discharge, but apparently they did not make a vibrational analysis. No other observations on the band spectra of lead halides seem to have been recorded.

To obtain the band spectra of the lead halides in absorption, the lead halide under investigation was placed in an open iron or graphite tube about 30 cm in length and heated in an electric resistance furnace to such a temperature that the band system was well developed when light from a 500-watt incandescent lamp was passed through the column of vapor. Since PbF, PbCl, and PbBr do not exist as stable chemical compounds, it was necessary to introduce PbF_2, $PbCl_2$, or $PbBr_2$ into the furnace and heat it to a temperature at which it dissociates into the diatomic halide. The PbCl and PbBr systems were well developed at about 900°C, while a temperature of 1500°C was found more suitable for PbF. In the case of lead chloride and lead bromide the band systems were also developed by passing chlorine or bromine, respectively, over molten lead in the electric furnace.

Preliminary observations were made on an E-1 quartz spectrograph, but all measurements were made from spectrograms taken on a 10-ft. concave grating which has a dispersion of 2.72A/mm in the second order. Both first- and second-order plates were measured in each case.

[1] Barratt, Trans. Faraday Soc. **25**, 758 (1929).
[2] Howell and Rochester, Univ. Durham Phil. Soc. Proc. **9**, 126 (1934).

PbF BANDS

In the case of PbF, a double-headed band system, degrading toward the red, was observed. The double heads are separated by about 7 cm^{-1}. Because of overlapping fine structure only one head has been measured in most cases, but where two heads of a given band have been measured the observed wave numbers of both have been tabulated. The vibrational quantum numbers, the estimated intensities, the observed wave numbers, and the difference between the observed and calculated wave numbers for the higher frequency heads are given in Table I. This table also shows the observed wave numbers

TABLE I. *Analysis of PbF band heads.*

v'	v''	I	$\nu_{obs.}$	$\nu_{obs.}-\nu_{calc.}$	v'	v''	I	$\nu_{obs.}$	$\nu_{obs.}-\nu_{calc.}$
8	14	00	18945.4	−4.7	4	5	2	21600.8	0.0
7	13	0	19019.9	−3.6	8	8	0	676.3	0.9
5	11	0	171.7	−1.4	3	4	1	702.8	1.7
3	9	00	328.4	1.5	1	2	5	905.5	0.6
8	13	0	388.9	−3.9	0	1	10	22008.4	−0.1
7	12	0	468.0	−2.6	4	4	2	085.5	0.7
6	11	1	548.0	−1.6	3	3	5	189.4	−0.3
5	10	1	628.1	−1.5	2	2	5	295.1	−0.5
3	8	1	792.9	0.3	1	1	1	405.0	2.3
2	7	0	877.5	1.9	5	4	2	465.7	0.8
7	11	0	921.0	−1.5	0	0		502.9*	
1	6	0	961.1	1.3	0	0	10	510.4	−0.4
6	10	1	20005.2	−0.9	4	3		568.8*	
5	9	1	089.8	−0.9	4	3	1	574.6	1.3
4	8	2	176.5	0.2	7	5	0	728.5	−1.9
3	7	2	263.0	0.2	2	1	5	793.6	0.2
8	11	0	291.3	−0.8	1	0		897.7*	
2	6	2	351.0	0.5	1	0	10	904.8	−0.2
1	5	1	440.0	0.8	4	2	3	23068.6	2.1
0	4	1	529.8	0.8	3	1		174.0*	
5	8	0	556.2	−0.2	3	1	6	180.8	0.2
4	7	1	646.5	0.0	2	0		288.3*	
9	11	0	658.1	0.0	2	0	8	295.6	−0.1
3	6	3	737.7	0.0	5	2	2	447.7	1.1
2	5	5	830.2	0.3	4	1		557.3*	
1	4		916.2*		4	1	4	564.6	0.3
1	4	6	923.6	0.4	3	0	5	682.9	0.0
0	3		21010.0*		6	2	1	825.1	2.0
0	3	5	017.8	0.2	5	1		938.4*	
3	5	1	216.0	−1.1	5	1	3	945.4	1.0
2	4	4	313.9	0.0	4	0	1	24068.0	1.4
1	3		404.0*		8	3	0	074.7	2.2
1	3	7	411.9	0.1	7	2	0	199.9	3.8
0	2		502.3*		6	1		315.4*	
0	2	8	510.7	0.0	6	1	0	322.8	1.9

* Indicates lower frequency head of band.

and the vibrational quantum numbers of the lower frequency band heads which could be measured. These lower frequency heads have been marked with an asterisk. The higher frequency heads are represented by the formula:

$$\nu = 22{,}565.2 + [397.8u' - 1.77u'^2] - [506.9u'' - 2.29u''^2],$$

where $u' = v' + \frac{1}{2}$ and $u'' = v'' + \frac{1}{2}$. They appear to be of greater intensity than the lower frequency ones. The intensity distribution of these bands is shown in Table II.

PbCl Bands

One system for each of the isotopes of chlorine, Cl^{35} and Cl^{37}, has been observed for PbCl. The bands degrade to the red and in some cases appear to be double-headed with a very small separation between the two heads. The vibrational analysis of these band heads is given by the formulas:

$$PbCl^{35}: \nu = 21{,}866.9 + [228.6u' - 0.76u'^2 - 0.006u'^3] - [304.2u'' - 0.89u''^2];$$

$$PbCl^{37}: \nu = 21{,}866.9 + [223.3u' - 0.72u'^2 - 0.006u'^3] - [297.1u'' - 0.85u''^2],$$

where $u' = v' + \frac{1}{2}$ and $u'' = v'' + \frac{1}{2}$. The constants of the second equation have been calculated from those of the first equation by the use of the formula $G^i(v) = \rho\omega_e(v+\frac{1}{2}) - \rho^2 x_e\omega_e(v+\frac{1}{2})^2 + \cdots$, where $G^i(v)$ is the vibrational term for the isotope and ρ is the square root of the ratio of the reduced masses of the two molecules. The analysis of the PbCl bands is recorded in Table III and the distribution of estimated intensities for the $PbCl^{35}$ bands is shown by Table IV. The ratio of the intensities of the bands of $PbCl^{35}$ and $PbCl^{37}$ is approximately the ratio (76 : 24) of the abundance of the chlorine isotopes.

PbBr Bands

As in the case of PbCl, one system of bands has been observed for each of the isotopes of bromine. These bands also degrade to the red and the band-intensity curve is a parabola

TABLE II. *Intensities of bands in PbF.*

v' \ v''	0	1	2	3	4	5	6	7	8	9	10	11	12	13	14
0	10	10	8	5	1										
1	10	1	5	7	6	1	0								
2	8	5	5		4	5	2	0							
3	5	6		5	1	1	3	2	1	00					
4	1	4	3	1	2	2		1	2						
5	0	3	2		2				0	1	1	0			
6		0	1								1	1			
7			0			0						0	0	0	
8				0					0			0		0	0
9												0			

TABLE IV. *Intensities of $PbCl^{35}$ bands.*

v' \ v''	0	1	2	3	4	5	6	7	8	9	10
0	4	2	4	8	7	4	2	1	0		
1	2	8	10	3	00		1	2	2	0	
2	6	10	4		1	2	0		0	1	0
3	5	7		1	2			0	0		
4	6	2		00						0	
5	7		1								
6	4		2								
7	3	0	0								
8	2	1									
9	1	1									
10	1	2									
11	1	3	0								
12		1	1								
13		0	0								

TABLE III. *Analysis of PbCl bands.*

v'	v''	I	$\nu_{obs.}$ ($PbCl^{35}$)	$\nu_{obs.} - \nu_{calc.}$	$\nu(PbCl^{35}) - \nu(PbCl^{37})$ Obs.	Calc.	v'	v''	I	$\nu_{obs.}$ ($PbCl^{35}$)	$\nu_{obs.} - \nu_{calc.}$	$\nu(PbCl^{35}) - \nu(PbCl^{37})$ Obs.	Calc.	v'	v''	I	$\nu_{obs.}$ ($PbCl^{35}$)	$\nu_{obs.} - \nu_{calc.}$	$\nu(PbCl^{35}) - \nu(PbCl^{37})$ Obs.	Calc.
2	10	0	19338.3	0.7			2	4	1	21083.8	1.1	−18.1	−18.1	4	0	6	727.4	−0.4	19.9	19.6
1	9	0	399.1	0.6			1	3	3	154.8	0.5	−16.1	−16.5	7	2	0	781.8	0.6		
0	8	0	459.9	0.3			0	2	4	226.2	0.1	−14.4	−14.8	5	0	7	949.1	0.8	23.9	24.4
2	9	1	624.8	0.8			3	4	2	306.9	0.4	−11.2	−13.1	7	1	0	23083.4	1.6		
1	8	2	687.2	0.5	−49.0	−49.6	1	2	10	453.1	−0.1	−10.4	−9.6	6	0	4	168.1	1.0	30.1	29.2
0	7	1	749.0	−0.6	−47.3	−48.3	0	1	2	528.0	1.3	−5.1	−7.9	8	1	1	297.4	0.3		
2	8	0	911.9	−0.3			3	3	1	603.8	0.2			7	0	3	384.8	0.6	33.5	33.9
1	7	2	977.2	0.5	−43.7	−43.1	2	2	4	679.0	−0.3	−5.4	−4.4	9	1	1	511.0	0.4		
0	6	3	20041.5	0.2	−42.4	−41.8	1	1	8	753.2	−0.6	−3.0	−2.7	8	0	2	600.2	0.7	38.3	38.6
4	9	0	069.6	−0.5			4	3	00	825.7	−0.2			11	2	0	632.6	1.3		
3	8	0	135.6	−0.4			0	0	4	829.8	0.7			10	1	2	722.9	0.7	38.9	40.8
1	6	1	268.8	0.4	−38.1	−36.6	2	1	10	978.5	−0.8	3.8	2.5	9	0	1	815.4	2.4		
0	5	4	335.1	0.3	−34.1	−35.2	1	0	2	22057.0	0.8	5.5	4.3	12	2	1	836.8	−2.2		
3	7	0	426.1	0.1			3	1	7	202.6	−0.5	7.8	7.5	11	1	3	931.0	−0.9	43.9	43.1
2	6	0	494.4	0.5			2	0	6	281.2	−0.5	10.7	9.5	10	0	1	24025.5	0.9		
0	4	7	630.2	0.1	−29.0	−28.5	5	2	1	345.1	−0.2	12.5	10.5	13	2	0	037.6	−7.2		
2	5	2	788.0	0.6	−25.4	−24.8	4	1	2	425.0	−0.4	13.3	12.6	12	1	1	137.3	−2.3	48.8	49.4
1	4	00	858.1	0.9			3	0	5	505.8	0.3	15.0	14.5	11	0	1	233.8	−0.5		
0	3	8	927.1	−0.1	−22.3	−21.7	6	2	2	563.2	−0.9	16.0	15.3	13	1	0	337.9	−7.5	51.7	53.7

TABLE V. *Analysis of PbBr bands.*

v'	v''	I	$\nu_{obs.}(PbBr^{79})$	$\nu_{obs.}-\nu_{calc.}$	$\nu(PbBr^{79})-\nu(PbBr^{81})$ Obs.	Calc.	v'	v''	I	$\nu_{obs.}(PbBr^{79})$	$\nu_{obs.}-\nu_{calc.}$	$\nu(PbBr^{79})-\nu(PbBr^{81})$ Obs.	Calc.	v'	v''	I	$\nu_{obs.}(PbBr^{79})$	$\nu_{obs.}-\nu_{calc.}$	$\nu(PbBr^{79})-\nu(PbBr^{81})$ Obs.	Calc.
1	11	0	18790.9	−1.0	−17.8	−18.5	2	4	1	339.0	0.0	−5.2	−5.0	6	3	1	132.2	1.4		
1	10	1	988.6	0.2	−14.9	−16.8	1	3	8	391.8	−0.1	−4.4	−4.5	5	2	0	190.3	−0.3		
0	9	2	19034.9	0.6	−15.6	−16.5	4	5	0	432.4	−1.4			4	1	4	249.4	−0.4	3.2	3.2
0	8	4	233.5	0.7	−13.2	−14.8	2	3	7	543.4	0.9	−3.2	−3.2	7	3	1	275.1	1.5	3.1	2.9
1	8	1	382.8	−1.6	−12.7	−13.4	1	2	3	597.7	1.3			3	0	0	300.1	0.8	4.3	3.8
0	7	6	432.7	0.4	−12.3	−13.2	4	4	0	638.6	2.3			5	1	5	396.4	0.3	4.7	4.3
2	8	2	535.6	0.6	−11.1	−12.1	7	6	00	667.8	1.7	−2.7	−2.5	4	0	2	455.5	−0.8	6.3	5.1
0	6	7	632.9	0.1	−10.9	−11.3	3	3	2	692.8	1.0			7	2	0	475.4	−2.7		
2	7	2	733.7	−0.6	−10.7	−10.4	2	2	8	747.6	0.6	−1.4	−1.4	6	1	3	540.9	0.1	5.2	5.5
1	6	1	785.2	1.1	−8.9	−9.9	5	4	1	784.1	1.5			5	0	5	602.1	−0.5	6.0	6.2
0	5	8	834.3	0.0	−8.9	−9.5	1	1	1	801.5	−0.4			8	2	0	620.2	1.4	5.2	5.8
2	6	0	933.4	−0.6	−8.7	−8.6	3	2	5	898.5	0.2			7	1	1	685.9	2.3	7.7	6.6
1	5	7	986.3	0.4	−7.8	−8.1	6	4	0	929.0	1.7			6	0	7	746.8	−0.5	6.6	7.4
0	4	5	20036.8	0.0	−7.3	−7.7	2	1	3	951.5	−1.0			8	1	00	829.6	5.3		
3	6	3	084.8	0.8	−6.8	−7.2	5	3	0	987.6	1.5			7	0	9	890.4	0.3	8.1	8.5
1	4	8	188.2	−0.2	−6.3	−6.3	1	0	0	21011.6	3.2			8	0	8	22032.2	1.4	10.3	9.6
0	3	2	240.4	0.1	−5.7	−5.9	4	2	3	044.5	0.2			9	0	7	169.1	−0.2	10.8	10.5
3	5	0	286.9	1.1	−4.4	−5.4	3	1	4	101.2	−0.6	2.5	1.9	10	0	6	303.4	−2.0	12.1	11.5

somewhat wider than the Franck-Condon parabola for $PbCl^{35}$. The intensities of corresponding band heads for the two isotopes are nearly equal as might be expected from the abundance ratio (1 : 1) of the two isotopes of bromine. In some cases these bands also appear to be double-headed. They are much less sharp than the bands of PbF or PbCl. Table V gives the vibrational analysis, the observed wave numbers for $PbBr^{79}$, the difference between the observed and calculated wave numbers and a comparison between the observed and calculated isotope shift. The following equations give the wave numbers of the band heads, the equation for $PbBr^{81}$ being calculated from that for $PbBr^{79}$.

$$PbBr^{79}:\ \nu = 20{,}884.3 + [152.5u' - 0.40u'^2 - 0.028u'^3] - [207.5u'' - 0.50u''^2];$$

$$PbBr^{81}:\ \nu = 20{,}884.3 + [151.1u' - 0.39u'^2 - 0.027u'^3] - [205.6u'' - 0.49u''^2],$$

where $u' = v' + \frac{1}{2}$ and $u'' = v'' + \frac{1}{2}$.

DISCUSSION

A striking similarity is noted between the lead halide bands and the longer wave-length systems of the bismuth halides.[3] In all cases the corresponding constants are nearly the same, as might be expected since the atomic weights of lead and bismuth are 207.22 and 209.00, while the charges are 82 and 83, respectively. The system origin of the PbF bands lies slightly to the red of the origin of the BiF bands, while the reverse is true in the case of the PbCl and PbBr and the corresponding bismuth halide bands.

From the similarity of the PbF, PbCl and PbBr molecules, the PbCl and PbBr systems would be expected to be double-headed if the corresponding system due to PbF were double-headed. However, since the Franck-Condon parabola is more open for PbCl and PbBr than for PbF, the separation between a band head and the origin of the band should be less for PbCl and PbBr than for PbF. Consequently the separation between the two heads of a double-headed band would be less for a PbCl or a PbBr band than for a PbF band. In the case of the PbF bands this separation was large enough to measure but it could not be observed with certainty in the case of either PbCl or PbBr. That the two heads, observed in the case of PbF, are not due to lead isotopes is evident since the maximum isotope shift in the case of $Pb^{208}F$ and $Pb^{206}F$ would be only about 1 cm^{-1}. Also if the two heads were the result of isotopy, the separation should increase almost linearly with the distance from the system origin while the observed separation between heads is almost constant.

Lead and tin are in the same subgroup in the periodic table. Since the number of electrons is odd for the halides of both tin and lead, the spin number must be half-integral. Hence a doublet system of levels may be expected and from the electron configuration the halides of both tin and lead might be expected to have a

[3] F. Morgan, "Band Spectra of BiBr, BiCl, BiF and BiI in Absorption," this issue.

quencies" at which the amplitude of the vibrational stress passes through a maximum. In analogy with Balamuth's Eq. (14), these resonance frequencies are, for the torsional oscillator, given by the solutions for f of the equation

$$m_1 \tan y_1/y_1+m_2 \tan y_2/y_2+m_3 \tan y_3/y_3 - (m_1m_2y_3/y_1y_2m_3) \tan y_1 \tan y_2 \tan y_3=0, \quad (1)$$

where m_i=mass of a cylinder, $(i=1, 2, 3)$

$$y_i=\pi f/f_i, \quad (2)$$

f=frequency of applied voltage,

and $$f_i=(n/2L_i)(\mu_i/\rho_i)^{\frac{1}{2}}, \quad (3)$$

where n=an integer, L_i=length of a cylinder, μ_i=modulus of rigidity for the direction of the cylinder axis, ρ_i=density, and the subscripts refer, respectively, to the specimen material, the quartz, and the intermediate material.

Eq. (1) is the fundamental working formula of the piezoelectric method for measuring *all* the elastic constants of any solid substance. For example, the resonance frequencies of a triple *longitudinal* oscillator are given by the solutions of this equation provided that, in the calculation, the symbols y_i and f_i be related to the physical constants of the materials by the formulae:

$$y_i=\pi(f/f_i)[1-(\tfrac{1}{2})\pi^2\sigma_i^2(\theta_i/A_iL_i^2)(1-f^2/f_i^2)],^3 \quad (4)$$

and

$$f_i=(n/2L_i)(G_i/\rho_i)^{\frac{1}{2}}(1-\pi^2n^2\sigma_i^2\theta_i/2A_iL_i^2), \quad (5)$$

where σ_i=Poisson's ratio, θ_i=moment of inertia of cross section about the cylinder axis, A_i=area of cross section, and G_i=Young's modulus for the direction of the cylinder axis.

Again, the resonance frequencies of a *two-part* oscillator, either torsional or longitudinal, are given by the solutions of Eq. (1) with m_1 set equal to zero, that is, by the solutions of

$$m_2 \tan y_2/y_2+m_3 \tan y_3/y_3=0, \quad (6)$$

in which the subscript 3 now refers to the specimen material and Eqs. (2), (3), (4) and (5) subsist.

If m_1 and m_3 are both set equal to zero Eq. (1) reduces to

$$\tan y_2=0, \quad (7)$$

the solutions of which yield the resonance frequencies of the quartz cylinder alone.

Lastly, the left-hand member of Eq. (1) plays exactly the same role in the description of the electrical behavior of triple oscillators as Balamuth's quantity Δ^1 plays in the description of two-part oscillators.

Experimental Method

The electric circuit arrangements for measuring the resonance frequencies are identical with those of Balamuth.[1] The experimental procedure is as follows: The fundamental resonance frequency of the quartz cylinder alone is measured. This frequency is the quantity f_2 by Eqs. (7), and (2), (3) or (4), (5). Next the intermediate cylinder is attached, the fundamental resonance frequency of the two-part oscillator is measured, and Eq. (6) is solved for f_3. If desired, the elastic modulus of this material may be calculated with the aid of Eqs. (2), (3) or (4), (5). A roughly approximate value only of Poisson's ratio is needed for an adequate evaluation of the terms in σ in Eqs. (4) and (5). Lastly, the specimen cylinder is attached, the fundamental resonance frequency of the triple oscillator is measured, Eq. (1) is solved for f_1, and Eqs. (2), (3) or (4), (5) for the elastic modulus.

In case the softness of the cement permits the removal of a cylinder without demounting the oscillator, it is desirable to obtain the resonance frequency data in the reverse of the above order; small remounting errors are thus eliminated. This procedure is adopted when the rubber-vaseline cement is used.

The lengths of the three cylinders should be adjusted so that the fundamental resonance frequencies of the single, double and triple oscillators are the same within ten percent or better. Such frequency matching minimizes the effect of inequality of areas at the interfaces, of the adhesive,[1] and of internal friction in the materials,[4] on the resonance frequency of the oscillator. It will also be noted that the term in σ in Eq. (4) vanishes when $f=f_i$. Furthermore, the specimen cylinder should be long enough to keep these frequencies below 100 kilocycles.

[3] The plus sign in this expression as printed in Balamuth's paper, reference 1, is an error.

[4] Zacharias, Phys. Rev. **44**, 118 (1933).

Above this value harmonics of low frequency modes of vibration are very likely to appear in the neighborhood of that under investigation, which vitiate the observations. Such spurious neighboring modes must always be sought and their absence established. They arise, of course, because the actual impressed piezoelectric stress in the quartz does not correspond exactly to that of any single mode of vibration, but their effect remains negligible so long as none of their resonance frequencies lies near that under observation.

The Elastic Moduli and Elastic Constants of a Cubic Crystal

Formulae which relate Young's modulus and the rigidity modulus for any direction in a cubic crystal to the elastic moduli are given by Voigt.[5] The present research is concerned with only two directions, namely (0, 0, 1) and (0, 1, 1). If the unprimed quantities refer to the former and the primed to the latter, then for the elastic moduli,

$$\begin{aligned} 1/G &= s_{11} \\ 1/G' &= s'_{11} = \tfrac{1}{2}(s_{11}+s_{12}+\tfrac{1}{2}s_{44}) \\ 1/\mu &= s_{44} \\ 1/\mu' &= \tfrac{1}{2}(s'_{44}+s'_{55}) = s_{11}-s_{12}+\tfrac{1}{2}s_{44} \end{aligned} \tag{8}$$

and for the compressibility, κ,

$$\kappa = 3(s_{11}+2s_{12}). \tag{9}$$

Furthermore,

$$\begin{aligned} c_{11} &= (s_{11}+s_{12})/(s_{11}-s_{12})(s_{11}+2s_{12}), \\ c_{12} &= -s_{12}/(s_{11}-s_{12})(s_{11}+2s_{12}), \\ c_{44} &= 1/s_{44}. \end{aligned} \tag{10}$$

From Eqs. (8),

$$s_{12} = 1/G' - \tfrac{1}{2}\mu', \tag{11}$$

or

$$= 1/G + \tfrac{1}{2}\mu - 1/\mu'. \tag{12}$$

Poisson's ratio for a (0, 0, 1)-cut cylinder is given by the formula[6] $\sigma = s_{12}/s_{11}$. When a right circular (0, 1, 1)-cut cylinder is stretched the cross section is no longer circular. The average radial displacement is readily evaluated with the aid of Voigt's analysis, and so the "average" Poisson's ratio. Thus

$$\bar{\sigma}' = (s_{11}+3s_{12}-\tfrac{1}{2}s_{44})/(2s_{11}+2s_{12}+s_{44}).$$

[5] Voigt, *Lehrbuch der Kristallphysik*, p. 739.
[6] Voigt, reference 5, p. 631.

TABLE I. *The elastic moduli and constants of rocksalt.*

T (°K)	Adiabatic Moduli $\times 10^{13}$ (cm²/dyne) s_{11}	$-s_{12}$	s_{44}	Adiabatic Constants $\times 10^{-11}$ (dyne/cm²) c_{11}	c_{12}	c_{44}	Isothermal Constants $\times 10^{-11}$ c_{11}	c_{12}
80	18.64	3.15	75.06	5.76	1.17	1.332	5.72	1.13
90	18.77	3.21	75.18	5.73	1.18	1.330	5.69	1.14
140	19.55	3.54	75.87	5.56	1.22	1.318	5.50	1.16
150	19.72	3.61	76.03	5.52	1.23	1.315	5.45	1.17
160	19.89	3.68	76.19	5.48	1.24	1.313	5.41	1.17
170	20.06	3.75	76.36	5.44	1.24	1.310	5.37	1.17
180	20.24	3.82	76.53	5.40	1.25	1.307	5.33	1.17
190	20.43	3.89	76.70	5.37	1.26	1.304	5.29	1.17
200	20.63	3.96	76.88	5.33	1.26	1.301	5.24	1.17
210	20.82	4.03	77.07	5.29	1.27	1.298	5.20	1.17
220	21.02	4.11	77.25	5.25	1.27	1.294	5.16	1.17
230	21.21	4.18	77.46	5.22	1.28	1.291	5.12	1.17
240	21.43	4.26	77.64	5.18	1.28	1.288	5.07	1.17
250	21.65	4.33	77.84	5.14	1.29	1.285	5.03	1.17
260	21.86	4.41	78.05	5.10	1.29	1.282	4.99	1.17
270	22.08	4.49	78.26	5.06	1.30	1.278	4.95	1.17

In accordance with the theory of Voigt,[7] the adiabatic and isothermal moduli and constants are related by the formulae

$$(s_{11})_{ad.}-(s_{11})_{is.} = (s_{12})_{ad.}-(s_{12})_{is.} = -T\alpha^2/\rho c_p, \tag{13}$$

$$(c_{11})_{ad.}-(c_{11})_{is.} = (c_{12})_{ad.}-(c_{12})_{is.} = T\alpha^2/(\rho c_p)(s_{11}+2s_{12})^2, \tag{14}$$

where T is the absolute temperature, α is the coefficient of linear expansion, and c_p is the specific heat at constant pressure. The adiabatic and isothermal s_{44} and c_{44} are the same.

Results

The adiabatic and isothermal moduli and constants for rocksalt over the temperature range 80°K to 270°K are given in Table I. The first column contains the adiabatic s_{11} as measured by Balamuth. The third column is the smoothed out mean of measurements of the adiabatic s_{44} taken on four different (0, 0, 1)-cut specimens. The values of s_{12} given in the second column were calculated with Eq. (12) from s_{11} and s_{44} together with the smoothed out mean of measurements of the torsion modulus on four different (0, 1, 1)-cut specimens. The specimen material was the finest grade of optical rocksalt obtainable, and was the same as that used by Balamuth. The adiabatic c's were calculated

[7] Voigt, reference 5, p. 789.

TABLE II.

T (°K)	$s_{11}' \times 10^{13}$ BALAMUTH	ROSE	$-s_{12} \times 10^{13}$ Eq. (12)	Eq. (11)
80	26.51	26.53	3.15	3.12
90	26.58	26.60	3.21	3.18
140	26.94	27.01	3.54	3.49
150	27.02	27.10	3.61	3.56
160	27.11	27.19	3.68	3.63
170	27.21	27.29	3.75	3.70
180	27.30	27.39	3.82	3.77
190	27.40	27.49	3.89	3.84
200	27.51	27.59	3.96	3.91
210	27.62	27.69	4.03	3.99
220	27.74	27.80	4.11	4.06
230	27.86	27.91	4.18	4.14
240	27.99	28.02	4.26	4.21
250	28.10	28.13	4.33	4.29
260	28.22	28.25	4.41	4.37
270	28.33	28.36	4.49	4.48

from the s's with Eqs. (10), and the isothermal c's with Eqs. (14).

The formula used in computing the density was[8]

$$\rho = 2.1680(1 - 11.2 \times 10^{-5} t - 0.5 \times 10^{-7} t^2).$$

Values of c_p were taken from the *International Critical Tables*.

PRECISION

Exhaustive tests, of the sort described by Balamuth, were made to demonstrate beyond doubt that the quantities calculated from the observed behavior of the triple oscillators are, in fact, the elastic moduli of the specimen material. The results of two such experimental checks are given in Table II. The first column contains the values of $1/G'$ measured by Balamuth with a two-part oscillator of square cross section. The second column contains values of the same quantity measured on a different set of specimens with a triple oscillator of circular cross section. The agreement is noteworthy. The third column contains values of s_{12} calculated *with Eq.* (*12*) from measurements of the Young's and rigidity moduli on a set of (0, 0, 1)-cut specimens and of the rigidity modulus on a set of (0, 1, 1)-cut specimens. The last column contains values of the same quantity calculated *with Eq.* (*11*) from measurements of the Young's and rigidity moduli on a set of two (0, 1, 1)-cut specimens. The agreement between the values of s_{12} obtained with these quite independent methods offers a very satisfactory overall test of the piezoelectric method, particularly as a small percentage error of measurement is very greatly magnified in the calculation of the difference quantity, s_{12}.

The accidental error in any observation on a single specimen is never greater than 0.03 percent. The source of largest systematic error is nonuniformity of cross section in the specimen cylinder. Such nonuniformity produces a shift parallel to itself of the entire modulus *vs.* temperature curve, and the curves for different specimens are invariably parallel. This is exemplified by, and accounts for, the systematic differences in Table II. Balamuth gives an observed average deviation among his specimens of 0.4 percent in s_{11}. This could have been reduced by using cylinders of circular instead of square cross section, for circular cylinders are in general more uniform. The average deviation for the torsional measurements was about 0.08 percent in s_{44}. The uncertainty in s_{12} is about 1 percent.

Steinebach[9] found the ratio of the value of s_{44} at 291°K to that at 88°K to be 1.065. This ratio, calculated from Table I, is 1.045. Voigt[10] gives $s_\nu = 78.85 \times 10^{-13}$ cm²/dynes, but does not specify the temperature. This is the value here found at 25°C. Voigt,[11] Madlung and Fuchs,[12] and Slater[13] have measured the isothermal compressibility at room temperature. They obtained, respectively, the values 41.3, 41.2, and 42.0 for $\kappa \times 10^{13}$ (cm²/dynes). The present value is 41.9 at 30°C, which was the temperature of Slater's specimens.

In conclusion, the writer desires to thank the Physics Department of Columbia University for the facilities generously placed at his disposal, and Dr. S. L. Quimby for helpful suggestions during the progress of the research.

[8] A. Henglein, Zeits. f. physik. Chemie **115**, 97 (1925).

[9] Steinebach, Zeits. f. Physik **33**, 674 (1925).
[10] Voigt, reference 5, p. 741.
[11] Voigt, reference 5, p. 742.
[12] Madlung and Fuchs, Ann. d. Physik **65**, 289 (1921).
[13] Slater, Phys. Rev. **23**, 488 (1924).

The Band Spectrum of OH^+

F. W. LOOMIS AND W. H. BRANDT, *University of Illinois*

(Received October 17, 1935)

Two bands at 3332 and 3565A discovered by Rodebush and Wahl in the electrodeless discharge in pure water vapor, and two new bands at 3695 and 3893A, are shown to be, respectively, the (1,0), (0,0), (1,1) and (0,1) bands of OH^+. Rotational analysis establishes that they correspond to a $^3\Pi \rightarrow {}^3\Sigma^-$ transition in which the $^3\Pi$ state is inverted, with coupling intermediate between cases *a* and *b*. The nine strong branches to be expected in this type of transition are found, and also enough satellite branches (nine in the 0,0 band) to determine the multiplet intervals in both states. The Λ type doubling is large and there are exceptionally large perturbations in the 3*b*, 2*a* and 1*b* levels of the $v'=1$ state, with maxima at approximately $K'=18.5$, 14.5 and 10.5, respectively. These perturbations are attributed to another $^3\Sigma^-$ state. The $^3\Sigma^-$ state concerned in the transition and the perturbing state are molecular levels which dissociate into the ground states of O and H^+ and O^+ and H, respectively, but one cannot tell which is which. The $^3\Pi$ state probably dissociates into the ground states of O and H^+.

I. INTRODUCTION

IN the course of an investigation of certain problems in the chemical behavior of the OH radical, Rodebush and Wahl[1] discovered two new bands with heads at 3564 and 3328A, degraded to the red. Their source was the electrodeless discharge in very pure water vapor, and the bands have the coarse structure characteristic of diatomic hydrides, so that it seemed very likely that the carrier of these bands is some form of OH, probably the ion OH^+. However, the spectrum of OH has been the subject of numerous investigations and it is a little surprising that, if these rather strong bands are due to its ion, they should not have been discovered before. Moreover, it is to be expected that the bands of OH^+ will be analogous to those of the isoelectronic molecule NH. But the latter are known and are, superficially at least, very different, since they are of the headless type, while the new ones are sharply degraded to the red. It was clear that the question could best be settled by a detailed investigation of the rotational structure of the new bands.

A preliminary investigation[2] disclosed the fact that the bands have an extraordinarily complex structure and that the resolving power of a large grating would be necessary for their analysis. This was undertaken, using some modifications of the source described by Rodebush and Wahl, the principal change being the use of a D-shaped discharge tube with the exciting coil wound around the curved part and the spectrum viewed along the straight part. A rather critical adjustment of the pressure in the discharge tube was necessary. If the pressure was too low, the conditions were apparently too spark-like, the discharge appeared purple and spectrograms showed that most of the energy went into the oxygen spark spectrum. If the pressure was too high, the discharge either did not occur or, if it did, was bluish white and the new bands were not intense. The actual pressure used was not measured, but was probably a few hundredths of a millimeter. The discharge was red and the Balmer series prominent. The "water" bands appeared with great intensity, nearly all of the lines which have been reported in the literature and which occur in the region measured being observed. An important advantage of this electrodeless discharge is the suppression of the hydrogen continuum, which ordinarily practically obscures the region where the new bands occur. This is due to the fact that, in the complete absence of a metal catalyst, the hydrogen molecules are not formed.

Satisfactory photographs were obtained in the first order of a 6-inch 30,000-line/inch, 21-foot concave grating with a dispersion of 1.25A/mm with 20 hours exposure. To increase the intensity a slit width of 0.04 mm was used which is too great to give the full resolving power of the grating. The photographs disclosed a new band with its head at 3983A, which is the (0,1) band of the system of which those discovered by Rodebush and Wahl are the (1,0) and (0,0)

[1] Rodebush and Wahl, J. Chem. Phys. **1**, 696 (1933).
[2] With H. M. Pepiot.

TABLE A. *Wave-lengths of OH^+ band heads.*

$v' \backslash v''$	0	1
0	3565	3893
1	3332	3695

bands. The analysis showed that the wave-lengths of the heads of the bands, as reported by Rodebush and Wahl, are slightly too low, because of a fortuitous accumulation of other lines in the neighborhood. The analysis also disclosed many of the stronger lines of the (1,1) band, especially of the Q branches, intermingled with those of the (0,0) band. The correct wave-lengths of the heads of these four bands (the R_3 branches) are given in Table A, that for the (1,1) band having been computed from the four band combination relations for the R_3 branches.

II. ANALYSIS

1. Strong branches

Observation of the bands reveals that the stronger lines occur in series of groups of three. This indicates that the states involved are triplets. By analogy[3, 4] with NH and PH one would expect to find bands in OH^+ belonging to a $^3\Pi \rightarrow {}^3\Sigma$ transition with the $^3\Pi$ state approaching case *a* for low K values and case *b* for high K values. The analysis shows that this is the case and that the $^3\Pi$ state is inverted. The possible transitions from a $^3\Pi$ to a $^3\Sigma$ state are shown in Fig. 1. The full lines represent strong transitions, the dashed lines weaker ("satellite") transitions and the dotted lines very weak transitions. There are nine strong branches, three P, three Q and three R. Most of these branches were found by inspection and extended by second differences. A few of the branches could not be accurately assigned before enough was known about the quantum numbers to use combination differences.

The three lines in each of the distinct triplets into which the strong lines arrange themselves at some distance from the origin are known to have the same value of K, since case *b* is here closely approached. The clue to the *relative* numbering of the lines lies in a consideration of the internal triplet spacings in the several

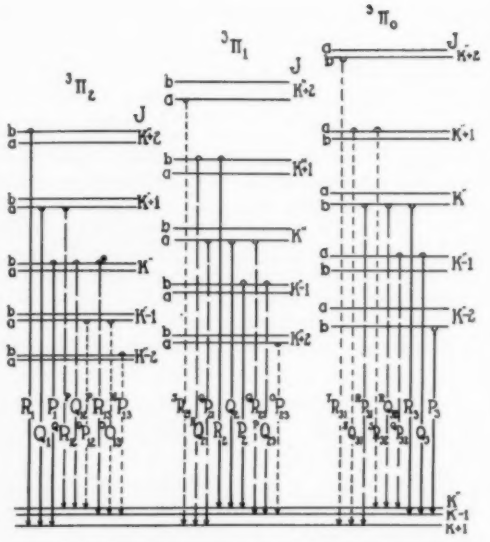

FIG. 1. Schematic representation of possible transitions between $a\ ^3\Pi$ and $a\ ^3\Sigma$ state. Full lines are strong transitions, dashed lines are weaker transitions and dotted lines are very weak transitions. The character of Λ type doubling is indicated qualitatively for K values <13.

branches. That is, the quantum numbers K' and K'' can be assigned, except for a single additive integer, common to all branches, from a study of the magnitudes of the intervals $Q_3(M)-Q_2(M)$, $Q_2(M)-Q_1(M)$, etc. Neglecting the presumably small variation of the internal spacing of the triplet levels in the $^3\Sigma$ state with K'', and also the variation in the internal triplet spacing with Λ type doubling, the same value of K' was assigned to triplets in each of the three sets of branches which have the same internal spacings; and similarly, neglecting the variation of the internal $^3\Sigma$ spacing with v'', the same value of K' was assigned to corresponding triplets in the (0,0) and (0,1) bands. The P, Q and R branches could then be distinguished by the criterion $\nu_R(K) > \nu_Q(K) > \nu_P(K)$. Subsequently the assignments were fully checked by the combination relations which are wholly independent of the above approximations. The assignment of relative K values to the (1,0) band was similar though less certain, but was eventually checked by combinations.

Absolute K values were determined by plotting $\Delta_2 F_2''(M)$ and extrapolating to zero at $K''=-\frac{1}{2}$. The set of components, F_2, was used since $\Delta_2 F_2''$

[3] Batsch, Ann. d. Physik **410**, 81 (1933).
[4] Pearse, Proc. Roy. Soc. **A129**, 328 (1930).

involves no term in $f_i(K, J-K)$. See Eqs. (2)–(5).

2. Perturbations

There are three perturbations in the $^3\Pi$ level ($v=1$). These appear only in the (1, 0) band, since the branches of the (1,1) band are too weak for observation in the perturbed regions. These perturbations occur as given in Table B.

TABLE B.

LEVEL PERTURBED	K' OF MAXIMUM PERTURBATION	BRANCHES INVOLVED
F_{2b}	18.5	P_3, R_3
F_{2a}	14.5	Q_2
F_{1b}	10.5	P_1, R_1

The perturbation in the F_{2a} level involves only the Q_2 branch and there are no exact combinations to check the assignment. However, since the Q branches are quite intense and since the Q_2 branch is the middle branch, this perturbation shows up strikingly on the figure and the assignments are evident by observation. Fig. 5 shows this perturbation. In the case of the P_3, R_3 and P_1, R_1 branches the intensities are not sufficiently greater than those of neighboring lines to establish the assignment beyond doubt. However, all attempts to assign smooth branches in these regions were unsuccessful and Tables II and V show that the intensities as assigned are smooth and that the Δ_2F'' values agree to within experimental error with those of the (0,0) band. These two factors make the assignment seem quite valid.

Accompanying a perturbation there should be faint lines due to transitions to the perturbing state. These lines may well be present but cannot be assigned because of the great number of faint lines in those regions.

3. "Satellite" and very weak branches

The assignment of "satellite" branches will be discussed in connection with multiplet splitting in the $^3\Sigma$ state. When all branches corresponding to full and dashed lines in Fig. 1 are known, the fainter branches can be accurately predicted by combinations.[5] Of these only the $^SR_{32}$ branch of the (0,0) band was observed. No "satellite" or very faint branches were observed in the (0,1) band since this band is comparatively weak.

From a consideration of the low lying states of O and O^+ which might, according to the rules of Wigner and Witmer,[6] yield the $^3\Sigma$ and $^3\Pi$ states involved in the spectral transition, and which might, according to Kronig's[7] rules, perturb the $^3\Pi$ state, one finds that only four states may be concerned: namely, a $^3\Sigma^-$ state which dissociates into $^4S^\circ$ of O^+ and 1^2S of H, a $^3\Pi$ state which dissociates into $^2D^\circ$ of O^+ and 1^2S of H, and a $^3\Sigma^-$ and a $^3\Pi$ state which dissociates into ^3P of O and H^+. One concludes that the $^3\Sigma$ state observed is one of these $^3\Sigma^-$ states, that the $^3\Pi$ state observed is one of these $^3\Pi$ states and that the perturbing state is either the other $^3\Sigma^-$ or the other $^3\Pi$ state. It is very likely that the perturbing state is $^3\Sigma^-$ since it could produce just the perturbations observed, whereas a $^3\Pi$ state would be likely to produce more. If the heats of dissociation which can be calculated from the values of ω and ωx given below can be relied upon even very roughly, within say 3 volts out of 4 and 1, respectively, one may conclude that the $^3\Pi$ state which dissociates into O^+ $^2D^\circ$ cannot be concerned in the transition observed. One may then conclude that one of the two $^3\Sigma^-$ states which dissociate into normal O and H^+ and normal O^+ and H, respectively, is the ground state of the OH^+ molecule, the other being the perturbing state; also that the observed $^3\Pi$ state is the one which dissociates into ^3P of O and H^+.

III. DATA

The frequencies of lines which have been assigned to branches are recorded in Tables I–III. The intensities are visual estimates made while measuring plates; d after the intensity indicates that the line is diffuse. A number in parenthesis indicates that the line has been assigned that number of times. Since the "water" bands overlap the (1,0) and the (0,0) bands, not all of these occur twice in the tables. Except in the region of the (0,0) band, there are numerous

[5] For the notation used here and for an exhaustive list of combination relations in $^3\Pi - {}^3\Sigma$ bands see Naudé, Proc. Roy. Soc. **A136**, 114 (1930).

[6] Wigner and Witmer, Zeits. f. Physik **51**, 859 (1928).

[7] Kronig, Zeits. f. Physik **50**, 347 (1928).

TABLE I. *Branches of (0,0) band.*

K	INT.	ν (vac)	INT.	ν (vac)	INT.	ν (vac)
		R_2		R_2		R_1
1	1	28040.55				
2	2	044.96	1	28009.23	1	27954.13
3	2	044.41	5	015.28 (2)	3	968.45
4	1	039.73	5	014.72 (2)	5	975.66 (2)
5	4	030.18 (2)	2	008.20 (2)	5	975.66 (2)
6	5	015.28 (2)	2	27995.89	4	967.61 (2)
7	2	27994.49	2	977.17	4	953.05 (2)
8	4	967.61 (2)	4	951.96	5	930.80 (2)
9	5	933.89 (4)	4	920.05 (2)	3	901.33
10	3	893.85	5	881.19 (3)	2	864.68
11	3	846.65	4	835.18 (3)	4	820.60
12	5	792.76 (2)	3	782.09 (2)	2d	769.15
13	2	731.09	3	721.81 (3)	3	710.08
14	2	662.24	4	653.64	2	643.34
15	4	585.69 (2)	10	578.15 (2)	2	568.66
16	1	501.32	2	494.23	2	485.96
17	2	408.91	2	402.40 (2)	2	395.20
18	2	308.36	2	302.55	2	296.05
19	2d	199.07	1	193.88	2	188.28
20	2	081.45	2	076.66	2	071.75
21	2	26954.72	2	26950.43	2d	946.19
22	1	818.90	3	815.08 (2)	2	811.47
23	1	673.66	1	670.18	2d	667.27
24	1d	518.52	0d	515.68	1d	512.81
25	1	353.65	1	350.83 (2)	1	349.28
26	1d	178.59	0	175.03	1d	176.70
27	0d	993.11				
28	1	796.44				
		Q_3		Q_2		Q_1
1	2	28008.20 (2)				
2	1	27982.69	5	27930.80 (2)	2	27864.68 (2)
3	4	953.05 (2)	2	909.00	3	855.02
4	4	920.05 (2)	5	881.19 (3)	4	837.66 (2)
5	3	882.45 (2)	3	848.36	5	812.35 (2)
6	4	840.22	5	809.54 (2)	5	779.65 (2)
7	5	792.76 (2)	3	764.94	20	739.78 (2)
8	20	739.78 (2)	5	714.39	7	692.86
9	7	680.96 (2)	6	657.42 (3)	6	638.99
10	5	616.24	4	594.36 (2)	10	578.15 (2)
11	7	545.21	6	524.69	3	510.79 (2)
12	6	467.70	6	448.47	7	436.28
13	5	383.66	7	365.59	6	354.85
14	6	292.92	6	275.87	6	266.39
15	5	195.25	7	179.12	8	170.84
16	5	090.64	6	075.33	6	068.03
17	6	26978.80 (2)	6	26964.23	6	26957.80
18	5	859.71	5	845.82	5	840.15
19	8	732.94	8	719.77	8	714.87
20	4	598.73	5	586.17	5	581.77
21	4	456.55	4	444.51	4	440.78
22	2	305.72	3	294.79	3	291.54
23	8	147.53	8	136.68	5	133.96
24	3	25980.85	3	25970.38	2	25968.07
25	4	805.23	2	795.01	2	793.17
26	1	620.32	1	610.75	1	609.38
27	0	426.31	1	417.17	1	416.32
28	00	222.89	2	213.90		
29	2	009.93 (2)	2	001.14 (2)		
30	0	24786.04				
		P_3		P_2		P_1
1						
2	5	27933.89 (4)	1	27684.97 (2)	1	27798.26
3	1d	876.56	4	835.18 (3)	1	766.07 (2)
4	1	815.19	5	779.65 (2)	1	724.44
5	1	749.84	1	720.53	1	674.79
6	7	680.96 (2)	1	655.93 (2)	1	617.52
7	2	607.22	4	585.69 (2)	3	553.25
8	2	528.87	1	509.80	3	482.03

K	INT.	ν (vac)	INT.	ν (vac)	INT.	ν (vac)
		P_3		P_2		P_1
9	3	445.29	3	428.35	2	404.33
10	4	356.27	5	341.08	5	320.12
11	4	261.65	3	248.03	6	229.60
12	4	161.29	4	148.94	5	132.65
13	5	054.98	5	043.81	6	029.43
14	6	26942.65	6	26932.59	6	26919.81
15	2	824.26	3	815.08 (2)	4	803.75
16	4	699.69	4	691.34	4	681.23
17	4	568.76	4	561.21	4	552.21
18	4	431.35	4	424.46	4	416.58
19	3	287.39 (2)	3	281.17	3	274.23 (2)
20	8	136.68 (2)	3	131.09	3	124.95
21	3	25979.29	3	25974.19	2	25968.71
22	2	814.56	2	810.04	4	805.23 (3)
23	1	642.71	1	638.67	1	634.73
24	0	463.64	1	459.98	1	456.56
25	1	276.74	1	273.69	1	270.67
26	0	082.09	0d	078.84 (2)	0	076.90 (2)
27	2	24877.65 (2)			1	24875.14
28					00	666.35
29					00	451.21
30					1	228.05
31					00	995.68
		$^RQ_{11}$		$^RQ_{21}$		$^QP_{21}$
1	1	28000.23				
2	2d	011.52 (2)	2d	28042.38 (2)	1	27980.42 (2)
3	2	017.29 (2)	2d	042.38 (2)	1d	949.86
4	2	017.29 (2)	1	037.82	1	918.29
5	2d	011.52 (2)	1	028.64	5	881.19 (3)
6	1	27999.06	5	014.72 (2)	1	838.89 (2)
7	1	980.42 (2)	1	993.20	1d	789.73 (2)
8	1	955.32	1	966.44		
9	1	923.45				
10	1	884.97 (2)				
11	1	838.89 (2)				
12	1d	786.41 (2)				
		$^QP_{11}$		$^QR_{11}$		$^QR_{12}$
2	5	27933.89 (4)	5	27933.89 (4)	2	27861.56
3	1	911.28 (2)	1	911.28 (2)	1d	852.29 (2)
4	1	27883.86	3	882.45 (2)	4	835.18 (3)
5	1	851.11	2	849.91 (2)	5	809.54 (2)
6	5	812.35 (2)	1	811.01	1	776.57
7			1	766.07	1d	736.52
8	1	717.67			1	689.40
9	1d	661.06	1d	659.19	1	635.42
10	1	598.15			0	574.62
11	2	528.87 (2)				
12	1	452.29 (3)				
		$^PQ_{21}$		$^PQ_{11}$		$^SR_{11}$
1					1	28112.64
2			1	27795.93	0	147.34
3	4	27837.66 (2)	1	763.38	1	175.28
4	3	782.09 (2)	3	721.81 (3)	1d	197.14
5	3	721.81 (3)	1d	671.88	2d	212.41 (2)
6	6	657.42 (3)	1	614.49	1	220.83
7	1	586.87	1	549.94		
8	3	510.79 (2)	1	478.65		
9	00	429.34	1	400.75		
10			1	316.52		
11			1	225.74		
12			0	128.67		
13			1	025.27		
14			0	26915.56		
15			00	799.48		

lines which have not been assigned, but none of them are stronger than intensity "2".

Combination differences are given in Tables IV–VII inclusive.

Corresponding values of $\Delta_2 F_i''$ agree to within experimental error for the (0,0) and (1,0) bands and corresponding values of $\Delta_1 F_{ab}'$, $\Delta_1 F_{ba}'$ and $\Delta_2 F_{ab}'$ agree to within experimental error for the (0,0) and (0,1) bands. Table IV(a) shows observed frequencies of Q branches of the (1,1) band. Table IV(b) shows the values of these frequencies calculated by 4 band combinations.

TABLE II. *Branches of (1,0) band.*

K	INT.	ν (vac)	INT.	ν (vac)	INT.	ν (vac)
		R_3		R_2		R_1
1						
2					3	29917.79
3	1	30004.72			2	926.38
4	1	29993.12	1	29964.26	2	925.04
5	4	973.20	3	947.77	3	914.67
6	3	946.23	2	923.68	5	895.14
7	2	911.63	5	891.52 (2)	5	866.94
8	5	869.27	3	850.97	4	829.91
9	3	818.78	6	802.05 (2)	5	785.03
10	4	759.90	6	744.73	6	724.43
11	10	692.58	8	678.62	5	662.44 (2)
12	6	616.70	6	603.83	6	589.78
13	6	532.11	6	519.99	8	507.49
14	5	438.54 (2)	5	427.08	3	415.96
15	5	335.89	4	324.81	5	314.98 (2)
16	6	224.73	3	213.23	2	204.60
17	3	107.47	10	091.96 (2)	10d	084.60 (2)
18	3	28958.06	3	28960.95 (2)	3	28954.17
19	1	822.58	7	819.84 (2)	2	814.04
20	2	672.25	3	668.37 (2)	4d	663.85
21	1	510.42	1	506.79	2	503.09 (2)
22	1	337.69	1	334.59 (2)	1	334.59 (2)
23	2	154.20 (2)	1	151.31		
24	1	27959.32	1	27956.92		
25			00	751.35		
26			0	534.23		

K	INT.	ν (vac)	INT.	ν (vac)	INT	ν (vac)
		Q_3		Q_2		Q_1
1			2	29926.38	3	29841.16 (2)
2	1	29955.22	2	904.29	1	835.07
3	1	920.02	5	875.21	3	819.37
4	4	879.42	3	841.16	6	795.25
5	5	833.41	4	799.94	5	761.41
6	5	780.59	6	751.10	6	718.49
7	6	721.33	9	694.78	6	666.78
8	6	654.72	7	630.20	10	606.30 (2)
9	10	580.78	7	558.87	8	537.37
10	10	498.95	10	479.18	10	459.84
11	10	409.40	10	391.38	10	373.87
12	8	311.74	6	295.85	7	279.36
13	5	206.04	6	193.27	6	176.45
14	10	091.96 (2)	7	089.20	7	064.72 (2)
15	5	28969.40	6	28944.99	6	28944.25
16	6	838.32	7	819.84 (2)	6	815.01
17	4	698.68	6	682.33	6	677.18
18	3	550.38 (2)	2	534.98	2	529.97
19	2	392.38 (2)	3	378.39	3	373.96 (2)
20	2	225.44	2d	212.41 (2)	3	208.45 (2)
21	1	049.27 (2)	1	037.02	1d	033.72 (2)
22	2	27863.70	1d	27852.29 (2)	2	27849.91 (2)
23	1	668.01	6	657.42 (3)	1	655.93 (2)
24	1	462.66	1	452.29 (3)	1	452.29 (3)
25	0	246.98	1	237.30 (2)	1	237.30 (2)
26	2	020.51	0	013.57		
27	0	26783.35				
28	0d	534.71				
29	3	274.23 (2)				

		P_3		P_2		P_1
4					1	29688.87
5	1	29710.31			1	632.45
6	2	634.08 (2)	10	29606.30 (3)	3	566.77
7	2	550.11	2	525.21	2	492.31
8	10	459.84 (2)	4	437.55	10	409.40 (2)
9	4	362.30	4	342.51	5	318.31 (2)
10	6	257.96	5	240.01	6	219.35
11	3	146.35	2	129.89	10	113.26 (2)
12	5	027.40	6	012.45	6	28992.51
13	6	28900.85 (2)	6	28887.19	5	871.33
14	2	766.87	3	754.33	3	740.39 (2)
15	2	625.08	2	613.68	2	601.30
16	2	476.08	2	464.90	2	454.06
17	2	319.13	3d	308.68	2	298.66 (2)
18	2	154.20	2	143.41	2	135.00
19	1	27985.97 (2)	1	27970.74	1	27963.39
20	1d	786.41 (2)	1d	789.73 (2)	1	783.33
21	1	602.80	1	600.25	4	594.36 (2)
22	0	405.30	2	402.40	1	397.36
23	0	198.56	5	195.25 (2)	1	192.07
24	0	26982.58	0	26979.82	6	26978.80 (2)
25	1	757.25	1	754.84		
26	1d	522.64	1d	520.48		

		$^RQ_{32}$		$^RQ_{21}$		$^QP_{32}$
3	1	30002.84			3	29917.79
4	0	29991.52	2	29967.37	4	877.24
5	0	971.61	1	950.81	2	831.49
6	0	944.61	2	926.38 (2)	0	779.26
7	1	910.60	5	895.14 (2)	0	719.98
8			1d	854.56	0	653.82
9	1	817.21	1	805.95		
10	1	758.79	1	748.30		
11	1	691.73 (2)	0	682.37		
12			10	606.30 (2)		

		$^QP_{21}$		$^QR_{12}$		$^PQ_{12}$
4			1	29792.54	1	29686.22
5	6	29802.05 (2)	1	758.79	1	629.62
6	1	754.22	1	715.32	1	563.58
7	3d	698.03	5	662.44 (2)	1	489.11
8	2	634.08 (2)	6	603.83 (2)	1	406.08
9	1	562.93	1	534.41	5	314.98 (2)
10	0	482.92	00	456.21	00	215.67
11	00	395.75	00	370.09	3	107.47
12	0	299.05			3d	28990.79
13					1d	867.08

These agreements constitute a rigorous check on the assignments.

IV. CALCULATION OF MOLECULAR CONSTANTS

1. Energy expressions[8]

In a multiplet state the energy is written[9] for case *a*

$$T=T^e+G+A\Lambda\Sigma$$
$$+B_v[J(J+1)-\Omega^2+\bar{G}^2+S^2_{\text{perp}}]+\varphi_i(\Sigma,J)$$
$$+D_vJ^2(J+1)^2+F_vJ^3(J+1)^3+\cdots. \quad (1)$$

In case *b*

$$T=T^e+G+B_v[K(K+1)-\Lambda^2+\bar{G}^2]$$
$$+f_i(K,J-K)+\varphi_i(K,J)$$
$$+D_vK^2(K+1)^2+F_vK^3(K+1)^3+\cdots. \quad (2)$$

The multiplet splitting in case *a* is given by the term, $A\Lambda\Sigma$, while in case *b* it is given by $f_i(K,J-K)$. $\varphi_i(\Sigma,J)$ and $\varphi_i(K,J)$ are both double valued for any value of J whenever $\Lambda>0$. The two values are distinguished by the subscripts *a* and *b*, as is shown in Fig. 1, the strong *Q* branches are transitions from *a* levels and the strong *P* and *R* branches are from *b* levels. The

[8] Mulliken, Rev. Mod. Phys. **2**, 60 (1932).

[9] It should be noted that F_v is a coefficient in the rotational part of the energy expression and is not to be confused with *F*, used to express rotational energy as a whole.

TABLE III. *Branches of (0,1) band.*

K	INT.	ν (vac)	INT.	ν (vac)	INT.	ν (vac)	K	INT.	ν (vac)	INT.	ν(vac)	INT.	ν (vac)
		R_2		R_2		R_1			R_2		R_2		R_1
1	0	25082.09 (2)			3	24974.16 (2)	15	0	801.24	0	793.38	1	784.10
2	0	090.53			2	25001.14 (2)	16	3	739.36 (2)	0	732.35	1	723.94
3	0	095.75 (2)	00	25067.38	1	020.83	17	1	670.84	1	664.28	1	657.01
4	00	097.73	0	072.76	2d	033.97	18	1	595.27	2	589.45	1	582.67
5	0	095.75 (2)	0	073.72	1	040.93	19	0d	512.66	0	507.15	0	501.46
6	1	089.49	2	069.81	1	041.82	20	1	423.30	1d	417.41	1d	412.33
7	0d	078.84 (2)	1	061.64	2d	037.05	21	0	324.34	1	320.03	0	315.70
8	1	063.21	1	047.72 (2)	3	026.31 (2)	22	2d	218.18 (2)	1d	214.80	1	210.86
9	1	042.70	1	028.67	2	009.93 (2)	23	0d	104.58	0	101.11	0	097.98
10	1	016.37	1	004.25 (3)	2	24987.64	24			1	23978.85	00	23976.13
11	1	24985.53	3	24974.16 (2)	1	959.40	25			0	847.82	0	846.18
12	1	948.36	2	938.09	2	924.96	26					1	708.03
13	1	905.57	3	895.92 (2)	2	884.37	27					00	561.92
14	1	856.60 (2)	1	847.91	1	837.48							
		Q_2		Q_2		Q_1			Q_2		Q_2		Q_1
1			1	25004.25 (3)	00	24909.53	14	3	487.11	3	470.03	4d	460.42
2	3	25026.31 (2)	0	24978.16 (2)	00	911.92	15	3	410.65	1	394.46	5d	386.09
3	1	004.25 (3)	00	961.24	1	907.34	16	3	328.56	3	313.22	4	305.88
4	0	24978.16 (2)	2	939.56	3	895.92 (2)	17	3	240.59	4d	225.94	3	219.37
5	1	947.87	2	913.75	2	877.65	18	4	146.40	4	132.59	5	126.81
6	2	914.25	2	883.66	2	853.65	19	2	046.12	2	033.03	2	027.95
7	2	877.09	2	849.03	2	823.79	20	2	23939.46	1	23926.92	1d	23922.35
8	2	835.59	2	810.03	2	788.50	21	1	826.24	3	814.04	1	810.23
9	2	789.87	2	766.12	2	747.61	22	1	706.05	1	694.58	2	691.02
10	3	739.36	2	717.38	2	701.30	23	1	578.50	0	567.62	0	564.83
11	2	684.08	2	663.55	3	649.49	24	0	442.10	0	433.37	0	431.07
12	2	623.66	1	604.46	3	592.21	25	0	295.42	00	291.66	0	289.53
13	2	558.09	4	539.97	4	529.17	26			00	142.04	0	140.37
		P_2		P_2		P_1			P_2		P_2		P_1
5	00d	24815.34					14	2	136.87	5	126.81 (2)	3	113.99
6							15	1d	039.67	1	030.58	3	019.11
7	1	691.57 (2)	00	24669.72	1	24637.38	16	1	23937.55	0	23929.22	3d	23919.11
8	0	624.75	0	605.44			17	0	830.56	2d	822.65	3	814.04 (2)
9					0d	512.66 (2)	18	0	718.52	0	711.38	0	703.39
10	1d	479.22	1	464.13	1d	442.90	19	0	600.71	0	594.34	00	587.38
11	1	400.35	0	386.41	1	368.28	20	0d	477.77	00	471.87	0	465.62
12	1	317.07	0	304.78	1	288.50	21	0	348.94			00	338.16
13	4d	229.34	2d	218.18 (2)	3	203.72	22					00	204.87

TABLE IV.

(a) *Branches of (1,1) band (observed).*

K	INT.	ν (vac)	INT.	ν (vac)	INT.	ν (vac)
		Q_2		Q_2		Q_1
4					0	26853.37
5	0	26898.78	0d	26865.48	0	826.68
6	1	854.99	00	825.44	1	792.65
7	1	805.57	1	779.02	2	750.88
8	2	750.88 (2)	0	726.64	1	702.11
9	0	689.55	2d	667.27 (2)	2	646.10
10	1	622.13	0	602.24	1	582.82
11	0d	548.20	1d	530.47 (2)	1d	512.81 (2)
12	1d	467.75	1d	451.57	1	435.07
13	0d	380.59	1d	367.66	1	350.83 (2)
14	3	287.39 (2)				
15	0d	184.90	1	160.78	1	159.50 (2)
16					0	052.90 (2)

(b) *Branches of (1,1) band (calculated by 4 band combinations).*

	Q_2	Q_2	Q_1
4			26852.28
5	26898.83	26865.33	826.71
6	854.62	825.22	792.49
7	805.66	778.87	750.79
8	750.53	725.84	701.94
9	689.69	667.57	645.99
10	622.07	602.20	582.99
11	548.27	530.24	512.57
12	467.70	451.84	435.29
13	380.47	367.65	350.77
14	286.15		
15	184.80	160.33	159.50
16			052.90

difference $\varphi_{ib}(K)-\varphi_{ia}(K)=\Delta\nu_{iba}(K)$ is known as Λ type doubling.

2. Multiplet splitting in the $^2\Sigma$ state

The energy in the lower state is represented by Eq. (2) since a Σ state is strictly case *b*. The term $\varphi_i(K, J)=0$ since $\Lambda=0$. Corresponding to the different values of J, the total angular momentum quantum number, the term $f_i(K, J-K)$ has the following values.[8]

$$J=K+1, \quad f_1=-\epsilon[1-3/(2K+3)]+\gamma K \qquad (3)$$

$$J=K, \quad f_2=2\epsilon-\gamma \qquad (4)$$

$$J=K-1, \quad f_3=-\epsilon[1+3/(2K-1)]-\gamma(K+1) \qquad (5)$$

ϵ and γ being constants. Subtracting (3) from (4) and (5) from (4),

$$\Delta f_{21}(K)=3\epsilon[1-1/(2K+3)]-\gamma(K+1), \qquad (6)$$

$$\Delta f_{23}(K)=3\epsilon[1+1/(2K-1)]+\gamma(K). \qquad (7)$$

Experimentally $\Delta f_{21}(K)$ and $\Delta f_{23}(K)$ were observed by taking the differences.[5]

TABLE V. $\Delta_2F_i''(K)=R_i(K-1)-P_i(K+1)$.

K	(0,0) band $\Delta_2F_3''(K)$	$\Delta_2F_2''(K)$	$\Delta_2F_1''(K)$	$\Delta_2F_3''(K)$	(1,0) band $\Delta_2F_2''(K)$	$\Delta_2F_1''(K)$	$\Delta_2F_3''(K)$	(0,1) band $\Delta_2F_2''(K)$	$\Delta_2F_1''(K)$
2	163.99								
3	229.77	229.58	229.69			228.92			
4	294.57	294.75	293.66	294.41		293.93	280.41		
5	358.77	358.79	358.14	359.04	357.96	358.27			
6	422.96	422.51	422.41	423.09	422.56	422.36	404.18	404.00	403.55
7	486.41	486.09	485.58	486.39	486.13	485.74	464.74	464.37	
8	549.20	548.82	548.72	549.33	549.01	548.63			524.39
9	611.34	610.95	610.68	611.31	610.96	610.56	583.99	583.59	583.41
10	672.24	672.02	671.73	672.43	672.16	671.77	642.35	642.26	641.65
11	732.46	732.25	732.03	732.50	732.28	731.92	699.80	699.47	699.14
12	791.67	791.37	791.17	791.73	791.43	791.11	756.19	755.98	755.68
13	850.11	849.50	849.34	849.83	849.50	849.39	811.49	811.28	810.97
14	906.83	906.73	906.33	907.03	906.31	906.19	865.90	865.34	865.26
15	962.55	962.30	962.11	962.46	962.18	961.90	919.05	918.69	918.37
16	1016.93	1016.94	1016.45	1016.76	1016.13	1016.32	970.68	970.73	970.06
17	1069.97	1069.77	1069.38	1070.53	1069.82	1069.60	1020.84	1020.97	1020.55
18	1121.52	1121.23	1120.97	1121.50	1121.22	1121.11	1070.13	1069.94	1069.63
19	1171.68	1171.46	1171.10	1171.65	1171.22	1170.84	1117.50	1117.98	1117.05
20	1219.78	1219.69	1219.57	1219.78	1219.59	1219.68	1163.72		1163.30
21	1266.89	1266.62	1266.52	1266.95	1265.97	1266.49			1207.46
22	1312.01	1311.76	1311.46	1311.86	1311.54	1311.02			
23	1355.26	1355.10	1354.91	1355.11	1354.77	1355.79			
24	1396.92	1396.49	1396.60	1396.95	1396.47				
25	1436.43		1435.91	1436.68	1436.44				
26	1476.02		1474.14						
27			1510.35						

TABLE VI. $\Delta_2F_{12}'(K)=R_1(K)-P_1(K)$.

K	(0,0) band $\Delta_2F_{32}'(K)$	$\Delta_2F_{12}'(K)$	$\Delta_2F_{12}'(K)$	$\Delta_2F_{32}'(K)$	(0,1) band $\Delta_2F_{12}'(K)$	$\Delta_2F_{12}'(K)$	$\Delta_2F_{32}'(K)$	(1,0) band $\Delta_2F_{12}'(K)$	$\Delta_2F_{12}'(K)$
2	111.07	124.26	155.87						
3	167.85	180.10	202.38						236.17
4	224.54	235.07	251.22				262.89		282.22
5	280.34	287.67	300.87	280.41			312.15	317.38	328.37
6	334.22	339.96	350.09				361.52	366.31	374.63
7	387.27	391.48	399.80	387.27	391.92	399.67	409.43	413.42	420.51
8	438.74	442.16	448.77	438.46	442.28		456.48	459.54	466.72
9	488.60	491.70	497.00			497.27	501.94	504.72	505.08
10	537.58	540.11	544.56	537.65	540.12	544.74	546.23	548.73	549.18
11	585.00	587.15	591.00	585.18	587.75	591.12	589.30	591.38	597.27
12	631.47	633.15	636.50	631.29	633.31	636.46	631.26	632.80	636.16
13	676.11	678.00	680.65	676.23	677.74	680.65	671.67	672.75	675.57
14	719.59	721.05	723.53	719.73	721.10	723.49	710.81	711.13	713.68
15	761.43	763.07	764.91	761.57	762.80	764.99	748.65	748.33	750.54
16	801.63	802.89	804.73	801.81	803.13	804.83	788.34	783.28	785.94
17	840.15	841.19	842.99	840.28	841.63	842.97	803.86	817.54	819.17
18	877.01	878.09	879.47	876.75	878.07	879.28	836.61	849.10	850.65
19	911.68	912.71	914.05	911.95	912.81	914.08	885.84	878.64	880.52
20	944.77	945.57	946.80	945.53	945.54	946.71	907.62	906.54	908.73
21	975.43	976.24	977.48	975.30		977.54	932.39	932.19	937.23
22	1004.34	1005.04	1006.24		1005.16	1005.99	955.64	956.06	962.13
23	1030.95	1031.51	1032.54				976.74	977.10	984.59
24	1054.88	1055.70	1056.25					996.51	
25	1076.91	1077.14	1078.61					1013.75	
26	1096.50		1099.80						
27	1115.46								

$$\begin{aligned}\Delta f_{21}(K)&=Q_1(K)-{}^QR_{12}(K)\\&={}^QP_{21}(K)-Q_2(K)\\&=P_1(K)-{}^PQ_{12}(K)\\&={}^RQ_{21}(K)-R_2(K),\end{aligned}\tag{8}$$

$$\begin{aligned}\Delta f_{23}(K)&=Q_3(K)-{}^QP_{32}(K)\\&={}^QR_{23}(K)-Q_2(K)\\&={}^PQ_{23}(K)-P_2(K)\\&=R_3(K)-{}^RQ_{32}(K).\end{aligned}\tag{9}$$

The differences defined in this way are all positive.

The satellites corresponding to $\Delta f_{21}(K)$ are easily picked out by observation while those belonging to $\Delta f_{23}(K)$ are less intense and in very many cases coincide with lines of greater intensity. For this reason, the constants, ϵ and γ, were determined by averaging all observed values of $\Delta f_{21}(K)$, ignoring coincidences, and fitting the resulting points by least squares. The values of ϵ and γ were then used to calculate the values of $\Delta f_{23}(K)$. The satellites corresponding to $\Delta f_{23}(K)$ could then be assigned by using relations (9).

TABLE VII. $\Delta_1F_{ibc}'(K+\frac{1}{2})=R_i(K)-Q_i(K)$; $\Delta_1F_{iab}'(K-\frac{1}{2})=Q_i(K)-P_i(K)$.

K	$\Delta_1F_{ibc}'(K+\frac{1}{2})$	$\Delta_1F_{iab}'(K-\frac{1}{2})$	$\Delta_1F_{ibc}'(K+\frac{1}{2})$	$\Delta_1F_{iab}'(K-\frac{1}{2})$	$\Delta_1F_{ibc}'(K+\frac{1}{2})$	$\Delta_1F_{iab}'(K-\frac{1}{2})$
			(0,0) band			
1	32.25					
2	62.27	48.80	78.43	45.83	89.45	
3	91.36	76.49	106.28	73.82	113.43	88.95
4	119.68	104.86	133.53	101.54	138.00	113.22
5	147.73	132.61	159.84	127.83	163.31	137.56
6	175.06	159.26	186.35	153.61	187.96	162.13
7	201.73	185.54	212.23	179.25	213.27	186.53
8	227.83	210.91	237.57	204.59	237.94	210.83
9	252.93	235.67	262.63	229.07	262.34	234.66
10	277.61	259.97	286.83	253.28	286.53	258.03
11	301.44	283.56	310.49	276.66	309.81	281.19
12	325.06	306.41	333.62	299.53	332.87	303.63
13	347.43	328.68	356.22	321.78	355.23	325.42
14	369.32	350.27	377.77	343.28	376.95	346.58
			(0,1) band			
2					89.22	
3	91.50		106.14		113.49	
4	119.57		133.16		138.05	
5	147.88	132.53	159.97		163.28	
6	175.24		186.15		188.17	
7	201.75	185.50	212.61	179.31	213.26	186.41
8	227.62	210.84	237.69	204.59	237.81	
9	252.83		262.55		262.32	234.95
10	277.51	260.14	286.87	253.25	286.34	258.40
11	301.45	283.73	310.61	277.14	309.91	281.21
12	324.70	306.59	333.63	299.68	332.75	303.71
13	347.48	328.75	355.95	321.79	355.20	325.45
14	369.49	350.24	377.88	343.22	377.06	346.43
			(1,0) band			
2					82.72	
3					107.01	
4	84.70		123.10		129.79	106.38
5	113.70		147.83		153.26	128.96
6	139.79	123.10	172.58	144.80	176.65	151.72
7	165.64	146.51	196.74	169.57	200.16	174.47
8	190.30	171.22	220.77	192.65	223.61	196.90
9	214.55	194.88	243.18	216.36	247.66	219.06
10	238.00	218.48	265.55	239.17	264.59	240.49
11	260.95	240.99	287.24	261.49	288.57	260.61
12	283.18	263.05	307.98	283.40	310.42	286.85
13	304.96	284.34	326.72	306.08	331.04	305.12
14	326.07	305.19	337.88	334.87	351.24	324.33

K	$\Delta_1F_{ibc}'(K+\frac{1}{2})$	$\Delta_1F_{iab}'(K-\frac{1}{2})$	$\Delta_1F_{ibc}'(K+\frac{1}{2})$	$\Delta_1F_{iab}'(K-\frac{1}{2})$	$\Delta_1F_{ibc}'(K+\frac{1}{2})$	$\Delta_1F_{iab}'(K-\frac{1}{2})$
			(0,0) band			
15	390.44	370.99	399.03	364.04	397.82	367.09
16	410.68	390.95	418.90	383.99	417.93	386.80
17	430.11	410.04	438.17	403.02	437.40	405.59
18	448.65	428.36	456.73	421.36	455.90	423.57
19	466.13	445.55	474.11	438.60	473.41	440.64
20	482.72	462.05	490.49	455.08	489.98	456.82
21	498.17	477.26	505.92	470.32	505.41	471.96
22	513.18	491.16	520.29	484.75	519.93	486.31
23	526.13	504.82	533.50	498.01	533.31	499.23
24	537.67	517.21	545.30	510.40	544.74	511.51
25	548.42	528.49	555.82	521.32	556.11	522.50
26	558.27	538.23	564.28	531.91	567.32	532.48
27	566.80	548.68				540.88
28	573.55					
			(0,1) band			
15	390.59	370.98	398.92	363.88	398.01	366.98
16	410.80	391.01	419.13	384.00	418.06	386.77
17	430.25	410.03	438.34	403.29	437.64	405.33
18	448.87	427.88	456.86	421.21	455.86	423.42
19	466.54	445.51	474.12	438.69	473.51	440.57
20	483.84	461.69	490.49	455.05	489.98	456.73
21	498.00	477.30	505.99		505.47	472.07
22	512.13	490.40	520.22		519.84	486.15
23	526.08		533.49		533.15	
24			545.48		545.06	
25			556.16		556.65	
26					567.66	
			(1,0) band			
15	346.58	325.09	379.82	331.31	370.73	342.95
16	366.49	344.32	393.39	354.94	389.59	360.95
17	386.41	362.24	409.63	373.65	407.42	378.52
18	408.79	379.55	425.97	391.57	424.20	394.97
19	407.68	396.18	441.45	407.65	440.08	410.57
20	430.20	406.41	455.96	422.68	455.40	425.12
21	446.81	439.03	469.77	436.77	469.37	439.36
22	461.15	446.47	482.30	449.89	484.68	452.55
23	473.99	458.40	493.89	462.17		463.86
24	486.19	469.45	504.63	472.47		473.49
25	496.66	480.08	514.05	482.46		
26		489.73	520.66	493.09		
27		497.87				

In Fig. 2 are plotted the average observed values of $\Delta f_{21}(K)$ and $\Delta f_{23}(K)$ (including coincidences) against K. The curves represent Eqs. (6) and (7) with the following values of the constants:

$$3\epsilon=2.29\ \text{cm}^{-1},\quad \gamma=-0.132\ \text{cm}^{-1}.$$

The approximate agreement of the full circles in Fig. 2 with the curve establishes the adequacy of Eqs. (6) and (7) in this case.

3. Fine structure of the $^3\Pi$ state

a. Λ type doubling. The Λ type doubling, as deducible from measured frequencies, is really the average of two successive doublings, i.e.,

$$2\Delta\nu_{iba}(K+\tfrac{1}{2})=\Delta_1F_{iba}'(K+\tfrac{1}{2})-\Delta_1F_{iab}'(K+\tfrac{1}{2})$$
$$=\Delta\nu_{iba}(K)+\Delta\nu_{iba}(K+1),$$

where

$$\Delta_1F_{iba}'(K+\tfrac{1}{2})=R_i(K)-Q_i(K),$$
$$\Delta_1F_{iab}'(K-\tfrac{1}{2})=Q_i(K)-P_i(K);$$

$\Delta\nu_{iba}(K+\frac{1}{2})$ plotted against K is shown in Fig. 3.

These values of the Λ type doubling can be used, as was done in the case of the first positive nitrogen bands by Naudé,[5] to determine whether the $^3\Pi$ level is normal or inverted. According to theory[10] the Λ type doubling in case *a* should behave as follows: The $^3\Pi_0$ level should show a comparatively large doubling independent of J, which should therefore exist even for $J=0$. The doubling of the $^3\Pi_1$ levels should be proportional to $J(J+1)$ and that of the $^3\Pi_2$ levels should be very small and approximately proportional to $J^2(J+1)^2$. In case *b* all three levels should show doublings approximately propor-

[10] Hill and Van Vleck, Phys. Rev. **32**, 250 (1928); J. H. Van Vleck, Phys. Rev. **33**, 467 (1929); R. S. Mulliken, Rev. Mod. Phys. **3**, 145 (1931).

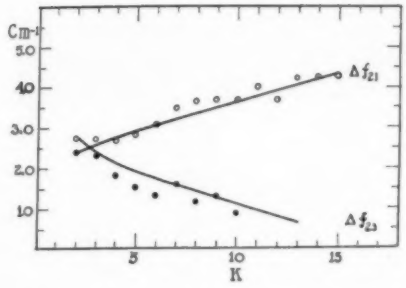

FIG. 2. Multiplet splitting in the $^3\Sigma$ state. Circles represent average of all observed values of $\Delta f_{21}(K)$. Dots represent average of all observed values of $\Delta f_{23}(K)$. Curves are drawn through points calculated, using $3\epsilon = 2.29$ cm^{-1}, $\gamma = -0.132$ cm^{-1}.

tional to $K(K+1)$. The curves in Fig. 3 do not correspond to either of these cases but are qualitatively in consonance with the assumption that the $^3\Pi$ state is intermediate between cases *a* and *b*, and that the high frequency set of levels, $^3\Pi_{high}$ is $^3\Pi_0$ that $^3\Pi_{med}$ is $^3\Pi_1$ and $^3\Pi_{low}$ is $^3\Pi_2$, that is, the $^3\Pi$ level is inverted. The method of distinguishing between these sub-levels by means of "missing lines" is not applicable here because of the large number of lines in the neighborhood of the origins.

The erratic behavior of the Λ type doubling in the $v'=1$ state is due to the perturbations in that state. The assignments, however, are checked by Δ_2F'' combinations.

b. Multiplet splitting. In the absence of a closed energy expression for the case of coupling intermediate between cases *a* and *b*, it seems that one can at best obtain a rough value of the coefficient, A, by assuming that case *a* is approximated at the lowest values of J. Then:

$$^3\Pi_2(2) - {}^3\Pi_1(1) = {}^3\Pi_1(1) - {}^3\Pi_0(0) = A + B$$

where J is the argument[4] or

$$^3\Pi_2(1) - {}^3\Pi_1(1) = {}^3\Pi_1(1) - {}^3\Pi_0(1) = A + B$$

where K is the argument. Λ type doubling is too great to neglect but a fair value should be obtained by averaging the *a* and *b* separations. These separations are observed by using

$$^3\Pi_{1a}(K) - {}^3\Pi_{0a}(K) = {}^QP_{32}(K) - Q_2(K),$$

$$^3\Pi_{2a}(K) - {}^3\Pi_{1a}(K) = {}^QR_{12}(K) - Q_2(K),$$

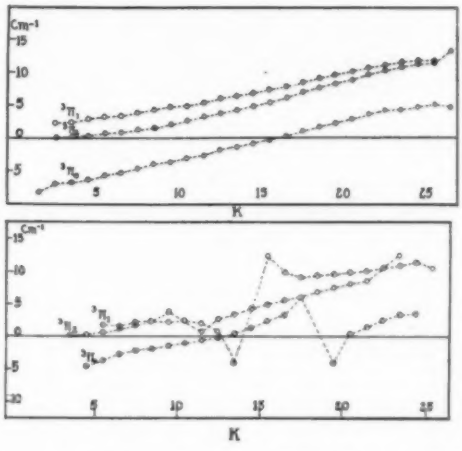

FIG. 3. Λ type doubling in the $v'=0$ and $v'=1$ levels of the $^3\Pi$ state. $\Delta\nu_{ab}$ $(K+1/2)$ plotted against $(K+1/2)$. Upper figure is for $v=0$. Lower figure is for $v=1$. Dotted lines are drawn between points corresponding to the same component of the $^3\Pi$ state. Erratic behavior of Λ type doubling when $v=1$ is due to perturbations.

$$^3\Pi_{1b}(K) - {}^3\Pi_{0b}(K) = {}^PQ_{23}(K+1) - P_2(K+1),$$

$$^3\Pi_{2b}(K) - {}^3\Pi_{1b}(K) = {}^PQ_{12}(K+1) - P_2(K+1).$$

These were plotted near the origin and extrapolated to $K=1$, when necessary. The values of A so determined are

$$^3\Pi_1 - {}^3\Pi_0, \quad A = -66 \text{ cm}^{-1},$$

$$^3\Pi_2 - {}^3\Pi_1, \quad A = -97 \text{ cm}^{-1}.$$

This considerable disagreement is probably due to the fact that the pure case *a* energy expression is inadequate even for these low values of J. Similar but smaller differences have been found in PH[4] and in the first positive bands of nitrogen.[5]

4. Rotational and vibrational constants

The constants B_v, D_v and F_v are evaluated by taking the second differences,

$$\Delta_2F_i(K) = F_i(K+1) - F_i(K-1). \qquad (10)$$

Eqs. (3), (4) and (5) show that in a $^3\Sigma$ state, the best value of the constants should be obtained by taking second differences of F_2 since the term $f_i(K, J-K)$ is constant for this component of the multiplet. Now

TABLE VIII. A *type doubling.*

	(0,0) band			(0,1) band			(1,0) band		
$(K+\frac{1}{2})$	$\Delta\nu_{2a}(K+\frac{1}{2})$	$\Delta\nu_{2a}(K+\frac{1}{2})$	$\Delta\nu_{1b}(K+\frac{1}{2})$	$\Delta\nu_{2a}(K+\frac{1}{2})$	$\Delta\nu_{2a}(K+\frac{1}{2})$	$\Delta\nu_{1b}(K+\frac{1}{2})$	$\Delta\nu_{2a}(K+\frac{1}{2})$	$\Delta\nu_{2a}(K+\frac{1}{2})$	$\Delta\nu_{1b}(K+\frac{1}{2})$
1.5	−8.22								
2.5	−7.11	2.30	0.25						
3.5	−6.75	2.37	.10						0.31
4.5	−6.46	2.85	.22	−6.48			−4.70		.41
5.5	−5.76	3.11	.59				−3.36	1.51	.77
6.5	−5.24	3.55	.71	−5.13	3.42	0.83	−2.79	1.50	1.09
7.5	−4.59	3.82	1.22	−4.54	4.01		−2.29	2.04	1.63
8.5	−3.92	4.25	1.64			1.43	−1.96	2.20	2.27
9.5	−3.52	4.67	2.15	−3.65	4.65	1.96	−1.49	2.00	3.58
10.5	−2.97	5.08	2.67	−3.11	4.86	2.56	−1.05	2.03	
11.5	−2.48	5.48	3.09	−2.57	5.46	3.10	− .58	1.92	.86
12.5	−1.81	5.92	3.72	−2.02	5.92	3.65	− .11	.95	2.65
13.5	−1.42	6.47	4.32	−1.38	6.36	4.38	.49	−4.07	3.35
14.5	− .83	6.86	4.94	− .74	7.00	5.04	1.13		4.14
15.5	− .25	7.52	5.51	− .21	7.46	5.62	2.12	12.44	4.89
16.5	.32	7.94	6.17	.38	7.92	6.36	3.43	9.87	5.53
17.5	.87	8.40	6.91	1.18	8.56	7.11	6.30	9.03	6.22
18.5	1.55	9.06	7.63	1.73	9.08	7.64		9.16	6.81
19.5	2.04	9.51	8.29	2.42	9.53	8.39	−4.41	9.38	7.48
20.5	2.73	10.08	9.01	3.02		8.95	.17	9.59	8.02
21.5	3.50	10.58	9.55	3.80		9.66	1.37	9.94	8.41
22.5	4.18	11.14	10.35				2.27	10.06	10.41
23.5	4.46	11.55	10.90				3.05	10.71	12.39
24.5	4.59	11.99	11.12				3.49	11.33	
25.5	5.09	11.95	11.81					10.38	
26.5	4.80		13.22						

$$\Delta_2F_2''(K)=4B_v''(K+\tfrac{1}{2})+8D_v''(K+\tfrac{1}{2})^3+12F_v(K+\tfrac{1}{2})^5+\cdots, \quad (11)$$

where terms small in comparison to $12F_v(K+\frac{1}{2})^5$ are dropped. Also

$$\Delta_2F_2''(K)=R_2(K-1)-P_2(K+1). \quad (12)$$

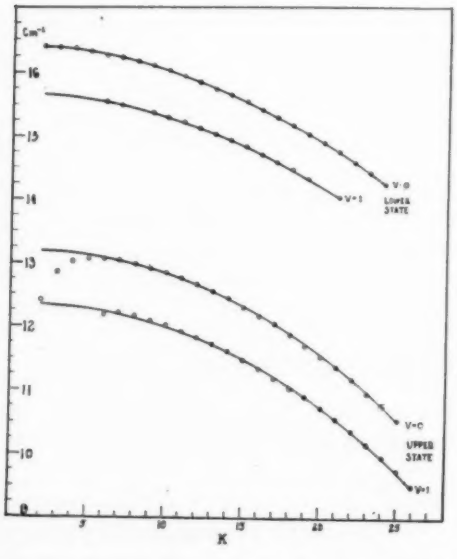

FIG. 4. Observed values of $\Delta_2F_2''(K)/4(K+1/2)$ are represented by circles. Curves are drawn through values calculated by using Table XI. In the case of the upper state observed values of Δ_2F_2' are the average of Δ_2F_{2a} and Δ_2F_{2b}.

The calculation is greatly simplified by dividing $\Delta_2F_2''(K)$ by $4(K+\frac{1}{2})$ giving $B_v''+2D_v''(K+\frac{1}{2})^2+3F_v''(K+\frac{1}{2})^4$. The value of F_v'' was determined by using 3 values of $\Delta_2F_2''/4(K+\frac{1}{2})$ and solving the resulting simultaneous equations. The values of $3F_v''(K+\frac{1}{2})^4$ were then subtracted from the observed values and B_v'' and D_v'' were calculated by least squares.

In the $^3\Pi$ state there should be an expression for Δ_2F_2' similar to Eq. (11) except for Λ type doubling. The theory of Λ type doubling for cases intermediate between *a* and *b* does not permit an exact correction for this, but fairly accurate results should be obtained by using the average,

$$\Delta_2\bar{F}_2'(K)=(\Delta_2F_{2a}'+\Delta_2F_{2b}')/2 \quad \text{where}$$

$$\Delta_2F_{2b}'(K)=R_2(K)-P_2(K), \quad (13)$$

$$\Delta_2F_{2a}'(K)=Q_2(K-1)-Q_2(K+1)-\Delta_2F_2''(K). \quad (14)$$

This procedure was followed in the $^3\Pi_2$ state ($v=0$) with observations from the (0,0) band, but it cannot be used in the $^3\Pi_2$ state ($v=1$) because of the perturbation in the Q_2 branch of the (1,0) band (see Figs. 3 and 5). Since taking this average simply amounts to adding the difference of two Λ type doublings to Δ_2F_{2b}', it is sufficiently accurate to add the same term as was added for $v=0$. The correction is small, averaging less than 1 cm^{-1}. In Fig. 4 the circles

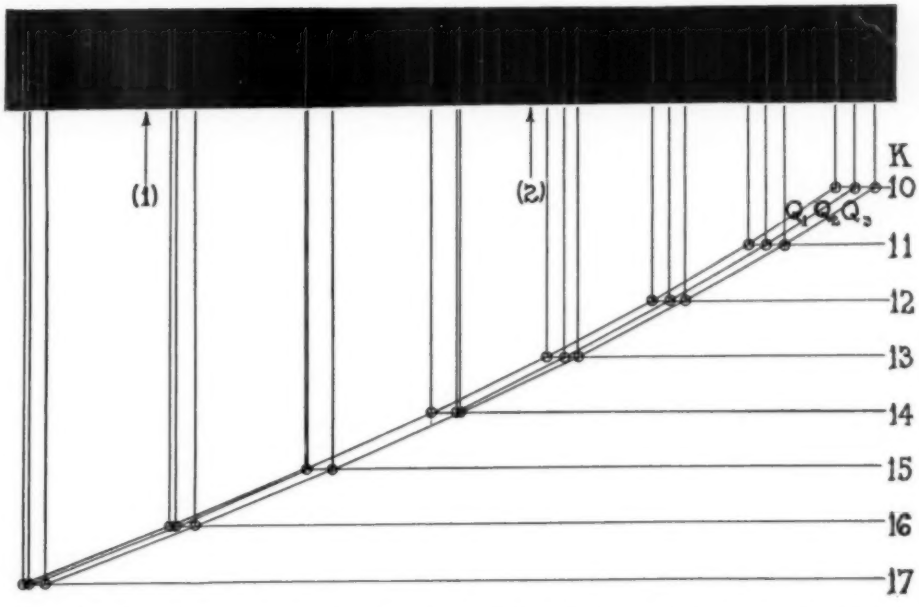

FIG. 5. The perturbation in the Q_2 branch of the (1,0) band. Circles show K plotted against plate position for all three Q branches. Heads of the OH bands at 3484A and 3428A are indicated by arrows; the former being marked (1), the latter (2).

show resulting values divided by $4(K+\frac{1}{2})$ and plotted against K. The Hill and Van Vleck[11] theory of multiplet separation would lead one to expect this curve to be almost constant near the origin and to have an intercept $=B_0'$, while the actual curve bends downward for values of $K<5$. This might be due to an error in assignment, but such an explanation seems improbable due to the fact that combination relations check well near the origin and that intensities of lines assigned to all branches run quite smoothly. Also Δ_2F_{2a}' and Δ_2F_{2b}' differ by less than 1 cm^{-1} near the origin which would hardly be expected if there were an error in assignment, and the $\Delta_2F_2''(K)$ values which are obtained from the same lines fit the theory very well.

Values of $\Delta_2\bar{F}_2'(K)$ for $K<5$ were ignored in computing constants. The calculation was carried out in the same manner as for the $^2\Sigma$ state.

The values of all constants are given in Table XI. In Table IX(a) are tabulated observed values of $[\Delta_2F_2''(K)]/[4(K+\frac{1}{2})]$ and values calculated from the constants. Table IX(b) gives corresponding values for the $^3\Pi$ state. These data are plotted in Fig. 4 with the curves drawn through points calculated from the constants. The differences $\Delta_2F_2(K)$(obs.)$-\Delta_2F_2(K)$(calc.) are also given in Table IX.

[11] Hill and Van Vleck, Phys. Rev. **32**, 250 (1928).

B_v and D_v depend upon the vibrational quantum number in the following manner:

$$B_v=B_e-\alpha_e(v+\tfrac{1}{2})+\cdots, \tag{15}$$

$$D_v=D_e+\beta_e(v+\tfrac{1}{2})+\cdots, \tag{16}$$

so that

$$\alpha_e=B_0-B_1, \tag{17}$$

$$\beta_e=D_1-D_0. \tag{18}$$

Using Table I with Eqs. (15)–(18) gives for the lower state,

$$\alpha_e''=0.732 \text{ cm}^{-1}$$

$$\beta_e''=-0.053\times10^{-3} \text{ cm}^{-1}$$

$$B_e''=16.793 \text{ cm}^{-1}$$

$$D_e''=-1.957\times10^{-3} \text{ cm}^{-1}$$

for the upper state,

$$\alpha_e'=0.841 \text{ cm}^{-1}, \quad B_e'=13.642 \text{ cm}^{-1},$$

$$\beta_e'=\text{very small}, \quad D_e'=D_e'=-1.782 \text{ cm}^{-1}.$$

TABLE IX (a). $\frac{\Delta_2 F_2''(K)}{4(K+\frac{1}{2})}$.

	$v=0$			$v=1$		
K	$\frac{\Delta_2 F_2''(K)}{4(K+\frac{1}{2})}$ (obs.)	$\frac{\Delta_2 F_2''(K)}{4(K+\frac{1}{2})}$ (calc.)	$\frac{\Delta_2 F_2''(K)}{4(K+\frac{1}{2})}$ (obs.) $-\frac{\Delta_2 \bar{F}_2''(K)}{4(K+\frac{1}{2})}$ (calc.)	$\frac{\Delta_2 F_2''(K)}{4(K+\frac{1}{2})}$ (obs.)	$\frac{\Delta_2 F_2''(K)}{4(K+\frac{1}{2})}$ (calc.)	$\frac{\Delta_2 F_2''(K)}{4(K+\frac{1}{2})}$ (obs.) $-\frac{\Delta_2 \bar{F}_2''(K)}{4(K+\frac{1}{2})}$ (calc.)
2	16.388	16.403	−0.15		15.672	
3	.399	.380	.27		.649	
4	.375	.349	.47		.619	
5	.309	.310	−.02		.581	
6	.250	.265	−.39	15.538	.537	0.03
7	.203	.211	−.24	.479	.482	−.09
8	.142	.150	−.27		.426	
9	.078	.081	−.11	.358	15.359	−.04
10	.000	.006	−.25	.292	.286	.25
11	15.918	15.923	−.23	.206	.205	.05
12	.827	.834	−.35	.120	.118	.10
13	.731	.736	−.27	.024	.024	.00
14	.633	.632	.06	14.920	14.924	−.23
15	.521	.522	−.06	.818	.817	.06
16	.408	.405	.20	.708	.703	.33
17	.282	.281	.07	.585	.585	.00
18	.150	.151	−.07	.459	.460	−.07
19	.017	.015	.16	.333	.328	.39
20	14.874	14.873	.08		.192	
21	.728	.726	.17	.044	.049	−.43
22	.575	.572	.27			
23	.416	.414	.19			
24	.250	.250	.00			

TABLE IX (b). $\frac{\Delta_2 \bar{F}_2'(K)}{4(K+\frac{1}{2})} = \frac{\Delta_2 F_{2a}'(K)+\Delta_2 F_{2b}'(K)}{8(K+\frac{1}{2})}$.

	$v=0$			$v=1$		
K	$\frac{\Delta_2 \bar{F}_2'(K)}{4(K+\frac{1}{2})}$ (obs.)	$\frac{\Delta_2 \bar{F}_2'(K)}{4(K+\frac{1}{2})}$ (calc.)	$\frac{\Delta_2 \bar{F}_2'(K)}{4(K+\frac{1}{2})}$ (obs.) $-\frac{\Delta_2 \bar{F}_2'(K)}{4(K+\frac{1}{2})}$ (calc.)	$K+\frac{1}{2}$	$\frac{\Delta_2 \bar{F}_2'(K)}{4(K+\frac{1}{2})}$ (obs.)	$\frac{\Delta_2 \bar{F}_2'(K)}{4(K+\frac{1}{2})}$ (calc.)	$\frac{\Delta_2 \bar{F}_2'(K)}{4(K+\frac{1}{2})}$ (obs.) $-\frac{\Delta_2 \bar{F}_2'(K)}{4(K+\frac{1}{2})}$ (calc.)
2	12.426	13.200	−7.74			12.359	
3	.859	.178	−4.46			.337	
4	13.033	.150	−2.11			.308	
5	.064	.113	−1.08			.272	
6	.059	.070	−.31	6	12.190	.228	−0.99
7	.040	.018	−.42	7	.201	.177	.66
8	12.992	12.960	.96	8	.147	.117	.88
9	.929	.893	1.36	9	.083	.051	.99
10	.850	.817	1.38	10	.007	11.976	1.30
11	.755	.734	.97	11	11.901	.893	.38
12	.654	.642	.60	12	.819	.801	.90
13	.545	.540	.22	13	.708	.702	.32
14	.425	.430	−.24	14	.592	.593	−.06
15	.297	.309	−.74	15	.459	.475	−.99
16	.158	.181	−1.45	16	.332	.348	−1.05
17	.010	.040	−2.10	17	.183	.212	−2.03
18	11.856	11.890	−2.52	18	.038	.065	−2.00
19	.694	.728	−2.57	19	10.879	10.908	−2.34
20	.524	.554	−2.46	20	.708	.741	−2.60
21	.345	.369	−1.98	21	.535	.563	−2.41
22	.161	.171	−.90	22	.352	.374	−1.97
23	10.968	10.961	.75	23	.166	.173	−.66
24	.767	.736	3.13	24	9.966	9.960	.48
25	.555	.498	5.92	25	.765	.735	3.04
				26	.559	.496	6.68

The following relation also exists between constants.

$$\omega_e^2 = -4B_e^3/D_e. \tag{19}$$

This gives the values

$$\omega_e'' = 3111 \text{ cm}^{-1}, \quad \omega_e' = 2387 \text{ cm}^{-1}.$$

By extrapolating the Q_2 branches to the origins, and subtracting, approximate values of ω_4 may be obtained where $\omega_3 = \omega_e - 2x_e\omega_e$. These values are,

$$\omega_1'' = 2955 \text{ cm}^{-1}, \quad \omega_1' = 1986 \text{ cm}^{-1}.$$

By comparison of the values of ω_e obtained from Eq. (19) with those of ω_3 it can be deduced that $x_e''\omega_e'' = 73$ cm^{-1} and $x_e'\omega_e' = 200$ cm^{-1}, but it is doubtful whether the constants in Eq. (19) are known with sufficient accuracy to justify much confidence in these values of $x_e\omega_e$. Certainly estimates of the energies of dissociation based upon them would be highly precarious.

F_v is a function of v, but it is not worth while

TABLE X. *Multiplet splitting in the lower state.*

K	$\Delta f_{23}(K)$ (obs.) (average)	$\Delta f_{23}(K)$ (calc.)	$\Delta f_{13}(K)$ (obs.) (average)	$\Delta f_{13}(K)$ (calc.)
2	2.72	2.36	2.40	2.80
3	2.71	2.57	2.30	2.36
4	2.67	2.74	1.81	2.10
5	2.80	2.90	1.52	1.89
6	3.06	3.06	1.30	1.71
7	3.46	3.21	1.60	1.55
8	3.66	3.36	1.16	1.40
9	3.66	3.50	1.29	1.25
10	3.67	3.64	.85	1.10
11	4.00	3.78		
12	3.70	3.92		
13	4.22	4.06		
14	4.25	4.19		
15	4.27	4.33		

TABLE XI. *Molecular constants.*

	$^2\Sigma$ STATE	$^2\Pi$ STATE
	$B_e'' = 16.427\ \text{cm}^{-1}$	$B_e' = 13.222\ \text{cm}^{-1}$
$v=0$	$D_e'' = -1.931\times10^{-3}\ \text{cm}^{-1}$	$D_e' = -1.782\times10^{-3}\ \text{cm}^{-1}$
	$F_0'' = 1.31\times10^{-7}\ \text{cm}^{-1}$	$F_0' = -3.21\times10^{-7}\ \text{cm}^{-1}$
	$B_1'' = 15.695\ \text{cm}^{-1}$	$B_1' = 12.381\ \text{cm}^{-1}$
$v=1$	$D_1'' = -1.878\times10^{-3}\ \text{cm}^{-1}$	$D_1' = -1.798\times10^{-3}\ \text{cm}^{-1}$
	$F_1'' = 1.41\times10^{-7}\ \text{cm}^{-1}$	$F_1' = -2.42\times10^{-7}\ \text{cm}^{-1}$
	$B_e'' = 16.793\ \text{cm}^{-1}$	$B_e' = 13.642\ \text{cm}^{-1}$
	$D_e'' = -1.957\times10^{-3}\ \text{cm}^{-1}$	$D_e' \cong D_0' = -1.782\times10^{-3}\ \text{cm}^{-1}$
	$\alpha_e'' = 0.732\ \text{cm}^{-1}$	$\alpha_e' = 0.841\ \text{cm}^{-1}$
	$\beta_e'' = -0.053\times10^{-3}\ \text{cm}^{-1}$	β_e' very small
	$I_e'' = 1.647\times10^{-40}\ \text{g cm}^2$	$I_e' = 2.028\times10^{-40}\ \text{g cm}^2$
	$r_e'' = 1.027\times10^{-8}\ \text{cm}$	$r_e' = 1.139\times10^{-8}\ \text{cm}$

to distinguish between F_e and F_v. F_e may be calculated by using

$$F_e = (D_e^2/B_e)[2-\alpha_e\omega_e/6B_e^2], \qquad (20)$$

giving

$$F_e'' = 1.51\times10^{-7}, \quad F_e' = 0.468\times10^{-7}$$

as compared with

$$F_0'' = 1.31\times10^{-7}, \quad F_0' = -3.21\times10^{-7},$$

$$F_1'' = 1.41\times10^{-7}, \quad F_1' = -2.42\times10^{-7}.$$

The agreement of F_e'' with F_0'' and F_1'' is as good as can be expected. F_e' does not agree with the values of F_0' and F_1', being of opposite sign. This is probably partly due to the fact that the constants used in calculating F_e' are not so reliable as those used in calculating F_e'' and partly to the fact that the values of F_0' and F_1' are erroneous because the observed values of $\Delta_2F_2'/4(K+\frac{1}{2})$ do not fit the assumed formula (see Fig. 4).

The constants, I_e and r_e, were calculated from B_e in the usual manner (see Table XI).

JANUARY 1, 1936 PHYSICAL REVIEW VOLUME 49

The Excitation of the Auroral Green Line by Metastable Nitrogen Molecules

JOSEPH KAPLAN, *University of California at Los Angeles*

(Received September 13, 1935)

The excitation of the auroral green line in tubes which show the two new afterglow spectra of nitrogen is described. The conditions of excitation in the present experiments are compared with those in the night-sky and in the aurora borealis. It is proposed that in both of these phenomena the $^1S_0$ state of oxygen which is responsible for the green line is produced by collisions between oxygen atoms and metastable nitrogen molecules in the $A^3\Sigma$ state. Processes by which oxygen atoms may be excited to the $^1S_0$ state in the night-sky and in auroras which have been proposed by other authors are discussed.

I. INTRODUCTION

ONE of the most striking characteristics of the auroral green line in both auroral and night-sky spectra is that, with the exception of the two relatively weak red lines λ6300 and λ6363, it is the only oxygen line present. This peculiar fact immediately suggests of course that some special process or processes are responsible for the production of this line. Naturally, many such processes have been proposed during the few years since the definite identification of this line as the transition $^1S_0 \rightarrow {}^1D_2$ in oxygen. Some of these proposals will be discussed briefly later in the paper. My own feeling has been that the most conclusive way by which to explain the excitation of the green line is to produce it in a laboratory experiment in such a way that both its appearance and mode of production fit in with observed and hypothetical facts about the upper atmosphere.

In 1928[1] a significant step toward the "natural" production of the green line was taken in the excitation of the line in active nitrogen. In all earlier studies of the excitation of oxygen by active nitrogen, only the band spectrum of nitric oxide had been observed. In this experiment the green line appeared most intensely in a mixture of 4 percent O_2 and 96 percent N_2. Soon after this experiment, I realized that much more had to be done before the above-mentioned "natural" production of the green line could be achieved. In addition to the green line, there were present in the spectrum the bands of NO and the first-positive bands of N_2. Now no nitric oxide bands have ever been observed in night-sky or auroral spectra, and furthermore the first-positive bands which were associated with the green line in my laboratory experiment were not the same as those which are associated with this line in auroral spectra. Thus, there was an obvious need for further study of the excitation of the green line. The results of this study will now be described and discussed.

II. Experimental Method and Results

The apparatus was the same as that in which the nitrogen radiations in auroral spectrum have been produced.[2] It was necessary first to bring the nitrogen tube to the condition in which it shows a strong afterglow when a strong uncondensed discharge is passed through it. It may be recalled here that the spectrum of the afterglow in this case, instead of consisting of the well-known first-positive bands of N_2, is made up of the first-negative bands of N_2^+, the second-positive bands of N_2 and a few first-positive bands which originate on very high vibrational levels. The spectrum of this afterglow has been published and discussed elsewhere. Into this tube there is introduced a trace of oxygen from a side tube containing $KMnO_4$. In the first experiments the discharge was rapidly interrupted in such a way that the current in the bulb did not reach a value as large as it would have in a steady state. The center of the bulb was in fact very much like a dark space although there was a feeble red discharge in that region. The reason for this procedure was that I expected an accumulation of nitrogen molecules in the $A^3\Sigma$ metastable state in the region of very low current because of the expected absence there of collisions which would cause transitions from the $A^3\Sigma$ to higher states. The spectrograph was pointed toward the center of the bulb and a long exposure on an Eastman Astronomical Green Sensitive plate yielded some startling results which have already been briefly described in *Nature*.[3] The green line was present with a relative intensity such that the normally strong first-positive bands in the region of the green line were almost completely missing on a plate which was strong enough to be enlarged and printed. This plate has been reproduced in the note in *Nature* to which we referred above. The N_2^+ bands which are usually strongly excited in the completely formed discharge, are absent from this rapidly interrupted discharge. No nitric oxide bands were present in the visible so that we apparently had a more "natural" green line excitation than in the 1928 experiments.

In a later experiment, which also has been briefly described in *Nature*,[4] it was possible to increase the relative intensity of the green line considerably over that described in the last paragraph. The method of production and observation of the line is essentially the same as before with the exception of the current through the tube. This was diminished almost to the point where it vanished, and once again the discharge was rapidly interrupted. Fig. 1 shows one of the resulting spectrograms.

After the completion of these experiments it was suspected that most of the green line radiation in rapidly interrupted discharges arises in the afterglow associated with the discharges. Because of the extreme weakness of this afterglow in the visible, no attempt has been made to observe it carefully, although this will be done. Evidence for the hypothesis that the green line is mainly an afterglow radiation is the discovery of a strong ultraviolet afterglow associated with rapidly interrupted weak discharges in nitrogen. This has been described elsewhere.[4] For our purposes here it is necessary only to say that the Vegard-Kaplan bands contribute a large fraction of the afterglow radiation, and that this

[1] Kaplan, Phys. Rev. **33**, 154 (1929).
[2] Kaplan, Phys. Rev. **42**, 807 (1932); **34**, 671 (1934).
[3] Kaplan, Nature **135**, 229 (1935).
[4] Reference 3, p. 1034.

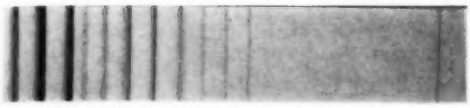

FIG. 1. Spectrogram showing the second-positive bands. The line 5577.35 is shown at the right.

contribution increases as the current decreases. Since the relative intensity of the green line also increases in the same way it is reasonable to suppose that the green line is produced in the afterglow.

III. DISCUSSION

The strong metastable molecular radiation in the afterglow, as well as the weak discharge in nitrogen, indicates that the metastable molecule is responsible for the excitation of the $^1S_0$ level in atomic oxygen. The green line corresponds to a transition from this level to the $^1D_2$ level. The Vegard-Kaplan bands are fairly intense in auroral spectra so that there must be a large number of metastable N_2 molecules present during auroral displays. It seems reasonable, in view of our experiments, to suppose that the green line in the aurora is produced by collisions between metastable nitrogen molecules and oxygen atoms.

Elsewhere, it has been reported that most of the night-sky radiation which is due to nitrogen and which lies at wave-lengths below λ5000, can be convincingly identified as members of the Vegard-Kaplan bands.[5] This clearly proves the presence in the upper atmosphere of a considerable number of metastable molecules even in the absence of auroras. While I do not propose at this time to discuss how these molecules are initially produced, I do wish to point out that most of the auroral green line radiation in the light of the night-sky must originate in collisions between oxygen atoms and metastable nitrogen molecules.

It should be of some interest to mention some of the other hypotheses as to the origin of the green line in night-sky and auroral radiations. S. Chapman, in his 1931 Bakerian Lecture,[6] proposed an extremely fruitful idea as to the origin of the green line. According to this proposal, if the emission of the green line takes place about 100 km, atomic oxygen is responsible, and the reaction associated with this atomic oxygen layer is $2O = O_2$. In an interesting discussion with Professor Chapman it was suggested that this energy of recombination is used in the production of metastable nitrogen molecules which in turn excite the oxygen atoms to the $^1S_0$ level. Further discussion of this point will be presented elsewhere.[7] This idea suggests other experiments which will be attempted soon.

As a result of a long and extensive series of experiments on the production of the green line in the laboratory, McLennan[8] and his colleagues have tentatively suggested metastable nitrogen molecules as responsible for the excitation of the oxygen. This is in agreement with our present suggestion, but it must be recalled that these experiments were performed in mixtures of argon and oxygen in which the oxygen was present in an infinitesimal amount. The argument was based on the hypothesis that in these mixtures the metastable $^3P_2$ state of argon provided the energy necessary for the excitation of the oxygen. This state requires an excitation potential of 11.8 volts, and in view of the recent new value for the $A\,^3\Sigma$ state of N_2 of about 6.15 volts it is apparent that the argument presented by McLennan and his collaborators is not valid.

In a paper written in 1932,[9] Kimura discussed four possible processes of producing oxygen atoms in the ^1S state. He states that it is generally considered that decomposition of ozone caused by light absorption is a cause of the emission of the green line. We wish to point out two objections to this suggestion. First, no experimental evidence has even been presented showing that the green line can be produced in the above manner, and again most of the ozone in the atmosphere occurs below 40 km,[10] and this is probably well below the region from which the green line is radiated.

In closing we wish to direct attention to the fact that we are now observing the visible afterglow, and a more careful study of the variation of relative green line intensity with oxygen contact is also in progress.

[5] Kaplan, Pub. Astronom. Soc. Pacific, October.
[6] Chapman, Proc. Roy. Soc. **A132**, 374 (1931).
[7] Proposed joint publication with Professor Chapman.
[8] McLennan and Ireton, Proc. Roy. Soc. **A129**, 31 (1930).
[9] Kimura, Sci. Papers Inst. Phys. and Chem. Res., Tokyo **18**, 166 (1932).
[10] Götz, Meethan and Dobson, Nature **133**, 698 (1934).

Mass Ratio of Hydrogen and Deuterium from Band Spectra

WILLIAM W. WATSON, *Yale University*

(Received October 21, 1935)

The size of the several corrections to the observed, apparent B_e constants of the usual rotational energy expression in order to obtain "true" B_e values is calculated for some diatomic hydride and deuteride molecules. It is shown that the corrections arising from the uncoupling terms due to the interaction of certain electronic levels (Van Vleck, Mulliken) and from the inclusion of the interactions between nuclear and electronic motions (Kronig) are by far the most important for the molecules considered. The calculations also show that, assuming 1.0081 to be the mass of the hydrogen atom, the mass of deuterium has to be greater than the 2.01423 value given in a number of recent articles. A value close to Aston's latest, 2.0148, is indicated.

THE investigation of the hydrogen isotope effect in the spectra of several diatomic hydride molecules[1–8] has shown that the constants B_e of the usual rotational energy expressions for the two isotopic molecules are never exactly in the ratio of their reduced masses. To explain this failure of the simple isotope theory one or more of the following effects have been mentioned with varying emphasis in each case:

(a) Quantum-mechanical interaction of the electronic level in question with other electronic levels of the molecule gives rise to uncoupling terms[9] which make the apparent B (Mulliken's B^*) different from the real B.[10]

(b) Inclusion of the usually neglected interactions between nuclear and electronic motions in the calculation of the effective potential function makes the equilibrium distance between the nuclei depend slightly upon the reduced mass of the molecule under certain conditions.[11]

(c) Small corrections to the observed B_e^* come from the higher order anharmonic terms because of the interaction of vibration and rotation.[12]

(d) The rotation of a few of the outermost electrons may have to be treated independently of the nuclear rotation, thereby causing an additional contribution to the moment of inertia of the molecule.[1, 13]

These corrections may be considered to be effectively independent of each other. We list them in the order of decreasing importance for most of the molecules. To support this statement and to aid in clearing up the confusion in the literature as to the relative magnitude of these reasons for the discrepancy between the B_e ratios and the ratios of the reduced masses, we shall discuss briefly the size of the corrections for some of these hydride and deuteride molecules. Of some interest also is the indicated maximum value for the ratio of the masses of the H and D atoms.

For the normal $^2\Sigma$ state of BeD, which has negligible spin doubling, the observed, apparent B_e ($=Y_{01}$ in Dunham's notation) is 5.6807, the corresponding quantity for BeH being 10.308. The ratio of these B's is 0.55110, whereas ρ^2, the ratio of the two reduced masses, is 0.55062. In calculating this ρ^2 we use the atomic weights 9.011, 1.0081 and 2.0148 for Be, H and D, respectively, the values for H and D being those recently obtained by Aston.[14] Application of the anharmonic corrections (c) (Dunham's Eqs. (15) and (19)) changes these B values to 5.6812 and 10.3095 which have the ratio 0.55106. This is but a small reduction of the total discrepancy. A considerably larger correction comes from effect (a), for which the q coefficient for the Λ-doubling of the interacting $^2\Pi$ state is to be added to the observed B^* to give the "true" B.[10] For BeD $q_0=0.0043$, while for BeH $q_0=0.0142$. Addition of these quantities raises the B values to 5.6855 and 10.3237 giving a ratio 0.55072.

The difference between this ratio and that of

[1] W. Holst and E. Hulthén, Zeits. f. Physik **90**, 712 (1934). (AlH)
[2] W. W. Watson, Phys. Rev. **47**, 27 (1935). (CaH)
[3] E. Olsson, Zeits. f. Physik **93**, 206 (1935). (NaH)
[4] E. Svensson, *Die Bandenspektren des CdH und CdD* (Stockholm, 1935).
[5] F. H. Crawford and T. Jorgensen, Jr., Phys. Rev. **47**, 358, 932 (1935). (LiH)
[6] P. G. Koontz, Phys. Rev. **48**, 138 (1935). (AgH)
[7] E. Hulthén and E. Knave, Zeeman Jubilee Volume of Physica (1935). (AgH)
[8] P. G. Koontz, Phys. Rev. **48**, 707 (1935). (BeH)
[9] J. H. Van Vleck, Phys. Rev. **33**, 467 (1929).
[10] R. S. Mulliken and A. Christy, Phys. Rev. **38**, 87 (1931).
[11] R. de L. Kronig, Physica **1**, 617 (1934).
[12] J. L. Dunham, Phys. Rev. **41**, 721 (1932).
[13] L. Hulthén, Nature **135**, 543 (1935).
[14] F. W. Aston, Nature **135**, 541 (1935).

the reduced masses may be further decreased by consideration of effect (b). Incidentally, both (a) and (b) involve the perpendicular components of the angular momentum of the electrons, but they are not the same. Kronig[11] shows that (b) introduces a correction term $\bar{U}(r)$ to the potential function given by

$$\bar{U}=\frac{h^2}{8\pi^2\mu}\left[\frac{L(L+1)}{r^2}+\Sigma\int\left(\frac{\partial\Phi}{\partial r}\right)^2 d\tau\right], \quad (1)$$

where L is the orbital angular momentum for the atom imagined to be formed by uniting the two atoms, r is the internuclear distance and Φ the electronic part of the wave function. The first term in (1) produces a difference in the equilibrium distance between the nuclei for the two isotopic molecules given by the difference Δr_1 in the correction

$$r_1=(h^2/8\pi^2\mu)2L(L+1)/fr_0^3 \quad (2)$$

for the two. In (2) f is the force constant for the vibrations. Computation of r_1 for BeD as against BeH (L for the "united atom" has the value 1) yields $\Delta r_1=0.63\times10^{-12}$ cm, r_1 being less for the heavier molecule. A difference in the equilibrium internuclear distance for the two molecules of 1.22×10^{-12} cm in this same sense would account for the whole of the discrepancy between the ratio 0.55072 and the mass ratio 0.55062. The first term of (1) thus accounts for half of this difference. The small remainder might well represent the effect of the second term in (1) which involves the perturbation of this state of BeH by other near-lying states and is of the same sign as the first term.

There is then at the most but very slight discrepancy between this legitimately corrected B_e ratio and the ratio of the reduced masses to be explained by any such effect as (d). Furthermore, if (d) were important, about the same discrepancies should exist for all the hydrides, whereas Koontz finds[6, 8] for BeH^+/BeD^+ and AgH/AgD considerably smaller deviations from mass ratios. This would follow from (b), since for both of these molecules $L=0$. These observed small differences would certainly also be reduced by consideration of (a), the second term in (1) and, in the case of BeH^+, effect (c). It should be emphasized that the observed B_e's are always B_e*'s, for the uncoupling terms are always at least incipiently present.

In the calculation of the reduced mass Casimir[15] has shown that it is proper to include the masses of the electrons in closed shells with the mass of the nucleus. The hydrogen electron, however, will be somewhat shared with the heavier atom. If BeH in its lowest state has a dipole moment as large as that of HCl, something like one-fifth of the H electron[16] may be considered to be associated with the Be atom. Adding one-fifth of the mass of an electron to that of the Be atom and subtracting it from that of the H or D atoms merely reduces ρ^2 to the value 0.55059, which would not affect our conclusions appreciably.

Accepting the value 1.0081 for the mass of the hydrogen atom, that of deuterium should be 2.01423 according to the mass-spectrograph measurements of Bainbridge.[17] These masses together with the value 9.011 for Be make $\rho^2=0.55075$. This mass ratio is so much higher than the ratio of the corrected B constants as to seem quite impossible. The corrected B ratio is consistent with the higher value 2.0148 for the deuterium mass, as outlined above, but of course cannot be used to indicate any exact value for this quantity.

Similar calculations on these ratios may be made for AlH/AlD. The observed B_e* values[1] for the normal $^1\Sigma$ state are 6.3962 and 3.3185. Correcting for effect (a) from the known Λ-doubling raises these to 6.4040 and 3.3208, which have the ratio 0.51855. The anharmonic corrections only drop this ratio to 0.51854. Taking the mass of the Al atom to be 26.97 and the masses of H and D as 1.0081 and 2.0148, respectively, as before, $\rho^2=0.51835$. The discrepancy between this mass ratio and the ratio 0.51854 for the B_e constants could be accounted for if the equilibrium internuclear distance for AlD were 3.0×10^{-12} cm smaller than for AlH. Now the difference between r_1 for the two molecules as calculated from (2) is 2.6×10^{-12} cm, AlD having the smaller r_e. The effect of the second term in (1) could well account for the

[15] H. Casimir, Physica **1**, 1073 (1934).
[16] J. D. Hardy, E. F. Barker and D. M. Dennison, Phys. Rev. **42**, 279 (1932).
[17] K. T. Bainbridge, Phys. Rev. **44**, 56 (1933).

remainder of the discrepancy, and so (d) would seem to have little validity. If the mass of deuterium is taken as 2.01423 and the other masses as before, the reduced mass ratio is 0.51849. Again this is considerably higher than the B_e ratio when the corrections (a), (b) and (c) have all been made to the observed B_e^* values.

JANUARY 1, 1936 PHYSICAL REVIEW VOLUME 49

Mass Ratio of the Lithium Isotopes from the Spectrum of Li_2

G. M. ALMY AND G. R. IRWIN, *Physics Department, University of Illinois*

(Received October 29, 1935)

It is shown from a study of the $^1\Sigma \rightarrow {}^1\Sigma$ Li_2 band system that the relative masses of the two isotopes of Li as calculated from the observed isotope effect in each of the two lowest states of Li_2 is in excellent agreement with the mass ratio obtained by other precise methods. Various methods of treating the data lead consistently to the conclusion that the mass-coefficient ρ is 1.04077 ± 0.00004 and that the mass ratio is 1.16640 ± 0.00016. This result disagrees with that of McKellar and Jenkins who, from a less extensive study of the $^1\Pi \rightarrow {}^1\Sigma$ system of Li_2, concluded that the mass ratio was 1.1678 ± 0.0008, a result which cast suspicion upon the band spectrum method of determining relative atomic masses. There has also been found a small but definite electronic isotope shift: $\nu_e^6 - \nu_e^7 = -0.064 \pm 0.010$ cm^{-1}.

THE accuracy of the band spectrum method of determining the mass ratio of isotopes has been called in question by two series of investigations. First, a consistent ratio of the masses of H^2 and H^1 has not been obtained when the simple theory of the isotope shift has been applied to measurements on various hydrogen and hydride band systems. On account of the large change of reduced mass in these instances, they form a rather special case. Although this problem is not yet completely solved, sufficient reasons for the discrepancies have been advanced from various quarters, by Kronig,[1] by Dieke[2] and by Holst and Hulthén.[3] Second, McKellar and Jenkins[4] have found from measurements on the blue-green system of Li_2 bands ($^1\Pi \rightarrow {}^1\Sigma$) that the mass coefficient $\rho (= (\mu/\mu^6)^{\frac{1}{2}}$, where μ is the reduced mass of $Li^7 Li^7$ and μ^6 that of $Li^7 Li^6$) and, therefore, the mass ratio of Li^7 to Li^6 are greater by several times the estimated probable errors than the corresponding quantities as determined by Bainbridge[5] who used the mass spectrograph. The latter have been corroborated by the recent extremely precise determinations of Oliphant, Kempton and Rutherford[6] who used the data from certain nuclear transformations. The comparison is given in Table IV. Since in some cases, notably that of oxygen, the mass ratio of the isotopes has been determined only from the band spectrum, it is worth while to examine the apparent discrepancy in the case of lithium, by determining spectroscopically the mass ratio of Li^7 to Li^6 under the more favorable conditions existing in the red band system of Li_2. This system has been analyzed by Wurm,[7] but the constants of $Li^7 Li^7$ were not determined with great precision, and the constants of $Li^7 Li^6$ not at all.

In a recent Letter to the Editor of this journal[8] we showed that the mass ratio of the Li isotopes calculated from the molecular constants obtained from a study of the $(v',0)$ progression of the red $^1\Sigma \rightarrow {}^1\Sigma$ system of Li_2 was in good agreement with the mass ratio obtained by other methods. Since the most accurate value of ρ came from the vibrational constant ω_e of the

[1] R. de L. Kronig, Physica **1**, 617 (1934).
[2] G. H. Dieke, Phys. Rev. **47**, 661 (1935).
[3] Holst and Hulthèn, Zeits. f. Physik **90**, 712 (1934).
[4] F. A. Jenkins and A. McKellar, Phys. Rev. **44**, 325 (1933); A. McKellar, Phys. Rev. **44**, 155 (1933).
[5] K. T. Bainbridge, Phys. Rev. **44**, 56 (1933).
[6] M. L. E. Oliphant, A. E. Kempton and Lord Rutherford, Proc. Roy. Soc. **A149**, 406 (1935).
[7] K. Wurm, Zeits. f. Physik **59**, 35 (1929).
[8] G. M. Almy and G. R. Irwin, Phys. Rev. **48**, 104 (1935).

upper $^1\Sigma$ state, a state not involved in the $^1\Pi \rightarrow {}^1\Sigma$ system, our result did not conflict directly with that obtained by McKellar and Jenkins. We have since measured the $(0,v'')$ progression of the same system and made the calculations of ρ from the constants of the lower state, common to the $^1\Pi \rightarrow {}^1\Sigma$ and $^1\Sigma \rightarrow {}^1\Sigma$ systems. Again we have found agreement with the value of ρ obtained by other methods; there seems to be no question but that, in the case of Li_2, the band spectrum method leads to the same mass ratio as other methods and that the probable error in the determination is not much larger than in the other methods.

An accurate calculation of the lower state constants has led to the determination, with considerable accuracy, of a small but definite electronic isotope shift. This point was in doubt in our letter.

Rotational and Vibrational Analysis

The plates used were photographed in absorption in the first order of a 21-foot, 30,000-lines per inch, concave grating. The dispersion is about 1.3A per mm. The standard lines were iron arc, second order. As in the case of the $(v',0)$ progression measurements, all comparator settings were made by each of two observers, except for the (0,4) band which was carefully remeasured by the only observer. Since the work on the $(v',0)$ progression showed consistent values of wave number among the various exposures, the $(0,v'')$ progression was measured on only one set of plates.

The method followed in the analysis was the same as that outlined in our previous letter. The first ten or twelve lines in each branch of each band were measured, $\Delta_2 F$'s were computed and corrected for a small D term, and the rotational B_v's calculated. By using the relation $B_v = B_e - \alpha_e(v+\frac{1}{2})$ the best values of B_e and α_e were obtained by least squares. Due weight was given to the fact that there were five determinations (six in $Li^7\,Li^7$) of B_0'' made in the analysis of the $(v',0)$ progression.

The band origins (ν_0) were calculated with reference to each measured line (ν), with the relation,

$$\nu = \nu_0 + (B_v' + B_v'')M + (B_v' - B_v'')M^2 + 2(D' + D'')M^3, \quad (1)$$

where $M = -K''$ for P lines, $M = K'' + 1$ for R lines. Smoothed values of B_v were used, obtained from $B_v = B_e - \alpha_e(v+\frac{1}{2})$. Only rough values of the D's were necessary on account of the smallness of the term in M^3 for small M; McKellar gives D_v'' accurately and we estimated D' with sufficient precision from measurements to large quantum numbers on the (3,0) band. In both the $(v',0)$ and $(0,v'')$ progressions ten to twenty lines free from serious blending were used in calculating the origin of each band, with the exceptions of the (0,0) $Li^7\,Li^6$ band where only four good lines were available, and the (3,0) bands, where almost exact coincidence of the P and R branches occurs near the origin.

The average deviation from the mean of the calculated origins was in the case of each band, with the exceptions mentioned, less than ± 0.025 cm^{-1}. The probable error of a mean origin, then, is less than ± 0.01 cm^{-1}. This is, however, a statement only of the consistency of the relative measurements of wave number within a band, or, at most, for one setting of the plate on the comparator. Since only one isotopic pair of bands were measured at one setting of the plate, and since small discrepancies occasionally appeared in the calculation of iron lines between standards we believe the probable error of an origin to be in the neighborhood of ± 0.02 cm^{-1}. This belief is supported by the fact that the fluctuations in the very small third differences (~ 0.05 cm^{-1}) formed on the origins can be smoothed by

Table I. *Rotational constants and origins of bands.*

v',v''	B_v''	$B_v''^{\delta}$	B_v'	$B_v'^{\delta}$	ν_0	ν_0^{δ}
0,0	0.6690	—	0.4949	0.5360	14,020.616	14,018.602
0,1	0.6622	0.7166	0.4949	0.53535	13,674.416	13,658.536
0,2	0.6552	0.7083	0.4945	0.5365	13,333.403	13,304.049
0,3	0.64785	0.7003	0.4953	0.5368	12,997.697	12,955.341
0,4	0.6404	0.6918	0.49505	0.5362	12,667.253	12,612.345
1,0	0.6696	0.7252	0.4898	0.5305	14,272.950	14,281.113
2,0	0.6691	0.7248	0.4837	0.5232	14,522.107	14,540.160
3,0	(0.6681)	0.7248	(0.4767)	0.5179	14,768.148	14,795.822
4,0	0.6692	0.7240	0.4744	0.5113	15,011.073	15,048.180
5,0	0.6693	0.7248	0.4687	0.5050	15,250.906	15,297.170
$B_e'' = 0.67293 \pm 0.00017$		$B_e''^{\delta} = 0.72892 \pm 0.00012$		$B_e' = 0.49754 \pm 0.00025$		$B_e'^{\delta} = 0.53933 \pm 0.00025$
$\alpha_e'' = 0.00719 \pm 0.00007$		$\alpha_e''^{\delta} = 0.00823 \pm 0.00005$		$\alpha_e' = 0.00522 \pm 0.00008$		$\alpha_e'^{\delta} = 0.00623 \pm 0.00008$
$\rho = [B_e''/B_e'']^{\frac{1}{2}} = 1.04077 \pm 0.00015$				$\rho = [B_e'^{\delta}/B_e']^{\frac{1}{2}} = 1.04114 \pm 0.0003$		
$\rho = [\alpha_e''^{\delta}/\alpha_e'']^{\frac{1}{2}} = 1.043 \pm 0.005$				$\rho = [\alpha_e'^{\delta}/\alpha_e']^{\frac{1}{2}} = 1.058 \pm 0.008$		
McKellar: $\rho = \left[\frac{B_e''^{\delta}}{B_e'}\right]^{\frac{1}{2}} = \frac{0.7302 \pm 0.0007}{0.6721 \pm 0.0003} = 1.0422 \pm 0.0006$						

TABLE II*a*. *Lower state vibrational constants.* Column (2) contains the best values.

	(1)	(2)	(3)	(4)
	$y_e''\omega_e''=-0.0063$ $y_e''^{\delta}\omega_e''^{\delta}=-0.0111$	$y_e''\omega_e''=-0.0097$ $y_e''^{\delta}\omega_e''^{\delta}=-0.0111$	$y_e''\omega_e''=0$ $y_e''^{\delta}\omega_e''^{\delta}=0$	McKellar
ω_e''	351.398	351.346±0.017	351.494	351.374
$\omega_e''^{\delta}$	365.658	365.658±0.021	365.828	365.993
$x_e''\omega_e''$	2.583	2.557±0.004	2.630	2.590
$x_e''^{\delta}\omega_e''^{\delta}$	2.768	2.768±0.004	2.851	2.844
E_ν	±0.010	±0.012	±0.014	
E_ν^{δ}	±0.015	±0.015	±0.020	
$\rho=\omega_e''^{\delta}/\omega_e''$	1.04058	1.040735 ±0.00008	1.04078	1.0416±0.0002
$\rho=[x_e''^{\delta}\omega_e''^{\delta}/x_e''\omega_e'']^{1/2}$	1.0352	1.0404±0.0011	1.0412	1.048±0.01
ν_0	14068.316	14068.291±0.020	14068.408	
ν_0^{δ}	14068.195	14068.215±0.032	14068.287	
$\nu_e^{\delta}-\nu_e$	−0.121	−0.076±0.038	−0.121	

TABLE II*b*. *Upper state vibrational constants.*

	(1)	(2)	(3)
	$y_e'\omega_e'=0.0039$ $y_e'^{\delta}\omega_e'^{\delta}=0.0067$	$y_e'\omega_e'=0.0039$ $y_e'^{\delta}\omega_e'^{\delta}=0.0044$	$y_e'\omega_e'=0$ $y_e'^{\delta}\omega_e'^{\delta}=0$
ω_e'	255.507	255.507±0.004	255.421
$\omega_e'^{\delta}$	265.963	265.914±0.015	265.816
$x_e'\omega_e'$	1.597	1.597±0.001	1.561
$x_e'^{\delta}\omega_e'^{\delta}$	1.745	1.725±0.003	1.685
E_ν	±0.003	±0.003	±0.013
E_ν^{δ}	±0.010	±0.013	±0.024
$\rho=\omega_e'^{\delta}/\omega_e'$	1.04092	1.04073 ±0.00006	1.04070
$\rho=[x_e'^{\delta}\omega_e'^{\delta}/x_e'\omega_e']^{1/2}$	1.0455	1.0394±0.0008	1.0387
ν_0	14068.295	14068.295±0.006	14068.344
ν_e^{δ}	14068.196	14068.222±0.023	14068.279
$\nu_e^{\delta}-\nu_e$	−0.099	−0.073±0.024	−0.065

shifting origins by 0.02 cm^{-1} or less. There may still be a small systematic shift throughout the spectrum due to the use of second order lines for standards. Since differences of wave number are used in determining the molecular constants and ρ such a shift could not affect the results.

The results of the rotational analysis are given in Table I. For completeness, some of the results of our previous letter are included. The B_v's and the origins of each of the twenty bands are listed, and the values of B_e and α_e given below. As mentioned above, due weight was given, in the calculation of the B_e's and α_e's, to the fact that several determinations were made of B_0' and B_0''. The table also contains the values of ρ obtained from the ratios of rotational constants, and, on this point, a comparison with McKellar's results for the ground state.

From the band origins the vibrational constants may be computed, since,

$$\nu_0(v',v'')=\nu_e+[\omega_e'(v'+\tfrac{1}{2})-x_e'\omega_e'(v'+\tfrac{1}{2})^2+y_e'\omega_e'(v'+\tfrac{1}{2})^3]-[\omega_e''(v''+\tfrac{1}{2})-x_e''\omega_e''(v''+\tfrac{1}{2})^2+y_e''\omega_e''(v''+\tfrac{1}{2})^3]. \quad (2)$$

The general method for obtaining the vibrational constants of the lower state was to take the primed constants from our previous work on the $(v',0)$ progression, insert the origins $(\nu_0(v',v''))$ from Table I and to compute ν_e, ω_e'', $x_e''\omega_e''$ and $y_e''\omega_e''$ by least squares. Several variations of this method were tried, the results of which are given in Table II*a*.

(1) The constants obtained by straight least squares with the third degree Eq. (2) are given in column (1). This gives values of $y_e''^{\delta}\omega_e''^{\delta}$ and $y_e''\omega_e''$ which have a much larger ratio than the theoretically correct ratio, $\rho^3\sim1.13$. One may, however, expect these small constants to be correct only as to order of magnitude since the small third differences $(=6y_e\omega_e)$ formed on the origins, though showing a trend, fluctuate even in sign. The constants have been tested by computing the origins with them; the calculated probable error E_ν of a single observed origin for each type of molecule is given. E_ν is equal to $0.674([rr]/n-q)^{\frac{1}{2}}$ where $[rr]$ is the sum of the squares of the residuals, n the number of observations, and q the number of constants being determined.

(2) If one assumes a particular value of $y_e''\omega_e''$, or $y_e''^{\delta}\omega_e''^{\delta}$, to be correct and requires the other to bear approximately the proper ratio, ρ^3, to it, appreciably different constants are obtained. Since Loomis and Nusbaum[9] have made a vibrational analysis of the ground state extending to $v=15$, their value of $y_e''\omega_e''(=-0.0097)$ is probably more reliable than that given in column (1). Their value bears a sufficiently correct ratio to the least squares $y''^{\delta}\omega_e''^{\delta}$ to let the latter stand. When the observed origins of $Li^7\,Li^7$ are

[9] F. W. Loomis and R. E. Nusbaum, Phys. Rev. **38**, 1447 (1931).

corrected by a term, 0.0097 $(v''+\frac{1}{2})^3$, and the corrected origins fitted by least squares to the second degree equation in $(v''+\frac{1}{2})$, the constants in column (2) were obtained. The fit as indicated by E_ν, is almost as good as with the constants in column (1).

(3) As a special case of (2) one may assume $y_e''\omega_e''$ and $y_e'^i\omega_e'^i$ to be negligibly small. Column (3) shows the results obtained by fitting both the Li^7Li^7 and Li^7Li^6 to second degree equations.

Now the calculated probable errors, E_ν and $E_\nu{}^i$, indicate that any of the three sets of constants will represent the observed origins rather more accurately than one could have expected from the estimate of experimental probable errors made above (± 0.02 cm^{-1} in an origin). A choice among them must therefore be made on the basis of considerations other than goodness of the fit. Since the $y_e\omega_e$'s of column (2) satisfy the theoretical condition on their ratio and since they agree with an independent determination of $y_e''\omega_e''$, the other vibrational constants of column (2) are presumably the best values in Table II*a*.

Before discussing the value of ρ obtained from the vibrational constants, we will reconsider the data from the $(v',0)$ progression according to the scheme outlined for the $(0,v'')$ progression. Table II*b* gives in column (1) the results of a straight least-squares calculation. Since the fit of the Li^7Li^7 bands to the equation is so surprisingly good ($E_\nu = \pm 0.003$ cm^{-1}), $y_e'^i\omega_e'^i$ was adjusted to $\rho^3 y_e'\omega_e'$ in column (2) and $\omega_e'^i$ and $x_e'^i\omega_e'^i$ recomputed. Column (3) shows the constants obtained when the $y_e'\omega_e''$s are assumed to be negligibly small. As in the case of the $(0,v'')$ progression the constants of column (2) represent the observed origins practically as well as those of column (1) and better than those of column (3). Moreover, they satisfy the condition that $y_e'^i\omega_e'/y_e'^i\omega_e' \sim (1.04)^3$ which the constants of column (1) do not, and they represent much better than column (3) the trend of the third differences. Column (2) is therefore the best choice. The constants therein do not differ significantly from those published in our previous report of the $(v',0)$ progression. The errors given in column (2) are probable errors obtained by multiplying E_ν and $E_\nu{}^i$ by the weight factors appropriate to each constant. In column (3) the errors would be somewhat larger, in column (1) some would be slightly smaller.

The values of ρ obtained from ratios of vibrational constants are also given in Table II. The most accurate values of ρ are obtained from the ratios of the ω_e's in column (2) and in this column the agreement between $\omega_e'^i/\omega_e''$ and $\omega_e'^i/\omega_e'$ is seen to be excellent. A comparison with column (3), however, shows that the assumption of any pair of constants $y_e\omega_e$ and $y_e{}^i\omega_e{}^i$ (at least any pair between the limits set in these columns) which have approximately the correct ratio will lead, in the ratios of the other constants, to sensibly the same values of ρ. The values of ρ in column (1) obtained by using uncritically the constants obtained from a least-squares calculation with the third-degree equation lie somewhat outside the probable errors of column (2), one too high, one too low. We believe it may fairly be said, however, that the same mass coefficient ρ is obtained from the vibrational analysis of each of the two lowest states of Li_2 and that this coefficient is 1.04073 ± 0.00008.

It should be remarked that if the more elaborate expression for the energy of a rotating vibrator, developed by Dunham,[10] is used the values of the constants are not appreciably changed. The correction terms to B_e and ω_e are, however, large enough to be important if one attempts to evaluate ρ to seven significant figures, instead of six.

The vibrational analysis also leads to the determination of the origin of the two isotopic systems and hence to the electronic isotope shift. In Table II the origins are given as obtained from the least-squares calculation outlined above for each of the columns. The difference $\nu_e{}^i - \nu_e$ is defined as the electronic shift. Added indication of the superiority of the constants of column (2) lies in the fact that with these constants both progressions extrapolate to practically identical values of ν_e and $\nu_e{}^i$. The mean electronic isotope shift is -0.074 ± 0.025 cm^{-1}.[11]

[10] J. L. Dunham, Phys. Rev. **41**, 721 (1932).

[11] In our previous account we found $\nu_e{}^i > \nu_e$. Improved constants for the lower state have made possible better values of the origins and it is found that $\nu_e{}^i < \nu_e$. The contradiction then existing between the values of the electronic shift as obtained by two methods has thus disappeared.

Alternative Calculation of ρ and Electronic Shift

There is an alternative method of determining ρ and the electronic shift which appears to be superior to the methods which have been discussed. It consists of taking as observed data the total isotope shifts of the band origins and calculating by least squares the values of ρ and $\Delta\nu_e$ which best fit the data. On the experimental side, the advantage of this method is that only isotope *shifts* are involved. The two bands concerned in one observed datum are measured without moving the plate and under nearly identical conditions so that an observed shift, though a difference of two measured origins, is probably correct to ± 0.02 cm^{-1}. The (0,0) and probably the (3,0) bands are exceptions. The former was omitted but the latter was used in this calculation.

The isotope shift of the origin of the (v',v'') band may be written,

$$\Delta\nu_0(v',v'')=\Delta\nu_e+(\rho-1)\times\{[\omega_e'(v'+\tfrac{1}{2})-\omega_e''(v''+\tfrac{1}{2})]-(\rho+1)[x_e'\omega_e'(v'+\tfrac{1}{2})^2-x_e''\omega_e''(v''+\tfrac{1}{2})^2]+(\rho^2+\rho+1)[y_e'\omega_e'(v'+\tfrac{1}{2})^3-y_e''\omega_e''(v''+\tfrac{1}{2})^3]\}, \quad (3)$$

where $\Delta\nu_e=\nu_e{}^i-\nu_e$ and all of the constants are those of $Li^7\,Li^7$. Writing the quantity in braces $\{V\}$ we have,

$$\Delta\nu_0(v',v'')/\{V\}=\Delta\nu_e/\{V\}+(\rho-1). \quad (4)$$

We wish to obtain $\Delta\nu_e$ and $\rho-1$ by least squares. This requires that we know $\{V\}$. Since it is $(\rho-1)$, rather than ρ which is the last term in Eq. (4), relatively high accuracy in ρ will be obtained without accurate knowledge of the ρ or the constants appearing in $\{V\}$. It does not matter, for example, which column of constants from Table II is used. Actually the constants of column (2) were used and $\{V\}$ rounded to the nearest integer ($\{V\}$ varies from 200 to 1300). In $\{V\}$, ρ was put at 1.04075; 1.041 would have done as well.

The chief assumption made in this calculation is the usual one in the theory of the isotope effect, that the ratio of each pair of vibrational constants is a power of ρ or, more specifically, that, in Eq. (3), the factor $(\rho-1)$ has the same value for each term within the braces that it is to be multiplied into.

Table III. $\Delta\nu_e$ and $(\rho-1)$ from Eq. (3).

Band	Observed Shift $\nu_0{}^i-\nu_0$	Calculated Shift Eq. (3)	O−C
	$(v',0)$ progression: $\rho-1=0.040810\pm0.000010$ $\Delta\nu_e=0.0683\ \pm0.0001$ cm^{-1}		
0,0*	−2.014	−2.002	−0.012
1,0	+8.163	8.159	+ .004
2,0	18.053	18.060	− .007
3,0	27.674	27.703	− .029
4,0	37.107	37.093	+ .014
5,0	46.264	46.231	+ .031
	$(0,v'')$ progression: $\rho-1=0.040773\pm0.000007$ $\Delta\nu_e=0.0542\ \pm0.0001$ cm^{-1}		
0,0*	− 2.014	− 1.987	−0.027
0,1	−15.880	−15.882	+ .002
0,2	−29.354	−29.341	− .013
0,3	−42.356	−42.356	.000
0,4	−54.908	−54.922	+ .014

* Not used in calculation of constants.

The results of the calculations are given in Table III. $(\rho-1)$ and $\Delta\nu_e$ as obtained from each progression are given as well as the detailed comparison of the observed and calculated shifts. Alternative calculations were made in one of which the observations were weighted approximately according to the magnitude of the shift. In still another calculation of the $(v'0)$ progression, the observations were thus weighted and the (3,0) band omitted. In each case the changes in $(\rho-1)$ and $\Delta\nu_e$ were of the order of magnitude of the formally calculated probable errors in Table III.

This method of calculation leads to somewhat higher values of ρ (though within the probable errors) than the earlier methods of comparing constants individually. The probable errors, as judged by internal consistency, of the two values of ρ obtained by the second method are so small as to indicate disagreement between these two values. This discrepancy can be traced to the chief assumption, that in Eq. (3) $(\rho-1)$ is the same factor for all terms in the braces. Actually $[x_e{}^i\omega_e{}^i/x_e'\omega_e']^{\frac{1}{2}}$ was found in Table II to differ from $\omega_e{}^i/\omega_e'$ by more than the probable errors; if this is actually the case Eq. (3) with a common $(\rho-1)$ factor is not strictly applicable. The difference of $[x_e{}^i\omega_e{}^i/x_e'\omega_e']^{\frac{1}{2}}$ and $\omega_e{}^i/\omega_e'$ is not definite enough to give the argument much weight but it may signify that there is a slight difference in the potential energy curves of the

TABLE IV. *Comparison of determinations of mass ratio.*

	ρ	m_7/m_6
McKellar-Jenkins: $\omega_e'^6/\omega_e'(^1\Pi)$	1.0411 ±0.0002	1.1678 ±0.0008
Li_2 spectrum $^1\Sigma \rightarrow {}^1\Sigma$: $\omega_e'^6/\omega_e'$	1.04073 ±0.00006	
$\omega_e''^6/\omega_e''$	1.040735 ±0.00008	
$[B_e'^6/B_e']^{\frac{1}{2}}$	1.04114 ±0.0003	
$[B_e''^6/B_e'']^{\frac{1}{2}}$	1.04077 ±0.00015	
From isotope shift: $(v',0)$	1.040810 ±0.000010	
$(0,v'')$	1.040773 ±0.000007	
Band spectrum value:	1.04077 ±0.00004	1.16640 ±0.00016
Bainbridge (mass spectrograph)		1.16628 ±0.00010
Oliphant, Kempton and Rutherford (nuclear transformation)		1.16635 ±0.00005

upper state for the two isotopic molecules. Such considerations would reduce the weight of the calculation of ρ from data on the upper state, especially by the use of Eq. (3). Since the constants of the lower state may be similarly but less affected one cannot claim to have determined ρ to the accuracy indicated by the consistency of the calculations based on Eq. (3). Considering the various determinations of ρ, reviewed in Table IV, one may, however, conservatively conclude that the band spectrum value of ρ is 1.04077 ± 0.00004.

The electronic shifts calculated from the two progressions by Eq. (3) do not agree within the probable errors suggested by internal consistency. This discrepancy is associated with the similar one found in $(\rho-1)$. Giving the determinations in column (2), Table II some weight, one may conclude that $\Delta\dot{\nu}_e = 0.064 \pm 0.010$ cm. This electronic shift, though definite, is probably too small to be discussed in terms of the incomplete theory of electronic shifts in molecular spectra at present available. Kronig has pointed out that even in the absence of rotation there is in the potential energy of Σ states a term $B_eL(L+1)$, which, with B_e, depends upon the reduced mass. For the ground $^1\Sigma$ state of Li_2, arising from $^2S+{}^2S$ atomic states, L must be zero. The excited $^1\Sigma$ state, however, arises from $^2P+{}^2S$ Li atoms and is presumably $\cdots 2p\sigma 2p\sigma\,{}^1\Sigma$ for which $L=1$. Hence there should be a difference in the electronic energies of the two isotopic molecules equal to $2(B_e'^{\frac{1}{2}}-B_e')$ or about 0.08 cm^{-1}, and the Li^7Li^6 state should lie higher. Actually, if one assumes the observed shift to be entirely in the upper state, the Li^7Li^6 state lies about 0.06 cm^{-1} lower. But until other small effects (see Kronig) on the electronic energy can be calculated, significance can hardly be attached to this discrepancy with theory. One must, for example, consider the fact that there is an isotope shift of about 0.35 cm^{-1} in the $^2P \rightarrow {}^2S$ atomic lines of Li,[12] the Li^7 lines being of greater frequency. That is to say, the products of dissociation of Li^7Li^7 and Li^7Li^6 have an isotope effect several times as large and in the same direction as the molecular electronic effect.

Note added to proof, December 6, 1935: Professor F. A. Jenkins has informed us of the results of recent measurements on the $^1\Sigma \rightarrow {}^1\Sigma$ system of Li_2 bands made by him and Dr. McKellar for the purpose of testing our conclusion[9] as to the value of ρ. Their results were reported at the Berkeley meeting of the Physical Society, December 20, 1935. Using the same bands but a different method of handling the data they secure values of $\rho: \omega_e'^6/\omega_e' = 1.04100$ and $\omega_e''^6/\omega_e'' = 1.04107$, lower than their previous estimates from the blue-green system but still higher than our present values. The remaining discrepancy is ascribed by them to the difference in the methods of handling the data. Their method has been described by McKellar.[4] It consists in forming differences such as $\Delta T''_{v+\frac{1}{2}}(K) = R^{v',\,v''}(K') - R^{v',\,v''+1}(K') = P^{v',\,v''}(K') - P^{v',\,v''+1}(K')$ which are equal to $\Delta G''_{v+\frac{1}{2}} - \alpha_e''(K''+\frac{1}{2})^2$ for not too large K''. From the series of ΔG's the vibrational constants are obtained.

To test our data by this method we have formed the differences $\Delta T''(K')$ for the $(0,v'')$ progressions of the bands of both kinds of molecules, added the correction terms $\alpha_e''(K''+\frac{1}{2})^2$, using our α_e''s from Table I, to get values of $\Delta G''_{v+\frac{1}{2}}$. The average $\Delta G''_{v+\frac{1}{2}}$ so obtained is, for each vibrational interval, exactly equal to the corresponding quantity obtained by taking the difference between origins in Table I; the greatest discrepancy is less than 0.02 cm^{-1}. Hence with our data, limited to low K, the two methods should give identical values of ρ, at least in the case of the $(0,v'')$ progression. The small remaining discrepancy in ρ then appears to be due to the fact that Jenkins and McKellar make use of lines of larger rotational quantum number while we use lines of $K<13$, which provide ample data for exact analysis and which do not involve any complication which might arise from rapid rotation of the molecule.

[12] H. Schüler and E. Wurm, Naturwiss. **15**, 971 (1927); D. S. Hughes, Phys. Rev. **36**, 698 (1930); ibid. **38**, 857 (1931).

Thermionic Emission from Tungsten and Thoriated Tungsten Filaments

W. B. NOTTINGHAM, *George Eastman Research Laboratory of Physics, Massachusetts Institute of Technology, Cambridge, Massachusetts*

(Received October 7, 1935)

The electron emission from pure and thoriated tungsten filaments has been investigated as a function of the applied potential over the entire range from a few volts retarding to 1400 volts accelerating including careful studies at zero field. The filaments were heated with pulsating currents from thyratrons to eliminate during the measurements any drop in potential along the filament. The energy distribution of electrons was found to be deficient in slow electrons. An empirical reflection factor of $R(p_x)=\exp -p_x^2/2m\omega$, where ω is a constant 3.05×10^{-13} erg, represents the observed data for all temperatures and all states of activation for the thoriated tungsten. Analysis shows that there is no disagreement between the new results and the experiments of Germer. Zero-field Richardson plots show that the reflection effect alters both the A and b of Richardson's equation. The resulting values after correcting for reflection are $A=204$ and $b=55{,}100$ for pure tungsten. This value of A indicates a negative temperature coefficient of the work function of 4.3×10^{-5} volt per degree, which has been verified by an independent experiment. New data on the electron emission in accelerating fields are given for many states of activation, showing that there are large deviations from the Schottky mirror image theory. Becker's patch theory is discussed briefly and a simpler strip theory is developed which serves to represent the observed data as an empirical result. This analysis shows that the patch theory is not suitable to explain the reflection effect since it is independent of the state of activation of the filament.

INTRODUCTION

THE thermodynamic treatment of Dushman,[1] as well as the Fermi-Sommerfeld[2] theory of metals, yields the equation

$$I=(4\pi m\epsilon k^2/h^3)T^2e^{-b/T} \qquad (1)$$

for the saturation emission from an ideal emitting surface at zero field. The constants m, ϵ, k, and h have their usual significance and if values are introduced so as to express the current in amp. per cm², this coefficient has the value 120 amp. per cm² per degree.[2] Experiment shows that no known emitting surface meets the requirements of being an *ideal surface*. Real surfaces are defective in the following respects: (1) The true surface area is generally not equal to the apparent area. (2) The work function b which would be appropriate for a given small area of the surface (for example, a single crystal facet) is generally not the same over the entire surface used in experiment because of defects at crystal boundaries and because evaporation often exposes two or more kinds of crystal facets. Surface contaminations produce regions of different work functions. (3) Real surfaces generally show electron reflection effects. (4) Instead of the true work function b, we usually measure another quantity b_0 which may be related to b by the equation[3]

$$b=b_0+\alpha T. \qquad (2)$$

It is the purpose of this paper to present certain new experimental facts which may be interpreted in terms of these differences between real and ideal emitting surfaces. The method of attack was to study the electron emission as a function of the electric field over the entire range from a few volts of retarding potential to over 1400 volts accelerating potential for as wide a range of temperature as possible and for all states of activation when using a thoriated filament.

ELECTRON EMISSION FROM A FILAMENT IN A RETARDING ELECTRIC FIELD

Experimental tubes

For accurate measurements of emission in a retarding field or with very low accelerating fields, it is absolutely necessary that there be no drop in potential along the filament being studied. The filament must be long and the emission must be uniform over the entire length which is able to deliver current to the observing

[1] S. Dushman, Phys. Rev. **21**, 623 (1923). Original treatment did not include effect of electron spin which doubles the earlier value of 60 amp. per sq. cm per degree.

[2] L. Nordheim, Physik. Zeits. **30**, 177 (1929).

[3] Within the accuracy of present day experiments, only these two terms of the power series expansion are needed.

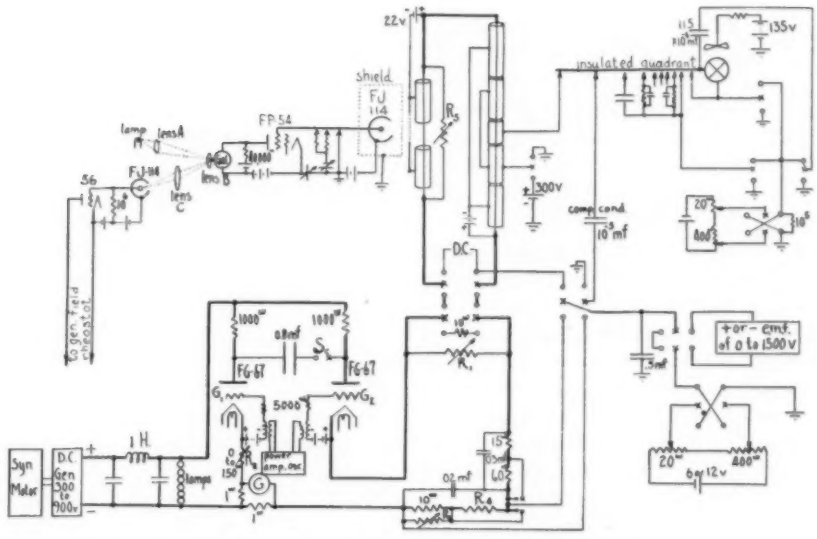

FIG. 1. Thyratron inverter circuit for heating filament with pulsating current.

instrument. The tubes used with thoriated tungsten filaments contained five tantalum collectors 1 cm in diameter, concentric with respect to the filament. The center collector, 2.5 cm long, was well insulated and served to deliver the electron current to the electrometer for measurement. The measuring circuit insured that this collector was always at ground potential. The two collectors adjacent to this one were 4.5 cm in length and were always maintained at ground potential. The two outermost collectors, also 4.5 cm in length, were generally maintained 12 volts negative with respect to the filament. This was done in order to suppress all electron emission from the ends of the filament which were never in the same condition as the middle because the temperature was lowered by the cooling effect of the leads and because the state of activation was very different from that at the middle. The filament material used is designated by the General Electric Company as "E" wire containing about one percent ThO_2 and no carbon. The filaments were about 21 cm in length and about 2.8 mils in diameter. The upper end of the filament was fixed while the lower end was held by a tungsten spring made in accordance with the information published by Langmuir and Blodgett.[4] The filament was welded to small "chips" of tantalum which in turn were welded to the supporting connections. Potential leads were also welded to these "chips" so that the true over-all potential of the filament could be measured accurately by a Leeds and Northrup type K potentiometer operated to give a 16-volt range instead of the usual maximum of 1 6 volts. The potential drop over a one-ohm resistance served to give an accurate measure of the filament current. The temperature of the filament was determined from these measurements after correction for end losses,[5] with both the Langmuir-Jones[6] and the Forsythe and Watson[7] temperature scales. Since these two scales yield temperatures which differ by about 3 to 5 degrees, a temperature was always taken lying between the two scales, generally a little nearer the F and W value. The temperatures were calculated from the functions, according to the Langmuir-Jones notation, $A/d^{\frac{1}{2}}$, $VA^{\frac{1}{2}}/l$ and

[4] Katharine B. Blodgett and I. Langmuir, Rev. Sci. Inst. **5**, 321 (1934).
[5] I. Langmuir, S. MacLane and K. B. Blodgett, Phys. Rev. **35**, 478 (1930).
[6] H. A. Jones and I. Langmuir, Gen. Elec. Rev. **30**, 310, 354, 408 (1927).
[7] W. E. Forsythe and E. M. Watson, J. Opt. Soc. Am. **24**, 114 (1934).

VA/ld. In terms of the resistivity R and the total watts W, these are $W^{\frac{1}{2}}/R^{\frac{1}{2}}$, $W^{\frac{1}{2}}R^{\frac{1}{2}}$ and W, respectively. In computing the final temperatures, the last two were given greater weight. When the filament was heated by pulsating current, the temperature was held constant within about 0.1 degree by a "photoelectric ammeter" which will be described below.

One of the tubes containing the pure tungsten wire (G. E. Co. 218) had only three collectors and consequently the results obtained are probably less reliable because of the shortness of the filament and the fact that impurities might have been present near the cool ends of the filament, giving an abnormal contribution to the emission. Another tube with a tungsten filament had five collectors as described above and also 0.6-mil potential leads welded directly to the filament at a distance far enough from the supporting leads so that the cooling effect could be neglected. In this tube the filament was not exactly on the axis of the collectors at all temperatures and therefore the results obtained in this case are subject to a little doubt, although calculation shows that the effect of noncentering should be of secondary importance.

An extensive outgassing schedule was used in every case, lasting between three and five days. All metal parts were outgassed before assembly and the cylinders were heated many hours at a high temperature by induction after the final assembly. Oven baking at 450°C was used. Before sealing off, two or three magnesium-barium getter caps were heated lightly to give a deposit of "getter" over the lower end of the tube. After heating the getter caps and also the seal-off constriction, the collectors were heated extensively by electron bombardment just before the final seal-off of the tube. Ionization current measurements were made by connecting the center collector to a potential 22 volts negative with respect to the filament and the two adjacent collectors to 220 volts positive with respect to the filament. The electron current to ion current ratio was generally about 10^7 to one. Although this corresponds to a pressure of about 10^{-8} mm of mercury, the fact that the condition of the filament would remain very accurately constant for weeks at a time without high temperature flashing proved that the partial pressure of any gas which could contaminate the filament had been reduced to a very small fraction of that indicated by the ionization current measurements. Early in the outgassing process the filament was heated to at least 3000°K for ten seconds and maintained at somewhat lower temperatures for some hours to remove the traces of impurities which so greatly distort results if this is not done.

Electric circuits

The filament heating circuit was patterned after the one described in a previous publication,[8] which will be referred to below as (PR–I). Certain improvements which make for a considerable increase in accuracy necessitate the reproduction of the circuit diagram in its modified form. Although one can see by an inspection of the diagram the main features, some of the others need explanation.

The galvanometer G gave a continuous indication that the heating current was on exactly one-half of the time. This was accomplished by first adjusting the resistance R_1 to give the correct heating current through the filament after which the switch S_c was opened so as to cause both thyratrons to remain on continuously. R_2 was then adjusted to bring about a "static" balance, as indicated by the galvanometer G. The resistances of the two branches of the circuit were thus equalized to better than 0.1 percent. With switch S_c closed, the 200-cycle oscillator input to the grids G_1 and G_2 was adjusted to give a "dynamic" balance as indicated by the galvanometer. After this was done, a check of the thermionic current, with an accelerating field high enough so that the drop in potential along the filament when heated by direct current was negligible, showed that the electron current delivered with pulsating heating current was accurately one-half that observed with d.c. heating.

Because of the fact that dielectrics are never perfect, compensation was necessary to eliminate the capacity currents which would otherwise flow in and out of the collector system because of the large changes of potential of the filament with respect to the collector as the heating current

[8] W. B. Nottingham, Phys. Rev. **41**, 793 (1932).

went on and off. In the extreme cases, this was as much as 75 volts. The compensation was accomplished by putting on a retarding potential V of about 6 volts, so as to cut off all electron emission, after which the ground key was opened while the electrometer circuit was arranged for the highest sensitivity. If the compensation was not correct, a throw to the right or left was observed, depending on whether the ground key was opened during a heating or nonheating cycle. By adjusting rheostat R_3 and resistance R_4 this throw was eliminated, thus showing perfect compensation.

For the smallest currents the rate of charging a condenser was used for the measurement. The condensers used were 11.5×10^{-12} farad and 403×10^{-12} farad, the smaller being mounted as part of the electrometer, while the latter was a quartz insulated 25-plate fixed condenser which also served as a standard for calibrating the high resistances used when the range of electron currents measured was so small that the one megohm standard could not be used satisfactorily. These condensers permitted the measurement of currents of 5×10^{-15} amp. to an accuracy of about 2 percent. The electrometer sensitivity was 6 mm per millivolt, and it was adjusted to be very slightly under-damped with a period of about 4 sec. The electrometer was of the Compton type of our own design with a needle of 2.5 mm radius.

Resistances between 6 and 5000 megohms were made by evaporating platinum in high vacuum on the inside of Pyrex bulbs. These, as well as wire wound resistances from 100 ohms to one megohm, were used for measuring the high currents. In every case the resistances were shunted by capacities such that the time constant CR was of the order of 0.6 sec. This is necessary in order that the collector potential remain essentially at ground potential as indicated by the balance of the electrometer, otherwise the collector will go negative with respect to ground about half the voltage required to give the compensation.

A General Electric FJ-114 photo-cell was used with the "photoelectric ammeter." Since this tube changed its sensitivity slowly after changes in illumination, it was kept under a constant state illumination continuously. The shunting resistance R_5 permitted the use of a constant current through the auxiliary filament. The output of the photo-cell was measured by a null method using an FP-54 amplifier. Thus the zero reading of the galvanometer in the plate circuit served as a continuous indication of the filament temperature. The sensitivity was such that a six to ten-cm deflection was produced by a one-degree change in temperature of the filament. While one galvanometer lamp was used to indicate the deflection, a second one was used for automatic compensation. The image of the condensing lens A of the galvanometer lamp was brought to focus by the galvanometer lens B on a large reading glass lens C fitted with a wedge-shaped aperture. This lens focused the image of the lamp filament on a FJ-114 photo-cell which controlled the plate current of a 56 type vacuum tube shunted across the field rheostat of the generator. By adjusting the intensity of the lamp, the system could be made to compensate almost perfectly for all rapid changes in the filament heating circuit due to changes in the power line voltage or frequency. This continuous temperature indication and automatic adjustment supplemented by manual control was absolutely essential for obtaining accurate results. Even though the absolute temperature is not known to better than two or three degrees, the temperature must be maintained *constant* to within a tenth of a degree because the emission change with the temperature corresponds to between the thirtieth and the fortieth power.

Experimental results

The curves of Fig. 2 illustrate in a qualitative way the sort of results one obtains for a thoriated filament at various states of activation. The energy distributions are all alike independent of the state of activation, and the contact potential shifts with changes in activation in the expected way. It is not difficult to determine zero field from these data when plotted on a much larger scale and fitted by a computed curve as is illustrated by Fig. 3. The applied potential at zero field is shown on each curve by a short vertical mark. Theoretically these zero-field points should have fallen on a straight line the slope of which is shown by the dotted straight line marked "theory." The fact that these points

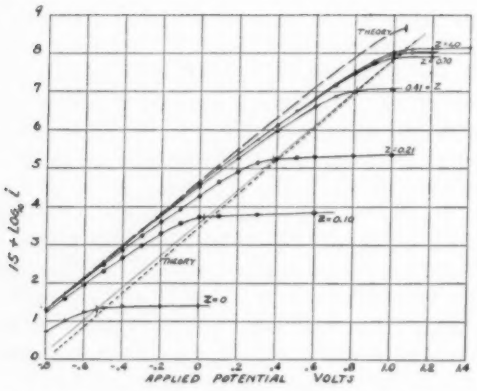

FIG. 2. Electron energy distributions from a thoriated filament for different states of activation. $T=1160°K$. Short vertical lines joined by light weight solid line show zero-field points. Dotted line shows theoretical slope of zero-field line. Dashed line shows theoretical energy distribution for $Z=1.0$ computed for cylinders and assuming no reflection.

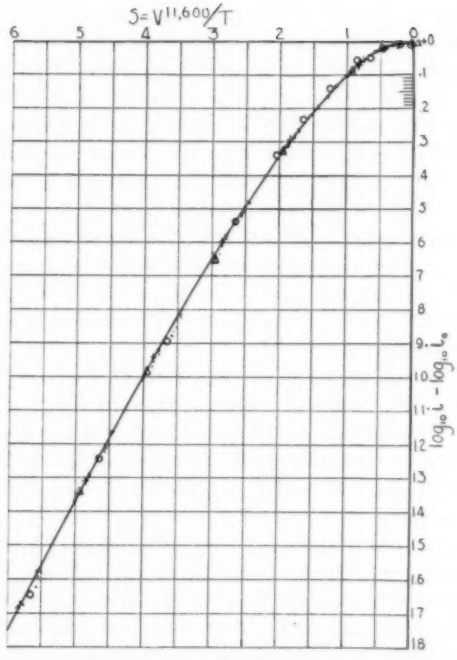

FIG. 3. Composite of electron energy distributions for nine states of activation. Circle, $Z=0.046$; cross, $Z=0.25$; triangle, $Z=1.3$. Line computed with $k/\omega=4.5\times10^{-4}$. i_0=current at zero field. $T=1160°K$.

do not fall exactly on the dotted theoretical line may be attributed to the rather unfamiliar effect* that the work function of a collector as indicated by its contact potential increases as a result of the flow of a large current of slow electrons. The flow of electrons with an energy of 50 electron volts or more produces the opposite effect. The time required for the collector to recover from such effects lasts for some minutes or even hours in the case of nickel collectors which have received considerable thorium. The time of recovery for clean tantalum collectors is less than the time required for measurement. Time lag effects have also been observed by Millikan,[9] Germer,[10] Mönch,[11] and Nottingham.[12]

It is important to notice that the curves *do not* follow the theoretical energy distribution curve, shown by the dashed line of Fig. 2. This is calculated assuming that the electrons have a Fermi-Dirac distribution within the metal and have a transmission coefficient of unity. The natural conclusion, of course, is that there is some mechanism producing reflection at the surface with the result that part of the slow electrons are not emitted. The distribution curve (PR–I, Fig. 6), obtained under much less satisfactory vacuum conditions, showed even more marked deviations from the theoretical curve. It is now known that the early results apply to a complex composite surface containing probably a layer of oxygen underlying the layer of thorium. The form of the potential barrier, shown PR–I, Fig. 13 and proposed as an explanation of the experimental results, seems to be reasonable if one recognizes that the "hump" assumed is due to the oxygen layer plus the thorium layer and not due to a thorium layer alone, as was originally thought. If the vacuum conditions are sufficiently perfect, this "post activated state"[13] is

* Dr. Irving Langmuir insists that this phenomenon should have a name. The author therefore suggests that it be called the "anode effect."

[9] R. A. Millikan, Phys. Rev. **18**, 236 (1921).

[10] L. H. Germer, Phys. Rev. **25**, 795 (1925).

[11] Günther Mönch, Zeits. f. Physik **65**, 233 (1930); W. Leo, Ann. d. Physik **9**, 347 (1931).

[12] W. B. Nottingham, Phys. Rev. **39**, 183 (1932).

[13] A thoriated filament may be activated, after the proper preliminary heat treatment, at a temperature of about 1920°K, for example, and the emission will increase as is illustrated in PR-I, Fig. 5. One may refer to the state of coverage which gives the maximum emission for strong fields as "$f=1.0$" as proposed by Brattain and Becker (Phys. Rev. **43**, 428 (1933)), or one may describe the coverage as in this paper by a "Z" scale, defining $Z=1.0$ as that coverage giving the maximum emission at zero field. The objection to the "f" scale is its dependence upon the

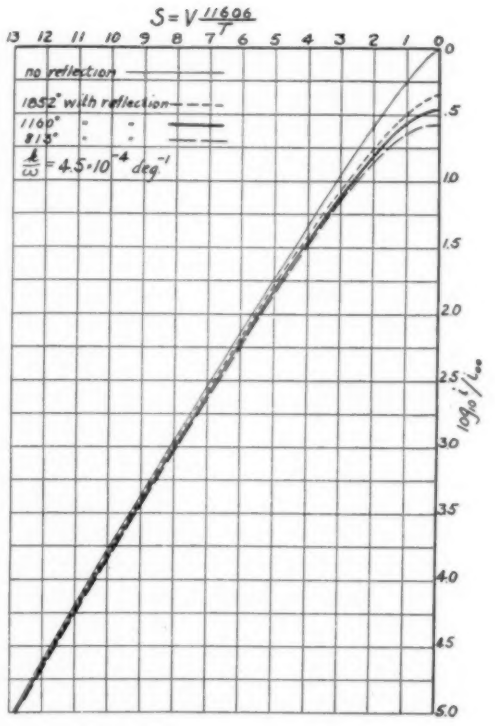

FIG. 4. Computed energy distributions.

not produced, and the distribution curves are not essentially different from those obtained for pure tungsten.

surface field. With a field of about 6000 volts per cm we find $f=1.5Z$. If the activation is carried on at 1800°K or lower, and the time required to produce the various states of activation noted, then Z is defined as $Z=t/t_m$ where t_m is the time required to activate to the maximum zero-field emission. This assumes that the average rate of arrival of thorium atoms on the surface is constant and that no evaporation takes place. These "f" or "Z" scales must be recognized as temporary. We need a "θ" scale which measures the true fraction of the surface covered. After having activated to a coverage of $Z=1$ or more, if the vacuum conditions are not "perfect," the emission may increase two- to six-fold even though the filament is cold between test readings. We have used the term "post-activation" to describe this increase in emission. As post-activation progresses, one observes that the emission passes through a maximum after which the emission decreases indefinitely until it practically disappears. A flash for less than a minute at 1850 not only removes the effect of post-activation, but if it has progressed far enough to give the maximum emission, practically the entire coating leaves the filament and it must be reactivated before even "normal" emission is obtained. The filament condition for most of the work reported in PR-I corresponded to that state of the filament for which the maximum emission occurred with post-activation. In the tubes studied for the present investigation, the vacuum conditions were so good that no detectable post-activation took place in a month's time.

Fig. 3 serves to illustrate the fact that the form of the energy distribution is independent of the state of activation. Eighty-five points taken at nine different states of activation were used to make up this composite curve. The three states of activation of particular interest are $Z=0.046$, $Z=0.25$ and $Z=1.3$ when considered from the standpoint of a patch theory. These points are identified by circle, cross and triangle, respectively. The extent to which these experimental data deviate from the expected Fermi (or Maxwellian) distribution is illustrated in Fig. 4, in connection with the theory of reflection which follows.

Theory of collection in a retarding field

There are two possible mechanisms which might produce reflection of electrons at an emitting surface. There is the possibility that reflection takes place due to the periodic structure of the metal lattice and the wave properties of electrons. This problem has been treated by Nordheim[14] and by Frank and Young[15] by approximate methods neglecting any possible effect of the crystal lattice with the result that a reflection of about 6 percent is expected for low energy electrons. As the energy of the emerging electrons increases to a number of volts, this reflection coefficient decreases very gradually. (See Fig. 21.) The nature of the curve is such that the effect could not be detected in the energy distribution of the electrons and would only show up as a five percent decrease in the total emission. Such a small effect would be masked by other things and therefore the theory could only be tested by shooting a beam of very slow electrons on the surface. Thus, the quantum theory as applied in the approximate form to the problem of reflection at the surface of a metal does not show promise of explaining the observed fact that the energy distribution has a shortage of low energy electrons as was seen above.

A second possibility is that the surface inhomogeneities such as work function differences between facets of a single crystal might produce potential hills of such a nature that reflection might be produced. It is a well-known

[14] L. Nordheim, Proc. Roy. Soc. **A121**, 626 (1928).
[15] N. H. Frank and L. A. Young, Phys. Rev. **38**, 80 (1931).

experimental fact that the emission from a composite surface such as thoriated tungsten, or caesium covered tungsten, changes greatly with the accelerating field if the surface is only partly covered. Langmuir and Compton[16] proposed a checkerboard patch theory to account for this effect. Becker[17] has also applied this sort of theory to emission in accelerating fields and has pointed out that patches would cause a reflection effect. The difficulty with this explanation of reflection is that throughout the entire range of activation from $Z=0.01$ to $Z=1.4$, the energy distributions are *exactly alike* indicating that whatever causes the reflection, it is *independent* of the state of activation of the surface.

Since it is not practical to work with anything but a cylindrical or filament type of emitter for accurate work, it is necessary to work out the method by which observed data taken with concentric cylinders can be correctly interpreted in terms of a reflection coefficient depending on the energy of the electron as it leaves the filament. A very simple form of reflection coefficient is the exponential type given by

$$R(p_x)=e^{-p_x^2/2m\omega}, \tag{3}$$

where ω is a constant and p_x is the momentum in the direction perpendicular to the surface in excess of that required to carry the electron to infinity when there is no external electrostatic field in the space, i.e., with "zero field." Thus, as the excess momentum approaches zero, the reflection approaches unity, while for large values of p_x the reflection goes to zero exponentially at a rate which depends on ω.

For an electron to arrive at a cylindrical collector, it must leave the emitting filament with enough radial and tangential momentum to overcome the retarding potential. The energy and momentum equations yield at once the limiting relationship

$$p_x^2+p_y^2(1-r^2/R^2)=2m\epsilon V, \tag{4}$$

where p_x and p_y are the radial and tangential momentum components just outside the filament, as defined more carefully above. Since the collector radius R is generally much larger than the filament radius r, Eq. (4) reduces simply to $p_x^2+p_y^2=2m\epsilon V$. Using the Fermi-Sommerfeld theory of metals we can write the expression for the emission current received by a cylindrical collector with a retarding potential V.

$$i=\frac{2\epsilon}{h^3}e^{-(W_a-W_i)/kT}\int_{p_x=-\infty}^{p_x=+\infty}\int^{p_y=\infty}\int^{p_z=\infty}(1-e^{-p_x^2/2m\omega})(p_z/m)e^{-(p_x^2+p_y^2+p_z^2)/2mkT}dp_xdp_ydp_z, \tag{5}$$

where $(W_a-W_i)/k$ is the same as b of Eq. (1). The limits of integration with respect to p_x and p_y exclude the region inside of the semicircle $p_x^2+p_y^2=2m\epsilon V$ but otherwise include the region of p_z from 0 to ∞, and of p_y from $-\infty$ to $+\infty$. The integration of Eq. (5) gives

$$i=i_{00}\{G(S)-F(S, kT/\omega)\}, \tag{6}$$

where

$$i_{00}\equiv(4\pi m\epsilon k^2/h^3)T^2e^{-(W_a-W_i)/kT}, \tag{7}$$

$S\equiv v(11{,}600/T)$, with v the retarding potential in volts.

$$G(S)\equiv(2/\sqrt{\pi})S^{\frac{1}{2}}e^{-S}+1-(2/\sqrt{\pi})\int_0^{S^{\frac{1}{2}}}e^{-x^2}dx, \tag{8}$$

$$F(S, kT/\omega)\equiv\frac{1}{1+kT/\omega}\left\{\left(\frac{\omega}{kT}\right)^{\frac{1}{2}}\frac{2}{\sqrt{\pi}}e^{-S(1+kT/\omega)}\int_0^{(SkT/\omega)^{\frac{1}{2}}}e^{y^2}dy+1-\frac{2}{\sqrt{\pi}}\int_0^{S^{\frac{1}{2}}}e^{-x^2}dx\right\}. \tag{9}$$

With the help of the Jahnke and Emde tables, $F(S, kT/\omega)$ was computed for various values[18] of (kT/ω) and selected values of S. Table I gives the results of this calculation in sufficient detail

[16] K. T. Compton and I. Langmuir, Rev. Mod. Phys. 2, 123 (1930).
[17] J. A. Becker, Rev. Mod. Phys. 7, 95 (1935).

[18] For $SkT/\omega>4$ the form of $F(S)$ given in Eq. (9) is not as convenient as the following:

TABLE I. *Values of $F(S, kT/\omega)$ for various values of S and kT/ω* (see Eq. (9)).

S	0	0.5	1	1.5	2	3	4	5	6	8	10
kT/ω											
0	1.0	8.01^{-1}	5.72^{-1}	3.91^{-1}	26.1^{-2}	11.2^{-2}	4.6^{-2}	18.6^{-3}	7.38^{-3}	11.3^{-4}	17^{-5}
0.06	0.943	7.47	5.25	3.51	23.1	9.5	3.78	14.3	5.62	8.4	11.8
.12	.893	6.98	4.83	3.18	20.5	8.14	3.12	11.7	4.35	6.05	7.9
.20	.833	6.41	4.31	2.81	17.7	6.75	2.45	8.85	3.20	3.99	5.00
.40	.714	5.30	3.42	2.09	12.6	4.39	1.47	5.00	1.75	1.96	2.33
.60	.625	4.47	2.75	1.62	9.12	2.69	0.974	3.21	1.00	1.12	1.25
.80	.556	3.86	2.28	1.29	7.23	2.25	.70	2.29	0.66	0.751	0.873
1.0	.500	3.38	1.90	1.05	5.13	1.73	.538	1.62	.502	.578	.672
1.2	.455	2.95	1.63	0.872	5.00	1.41	.401	1.28	.450	.461	.552
1.4	.417	2.62	1.40	.739	4.00	1.19	.331	1.06	.40	.386	.470
1.6	.385	2.34	1.23		3.37						
2.0	.337	1.92	0.959		2.61	0.718					
3.0	.250	1.29	.611		1.54	.453	.143				
5.0	.167	0.735	.325		0.879						

Note 1. The row for $kT/\omega=0$ is $G(S)$ since the first term of Eq. (9) reduces to $2S^{1/2}e^{-S}/\sqrt{\pi}$ in the limit.
Note 2. The superscript at the top of each column indicates the power of ten by which the numbers in that column should be multiplied.

for interpolation curves to be plotted by the user so that the theoretical curves for a limited range of values of (kT/ω) may be produced readily.

It was the original intention at the time these computations were made simply to "translate" observed curves such as those shown in Figs. 2 and 3 into corresponding transmission or reflection curves. For that reason, a method was worked out to evaluate the three constants of the following equation

$$R(p_z)=(1-f)e^{-p_z^2/2m\omega_1}+fe^{-p_z^2/2m\omega_2} \quad (10)$$

and thus make the empirical curve pass through three points of the observed curve. Here ω_1 and ω_2 are constants and f is a constant less than unity. All three constants are to be selected best to fit the data as an empirical equation. To do this, one chooses the three values of S at which the experimental and the empirical curves are to intersect. The ones selected were $S=0$, 2 and 6. Two curves were made by plotting $F(0, kT/\omega)$ as the abscissa and $F(2, kT/\omega)$ as the ordinate for one, while $F(0, kT/\omega)$ and $F(6, kT/\omega)$ were used for the abscissa and ordinate of the second. Since $F(S, kT/\omega)$ measures the amount the calculated curve falls below the Maxwellian curve $G(S)$, the experimental values of the deficiency may be called $E(S)$ and plotted as points $(E(0), E(2))$ and $(E(0), E(6))$ on the two graphs described above. If a straight line can be found which passes through the E points intersecting the F curves so as to give common values of $F(0, kT/\omega_1)$ and $F(0, kT/\omega_2)$ for the two curves, then two of the constants, *viz.*, ω_1 and ω_2, will have been determined. If such common values do not exist, then the empirical curve cannot be made to pass through the three experimental points selected. The third constant is given by the equation

$$f=\frac{F(0, kT/\omega_1)-E_0}{F(0, kT/\omega_1)-F(0, kT/\omega_2)}. \quad (11)$$

When this method was applied to the experimental data shown in Fig. 3, the points $(E(0), E(2))$ and $(E(0), E(6))$ fell exactly on their respective lines at a common value of $F(0, kT/\omega)$ thus giving $kT/\omega_1=kT/\omega_2$ and showing that the simple one constant expression of Eq. (3) represents the experimental data with accuracy. The solid line of Fig. 3 is the computed curve using $k/\omega=4.5\times10^{-4}$ degree^{-1}. This value of ω is 3.05×10^{-13} erg or 0.191 electron volt. The three curves of Fig. 4 are computed for the temperatures 813°K, 1160°K and 1852°K as indicated.

$$F(S, kT/\omega)=\frac{1}{1+kT/\omega}\left\{\frac{2}{\sqrt{\pi}}\frac{e^{-S}}{(kT/\omega)^{\frac{1}{2}}}f(a)+1-\frac{2}{\sqrt{\pi}}\int_0^{S^{\frac{1}{2}}}e^{-x^2}dx\right\},$$

where $a\equiv SkT/\omega$ and $A\equiv(a/(a-1))^{\frac{1}{2}}$,

$$f(a)=[A/a-e^{-a}\{(A+0.312)/a+(A-1.25)+(a/2)(A-1)\}].$$

A short table of values of $2f(a)/\sqrt{\pi}$ follows.

a	3	4	5	6	7
$(2/\sqrt{\pi})f(a)$	0.403	0.307	0.249	0.205	0.1735
a	8	9	10	12	14	16
$(2/\sqrt{\pi})f(a)$	0.1506	0.133	0.119	0.0986	0.0837	0.0728
a	18	20	21	24	27	30
$(2/\sqrt{\pi})f(a)$	0.0645	0.0579	0.055	0.0481	0.0426	0.0382

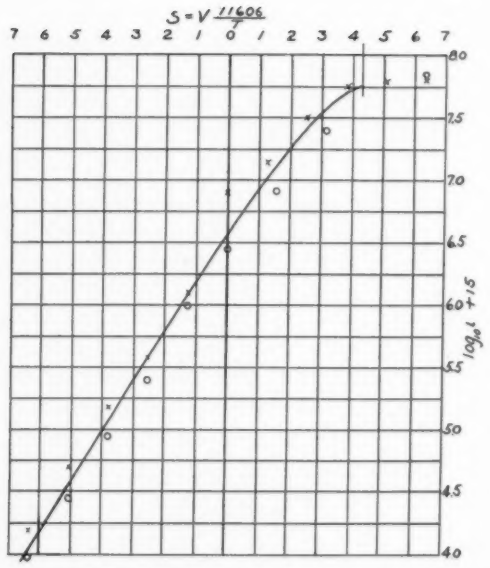

FIG. 5. Germer's data on electron energy distribution for $T=1830°K$. Curve computed with $k/\omega=4.5\times10^{-4}$ deg.$^{-1}$. Circles, increasing retarding potentials; crosses, decreasing potential.

All data observed at all states of activation and all temperatures using the thoriated filament were found to be accurately represented with the single reflection constant of $(k/\omega)=4.5\times10^{-4}$ deg.$^{-1}$. This same coefficient also represented the observed results for pure tungsten filaments almost as perfectly. This qualification is necessary because the fit was not quite perfect and it remains to be determined with an improved experimental tube whether or not there is a real difference in the reflection curve of pure tungsten as compared with thoriated tungsten.

As was stated above, the mechanism for producing this reflection is as yet undetermined, but the fact that there is a reflection effect seems to be established. The work previously quoted as the best authority for the fact that electrons are emitted with a Maxwellian distribution of energies and that no reflection takes place is that of Germer.[19]

Fig. 5 is produced here to show that there is no conflict between Germer's data and the reflection hypothesis. Here Germer's experimental points are shown and the curve drawn was computed, using $(k/\omega)=4.5\times10^{-4}$. The circles represent the observations made with increasing retarding potentials, while the crosses correspond to the series taken with decreasing retarding potentials.

[19] L. H. Germer, Phys. Rev. **25**, 795 (1925).

Reflection interpreted as excluded areas

According to the patch theory, which is discussed below, we might interpret the reflection in terms of a nonuniform transmission of electrons as a function of the coordinates of the surface. From the observed energy distribution data above, it is possible to construct a picture which shows essentially the fraction of the surface which should be allotted to transmission and reflection as a function of the energy. In Fig. 6 the cross-hatched part indicates a reflection, while the remainder represents the transmission. Thus, at any specified energy level ϵ_z a horizontal line started at $z=0$ passes through shaded territory for part of its length and nonshaded territory for other parts of its length. If we consider a segment of such a line of unit length, the fraction of it found in the shaded part of the figure measures the reflection coefficient, while the fraction in the nonshaded part measures the transmission. The figure is made up by repeating the line given by $\epsilon_z=2.3\omega\log_{10}z_0/2z$ where $\omega=0.191$ electron volt, the value shown above to fit the experimental data, and z, which is directly proportional to the area of the excluded region, takes on values between zero and $z_0/2$. The distance between adjacent peaks is taken as z_0 in order to fit in with the patch theory discussion below. For an energy of $\epsilon_z=0.2$ electron volt, 35 percent of the surface area would be assumed to be nonemitting, according to this interpretation. The object in presenting this figure is to show the kind of selectivity which

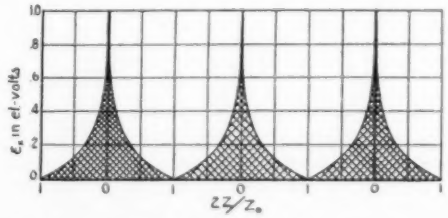

FIG. 6. Pictorial representation of reflection and transmission properties of a surface. $\epsilon_z=P_z^2/2m$.

a patch theory would have to exhibit in order to be consistent with the experimental data. Since the analysis below indicates that patch theories are not likely to give effects of this kind, it might be worth while to investigate theoretically the possibility that the surface layer of atoms is responsible for the reflection effect in which case z_0 would be the interatomic distance.

Zero-Field Richardson Plots

Since the entire energy distribution curve can be fitted so accurately by a computed curve, there is no difficulty in establishing zero field and therefore the emission which would have been observed in the absence of reflection is easily computed. At zero field Eq. (6) reduces to

$$i_0 = i_{00}\left(1-\frac{1}{1+kT/\omega}\right) = i_{00}\left(\frac{1}{T_\omega/T+1}\right), \quad (12)$$

where T_ω is defined by $T_\omega \equiv \omega/k$ and i_{00} is the emission which would have been observed at zero field with no reflection. Thus, after observing i_0, we can compute i_{00} at once. The zero-field emission should be uninfluenced by surface excess effects and also patch effects, since these will be absorbed in the reflection coefficient if they have any influence on the zero-field emission. This leaves only the temperature coefficient of the work function as an undetermined factor, and one may write

$$\log_{10}(i_{00}/T^2) = \log_{10} 120 - 0.4343\alpha - 0.4343(b_0/T). \quad (13)$$

We plot $\log_{10}(i_{00}/T^2)$ as a function of $(1/T)$ as in Fig. 7.

The slope of the upper straight line gives the work function at 0°K as defined by Eq. (2) and the intercept or the observed value of $\log_{10} A$ (according to the usual notation) allows us to calculate α as

$$\alpha = 2.3(\log_{10} 120 - \log_{10} A). \quad (14)$$

The lower straight line of Fig. 7 represents the observed emission at zero field i_0. Both curves have been plotted to show that in either case the Richardson line is straight within the experimental error. The largest error is in the temperature scale and can be reduced only by making an accurate scale for the particular filament being used.

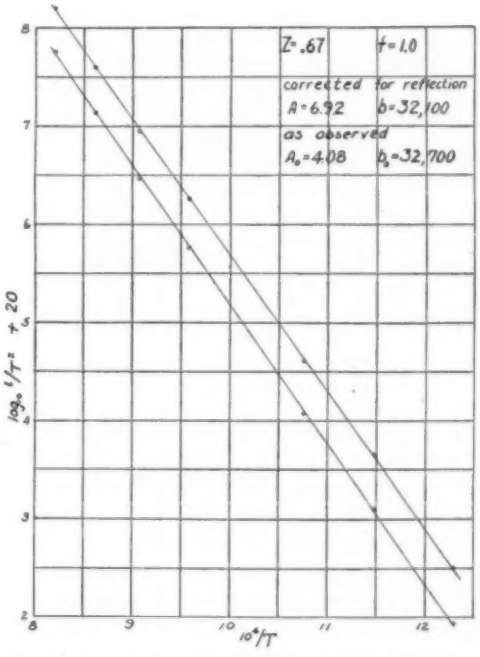

Fig. 7. Zero-field Richardson plots for a thoriated filament $Z=0.67$. Upper line includes correction for reflection.

The reflection effect not only alters the value of A, but also the value of b. By plotting $\log_{10}(T_\omega/T+1)^{-1}$ against $1/T$ for a particular range of observation, we may find the approximate correction to the A and the b brought about by the reflection. Richardson plots were made like Fig. 7 for $Z=0.67$, 1.0 and 1.3, but it was found impractical to attempt it for values of Z less than 0.67 on account of the changes which took place in the surface with the time. The existence of the effect is illustrated by the curves shown in Figs. 8 and 9. The heavy line of Fig. 8 shows a Schottky plot for Z approximately 0.1 and a temperature of 1160°K after ten hours heating at 1160°K. After heating the filament for three minutes at 1435°K, the emission at 100 volts was observed to have dropped to less than half its original value after which it returned to "normal" in about three hours time at 1160°K. The light line of Fig. 8 shows the shape of the

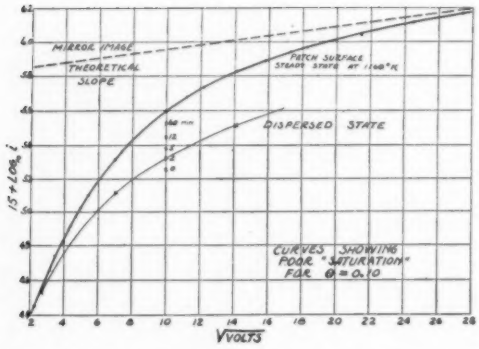

FIG. 8. Schottky curves for a thoriated filament. $T=1160$.

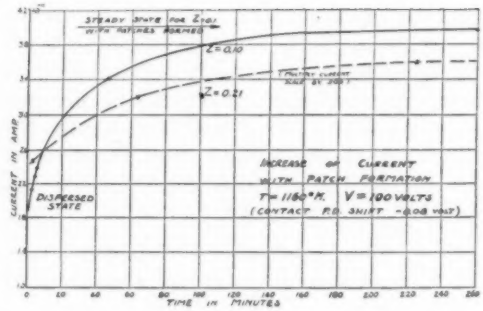

FIG. 9. Increase of current with patch formation.

curve two minutes after the high temperature treatment. Any form of patch theory suggests at once that the steady state at 1160°K corresponds to a more patchy state than that at 1435°K which we chose to call a "dispersed" state. With the patch state we have regions of relatively low work function which give a high emission with the help of a strong field, but at the same time the *average dipole moment* per unit area of the whole filament is actually less in the patch state than it is in the dispersed state. This is to be expected from Langmuir's[20] deductions that there is a depolarizing effect of the thorium atoms on each other. The emission at zero field is a direct measure of the average dipole moment per unit area and this has been found experimentally to follow the expected course, i.e., as the patch is formed the zero-field emission *decreases*, while the strong field emission *increases* as shown above. Fig. 9 shows the change in current with the time for the two states of activation $Z=0.1$ and $Z=0.21$.

After having produced the dispersed state at some relatively high temperature, it may be maintained for fairly long periods of time if the temperature is not raised above 925°K.

Richardson constants were computed from two observations for the values of Z less than 0.67. The filament surface was conditioned by maintaining it some hours at the highest temperature at which zero-field emission was not limited by space charge for the higher states of activation* and then the temperature was dropped to that for which the zero-field emission was about 5×10^{-14} amp. At these two temperatures energy distribution and Schottky plot data were taken, so that the emission at zero field could be determined accurately. After making the reflection correction, Richardson's A and b were computed. The results are summarized by Figs. 10, 11 and 12.

There are three important points to notice in Fig. 10. First, the observed points fall on a smooth curve which is not a straight line, showing that the temperature coefficient is not directly proportional to the average dipole moment (or the work function change) as has often been thought to be true from strong field measurements. Secondly, the point observed on a pure tungsten filament falls very naturally on the line as indicated by the double circle. This must be taken as provisional, however, because of the tube limitations described above. Thirdly, we see that the A thus observed is greater than 120, which suggests that the temperature coefficient of the zero-field work function for pure tungsten is *negative*,[21] contrary to Becker's[22] assumptions based on strong field data.

[20] I. Langmuir, J. Am. Chem. Soc. **54**, 2798 (1932).

* For low states of activation, 1393°K was selected as the maximum temperature. At temperatures much higher than this, measurable activation took place during the time of measurement.

[21] P. W. Bridgman in his *Thermodynamics of Electrical Phenomena in Metals* (Macmillan, New York, 1934), p. 100, shows that if the entropy of the surface charge at 0°K is not zero, the effect on the emission would be indistinguishable from a negative temperature coefficient of the work function. According to the Fermi-Sommerfeld model for a metal, the pressure of an electron gas in equilibrium with a metal of work function $b\equiv(W_0-W_i)/k$ should be

$$p=(4\pi mek^2/h^3)(k/2\pi m)^{1/2}\,T^{3/2}\exp(-b/T).$$

The latent heat per electron η as given by the Clapeyron equation is related to b as follows:

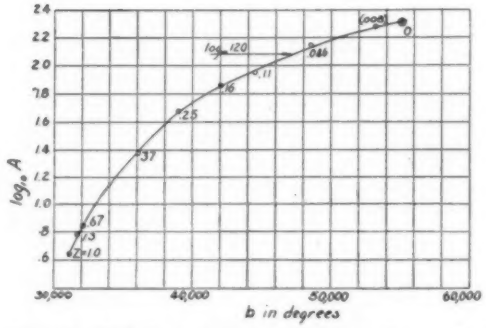

FIG. 10. Relation between $\log_{10} A$ and the zero-field work function from zero-field data corrected for reflection using $k/\omega = 4.5\times10^{-4}$ deg.$^{-1}$.

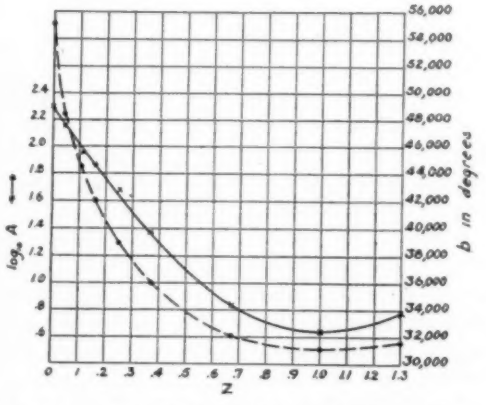

FIG. 11. $\text{Log}_{10} A$ (solid line) and b_0 as a function of Z after correction for reflection ($0.67f = Z$).

Fig. 11 shows the relation between $\log_{10} A$ and Z by the solid line while the dashed line relates

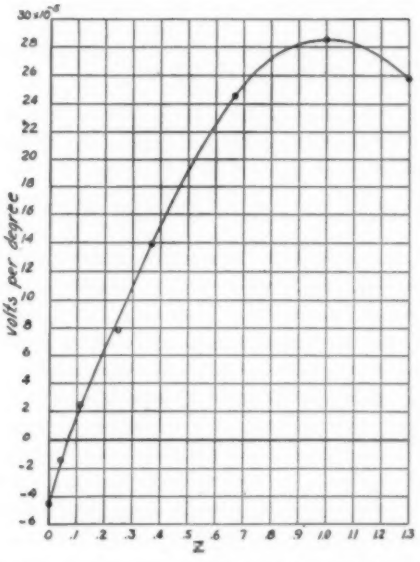

FIG. 12. Temperature coefficient of the work function as computed from $\log A$.

b to Z. The surprise brought out by this curve is that both $\log A$ and b pass through a minimum at $Z=1$. It was to be expected that b should pass through a minimum for about this coverage, but not so for $\log A$.

These data translated in terms of the temperature coefficient of the work function by Eq. (14) are illustrated by Fig. 12.

Here we see that the temperature coefficient for pure tungsten seems to be -4.3×10^{-5} volt per degree. The work function thus *decreases* as the temperature increases. D. B. Langmuir has investigated this point by a direct experiment using an improved Langmuir-Kingdon[23] method over the range of temperature 350°K to 1050°K and obtains results which agree in sign and order of magnitude with this value. The method involved the measurement of the contact potential of the tungsten filament used as a collector and not as an emitter. This result is so important if true that we are not satisfied with the present experiments and expect to redetermine these constants with improved apparatus.

$$\eta = kT^2\partial(\ln p)/\partial T = (5/2)kT + kb - kT(\partial b/\partial T).$$

We recognize $(5/2)k$ as the atomic heat of an ideal gas at constant pressure and can therefore write for the slope of the Richardson line,

$$\eta - (5/2)kT = \eta_0 - \phi(T) = kb - kT(\partial b/\partial T)$$

where η_0 is the latent heat at 0°K and $\phi(T)$ is determined by the heat absorbed in the metal due to the specific heat of the electrons and of the surface charge. The slope of a Richardson line such as that of Fig. 7 is constant within the experimental error. Therefore $\phi(T)$ is experimentally negligible compared to η_0. Within these limitations, $(\partial b/\partial T)$ must be a constant independent of the temperature and it follows that $kb_0 = \eta_0$. The temperature coefficient of the *work function* b may be *positive* or *negative* without conflicting with thermodynamic relationships.

[22] J. A. Becker and W. H. Brattain, Phys. Rev. **45**, 694 (1934). It should be emphasized that temperature coefficients cannot properly be calculated from strong field data without detailed knowledge of the surface structure.

[23] I. Langmuir and K. H. Kingdon, Phys. Rev. **34**, 129 (1929).

Electron Emission in an Accelerating Field

Test of Schottky theory with pure tungsten and fully activated thoriated tungsten

The Schottky mirror image theory[24] predicts that the electron current from a hot filament should increase according to the equation

$$\log_{10} i_V = \log_{10} i_0 + 1.905(fV)^{\frac{1}{2}}/T, \qquad (15)$$

where for cylinders $f=(r \ln R/r)^{-1}$ with r and R the filament and collector radii, respectively. If the filament were perfectly smooth and the image force the only one acting on the electron at distances large compared with interatomic distances, then Eq. (15) should be accurate from voltages less than 2×10^{-3} volt to many thousand volts for ordinary sized filaments. The fact that the image law applies strictly for an infinite plane becomes a limitation only for voltages between zero and one millivolt. Experiment however shows that the current rises as predicted by the Schottky theory only for fields higher than 500 volts per cm.

According to Eq. (15), if we plot $\log_{10} i_V$ (i_V = observed current with the accelerating voltage V)* as a function of $11{,}600V^{\frac{1}{2}}/T$ the slope of the theoretical line should be $1.64\times10^{-4}f^{\frac{1}{2}}$. We see from Fig. 13 that this is true for the higher voltages since the straight line drawn with this slope fits the experimental points accurately. As the field is lowered the departure from the Schottky theory becomes more and more marked. That this is not an effect due to space charge is proven by Fig. 14, in which the departure from theory, plotted as a function of the voltage, is seen to be *greater the lower the temperature.*

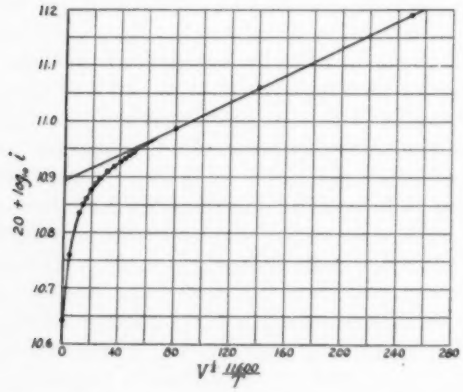

Fig. 13. Schottky plot for pure tungsten. $T=1434°K$.

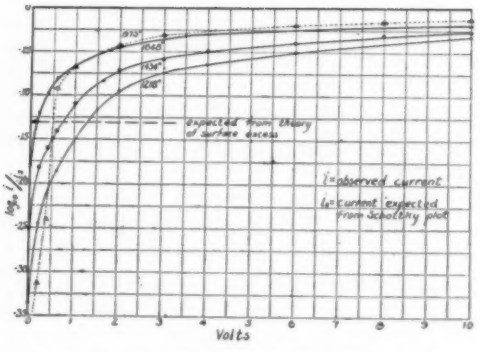

Fig. 14. Departure from Schottky line as a function of accelerating potential.

Observations taken at 1973°K do show the effect of space charge and even those at 1848°K are very slightly influenced near zero field. We also see that the lower the temperature the higher the applied field must be before the Schottky line is followed.

A comparison between Schottky curves obtained with pure tungsten and those observed with thoriated tungsten activated to $Z=1.3$ showed them to be very similar at 1218°K although the current received by the collector was over two million times greater for the thoriated filament. The three curves shown by Fig. 15 may therefore be considered as part of the tungsten family, thus showing quantitatively the extent to which observed Schottky curves actually deviate from the theoretical line as the temperature is lowered.

In seeking an explanation for these experimental observations, it seems obvious that there are only two possibilities. The first is that the transmission properties of a surface considered from a wave-mechanical point of view are very strongly influenced by a change in the form of the potential barrier at the surface. This suggestion seems so far fetched that it can perhaps be eliminated without further consideration. Grant-

[24] Schottky, Physik. Zeits. **15**, 872 (1914). See K. T. Compton and I. Langmuir, Rev. Mod. Phys. **2**, 123 (1930) for short discussion.

* The applied voltage must be corrected by the contact potential to obtain V.

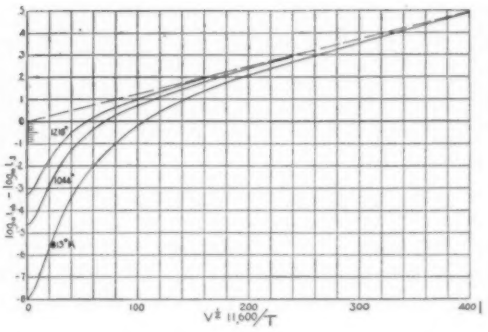

FIG. 15. Schottky plots for thoriated tungsten. $Z = 1.3$.

ing this, we are forced to the conclusion that there must be some electrical forces acting on the electrons at distances of the order of 10^{-6} to 10^{-4} cm which are *larger* than the mirror image forces. If the work function of the surface is not uniform but varies perhaps periodically from one crystal facet to another, then the contact potential fields might give rise to the electric fields which would account for the observed effect. Let us call this the "patch effect."

Two other complicating factors of the problem are the effect of field concentration at sharp points and the geometrical effect of surface excess.[25] The first of these would be temperature dependent in the direction observed but the fact that all experimental curves either fit the theoretical curve accurately for high fields or else approach it asymptotically is an indication that field concentration is of secondary importance in this problem. The "surface excess" effect would not be temperature dependent and therefore although this might account for a ten to thirty percent increase in current as the field is increased, it is not as important as the "patch effect" as a possible explanation of the experimental observations.

The sky-line and the patch theory*

No patch theory so far proposed can be applied to the problem of emission as a function of the electric field except in an approximate form as was done by Becker[26] and will also be done below in connection with the "strip theory." In order to demonstrate this, let us consider the problem in terms of the statistics of a perfect gas. We imagine an infinite conductor essentially in a plane and take the Y and Z axes of a coordinate system in this plane with the X axis extending into space. Designate this plane as the A plane. We assume that the work function for electrons is independent of y but varies periodically with z. Consider also a second conducting plane, known as the B plane, parallel to the first at a distance D which is very large compared with the fundamental wave-length of work function differences in the z direction or the distance between similar regions in the first plane. We have "zero field" in the space between these planes when no lines of electric force extend from A to B. There will then be no *net* surface charge on either plane.

Consider the boundaries to be at the temperature T and of such work functions that there is no net flow of electricity from A to B or B to A. The time average of the relative electron densities at all points in this space will be governed by the Boltzmann equation and furthermore over any small region where the change in motive* is small, the time average of the energy or the velocity distribution will be governed strictly by Maxwell's distribution function characterized by the temperature T. The motive must be used in the Boltzmann equation because differences in motive measure the work per unit charge required to move an *electron* from place to place. In the absence of an electric field between A and B, the motive will be constant everywhere except in the neighborhood of A where it will be the sum of the electrostatic potential due to the nonhomogeneous surface and the mirror image potential which, of course, does not satisfy Laplace's equation. If the temperature is low, the electrons

[25] L. Tonks, Phys. Rev. **38**, 1030 (1931).

* Some of the ideas presented here were worked out in collaboration with Dr. Irving Langmuir, to whom the author is greatly indebted. Part of the terminology therefore follows that of Mott-Smith and Langmuir, Phys. Rev. **28**, 727 (1926) and Langmuir and Compton, Rev. Mod. Phys. **3**, 191 (1931).

[26] J. A. Becker, Rev. Mod. Phys. **7**, 95 (1935).

* The term "motive" has been defined by Langmuir as ". . . a scalar quantity whose gradient, in any direction at any point, represents the force-component per unit charge which *acts on an electron or ion*." I. Langmuir and K. H. Kingdon, Proc. Roy. Soc. **A107**, 61 (1925), see p. 68. For an earlier discussion, see I. Langmuir, Trans. Am. Elec. Chem. Soc. **29**, 125, 137 (1916). P. W. Bridgman, reference 21, p. 37, uses the term "electric potential" in contrast to "electrostatic potential" where the former is the equivalent of the "motive" while the latter is a potential which satisfies Poisson's equation.

will be so far apart that one may neglect any interaction between electrons, i.e., we may disregard space-charge effects. We may imagine the phase space as the six-dimensional μ space of an ideal gas and focus our attention on a small region extending over the coordinates $dxdydz$ at (x, y, z) while the extention in momenta may be taken as p_x, p_y, p_z from $-\infty$ to $+\infty$. Since it is assumed that the motive is essentially constant throughout the volume $dxdydz$, we may picture the momentum space alone, remembering that the divisions in this space discussed below are determined by the space coordinates x, y, z.

Let us classify the electrons, whose representative points are seen in the momentum space, as AA electrons, AB electrons, BA electrons, or BB electrons, according to their trajectories. In the absence of space-charge effects there can be no periodic orbits which do not intersect planes A or B. It is evident that for every AB electron there is a corresponding BA electron such that their representative points, in the momentum space, lie diametrically opposite each other. That is, the line joining them will always be bisected by the origin. Thus, within the confines of a certain extended region in the momentum space, we will find all of the AB electrons and an exactly similar region will contain all of the BA electrons with the bounding surface "reflected" in the origin. All of the remaining momentum space will contain the AA and the BB electrons.

The problem of computing the current which would flow from electrode A to B could be solved if we could find some closed surface in the coordinate space between electrodes A and B over which we could correctly bound the above regions in momentum space and thus compute the flux of AB electrons crossing this coordinate surface.

With the system of strips described above, we can easily visualize a hill and valley system. The motive will be a point function depending only on the x and z coordinates. Since we have postulated the work function to be a periodic function of z, we know that we can represent the "surface potential" by a series

$$V(0, z)=\sum_{n=0}^{\infty} a_n \cos n\frac{2\pi z}{z_0}+\sum_{n=0}^{\infty} b_n \sin n\frac{2\pi z}{z_0}. \quad (16)$$

For the purpose of this discussion, let us take only the second term of the first sum, namely, $a \cos 2\pi z/z_0$ as the "surface potential." At $x \gg z_0$ the electrostatic potential must be constant and may be taken as zero. The potential at any point (x, z) must then be

$$V(x, z)=ae^{-2\pi x/z_0}\cos(2\pi z/z_0). \quad (17)$$

since this is a solution to Laplace's equation and fits the boundary conditions. With zero impressed field, the motive will then be

$$M_0(x, z)=ae^{-2\pi x/z_0}\cos(2\pi z/z_0)-\epsilon/4x. \quad (18)$$

Eq. (18) is, of course, not correct for $x<10^{-7}$ cm on account of the failure of the image laws, but it will serve to bring out certain points to follow. Let us now visualize $M_0(x, z)$ as a system of hills constructed on the x, z plane with the altitude at any point (x, z) equal to $M_0(x, z)$.

The form of this surface as seen by an analysis of Eq. (18) has interesting and rather unexpected properties. Differentiating with respect to x and setting the result equal to zero, we have

$$\frac{\partial M_0(x, z)}{\partial x}=0=-\frac{2\pi a}{z_0}\cos\frac{2\pi z}{z_0}e^{-2\pi x/z_0}+\frac{\epsilon}{4x^2}. \quad (19)$$

By substituting $u=2\pi x/z_0$ and rearranging, we find

$$\{(2z_0a/\pi\epsilon)\cos(2\pi z/z_0)\}e^{-u}=1/u^2=Ae^{-u}, \quad (20)$$

where A is defined by this equation. If we express A in terms of u and set $dA/du=0$ we see that for $u=2$, A passes through a minimum value of $e^2/4=1.847$. This means that if A is less than $e^2/4$, Eq. (20) can be satisfied only for $u=\infty$ while if A is greater than $e^2/4$ a *maximum* occurs in the motive as we follow a line of constant z at some value of $x<z_0/\pi$ and a *minimum* comes at $z_0/\pi<x<\infty$.

Thus we see that with zero field all electrons at distances greater than that to the minimum of the motive are accelerated toward the surface A for any finite value of a or z_0. This analysis brings out the fact that even though the "patch" fields may greatly exceed the image field at intermediate distances, the image field finally outlasts the patch field because the latter falls off exponentially with the distance.

If we could solve Eq. (19) for x, we would have an expression by which we could calculate the distance from the plane to the maximum in the motive as a function of z for any given values of a and z_0. These values of x and z could then be substituted into Eq. (18) and the motive along the line of maximum motive could be computed. Since the motive is a function of x and z and is independent of y we see that by the elimination of x between Eqs. (18) and (19) we would have M_0 as a function of z. Let us visualize this as the "sky-line" of the system of "hills" as viewed from a great distance. This "sky-line" intersects the $M_0=0$ contour at $x=z_0/2\pi$ and therefore it is seen to shift to $x=\infty$ and remain constant at $M=0$ for a distance in z approximately equal to $z_0/2$ after which the "sky-line" again returns to $x=z_0/2\pi$. Other contours are intersected at

$$x=z_0/\pi(1+(8M_0z_0/\epsilon\pi+1)^{\frac{1}{2}}). \quad (21)$$

Although all of this discussion has been for the case of zero field, it is possible to determine the motive along the "sky-line" for either accelerating or retarding fields and it is from these values of motive that the emission current is computed using the "sky-line" approximation. According to this approximation, we assume that those electrons escape which leave the surface at a particular value of z with energy $p_z^2/2m$ greater than the sky-line motive at that value of z and that electrons with energy less than this do not escape. The approximation made by Becker[26] in his computation is in reality the same as this one.

The form of the sky-line is shown graphically in Fig. 21 for $Z=0.25$ and $Z=1.3$. The ordinate is determined by z and the abscissa is equal to M_0. Some of the electrons included in the current calculated by this method are most certainly AA and not AB electrons. Other electrons with energy enough to escape, given the proper z component of momentum, will be excluded, while in reality they are AB electrons. Thus, it is not possible to state either the amount or the direction of one's error when the sky-line approximation is used.

There must be a line somewhere over the $M_0(x, z)$ surface at which marbles allowed to roll freely from rest go indeterminately either to A or to B. Defining this as the "marble-shed" line, it will probably be true that practically all electrons crossing this line are AB or BA electrons. If so, it would be a better approximation to compute the flux of electrons across a surface so defined but since it would generally be too difficult a problem to find the marble-shed line, this suggestion serves little purpose. This discussion, it is hoped, brings out the difficulties in the way of a proper solution to the problem, and perhaps shows that we cannot expect to get one in the near future.

The Strip Theory with Accelerating Fields

If Becker's[26] "checker-board" patch theory is correct in principle, then a certain amount of reflection of slow electrons should be expected, as was shown to be experimentally true. It was therefore thought desirable to investigate the properties of his equations in the retarding potential region. A partial examination showed that the labor involved would be so great that it would be just as easy to work out the simpler "strip theory" and then examine its predictions instead of those of the checkerboard patch theory. It is the purpose of this part to work out this theory and make application for both accelerating and retarding potentials.

In the presence of an accelerating field of electric intensity E the motive is given by

$$M=a\cos(2\pi z/z_0)e^{-2\pi x/z_0}-\epsilon/4x-Ex. \quad (22)$$

Using u and A as above and differentiating with respect to u we see that

$$\partial M/\partial u=(\pi\epsilon/2z_0)(-Ae^{-u}+1/u^2-Ez_0^2/\epsilon\pi^2). \quad (23)$$

If we set $\partial M/\partial u=0$, we have an equation relating u and E along the sky-line. In principle, we must solve this equation for u and substitute it into Eq. (22) and thus obtain M_E as a function of E and z along the sky-line. Since this is mathematically impractical we can use the following equations and method to obtain the desired result.

$$M_E=a\cos(2\pi z/z_0)(1+u)e^{-u}-\pi\epsilon/z_0\cdot 1/u, \quad (24)$$

$$E=\epsilon\pi^2/z_0^2u^2-(2\pi a/z_0)\cos(2\pi z/z_0)e^{-u}. \quad (25)$$

To use these equations, one chooses values of u for which E has positive values of a magnitude in the range of interest. Using these same values of u we can compute the corresponding values of M_E. In order to compute the current as a function of E or $E^{\frac{1}{2}}$, as is done here, we choose an arbitrary value of z_0 and an arbitrary set of values of $a\cos 2\pi z/z_0$. For example, we have taken $z_0=5\times10^{-4}$ cm, $a=0.5$ volt, and values of z which give $\cos 2\pi z/z_0$ the values 1, 0.8, 0.6, 0.4, 0.2, and 0 and also the negatives of these values. For each selection of z a curve was plotted giving M_E as a function of $E^{\frac{1}{2}}$ as computed from Eqs. (24) and (25). This step was necessary since it was easier to choose arbitrary values of u and find the corresponding values of M_E and E than it was to take definite values of E and then compute the value of M_E. From the curves, however, the desired M_E values for specific values of $E^{\frac{1}{2}}$ were selected. The sky-line curves were then given by plotting M_E as a function of z for chosen $E^{\frac{1}{2}}$ values. The current was computed by graphically evaluating

$$I_E=I_0\int_0^{z_0} e^{-M_E 11,600/T}dz. \qquad (26)$$

This method of computation is certainly more accurate than Becker's method of sub-squares, although in principle they are much alike. The constant I_0 is of no particular importance since it is the change in $\log_{10} I_E$ with $E^{\frac{1}{2}}$ which is of interest. We therefore take I_0 as unity.

We notice that Eq. (26) shows that the theoretical curves approach the slope of the mirror image curve for very high fields since in this case $u=\epsilon^{\frac{1}{2}}\pi/z_0E^{\frac{1}{2}}$ and Eq. (26) may be approximated by

$$I_E=I_0\exp\frac{(300)^{\frac{1}{2}}\epsilon^{\frac{1}{2}}E^{\frac{1}{2}}\cdot 11,600}{T}$$

$$\int_0^{z_0}\exp\{-(11,600\,a/T)\cos(2\pi z/z_0)\}dz \qquad (27)$$

for high values of E. In Eq. (27) E is expressed in volts per cm.

The final check between theory and experiment was made easy by the use of the curves of Fig. 16. Here $(\log_{10} I_E-\log_{10} I_S)$ is plotted as a function of a as computed with various values of $E^{\frac{1}{2}}$ for the temperature 1160°K. The constant I_S is defined by the following equation:

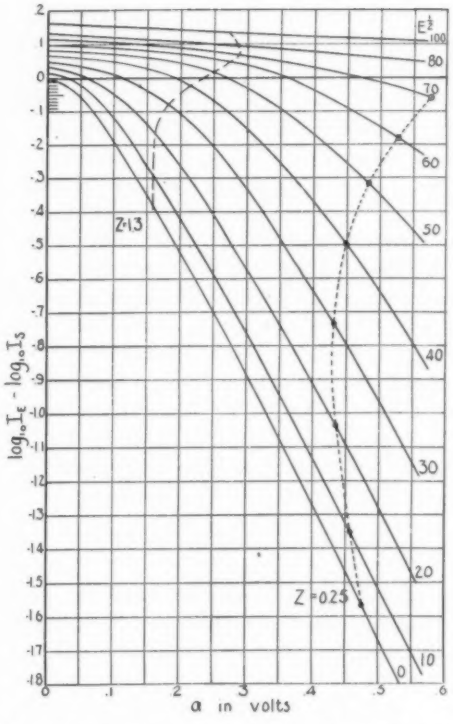

FIG. 16. Chart for computing Schottky curves for $T=1160$°K, using $z_0=5\times10^{-4}$ cm. Dotted line, observed results for $Z=0.25$. Dashed line, observed results for $Z=1.3$.

$$I_S=I_0\int_0^{z_0}\exp\{-(11,600\,a/T)\cos(2\pi z/z_0)\}dz, \qquad (28)$$

Table II gives $\log_{10} I_S$ for enough values of $11,600\,a/T$ so that an interpolation curve may be constructed for $I_0=$ unity.

In order to find an appropriate value of a to fit a given experimental curve, we determine the

TABLE II. *Values of $\log_{10} I_S$ for various values of $11,600\,a/T$* (see Eq. (28)).

$11,600\,a/T$	0.5	1.0	1.5	2.0	2.5	3.0	3.5
$\log_{10} I_S$	.027	.102	.214	.365	.520	.691	.865
$11,600\,a/T$	4.0	4.5	5.0	5.5	6.0	6.5	7.0
$\log_{10} I_S$	1.045	1.232	1.426	1.624	1.825	2.025	2.240

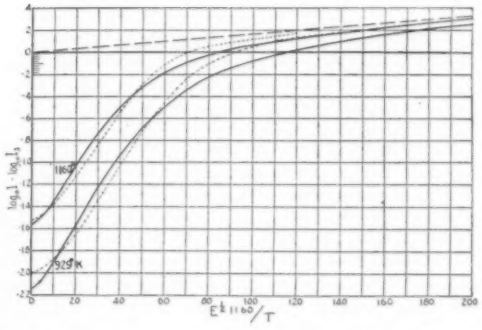

FIG. 17. Computed and experimental Schottky curves for $Z=0.25$. Dotted lines computed with $z=5\times10^{-4}$ cm and $a=0.465$ volt. Asymptotic Schottky line shown dashed.

values of $(\log_{10} i_{ob}-\log_{10} i_S)$ where $\log_{10} i_{ob}$ is the logarithm of the observed current for the values of field specified on Fig. 16. We define $\log_{10} i_S$ as the intercept on the $E^{\frac{1}{2}}=0$ axis of the Schottky line to which the observed Schottky curve is found to be asymptotic. Such Schottky lines are illustrated by Figs. 8, 13 and 15. These values $(\log_{10} i_{ob}-\log_{10} i_S)$ may be located on the corresponding $E^{\frac{1}{2}}$ lines as is shown by the circles which are joined by a dotted line in Fig. 16. The observed data were obtained at 1160°K with the filament activated to $Z=0.25$. For a perfect agreement between theory and experiment, this line would be straight and follow up a constant value of a. On the basis of this curve, however, we choose $a=0.465$ volt as perhaps the best value of a to represent this set of data and read off computed values of $(\log_{10} I_E-\log_{10} I_S)$ which are plotted as a function of $E^{\frac{1}{2}}$ to be compared with the observed values as shown in Fig. 17. The theoretical curve and the experimental one certainly have the same general shape and intersect at two points as they should, since we have two adjustable constants z_0 and a. A more important test is obtained if we compute the curve for a different temperature using the constants thus determined from the 1160°K data and compare this curve with the observed data. This test is also shown in Fig. 17 for here we have the observed and computed curves for 929°K and $Z=0.25$ and have used the values of z_0 and a found most suitable to fit the data observed at 1160°K. The observed points have been omitted from these curves since the accuracy of measurement was so great that all of the points lie accurately on the smooth curves shown.

Fig. 18 summarizes the observed results for a wide range of activation states. The state defined by $Z=0.25$ is thought to be the one for which the deviation from the Schottky mirror image theory is the greatest.

Using these methods, we have determined the most suitable values of a to represent all of the states of activation shown by Fig. 18 and have

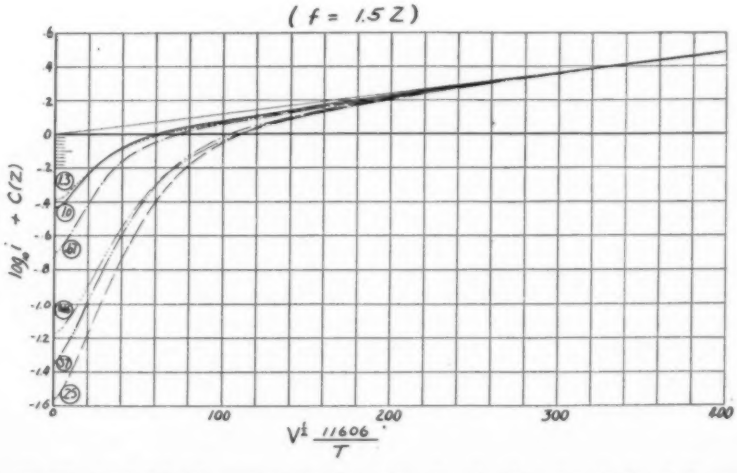

FIG. 18. Observed Schottky curves for six states of activation of a thoriated filament at $T=1160$°K.

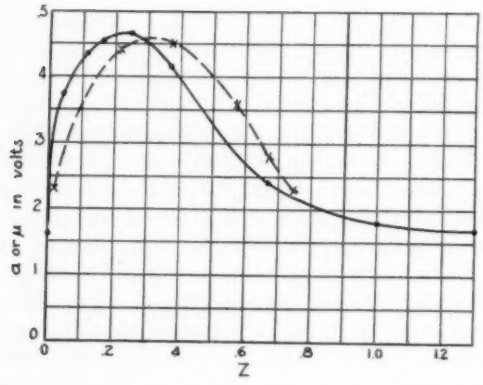

FIG. 19. Dependence of a on the state of activation Z compared with Becker's values of μ shown by solid and dashed lines respectively.

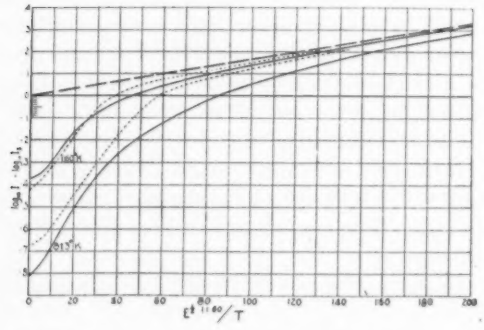

FIG. 20. Computed and observed Schottky plots for $Z=1.3$. $z_0=5\times10^{-4}$ cm and $a=0.17$ volt.

plotted a as a function of Z in Fig. 19. Here also are plotted Becker's[26] values of μ which is the corresponding quantity in his patch theory. It is interesting to note the rather close similarity of the two curves.

As was pointed out above, Schottky curves obtained with $Z=1.3$ are very similar to those obtained with pure tungsten. It is therefore thought desirable to show graphically the comparison between observation and theory for this case. Fig. 20 presents the data for the temperature 1160°K and 813°K.

Again the 1160°K data were used to determine the value of a which was also used to represent the 813°K observations. The agreement as regards the temperature effect is thus seen to be less satisfactory for $Z=1.3$ than for $Z=0.25$. It is

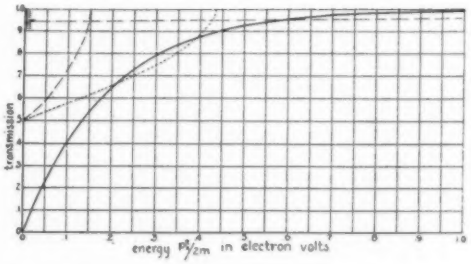

FIG. 21. Surface transmission as function of energy. Solid line for exponential accurately representing observed data. Dotted and dashed lines demanded by strip theory for $Z=0.25$ and $Z=1.3$. Dot-dash for Frank and Young quantum theory.

even more evident in this case that the computed curve approaches the Schottky line too rapidly for the high fields. This difficulty could be partially removed by choosing a smaller value of z_0 but then the rise for low fields would be entirely too slow.

It is easy to see from these curves that an improved theory would introduce narrow regions of low work function surface separated by wide regions of higher work function surface. This could no doubt be worked out by using more terms of Eq. (16), but since a new adjustable constant would come with each term and since there is no way yet available to evaluate these independently, it would not be of much value to show that the experimental curves could be represented very accurately by using a strip or patch theory with many terms.

Influence of strips on retarding potential curves

From the sky-lines computed, with $a=0.46$, $z_0=5\times10^{-4}$ and $a=0.17$, $z_0=5\times10^{-4}$, the effect on the energy distributions to be expected by using retarding potentials was determined. These results are best illustrated by curves showing the "transmission coefficient" of the surface as a function of the energy and comparing it with that obtained directly from experiments using retarding potentials.

The solid curve of Fig. 21 accurately represents the observed data for all states of activation of the thoriated filament and very nearly represents the results for pure tungsten. In the case of tungsten, the slight deviations may have been due to experimental error as pointed

out above. The two curves which result from this strip theory are thus seen to be in definite disagreement with experiment. Again it is not difficult to see that with the narrow regions (order of 10^{-5} cm) of low work function surface separated by wide regions (order of 5×10^{-4} cm) of high work function area, the effect of the strips on the retarding potential side would be greatly reduced and at the same time they would serve to give the large deviations from the Schottky theory which have been known to exist, especially with composite surfaces. If it is reasonable to suppose that such a theory of strips or patches might give a satisfactory explanation for the poor saturation effects for accelerating fields without appreciably influencing the currents predicted as a function of retarding potentials, then we must abandon hope of explaining the observed reflection effects by patches and must look to some "atomic explanation" for the excluded areas or the variable transmission coefficient.

I wish to acknowledge my indebtedness to Mr. N. B. Reynolds and Mr. J. E. Ryan for their careful technical assistance and to my students for many helpful discussions.

JANUARY 1, 1936 PHYSICAL REVIEW VOLUME 49

Negative Atomic Hydrogen Ions

WILLARD H. BENNETT AND PAUL F. DARBY, *Mendenhall Laboratory of Physics, Ohio State University*

(Received October 14, 1935)

Negative atomic hydrogen ions have been directly observed to exist at the heads of striations in discharges in water vapor. The ions appear to form surprisingly readily in these regions of high density of slow electrons, but they are lost very easily by collision.

NEGATIVE ions are supposed to exist in discharges through gases, as necessary for the explanation of the existence of striations[1] as well as for other reasons. They have not been observed there directly, but have been detected and studied in the past at extremely low currents differing greatly from those of the usual kinds of discharge through gases.

In work begun recently at this laboratory, negative atomic hydrogen ions have been observed directly at relatively high densities in the heads of striations in discharges through water vapor, and some information about their properties and behavior in a discharge obtained. The results establish that the ions exist at the heads of striations at high enough densities to play the role assigned them.

METHOD OF OBSERVATION

Various forms of discharge in water vapor were used as sources. In order to analyze the beams obtained through an aperture in the anode of the discharge, an electric lens system was used, shown in Fig. 1. The products from the source came through a sharp-edged aperture in A, 1 mm in diameter, and were accelerated by about 1200 volts into B. Approaching C, which had an accelerating potential of about 16,000 volts, the particles were focused, and going from C into D they were defocused less, thus producing a real image of the source aperture on the willemite-covered copper screen, F. The spot was observed through a screened narrow slot, E, and focused by adjustment of the middle electrode on the xylene-alcohol 10-megohm potential divider. A magnetic field from the Helmholtz coils HH deflected the particles through a hole in the screen on a collecting electrode, G, for measurement. The hole in F should be out from the plane of the figure when the coils HH are oriented as shown.

A great advantage of the electric lens system used was that when the potential divider was set for focus of the slowest electrons emerging

[1] See Thomson, *Conduction of Electricity Through Gases* (1933), vol. 2, pp. 387ff.

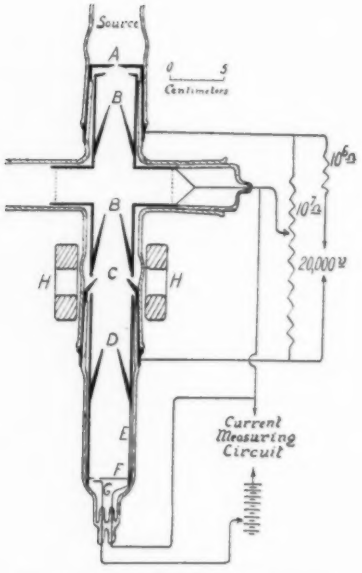

FIG. 1. Section of electric lens system.

through A, the same adjustment focused all singly charged particles in the plane of F, regardless of mass, and variations of potential drop across the potential divider were without effect on the focus.[2]

Whenever question arose as to whether the gas pressure in the tube below A had risen to too high a value through use of too high a water-vapor pressure in the arc chamber above A, liquid air could be put on the lower end of the tube, freezing out water vapor and greatly increasing the pumping speed. This question has seldom arisen, but the greatly increased pumping speeds so easily available have occasionally been very convenient in testing this point. Water vapor was admitted to the discharge chamber from a reservoir containing water cooled to any temperature desired from $-20°C$ to $-45°C$ at will.

ARC IN WATER VAPOR

An arc of the shape shown in Fig. 2 was used with all water-vapor pressures from 1 mm down. The cathode, K, was cup-shaped to concentrate the discharge towards the axis. The glass funnel, S, served further to concentrate the discharge on the aperture. Omitting S gave similar results but weaker beams of negative ions. A potential of 2000 volts was applied through a variable resistance limiting the arc current to 10–50 ma while at lower pressures the current fell to less than 1 ma before being extinguished.

Beginning with a high pressure and slowly reducing the pressure, it was found that no H^- spot appeared until the discharge had become of the "abnormal" type and well-defined striations had appeared in S. As the pressure fell, successive striations disappeared at the anode, and just as each striation disappeared at the anode the H^- spot faded out and then reappeared, becoming most intense just as the next striation had become a well-defined positive column in front of the anode. The most intense H^- spot was obtained when the last striation had become the positive column. At this point the pressure was roughly 5.10^{-2} mm, the current in the arc was 10 ma, the voltage on the arc 1800 volts and the current in the H^- beam was 2.10^{-8} ampere.

With further reduction of the pressure, the positive column faded out and the H^- beam decreased proportionally with the arc current.

Various shapes and smaller sizes of electrodes and tubes were tried, but these all gave smaller H^- currents. In all cases, the beam was strongest when there was a well-defined positive column above the anode without any striations.

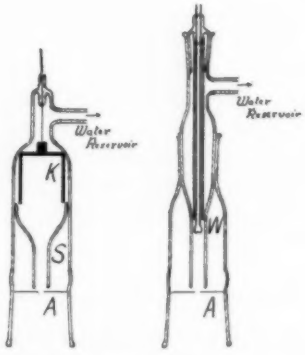

FIG. 2. (left) Water vapor arc.
FIG. 3. (right) Form of arc with oxide-coated filament.

[2] For a discussion of electron optics, see Bruche and Scherzer, *Electronenoptik*.

Discharge with Filament Cathode

An oxide-coated platinum filament, *W* (see Fig. 3), conditioned in vacuum was used as cathode. If enough water vapor was admitted to give several striations, the filament was poisoned and had to be reconditioned in vacuum. At lower vapor pressures, a dense discharge was easily obtained at as low a potential as 88 volts with the positive column extending nearly to the cathode. The current was 50 ma and a more intense H^- beam was obtained than with the high voltage arc. The gas pressures used here were about the same as those used before with the arc.

In this discharge, when the dense discharge was first obtained a second ion spot appeared as strong as the H^- spot. The mass of this second spot was tested for and found to be about 16 or 18. The resolution of the tube was not sufficient to distinguish between masses 16, 17, and 18, although quite adequate to identify the H^- ions by comparison with electrons. This heavy ion beam soon disappeared with operation of the tube and could be reproduced only by giving the tube a long rest. At no point in the experiments has a spot with mass 2 been seen although such a spot could easily have been detected.

Discussion

Negative atomic hydrogen ions were detected in Thomson's early experiments[3] in which he used a canal-ray tube with the applied field in the wrong direction to eject negative ions. That they were observed at all suggests that they may be remarkably easy to form because they had to be formed from high velocity positive hydrogen ions by the capture of two electrons in the canal. No other process would give the negatives the velocity observed, except head-on collisions of H^+ on molecules containing hydrogen and simultaneous retention of an extra electron by the recoil hydrogen atom. Hylleraas[4] has calculated the dissociation potential for the negative hydrogens as 0.715 volt. Lozier[5] has reported some measurements giving the result that H_2O vapor can acquire an electron at 6.6 or 8.8 volts and the resulting H_2O^- breaks up to give neutral OH and H^- with the recoil of the H^- having an energy of 1.5 or 3.2 for the two association energies, respectively. He found further that H^- currents could not be obtained as readily in purified hydrogen gas as in the water vapor.

The hypothesis made by Lozier to explain the formation of negative hydrogen ions in water vapor is supported by several points in our observations. The head of the positive column and the heads of striations are regions of slowly moving electrons necessary for attachment to water molecules. Heavy ions (presumably negative water ions, although not yet definitely identified) appeared sometimes with the negative hydrogen ions. The observed ion currents were much larger when the luminous part of a striation was close to the aperture. The rapidity with which the negative ions were otherwise lost by collisions necessitates the assumption of a high density for their formation.

It would seem that a negative hydrogen would be much more apt to be dissociated by a collision with a positive ion than with electrons or neutrals, because the attractive force would draw the colliding particles nearer to each other during a collision when they are oppositely charged than when they are not. Thus the use of the filament cathode has the advantage of a lower positive ion density since the discharge does not depend on ionization for the supply of electrons.

The writers wish to express appreciation to Professor L. H. Thomas for helpful discussions of the problem.

[3] Reviewed in Thomson's *Conduction of Electricity Through Gases*, vol. 1, Chap. 5.

[4] Hylleraas, Zeits. f. Physik **63**, 291 (1930).

[5] Lozier, Phys. Rev. **36**, 1417 (1930).

LETTERS TO THE EDITOR

Prompt publication of brief reports of important discoveries in physics may be secured by addressing them to this department. Closing dates for this department are, for the first issue of the month, the twentieth of the preceding month; for the second issue, the fifth of the month. The Board of Editors does not hold itself responsible for the opinions expressed by the correspondents.

Communications should not in general exceed 600 words in length.

On the Rotation-Vibration Spectrum of Acetylene in the Photographic Infrared

We have reinvestigated the absorption spectrum of C_2H_2 in the photographic infrared in order to obtain more information about the rotational and vibrational structure of this molecule. Using an absorbing length of 16.5 m and pressures up to 1.6 atmos., we have found 9 new absorption bands and in connection with that have remeasured some bands which were formerly incompletely known. Table I gives the wave-lengths and the wave numbers of the origins of the newly found bands as well as their probable interpretation following the scheme recently proposed by Herzberg and Spinks.[1] Two very weak bands have been added in parentheses, which, because of bad overlapping involve some uncertainty. As is well known C_2H_2 is a *linear* polyatomic molecule. It therefore shows $\parallel$ and $\perp$ bands depending on the direction of the oscillations of the dipole moment. The $\parallel$ bands have P and R branches only, whereas the $\perp$ bands have in addition one strong Q branch. Three of our new bands show Q branches and are therefore $\perp$ bands. For two of these, however, only the heads of the Q branches have been measured so far on account of their weakness. The third $\perp$ band which could be completely resolved and measured is rather interesting because from it information may be derived about the doubling of the degenerate upper state. This, according to theory,[2] is expected to be similar to the Λ-type doubling of diatomic molecules. We in fact found a slight but definite doubling which increases proportionally to $J(J+1)$ as does also Λ-doubling. The difference is that in this case the doubling originates not in an electronic but in a vibrational degeneracy.

Two or possibly three of the new bands (9801.7 cm^{-1} 12,618.4 cm^{-1} (11,591.0 cm^{-1})) do not show the usual alternation of intensities. In order to explain this the same assumption has been made as was advanced by Herzberg and Spinks for the band at 10,410A; namely, that both in the upper and in the lower state the transverse vibration ν_5 is excited. Then both the upper and the lower states are degenerate for zero rotation. If the splitting occurring at higher rotations is small then no intensity alternation should occur. This is quite analogous to the case of Π–Π transitions of diatomic homonuclear molecules. In order to test this assumption we have made exposures with the absorption tube imbedded in solid carbon dioxide. At the corresponding temperature (−80°C) the percentage of molecules excited to the first vibrational state (ν_5) is greatly diminished. In fact we found as is to be expected on the above assumption, that the band 10,410A disappeared completely, whereas the bands *with* alternating intensities did not change their total intensities.

TABLE I.

λ(A)	ν(cm⁻¹)	INTERPRETATION	TYPE	
11007	9085	$\nu_1+\nu_2+\nu_3+\nu_5$	$\perp$	Q only
10924	9151.7	$3\nu_1+\nu_3$	$\parallel$	
10677	9366	$2\nu_1+\nu_2+3\nu_4$?	$\perp$	Q only
10202	9801.7	$2\nu_2+\nu_3+\nu_4-\nu_5$	$\parallel$	
9645	10364.8	$\nu_3+2\nu_3+\nu_4$	$\perp$	*
8640	11570.8	$2\nu_1+2\nu_2+\nu_4+\nu_5$	$\parallel$	
(8625	11591.0	$\nu_1+3\nu_2+\nu_5-\nu_5$)	$\parallel$	
(8614	11605.0)	?	$\parallel$	
7923	12618.4	$\nu_2+3\nu_3+\nu_5-\nu_5$	$\parallel$	
7865	12710.7	$\nu_1+3\nu_3+2\nu_5$	$\parallel$	**
7671	13033.3	$3\nu_1+\nu_3$	$\parallel$	
6839	14617.0	$\nu_1+\nu_3+3\nu_3$	$\parallel$	

* The occurrence of this band has previously been noted by K. Hedfeld and P. Lueg (Zeits. f. Physik **77**, 446 (1932)) but was not measured by them. R. Mecke in his report (Hand- and Jahrbuch d. Chem. Phys. **9**, II (1934)) mentions that it is a $\perp$ band though he, too, gives no data.

** This band has already been found by C. A. Bradley and A. McKellar, Phys. Rev. **47**, 914 (1935) who have given a slightly different origin.

The experimental work was carried out at the Physikalisches Institut der Technischen Hochschule Darmstadt, Germany. Our thanks are due to the Agfa firm which generously supplied us with its excellent new infrared plates.

GÖSTA W. FUNKE
Department of Physics,
University of Stockholm, Sweden.

GERHARD HERZBERG
Department of Physics,
University of Saskatchewan, Canada,
December 9, 1935.

[1] G. Herzberg and J. W. T. Spinks, Zeits. f. Physik **91**, 386 (1934).
[2] Cf. D. M. Dennison, Rev. Mod. Phys. **3**, 280 (1931); R. S. Milliken, Phys. Rev. **42**, 364 (1932).

Alpha-Particle Yield from Lithium under Proton Bombardment

Cockcroft and Walton,[1] Henderson,[2] and Oliphant and Rutherford[3] have studied the yield of 8.5-cm alpha-particles from lithium under proton bombardment. The results of these studies have been interpreted as indicating that the probability of disintegration of Li^7 tends to become constant for proton energies around 400 kv. More recently Herb, Parkinson and Kerst[4] have measured the yield from both thick and thin films of lithium at voltages ranging from 70 to 400 kv. Their results indicate that the disintegration probability increases practically uniformly between 200 and 400 kv, with no appreciable tendency toward a constant value in this range. Further, the thick film yield of the latter observers is of the order of ten times that reported by Cockcroft and Walton around 400 kv. Also Hafstad and Tuve,[5] using thin films, have determined the excitation function of the disintegration in question at voltages up to above 1000 kv, and found that the probability increases continually in the observed

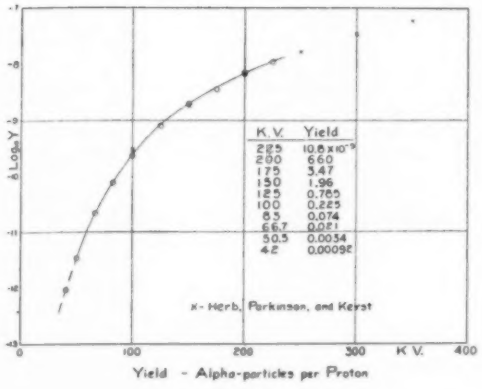

FIG. 1.

range of voltage, but tends to increase less rapidly at the higher voltages.

It is of interest for the theory of the nucleus to know the yield also at lower voltages than those covered so far because more accurate information can then be obtained about the potential inside the nucleus.[6] Since the data of Herb, Parkinson and Kerst are less accurate at the lower voltages it was thought worth while to extend observations to still lower voltages as well as to repeat them in a region overlapping theirs in order to obtain an independent determination with a different experimental arrangement.

Observations have been made of the thick film yield for proton energies ranging from 40 to 225 kv. Ions, including protons, were obtained from a low voltage hydrogen arc of the type described by Tuve, Dahl and Van Atta.[7] The high voltage was generated by a doubling rectifier circuit of the type used by Cockcroft and Walton. The ions were drawn from the arc by a small probe, focused by a metal cylinder, and then accelerated down a tube consisting of four glass sections separated by metal plates. The potential adjustment of the focusing cylinder and the potential distribution down the accelerating tube were maintained by corona leaks. The protons were separated from the other ions in the beam by passing them through a magnetic field, which after careful plotting and numerical integration served also to measure their equivalent voltage.

The protons were allowed to fall onto a lithium target, obtained by evaporation in vacuum onto a small sheet of nickel, and placed at an angle of 45° to the beam. The alpha-particles were let pass through a mica window into an ionization chamber, and then counted by means of a linear amplifier, of the type used by Dunning, together with a scale-of-four thyratron circuit coupled to a mechanical counter. The average proton current was measured by taking continuous readings on a galvanometer.

The absolute yields were calculated on the assumption of uniform angular distribution of the alpha-particles, and are expressed as the total number of alpha-particles per impinging proton. The results are shown in the accompanying figure together with the data of Herb, Parkinson and Kerst, both plotted on a logarithmic scale. Except for the lowest two points the yield values correspond to observations of from 5000 to 20,000 counts. At the lowest point about 90 counts were observed; and at the next point, about 900—so that these two points are subject to correspondingly greater statistical errors. It is seen from Fig. 1 that, within the limits of experimental error, these data are in good agreement with those of Herb, Parkinson and Kerst (except for their lowest point at 100 kv, for which they do not claim as high accuracy as for the other points). The theoretical significance of these data is discussed in an article by Ostrofsky, Briet and Johnson.[6]

The authors wish to express their thanks to Professor G. Breit, at whose instigation this problem was undertaken, for his generous interest and advice throughout the progress of the work. It is also desired to acknowledge indebtedness for grants-in-aid made to G. Breit by the Carnegie Institution of Washington and to C. E. Mendenhall and G. Breit by the American Philosophical Society, which made it possible to carry on this work.

N. P. HEYDENBURG
C. T. ZAHN
L. D. P. KING

Physics Department,
University of Wisconsin,
October 26, 1935.

[1] J. D. Cockcroft and E. T. S. Walton, Proc. Roy. Soc. **A137**, 229 (1932).
[2] M. C. Henderson, Phys. Rev. **43**, 98 (1933).
[3] M. E. Oliphant and Lord Rutherford, Proc. Roy. Soc. **A141**, 259 (1933).
[4] R. G. Herb, D. B. Parkinson and D. W. Kerst, Phys. Rev. **48**, 118 (1935).
[5] L. R. Hafstad and M. A. Tuve, Phys. Rev. **48**, 314 (1935).
[6] See M. Ostrofsky, G. Breit and D. P. Johnson, this issue.
[7] M. A. Tuve, O. Dahl and C. M. Van Atta, Phys. Rev. **46**, 1027 (1934).
We are indebted to Dr. Tuve for providing us with detailed specifications for the construction of this arc.

Ionic Dispersion in the Extreme Infrared

In many respects the following problem resembles that of the application of Maxwell's equations to the reflection and absorption of infrared radiation by thin metallic films, except that in the case of electrolytes the mass of an ion is sufficiently greater than the mass of an electron to introduce an inertia term.

Assuming the motion of an ion to satisfy the equation

$$M dv/dt + \rho v = e\mathcal{E}e^{i\omega t}, \tag{1}$$

where M is the mass of an ion, ρv the frictional force and $e\mathcal{E}e^{i\omega t}$ force from the alternating electric field, a characteristic value is obtained when $\rho = \omega M$. If Stokes' law of friction is applied, the characteristic wave-length, λ_0 (in μ) for which the inertia of an ion becomes important is given by:

$$\lambda_0 = 1.65 M/\eta r, \tag{2}$$

where r is the radius of an ion (in A) and η is the specific viscosity of the solution. For electrolytes of KCl and KI, $\lambda_K = 48\mu$, $\lambda_{Cl} = 32\mu$ and $\lambda_I = 95\mu$.

In Fig. 1 are shown the absorption coefficients and the reflecting powers of water, 3 normal KCl and 4 normal KI solutions. These data are chosen as illustrative of ionic dispersion and are taken from investigations on different concentrations of HCl, LiCl, NaCl, KCl, KBr, LiI, KI, ZnI_2, H_2SO_4, $MgSO_4$ and KOH.

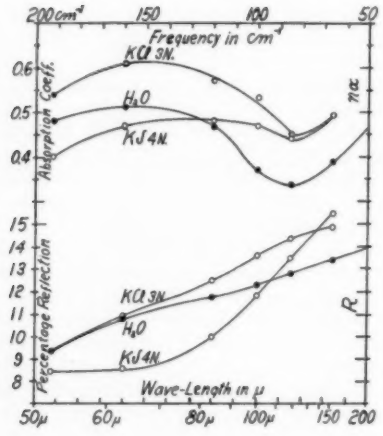

FIG. 1.

The characteristic wave-lengths for K, Cl, and I ions given above were calculated under the assumption that the ions were free to move with respect to the water molecules surrounding them. A comparison of the curves for KCl with those for KI seems to justify this assumption, at least for the amplitudes produced by the radiation employed. The rigid attachment of water molecules to the ions might be expected to change the ratio of M to r in Eq. (2) so that the characteristic wave-lengths would not be consistent with the data shown in the figure. A better criterion for deciding if there are water molecules attached to the ions is offered by considering the value of the absolute absorption as obtained from inserting the above equations in Maxwell's equations. A calculation shows that the ions in KCl and KI solutions are free to move with respect to the surrounding water molecules. However, in electrolytes of LiCl and $MgSO_4$ our data indicate that water molecules move with the ions. It seems noteworthy that the viscosities of KCl and KI solutions are practically the same as that of pure water while LiCl and $MgSO_4$ solutions are considerably more viscous. Also electrolytes of Li and Mg ions have abnormally small electrical conductivities.

We conclude that the dispersion of electrolytes in the extreme infrared can be pictured classically by considering the ions to follow in translation the alternations of electromagnetic waves. The motion of the ions decreases in amplitude as the frequency of the radiation increases because of their inertia and the friction against the neighboring molecules. In electrolytes of KCl and KI, the ions seem to move with respect to the water molecules except for friction.

I am indebted to Professor P. Debye, for having kindly derived the appropriate equations, and to Professor J. Errera, the University of Brussels, the Fonds National Belge de la Recherche Scientifique, and C. R. B. Educational Foundation for their generous help.

C. HAWLEY CARTWRIGHT

University of Michigan,
November 30, 1935.

Exchange Forces and the Structure of the Nucleus

The forces between elementary particles in the nucleus have been supposed to be of three types, which may be denoted as Wigner, Heisenberg or Majorana. The Wigner forces are of the ordinary kind, not involving exchange; the Heisenberg forces involve an exchange of both spin and space coordinates; and the Majorana forces involve an exchange of space coordinates alone.

According to Wigner,[1] one might account for the large neutron-proton scattering cross section by assuming the interaction of neutron and proton to depend on the relative orientation of the spins. Van Vleck[2] has suggested that, since the Heisenberg forces depend on spin orientation and the Majorana forces do not, the interaction could be described by a linear combination of Heisenberg and Majorana forces. Feenberg and Knipp[3] have shown that such an interaction can give an arbitrarily large scattering cross section, provided that the proper linear combination is chosen. It does not seem to the present writer, however, that the treatment is complete, since there is still another type of exchange conceivable, and this is obtained by making a Heisenberg exchange and then a Majorana exchange. This amounts to interchanging the spin coordinates and not the space coordinates. (We could perhaps compare the present situation to the interaction of an excited atom with a normal atom. Two types of processes occur here, and have been denoted by "austausch" and "resonance," respectively. The effect due to combination of the two is of the same order of magnitude as that of each alone.) The most general exchange operator would then include this spin exchange term as well as the others.

In this connection, a rather convenient formalism for treating the nucleus as a many-body problem suggests itself. Following Heisenberg,[4] one can suppose all the particles in the nucleus to be identical, but just in different states. The interaction operator will then be, in this scheme, the same for all pairs of particles. If now, we take the resulting wave function for the total system to be a determinant wave function, an analysis similar to that of Slater[5] can be carried through. If $V(12)$ is the above interaction operator, and if m and n denote space-spin states, while ν, π denote proton, neutron, respectively, then we obtain integrals of the type $\int u^*(m\nu/1)u^*(n\pi/2)\,V(12)u(m\nu/2)u(n\pi/1)d\tau_1 d\tau_2$. Here, particle 1 makes a transition from state m, ν to state n, π, while particle 2 does the opposite. That is, this integral represents a matrix element of the interaction between neutron and proton. It may be possible, from the observed masses of the light elements, to determine these matrix elements. A study of this is now being made, and will be reported later.

I wish to thank Dr. Feenberg for allowing me to see his manuscript before publication.

JAMES H. BARTLETT, JR.

University of Illinois,
December 14, 1935.

[1] Feenberg and Knipp, Phys. Rev. **48**, 906 (1935); footnote 13.
[2] Feenberg and Knipp, Phys. Rev. **48**, 906 (1935).
[3] Reference 1, footnote 14.
[4] W. Heisenberg, Zeits. f. Physik **77**, 1 (1932).
[5] J. C. Slater, Phys. Rev. **34**, 1304 (1929).

The Velocities of Slow Neutrons

Further experiments with a mechanical velocity selector[1] have been made on slow neutrons from sources at room and liquid-air temperatures. Fig. 1 shows the averaged results of the runs at room temperature. The limits of probable error are indicated by the vertical lines of lengths inversely proportional to the square root of the number of counts. The curve shows the experimental results that would be expected if the slow neutrons operated upon by the selector system have a Maxwellian distribution of velocities resulting from thermal equilibrium with the paraffin at its temperature of 300°K. The experimental points agree fairly well, for this type of measurement, with the calculated curve, although they would fit better a curve with a velocity maximum about 10 percent lower. If this shift is significant, then one factor which might account for this would be that the maximum of the Li detection region is somewhat below the most probable neutron velocity at 300°K. However, considering the poor resolution of the present selector with one to one ratio of slit width to width of Cd selector and the limited statistical accuracy on account of the small number of slow neutrons passing through the selector in comparison with the background effect of the fast neutrons, all that can be claimed is that the neutrons readily stopped by Cd and detected by Li have a maximum intensity in velocity distribution close (within ±250 meters/sec.) to the maximum in a Maxwellian distribution at 300°K (about 2500 meters/sec.).

Experiments in which the source of slow neutrons was a paraffin cylinder as before, except that a hole 3 cm in diameter was made in the paraffin extending axially 12 cm to the Rn-Be neutron source, also showed approximate thermal equilibrium in spite of the lack of paraffin in the direct beam. A measurement was made of the absorption in Cd of neutrons selected from the higher and lower velocity portions of the distribution curve. The mean velocities of the one group was estimated to differ from that of the other by about 10 percent, or 250 meters/sec. No difference in absorption by Cd was found, the probable error being ±3 percent, which is in accord with other observations as to the nonsensitiveness of Cd absorption to neutron velocity change.

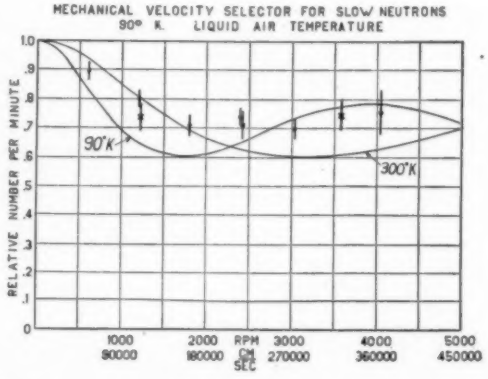

FIG. 1. Average results for the velocity distribution of slow neutrons from source at room temperature (300°K).

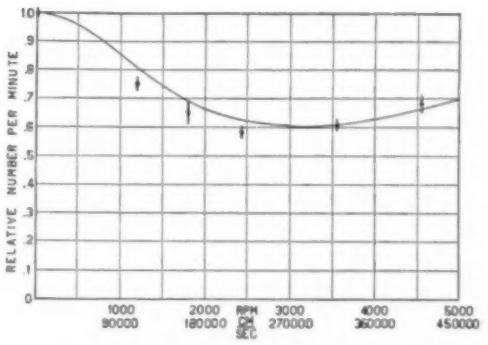

FIG. 2. Average results for the velocity distribution of slow neutrons from source at liquid-air temperature (90°K).

The experimental results with neutrons emerging from a soft glass Dewar flask containing about 2000 cc of paraffin at about 90°K are shown in Fig. 2 by the small circles, and the results of another group of runs with the source arranged to use only the neutrons emerging from a layer of cold paraffin 8 to 10 mm thick are indicated by the crosses. The theoretical curves to be expected at 90°K and at 300°K are also shown. The results are not very precise, but they do not appear to show complete thermal equilibrium in either case. The points seem to lie more between the two curves, while the maximum is not as well defined as at 300°K, and although it is probably shifted toward lower velocities, it is not shifted as far as would be expected for 90°K.

While the attempts to show temperature effects with artificial radioactive detectors[2,3] have indicated that thin cold layers of paraffin are more effective than thick cold paraffin layers, possibly due to increased probability of capture in the cold paraffin of neutrons on the slow side of the velocity distribution, under our conditions the results with Li detection and Cd absorption do not show any significant differences between thick and thin layers. It is possible that Li detection and Cd absorption are not as effective with the very slow neutrons as with those further up in the velocity distribution. If so, this might explain the failure to observe a velocity distribution appropriate to 90°K. The number of disintegrations of Li and the absorption of Cd show no changes larger than ±3 percent with the source at 90°K compared to the same source at 300°K.

G. A. FINK
J. R. DUNNING
G. B. PEGRAM
D. P. MITCHELL

Pupin Physics Laboratory,
Columbia University,
December 14, 1935.

[1] Dunning, Pegram, Fink, Mitchell and Segrè, Phys. Rev. **48**, 704 (1935).
[2] Moon and Tillman, Nature **135**, 904 (1935).
[3] Lukirsky and Zarewa, Nature **136**, 682 (1935).

On the Absorption Law for Slow Neutrons

The theory of the capture of slow neutrons by nuclei, developed by Fermi,[1] Bethe[2] and Perrin and Elsasser[3] on the basis of a simple model for the neutron-nucleus interaction (deep potential hole of radius of the order of magnitude of the nuclear radius) shows that, whatever the absolute value of the capture cross section may be, it must be inversely proportional to the velocity of the neutron. This statement can be expressed in other words by saying that the probability of absorption of a slow neutron depends only upon the time which the neutron spends in the material.

However, phenomena of selective absorption observed by several experimenters[4] using different absorbers and detectors suggest that this law does not hold, at least for some of the elements investigated.

In order to test the validity of the $1/v$ law in a more direct way, and also to find out in which direction the possible deviations lie, we performed the following experiment. It is known already from experiments with a velocity selector[5] that the slow neutrons are approximately in thermal equilibrium at room temperature; it must then be possible to produce appreciable changes in the absorption by altering the relative velocity of the neutrons and the absorber, i.e., by moving the latter. We rotated a 50-cm diameter steel disk coated with a thin film of cadmium (about 0.02 mm) at 6000 r.p.m., so that the linear velocity near the edge was about 140 meters/sec. A beam of slow neutrons was sent through the disk near the edge at an angle of about 25° with the face of the rotating wheel so that by rotating the disk in one direction or the other a large component of the velocity of the cadmium was added to or subtracted from the velocity of the neutrons. It is clear that under these conditions if the $1/v$ law holds, no change in absorption must be found when the direction of rotation is reversed, because the time spent by the neutron in the cadmium sheet is not changed; in other words, the longer or shorter effective path is compensated by the change in cross section. However, if the cross section does not vary inversely as the velocity but follows a different law, then a change in absorption should be observed. For instance, if the cross section is a constant we must find more absorption when the absorber moves against than when it moves with the neutrons.

We found that 8.2 ± 0.8 percent fewer slow neutrons came through when the cadmium was moved against than when it was moved with the neutrons (about 150,000 particles were counted by means of a lithium lined ionization chamber). This, under the experimental conditions, corresponds to a change in absorption coefficient of 6.3 percent. If we assume the Maxwellian distribution at room temperature for the slow neutrons, and calculate the apparent change in absorption coefficient resulting only from the changed length of path in cadmium (i.e., we assume the cross section to be constant), this turns out to be about 9 percent, which is not much larger than the observed effect.

In the case of cadmium we conclude therefore that the anticipated $1/v$ law does not hold, but the cross section varies with the velocity less rapidly than $1/v$, and approximates constancy.

However, the same experiment done with silver as an absorber, using a disk 0.8 mm thick gave a different result. In this case we could detect no change in absorption coefficient larger than the statistical fluctuations (by counting 92,000 particles we found a change of 0.7 ± 0.9 percent). The absorption of slow neutrons in silver thus appears to follow closely the $1/v$ law.

We plan to make similar experiments with boron and other elements.

F. RASETTI
E. SEGRÈ
G. FINK
J. R. DUNNING
G. B. PEGRAM

Pupin Physics Laboratories,
Columbia University,
December 14, 1935.

[1] Amaldi, d'Agostino, Fermi, Pontecorvo, Rasetti and Segrè, Proc. Roy. Soc. **A149**, 522 (1935).
[2] Bethe, Phys. Rev. **47**, 747 (1935).
[3] Perrin and Elsasser, Comptes rendus **200**, 450 (1935).
[4] Moon and Tillman, Nature **135**, 904 (1935); Bjerge and Westcott, Proc. Roy. Soc. **A150**, 709 (1935); Arsimovitch, Kourtschatow, Miccovskii and Palibin, Comptes rendus **200**, 2159 (1935); Ridenour and Yost, Phys. Rev. **48**, 383 (1935), Pontecorvo, Ricerca Scient. VI–II, 145 (1935).
[5] Dunning, Pegram, Fink, Mitchell and Segrè, Phys. Rev. **48**, 704 (1935).

Absorption Bands of Gaseous HI

Infrared absorption measurements by Czerny[1] first indicated the $1\leftarrow0$ band of gaseous HI to be centered at 2270 cm^{-1}. Measurements of the same band in Raman effect by Salant and Sandow[2] placed it at 2233 cm^{-1}. The discrepany was attributed to the difficulty of separating the band in absorption from the strong atmospheric band of CO_2. Recently, Nielsen and Nielsen,[3] using an echelette grating, have determined the center to be at 2230.08 cm^{-1}, in satisfactory agreement with the value of Salant and Sandow. In view of the importance of establishing the existence or absence of any such disagreement as that between the original absorption measurement and the Raman effect, it seems worth while to report that measurements of the centers of both the $1\leftarrow0$ and the $2\leftarrow0$ absorption bands have been made in this laboratory by means of a small Hilger rocksalt prism spectrometer. The results are 2260 ± 30 cm^{-1} for the fundamental and 4416 ± 75 cm^{-1} for the first overtone band. Within the limits of accuracy set by the necessarily wide spectroscopic slit widths, these results are in satisfactory agreement with the values found by Salant and Sandow and by Nielsen and Nielsen for the $1\leftarrow0$ band and with that found by the latter authors for the $2\leftarrow0$ band.

D. E. KIRKPATRICK

Washington Square College,
New York University,
December 4, 1935.

[1] M. Czerny, Zeits. f. Physik **44**, 235 (1927).
[2] E. O. Salant and A. Sandow, Phys. Rev. **37**, 373 (1931).
[3] A. H. Nielsen and H. H. Nielsen, Phys. Rev. **47**, 585 (1935).

The Infrared Absorption Spectrum of Water and Alcohols in Nonpolar Solvents

The vapor-like behavior of the electric moment of water dissolved in carbon tetrachloride and the colligative properties of the alcohols dissolved in nonpolar solvents are usually regarded as evidence for the existence, in the solution, of essentially vapor-like molecules. If this view is correct the infrared absorption spectra of water and the alcohols dissolved in carbon tetrachloride and carbon disulfide should be vapor-like. This point was investigated by studying the absorption in the 1.0–2.5μ region of water dissolved in carbon disulfide and of some of the alcohols dissolved in carbon tetrachloride. Preliminary results are shown in Fig. 1. The curves, representing the galvanometer deflections as ordinates and wave-lengths in μ as abscissae, show *A* the absorption of a thin cell of liquid water, *B* the absorption of 1 meter of carbon disulfide saturated with water at room temperature, *C* the radiation of the source containing the atmospheric water-vapor bands, *D* the absorption of 96 cm of methyl alcohol vapor at room temperature, *E* the absorption of liquid methyl alcohol and *F* the absorption of a solution of methyl alcohol in carbon tetrachloride. The solution and liquid cell lengths were chosen in each case so that the radiation traveled through approximately the same number of molecules. The bands marked W and OH, which occur in approximately these positions in all compounds containing the OH group, including water, with small variations in wave-length, are the ones to be noted. Curve *C* for the liquid alcohol shows the characteristic broad OH band of any alcohol at 1.45–1.65μ, cut by a water vapor band of the atmosphere on its short wave-length slope. Curve *F* shows, among others, a remarkably sharp band which appears very near the vapor position as shown in Curve *D*. In this set of curves the fact that the OH bands in solution are the sharpest of the three states of vapor, liquid and solution is even more apparent than in the case of water. Another fact appears significant. The bands marked CH which occur in approximately these positions whenever carbon-hydrogen groups are present, and which therefore are due to vibrations essentially characteristic, in the alcohol case, of the methyl group, are weak in the vapor and practically unchanged in the passage from the liquid to the solution state.

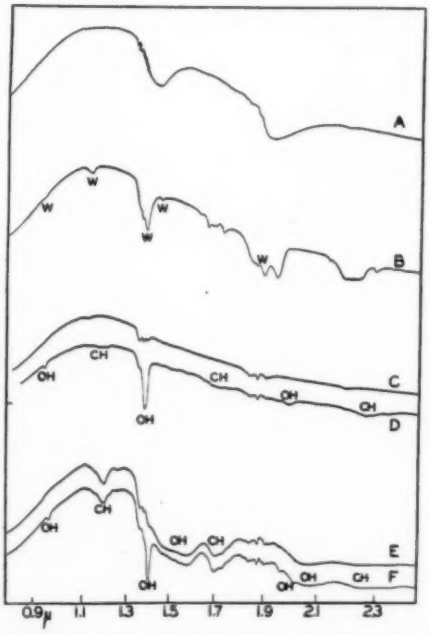

FIG. 1. *A*, 0.15 mm of water. *B*, 1 meter of water+carbon disulfide, ratio of numbers of molecules, 1 : 300. Water bands marked W. *C*, Intensity distribution, showing atmospheric water vapor bands. *D*, 96 cm of methyl alcohol vapor. *E*, 2 mm of methyl alcohol liquid. *F*, 4 cm of methyl alcohol+carbon tetrachloride, 1 : 7.9.

These observations are in agreement with the view that the interaction, whatever its nature, that occurs between molecules in the liquid is very much weakened, if not destroyed, in the solution state. They show also that the interaction affects, relatively, only the polar part of the molecule, for perhaps the most striking thing in the figure is the vast difference between the behavior of the so-called "OH" and "CH" bands of the alcohol when dissolved in carbon tetrachloride. Whether definite polymers consisting of double, triple or multiple molecules exist and produce the vapor-liquid differences, or whether indefinite aggregates held together by dipole forces which, acting upon a single molecule shift and broaden its absorption bands, is an open question.

But whatever view is taken, the existence of violent disturbances in the structure of the OH group must be recognized. Such disturbances may be due to strong dipole interaction between the OH ends of the alcohol, or in the case of water between two or more entire molecules, which results in the destruction of sharp quantization and the consequent production of broad absorption maxima for the OH bands, and for these alone. Another type of interaction however may be possible. The strong disturbing forces which arise may be caused by an interchange of protons between the OH groups in the manner postulated by Bernal and Fowler[1] to account for the high mobility of the H and OH ions in water solution. The existence of such a resonance phenomenon in liquid water and liquid alcohols in which the probability of occurrence would depend upon the proximity of neighboring molecules could easily account for the destruction of sharp quantization. The diffuse nature of the Raman bands in liquid water would also be a consequence of this interaction. It is evident however that a choice between these two views cannot be made at the present time.

Studies of these effects in the 3μ region are being made, and it is hoped that they may be carried out also under high resolving power and dispersion.

E. L. KINSEY
J. W. ELLIS
University of California at Los Angeles,
November 29, 1935.

[1] J. D. Bernal and R. H. Fowler, J. Chem. Phys. 1, 515 (1933).